

Naval Research Laboratory

Washington, DC 20375-5320



AD-A270 967



NRL/FR/8121--93-9526

# Ultraviolet Plume Instrument Imaging from the LACE Satellite The Strypi Rocket Plume

H.W. SMATHERS AND D.M. HORAN

*Space Systems Development Department  
Naval Center for Space Technology*

J.G. CARDON, E.R. MALARET, AND M. SINGH

*Applied Coherent Technology Corporation  
Herndon, Virginia*

T. SORENSEN

*AlliedSignal Technical Services Corporation  
Alexandria, Virginia*

P.M. LAUFER, M.R. CORSON, J.E. BRANDENBURG, AND J.A. MCKAY

*Research Support Instruments  
Alexandria, Virginia*

R.R. STRUNCE, JR.

*Star Technologies Corporation  
Great Falls, Virginia*

September 17, 1993

Reproduced From  
Best Available Copy

Approved for public release; distribution unlimited.

93-24123

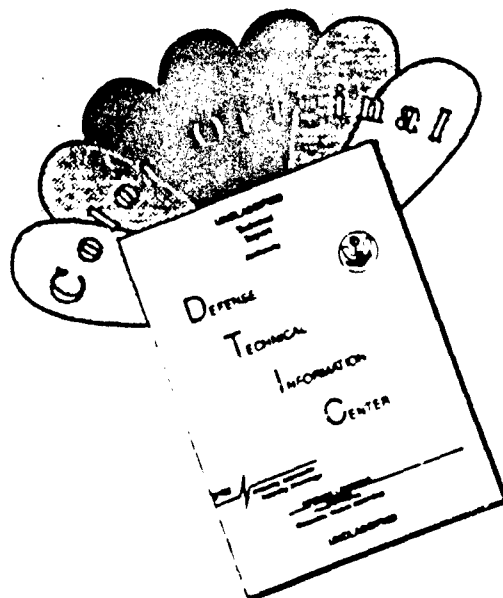


93 10 12 103

DTIC  
ELECTE  
OCT 15 1993  
S E D

20000920219

# DISCLAIMER NOTICE



THIS DOCUMENT IS BEST QUALITY AVAILABLE. THE COPY FURNISHED TO DTIC CONTAINED A SIGNIFICANT NUMBER OF COLOR PAGES WHICH DO NOT REPRODUCE LEGIBLY ON BLACK AND WHITE MICROFICHE.

REPORT DOCUMENTATION PAGE			Form Approved OMB No. 0704-0188
Public reporting burden for the collection of information is estimated to average 1 hour per response, including the time for reviewing instructions, searching existing data sources, gathering and maintaining the data needed, and completing and reviewing the collection of information. Send comments regarding the burden estimate or any other aspect of the collection of information, including suggestions for reducing the burden, to Washington Headquarters Services, Directorate for Information Operations and Reports, 1215 Jefferson Davis Highway, Suite 1204, Arlington, VA 22202-4302, and to the Office of Management and Budget, Paperwork Reduction Project (0704-0188), Washington, DC 20503.			
1. AGENCY USE ONLY (Leave Blank)	2. REPORT DATE September 17, 1993	3. REPORT TYPE AND DATES COVERED Interim	
4. TITLE AND SUBTITLE UVPI Imaging from the LACE Satellite: The Strypi Rocket Plume			5. FUNDING NUMBERS PE - 63217C PMA - N1305
6. AUTHOR(S) H.W. Smathers, D.M. Horan, J.G. Cardon, <sup>1</sup> E.R. Malaret, <sup>1</sup> M. Singh, <sup>1</sup> T. Sorensen, <sup>2</sup> P.M. Laufer, <sup>3</sup> M.R. Corson, <sup>3</sup> J.E. Brandenburg, <sup>3</sup> J.A. McKay, <sup>3</sup> and R.R. Strunce, Jr. <sup>4</sup>			
7. PERFORMING ORGANIZATION NAME(S) AND ADDRESS(ES) Naval Research Laboratory Washington, DC 20375-5320			8. PERFORMING ORGANIZATION REPORT NUMBER NRL/FR/8121-93-9526
9. SPONSORING/MONITORING AGENCY NAME(S) AND ADDRESS(ES) Strategic Defense Initiative Organization Washington, DC 20301-7100			10. SPONSORING/MONITORING AGENCY REPORT NUMBER
11. SUPPLEMENTARY NOTES <sup>1</sup> Applied Coherent Technology Corp. <sup>3</sup> Research Support Instruments <sup>2</sup> AlliedSignal Technical Services Corp. <sup>4</sup> Star Technologies Corp.			
12a. DISTRIBUTION/AVAILABILITY STATEMENT Approved for public release; distribution unlimited.			12b. DISTRIBUTION CODE
13. ABSTRACT (Maximum 200 words) <p>The Ultraviolet Plume Instrument (UVPI) is a small plume-tracking instrument that was flown on the Naval Research Laboratory's Low-power Atmospheric Compensation Experiment (LACE) satellite. The UVPI plume camera has a narrow field of view (0.180° by 0.135°), and it observes sources through any of four filters with passbands of 195 to 295 nm, 220 to 320 nm, 235 to 350 nm, and 300 to 320 nm. The Strypi rocket was launched from Hawaii on 18 February 1991. The second (Antares) and the third (Star 27) stages reached 110 km altitude and were successfully detected and tracked by the UVPI from a range of 450 to 550 km. The spectral radiance and spectral radiant intensities of the missile plumes were extracted from these images for the four passbands.</p>			
14. SUBJECT TERMS Ultraviolet Plume Instrument      LACE satellite      Spectral radiant intensity      Plume imaging UVPI      Plume tracking      Missile plumes UV      Spectral radiance      Strypi			15. NUMBER OF PAGES 263
			16. PRICE CODE
17. SECURITY CLASSIFICATION OF REPORT UNCLASSIFIED	18. SECURITY CLASSIFICATION OF THIS PAGE UNCLASSIFIED	19. SECURITY CLASSIFICATION OF ABSTRACT UNCLASSIFIED	20. LIMITATION OF ABSTRACT UL

NTIS GRA&I	<input checked="" type="checkbox"/>
DTIC TAB	<input checked="" type="checkbox"/>
Unannounced	<input type="checkbox"/>
Justification	
By	
Distribution/	
Availability Codes	
Dist	Avail and/or Special
A-1	

DTIC QUALITY INSPECTED 2

## Contents

EXECUTIVE SUMMARY.....	E-1
1.0 INTRODUCTION.....	1
1.1 Background.....	1
1.2 Capability of UVPI.....	2
1.2.1 Description of UVPI.....	2
1.2.2 Description of LACE Satellite.....	4
2.0 STRYPI MISSION PLAN.....	5
2.1 Scientific Objectives for UVPI.....	5
2.1.1 Radiometrics.....	5
2.1.2 Spatial Features.....	5
2.1.3 Temporal Features.....	6
2.1.4 Spectral Features.....	6
2.2 Strypi Description and Planned Trajectory.....	6
2.2.1 Strypi Description.....	6
2.2.2 Planned Strypi Trajectory.....	9
2.3 Planned Plume Observation.....	11
2.4 Viewing Expectations.....	11
2.4.1 Expected Geometry and Pointing.....	11
2.4.2 Expected Radiometrics (CHARM 1.3 Predictions).....	12
3.0 STRYPI OBSERVATION.....	13
3.1 Strypi Performance.....	15
3.2 UVPI Operations, Actual Scenario.....	16
3.2.1 UVPI Pre-Encounter Activities.....	18
3.2.2 Antares Plume Observation.....	19
3.2.3 Star 27 Plume Observation.....	19
3.2.4 Bow Shock Observation.....	19
3.3 Encounter Geometry.....	20
3.4 Pointing and Tracking Overview.....	21
3.4.1 Mode Sequence.....	21
3.4.2 Gimbal Angles.....	22
3.5 Tracker Performance Summary.....	22
3.5.1 Tracking Jitter During Antares Burn.....	23
3.5.2 Tracking Jitter During Star 27 Burn.....	23
3.5.3 Comparison with Previous Encounters.....	23
4.0 PLUME IMAGES.....	24
4.1 Definition of Data Intervals.....	24
4.1.1 Camera Parameters.....	24
4.2 UVPI Data Analysis Methodology.....	26
4.2.1 Photoevent Calculation.....	26
4.2.2 Extraction of Radiometric Quantities.....	27
4.2.2.1 Relation of Photoevents to Spectral Radiance.....	27
4.2.2.2 Peak Normalized Radiance.....	28
4.2.2.3 Formulation and Comparison of a Model Plume Spectrum.....	29
4.2.3 Specific Radiometric Values.....	31
4.2.3.1 Spectral Radiance.....	31
4.2.3.2 Radiance.....	32
4.2.3.3 Radiant Intensity and Spectral Radiant Intensity.....	32
4.2.4 Point Spread Function Effects.....	32
4.2.5 Radiometric Data Analysis Summary and Conversion Values.....	33



## Contents (Cont'd)

4.3	Examples of Single Plume Camera Images.....	34
4.4	Calibrated Plume Camera Images.....	34
4.5	Calibrated Tracker-Camera Images.....	55
4.6	Error Analysis for Radiometric Observations.....	72
4.6.1	Error Due to Measurement Noise.....	72
4.6.2	Error in Gain Conversion Factor.....	73
4.6.3	Calculation of Total Error.....	73
4.7	Noise Equivalent Radiance.....	75
5.0	SPATIAL FEATURES.....	77
5.1	Delineation of Plume Central and Outer Regions.....	77
5.2	Calibrated Plume Contours.....	78
5.3	Calibrated Tracker-Camera Spatial Features.....	98
5.4	Plume Extent and Point Spread Function.....	118
5.5	Comparison of Results to CHARM 1.3 Predictions.....	126
6.0	TEMPORAL FEATURES.....	130
6.1	Plume Camera Radiant Intensity Plots.....	132
6.2	Tracker Camera Intensity Plots.....	137
7.0	SPECTRAL ANALYSIS OF PLUMES.....	139
7.1	Observed Spectral Radiant Intensities.....	139
7.1.1	Antares Observation.....	139
7.1.2	Star 27 Observation.....	140
7.2	Discussion.....	141
8.0	TRAILING CLOUD OBSERVATIONS.....	141
8.1	Initial Transient.....	141
8.1.1	Size and Radiometrics of Initial Cloud.....	141
8.2	Antares Cloud Trail.....	143
8.2.1	Size and Radiometrics of the Cloud Trail.....	144
8.3	The Star 27 Dim Trail.....	145
9.0	SUMMARY AND CONCLUSIONS.....	146
9.1	Summary.....	146
9.2	Achievement of Objectives.....	147
9.2.1	General Objectives.....	147
9.2.2	Spatial Features.....	148
9.2.3	Temporal Features.....	148
9.2.4	Spectral Features.....	148
9.3	Conclusions.....	149
	ACKNOWLEDGMENTS.....	150
	REFERENCES.....	150
	APPENDIX A: The Ultraviolet Plume Instrument.....	153
	APPENDIX B: UVPI Characterization and Calibration.....	163
	APPENDIX C: Preflight Planning.....	171
	APPENDIX D: Tracker Performance.....	179
	APPENDIX E: UVPI Parameters.....	191
	APPENDIX F: Strypi Trajectory Parameters.....	239
	ADDENDUM: Statistical Discrimination of Photoevents.....	251

## Figures

1	Tracker camera: net quantum efficiency curve.....	3
2	Plume camera: net quantum efficiency curves.....	4
3	Schematic of LACE satellite.....	4
4	Strypi XI rocket.....	7
5	Antares II rocket motor.....	8
6	Star 27 rocket motor.....	9
7	LACE trajectory relative to Strypi trajectory.....	10
8	Strypi nominal altitude and velocity profiles.....	10
9	Planned sequence of events.....	10
10	Effective emissivity of a 2.3- $\mu$ m alumina particle.....	12
11	LACE ground track for orbit 5582 - 18 February 1991.....	14
12	Strypi altitude and velocity profiles.....	15
13	Antares chamber pressure and angle of attack.....	15
14	Star 27 chamber pressure and angle of attack.....	15
15	Telemetry frame vs time after liftoff.....	18
16	Strypi/UVPI encounter geometry.....	20
17	Strypi/UVPI image factors.....	21
18	Mission mode vs time after launch.....	21
19	Azimuth gimbal angles vs time after launch.....	22
20	Elevation gimbal angles vs time after launch.....	22
21	Tracker and plume camera gain.....	26
22	Tracker and plume camera exposure times.....	26
23	Spectral shape function based on reference spectrum model.....	30
24	Single unprocessed plume camera images of Antares plume.....	35
25	Single image of Antares plume.....	36
26	Plume camera image of ground-based beacon illustrating the point spread function.....	38
27	Composite plume camera image for interval 1.....	39
28	Composite plume camera image for interval 2.....	41
29	Composite plume camera image for interval 3.....	43
30	Composite plume camera image for interval 4.....	45
31	Composite plume camera image for interval 5.....	47
32	Composite plume camera image for interval 6.....	49
33	Composite plume camera image for interval 7.....	51
34	Comparison of image superposition methods for data interval 2.....	53
35	Comparison of image superposition methods for data interval 5.....	55
36	Tracker-camera image of ground-based beacon illustrating the point spread function.....	57
37	Composite tracker-camera image for interval 1.....	59
38	Composite tracker-camera image for interval 2.....	61
39	Composite tracker-camera image for interval 3.....	63
40	Composite tracker-camera image for interval 4.....	65
41	Composite tracker-camera image for interval 5.....	67
42	Composite tracker-camera image for interval 6.....	69
43	Composite tracker-camera image for interval 7.....	71
44	Highlighted plume central regions for Antares.....	79
45	Highlighted plume central regions for Star 27.....	81
46	Photoevents as a function of defined central region size, Antares interval 1.....	82
47	Photoevents as a function of defined central region size, Antares interval 2.....	82

## Figures (Cont'd.)

48	Photoevents as a function of defined central region size, Antares interval 3.....	82
49	Photoevents as a function of defined central region size, Antares interval 4.....	82
50	Plume-camera contour plot for ground-based beacon.....	83
51	Plume-camera contour plot for interval 1.....	85
52	Plume-camera contour plot for interval 2.....	87
53	Plume-camera contour plot for interval 3.....	89
54	Plume-camera contour plot for interval 4.....	91
55	Plume-camera contour plot for interval 5.....	93
56	Plume-camera contour plot for interval 6.....	95
57	Plume-camera contour plot for interval 7.....	97
58	Tracker-camera contour plot for ground-based beacon.....	99
59	Tracker-camera contour plot for interval 3.....	101
60	Tracker-camera contour plot for interval 6.....	103
61	Tracker-camera response over a 64 by 64 pixel region, interval 1.....	105
62	Clipped tracker-camera response over a 64 by 64 pixel region, interval 1.....	105
63	Tracker-camera response over a 64 by 64 pixel region, interval 2.....	107
64	Clipped tracker-camera response over a 64 by 64 pixel region, interval 2.....	107
65	Tracker-camera response over a 64 by 64 pixel region, interval 3.....	109
66	Clipped tracker-camera response over a 64 by 64 pixel region, interval 3.....	109
67	Tracker-camera response over a 64 by 64 pixel region, interval 4.....	111
68	Clipped tracker-camera response over a 64 by 64 pixel region, interval 4.....	111
69	Tracker-camera response over a 64 by 64 pixel region, interval 5.....	113
70	Clipped tracker-camera response over a 64 by 64 pixel region, interval 5.....	113
71	Tracker-camera response over a 64 by 64 pixel region, interval 6.....	115
72	Clipped tracker-camera response over a 64 by 64 pixel region, interval 6.....	115
73	Tracker-camera response over a 64 by 64 pixel region, interval 7.....	117
74	Clipped tracker-camera response over a 64 by 64 pixel region, interval 7.....	117
75	Plume-camera PSF for ground-based beacon.....	118
76	Axial profile through plume-camera PSF for ground-based beacon.....	118
77	Axial profile along plume central region for data interval 1, plume camera.....	119
78	Axial profile along plume central region for data interval 2, plume camera.....	121
79	Axial profile along plume central region for data interval 3, plume camera.....	121
80	Axial profile along plume central region for data interval 4, plume camera.....	123
81	Axial profile along plume central region for data interval 5, plume camera.....	123
82	Axial profile along plume central region for data interval 6, plume camera.....	125
83	Axial profile along plume central region for data interval 7, plume camera.....	125
84	Tracker-camera PSF for ground-based beacon.....	126
85	Axial profile through tracker-camera PSF for ground-based beacon.....	126
86	High-resolution and PSF-convolved CHARM 1.3 image prediction of UVPI's Antares observation using PC-4.....	127
87	PSF convolved CHARM 1.3 contour plot prediction of UVPI's Antares observation using PC-4.....	127
88	CHARM 1.3 predicted axial profile along plume for data interval 1, plume camera.....	128
89	CHARM 1.3 predicted axial profile along plume for data interval 2, plume camera.....	128
90	CHARM 1.3 predicted axial profile along plume.....	128
91	CHARM 1.3 predicted axial profile along plume for data interval 4, plume camera.....	128
92	CHARM 1.3 predicted axial profile along plume for data interval 5, plume camera.....	128
93	CHARM 1.3 predicted axial profile along plume for data interval 6, plume camera.....	128
94	CHARM 1.3 predicted axial profile along plume for data interval 7, plume camera.....	129
95	Mean central region spectral radiant intensity, plume camera, Antares stage.....	131
96	Mean central region spectral radiant intensity, plume camera, Star 27 stage.....	131
97	Mean spectral radiant intensity, tracker camera, Antares stage.....	131
98	Mean spectral radiant intensity, tracker camera, Star 27 stage.....	131
99	Mean outer region spectral radiant intensity, plume camera, Antares stage.....	132
100	Mean outer region spectral radiant intensity, plume camera, Star 27 stage.....	132
101	Antares, plume camera, total intensity for interval 1.....	133
102	Antares, plume camera, central region intensity for interval 1.....	133
103	Antares, plume camera, outer region intensity for interval 1.....	133

## Figures (Cont'd.)

104	Antares, plume camera, total intensity for interval 2.....	133
105	Antares, plume camera, central region intensity for interval 2.....	134
106	Antares, plume camera, outer region intensity for interval 2.....	134
107	Antares, plume camera, total intensity for interval 3.....	134
108	Antares, plume camera, central region intensity for interval 3.....	134
109	Antares, plume camera, outer region intensity for interval 3.....	134
110	Antares, plume camera, total intensity for interval 4.....	134
111	Antares, plume camera, central region intensity for interval 4.....	135
112	Antares, plume camera, outer region intensity for interval 4.....	135
113	Star 27, plume camera, total intensity for interval 5.....	135
114	Star 27, plume camera, total intensity for interval 6.....	135
115	Star 27, plume camera, total intensity for interval 7.....	135
116	Antares, tracker camera total intensity for interval 1.....	137
117	Antares, tracker camera total intensity for interval 2.....	137
118	Antares, tracker camera total intensity for interval 3.....	137
119	Antares, tracker camera total intensity for interval 4.....	137
120	Star 27, tracker camera total intensity for interval 5.....	138
121	Star 27, tracker camera total intensity for interval 6.....	138
122	Star 27, tracker camera total intensity for interval 7.....	138
123	Measured spectral radiant intensity for the Antares central region.....	139
124	Measured spectral radiant intensity for the plume-camera field of view for Antares.....	140
125	Measured spectral radiant intensity for the plume-camera field of view for Star 27.....	141
126	X target and Y target size during the Antares burn.....	142
127	Initial cloud imaged by tracker camera at 158.9 seconds.....	142
128	Tracker camera images of Antares cloud trail.....	143
129	Color mosaic of Antares cloud trail.....	144
130	Antares cloud trail profile.....	144
131	Star 27 dim trail.....	145

## Tables

1	Strypi XI Rocket Motor Characteristics .....	7
2	Expected Intensities for Antares Stage .....	13
3	Expected Intensities for Star 27 Stage .....	13
4	Strypi Sequence of Events .....	14
5	Strypi Encounter List of Commands .....	16
6	Antares and Star 27 Tracking Analysis Intervals .....	22
7	Tracking Error Statistics During Antares Burn .....	23
8	Tracking Error Statistics During Star 27 Burn .....	24
9	Tracking Error Comparison .....	24
10	Definitions of Data Intervals .....	25
11	Parameters Associated with Data Intervals .....	25
12	Camera Filter, Wavelength of Peak Quantum Efficiency, .....	28
13	Photoevents Per Second and Peak Normalized Radiance .....	29
14	Photoevents Per Second from Antares Plume and Reference .....	31
15	Plume Camera Filter Bandpass Limits, Full-Width-Half-Maximum, .....	31
16	Radiometric Values Corresponding to Single Photoevents .....	33
17	Description of Basic Parameters .....	36
18	Apparent Velocity Vector Direction for Each Interval .....	37
19	Centroid Statistics for Plume-Camera Images .....	53
20	Tracker Camera Exposure Time .....	55
21	Percent Error per Image Due to Measurement Noise, $\epsilon_N$ .....	73
22	Average Error in $1/G_g$ for Tracker and Plume Cameras .....	73
23	Plume Central Region Radiometric Percent Errors for Plume Camera .....	74
24	Central Region Plus Outer Region Radiometric Percent Errors for Plume Camera .....	75
25	Radiometric Percent Errors: Tracker Camera Over 19 x 19 Pixel Window .....	75
26	Total Radiometric Percent Errors, $\epsilon_T$ .....	75
27	Plume Camera NER Per Pixel for Data Intervals .....	77
28	Tracker Camera NER Per Pixel for Data Intervals .....	77
29	Central Region Extent in Plume Camera .....	81
30	Plume Camera Apparent Peak Radiometric Value .....	98
31	Observed Axial Length of Plume Central Region .....	118
32	Strypi Data Quality Estimate .....	129
33	Peak Radiance Comparison .....	130
34	Comparison of Measured to Predicted Plume Length .....	130
35	Radiant Intensity Figures .....	132
36	Summary of Plume Camera Average Radiant Intensities Using Reference Spectral Response .....	136
37	Summary of Plume Camera Average Radiant Intensities Using Flat Spectral Response for the Outer Region .....	136
38	Summary of Tracker-Camera Average Radiant Intensities .....	138
39	Measured and Scaled Spectral Radiant Intensity in Units of W/sr- $\mu$ m for Antares .....	140
40	Measured and Scaled Spectral Radiant Intensity in Units of W/sr- $\mu$ m for Star 27 .....	141

## EXECUTIVE SUMMARY

Missile tracking in the ultraviolet is advantageous because of extremely low Earth and solar backgrounds; extremely sensitive photodetectors that do not require cryogenic cooling; and very high optical resolution, which is possible with optics of relatively modest size. The Ultraviolet Plume Instrument (UVPI) is a small, plume-tracking-instrument that was flown on the Naval Research Laboratory's Low-power Atmospheric Compensation Experiment (LACE) satellite, which was launched on 14 February 1990.

The UVPI system aperture is only 10 cm in diameter. However, it can detect and image missile plumes at a 500-km range. The two cameras of the instrument use narrowband filters, image intensifiers, and charged coupled device (CCD) detectors to observe sources in the ultraviolet. The primary function of the tracker camera, viewing over a relatively wide field, ( $1.97^\circ$  by  $2.62^\circ$ ) and broad spectrum (255 to 450 nm) is to locate and track a source for higher resolution observation by the plume camera. The plume camera has a narrow field of view ( $0.180^\circ$  by  $0.135^\circ$ ); it observes sources through any of four filters with passbands of 195 to 295 nm, 200 to 320 nm, 235 to 350 nm, and 300 to 320 nm. The wavelengths shorter than 310 nm are essentially invisible from the ground because of atmospheric absorption. The limiting resolution of the tracker camera is about 230  $\mu$ radians; that of the plume camera is about 90  $\mu$ radians. These are equivalent to 115 m and 45 m, respectively, at a 500-km range.

The Strypi XI was the fourth demonstration of the ability of the UVPI to observe missiles in flight above the atmosphere. The Strypi was launched from the U.S. Navy Pacific Missile Range Facility in Hawaii before sunrise on 18 February 1991. The launch time and trajectory were selected to synchronize the flight with the LACE pass and permit ground observations from the AMOS site on Maui.

The first stage of the three-stage Strypi fired only at low altitude, below 20 km, and was not expected to be visible in the ultraviolet from space. The second (Antares) and the third (Star 27) stages reached 110-km altitude and were successfully detected and tracked by the UVPI from a range of 450 to 550 km.

The Antares plume was successfully tracked for about 30 seconds, and 480 1/30th-second images of plume data were acquired by using the four plume-camera filters. The tracking of the Antares plume was of sufficient quality to permit the superposition of images for plume radiance determination. Image superposition to enhance the signal level is needed for accurate radiometry because of the small telescope aperture. The weaker plume from the Star 27 stage was also tracked, and 304 images were acquired by using three plume-camera filters. However, the weak signal reduced the quality of the superposed images.

The spectral radiance and spectral radiant intensities of the missile plumes were extracted from these images. Absolute values are necessarily obtained on the basis of an assumed spectral shape, namely, one that is derived from a physical model of the plume as a nearly transparent stream of micron-sized alumina particles at their melting points. This spectral shape is simply termed the reference model spectrum. A comparison of the results for the four UVPI filters indicates that the reference spectral shape is not inaccurate, but the new data suggest a stronger component in the far UV ( $\lambda < 300$  nm) than the reference model predicts.

The images reveal not only a radiant plume but also an extensive outer region with a passband-integrated radiant intensity comparable to that of the plume central region. The far UV

component of this outer region appeared to be even stronger, relative to the near UV component, than that of the central region. The mechanism of excitation of this outer region has not been established. Although spectral radiant intensity values for the outer region were calculated based on the reference spectral shape and a spectrally flat model, these values must be considered tentative until a reliable spectral model is available.

The time dependence of the plume central region radiant intensity within each filter interval showed no pronounced trends or variations. Momentary, single-frame peaks exceeding the range of normal statistical variation were detected. Whether these can be correlated with missile engine events or other sensors remains to be seen.

The tracker camera, within its relatively limited resolution, obtained radiant intensity data to 450-nm wavelength. These data, taken with the plume camera data in the 195 to 350-nm band, support the conclusion that the central region spectrum is quite close to the reference model, with a relative enhancement of the emission in the far UV.

The third stage of the missile rose to a higher altitude than planned and burned out before descending to altitudes where a bow shock might occur. The UVPI tracker lost track when the missile ceased firing and, therefore, could not follow the third stage to lower altitudes. Thus, the observation did not provide a test of the existence of a luminous bow shock.

A very large, persistent cloud trail from the Antares stage was observed. This 43-km trail was sufficiently bright and persistent: it briefly confused the UVPI tracker.

This base of UV radiometric data is the foundation for further analysis to provide refined interpretations and evaluation. Comparison with models and with data from sensors on other platforms will also yield improved radiometric results and an enhanced phenomenological understanding of UV emission by solid rocket motors in the upper atmosphere.

## UVPI IMAGING FROM THE LACE SATELLITE: THE STRYPI ROCKET PLUME

### 1.0 INTRODUCTION

#### 1.1 Background

For 25 years or more, the military establishment has been interested in the infrared (IR) exhaust plumes of rockets and jet airplanes because heat-seeking missiles can be built and used as counter-threat weapons. A great deal of time and money has been spent:

- (a) developing these heat-seeking missiles and their sensors, and
- (b) measuring and modeling the spectral signatures of their exhaust plumes.

For example, the Standardized Infra-Red Radiation Model (SIRRM) and the Composite High Altitude Radiation Model (CHARM) [1] are software codes that can predict the size, shape, intensity, and other pertinent parameters of most infrared rocket plumes (given the altitude, velocity, fuel type, thrust, and nozzle characteristics). In short, (a) indicates that IR technology and phenomenology are mature sciences, and (b) clarifies why Phase I of the Strategic Defense Initiative Organization's (SDIO) program is dominated by IR instrumentation in most major areas. [A Glossary is located at end of report, following References.]

Other spectral regions, in particular the ultraviolet (UV), have not attracted as much attention from the defense industry as IR. Nevertheless, during the past few years, interest in the ultraviolet emissions of plumes and their use in passive sensor applications has increased, partly as a result of plume observation data obtained from several missions carrying UV sensors. Lawrence Livermore National Laboratory's PROBE [2] and the SDIO's Delta 180 [3] and 181 [4] missions are examples. The new hope is that two items - the UV passive emissions from the plumes of the booster and postboost vehicle and the solar scattering from the plume and hardbody - can be used effectively in addition to, or instead of, IR emissions. Signal contrast may be better in the UV because the background sunlight reflected from Earth is severely reduced by the ozone layer. Also, because a rocket plume is essentially a thermal radiator, only the hottest regions of the plume will tend to be bright in the UV. Thus, the UV plume will tend to be more compact than the IR plume, so that aimpoint and hardbody hand-off problems can be more easily solved with the UV plumes.

Another factor favoring the use of UV is less complex hardware. There is an increasing awareness that infrared sensors are destined to require relatively large, cryogenically cooled focal plane arrays. Small, high-quality, ultraviolet sensors, which do not require cryogenic cooling, are currently mass producible at modest cost. Thus, a relatively small ultraviolet optical system can achieve diffraction-limited resolution equivalent to that of a much larger IR optical system while providing significant weight, volume, and cost savings. As a result, more SDIO missions are proposing to use UV sensors [for example, the Brilliant Pebbles program and the Air Force Armament Laboratory's ULTRASEEK (Ultraviolet Seeker) program]. In addition to these acquisition and tracking applications, boost-phase surveillance and tracking systems performing early warning, identification, and initial trajectory determination functions are examining the potential that ultraviolet may offer.



Although the UV sensors are available, there is a general shortage of information as to what to expect in real flight situations for this relatively new UV technology. Additional data are needed to facilitate the application of this technology. For example, additional data are needed for the selection of wavebands best suited to the application, the design and evaluation of new flight systems, and the development of algorithms for tracking and handoff. Recently, an ad hoc subcommittee of the SDIO Phenomenology Steering and Analysis Group (PSAG) was convened to determine the current state of knowledge of plumes and backgrounds in the ultraviolet and visible portions of the spectrum. After considerable evaluation of existing data and system requirements, the subcommittee made recommendations regarding plume data requirements [5]. The need for more UV data is critical. Both plume and background data are needed; in-flight and ground-based measurements are desired. Operational, solid-fueled, upper-stage plumes in normal boost trajectories, both dark and sunlit, are the third highest priority after liquid-fueled upper stages and post-boost vehicles at operational velocities.

The Ultraviolet Plume Instrument (UVPI), carried aboard the Low-power Atmospheric Compensation Experiment (LACE) satellite launched in February 1990, was designed to collect such plume imagery. A moderately priced rocket was sought to serve as a dedicated target. A Strypi XI three-stage rocket was selected. The overall objective of the observation was to gather data at high altitude (above 100 km) from space in the solar blind UV bands. These data were to enhance the understanding of plume physics and chemistry and to help answer questions about radiance, spatial extent, and temporal variability of plumes. A number of more specific objectives are listed in Section 2.0, which describes the Strypi mission plan.

## 1.2 Capability of UVPI

The Ultraviolet Plume Instrument (UVPI) is carried aboard the Low-power Atmospheric Compensation Experiment (LACE) spacecraft. The UVPI's mission is to collect images of rocket plumes in the ultraviolet waveband and to collect background image data on Earth, Earth's limb, and celestial objects. Background object imagery already collected with the UVPI includes the day and night Earth limb air glow, aurora, sunlit and moonlit clouds, solid Earth scenes with varying solar illumination, cities, and stars.

The UVPI was assigned to the LACE spacecraft's experiment complement after the spacecraft was designed and after its fabrication was started. Therefore, the UVPI was constrained in size, weight, power consumption, and telemetry to whatever margin remained on the LACE spacecraft. The requirement that the UVPI be capable of high spatial resolution created a need for highly accurate instrument pointing on a gravity-gradient-stabilized spacecraft. The instrument did not have direct access to spacecraft attitude measurements. Subsequently, this led to the requirement for flexible software to control the instrument.

The LACE satellite was launched on 14 February 1990, into a circular orbit at an altitude of 292 nautical miles (nmi) and a 43° inclination. The UVPI is mounted within the satellite and looks through an aperture in the Earth-oriented panel. A gimballed mirror provides UVPI with a field of regard of a 50°-half-angle cone about the satellite's nadir. When the UVPI is not in use, a door covers the aperture. Attached to the inside of this door is a flat mirror that allows the UVPI cameras to view celestial objects or the Earth's limb when the door is partially opened.

### 1.2.1 Description of UVPI

The UVPI sensor assembly [6,7] contains two coaligned camera systems that are used in concert to acquire the object of interest, control UVPI, and acquire UVPI images and radiometric data. The two camera systems are the tracker camera and the plume camera; they are discussed briefly below. The two cameras share a fixed 10-cm diameter Cassegrain telescope, which uses a gimballed-plane-steering mirror to view a field of regard that is a 50°-half-angle cone around the nadir. In addition, UVPI contains a second plane mirror on the instrument door that can be set at an angle of approximately 45° relative to nadir. It can be used in conjunction with the steering mirror to view Earth's limb and stars near the limb. The configuration of the UVPI is described in detail in

Appendix A, and the radiometric response of UVPI is discussed in Appendix B. The characteristics of the UVPI have been previously reported [7,8].

The tracker camera is an intensified CCD camera, which is sensitive over a wide wavelength range extending from 255 to 450 nm. The overall response of the tracker camera as a function of wavelength, including the effects of the bandpass filter in the camera system, the photocathode response, and the other optical elements, is shown in detail in Fig. 1. This camera has a relatively wide total field of view of 1.97 by 2.62° and images over this full field of view can be recorded at the 5 Hz image rate. The tracker camera can also be operated in a mode where the field of view is restricted to the central 17% of the full field of view, and the image rate is increased to 30 Hz. The intensifier gain and the exposure time of the camera can be controlled to provide a radiometric dynamic range greater than  $10^6$ .

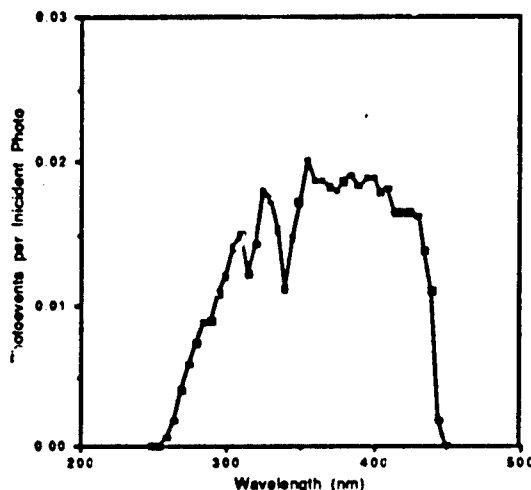


Fig. 1 - Tracker camera: net quantum efficiency curve

The tracker camera has three primary functions that are important for UVPI operation. First, the tracker camera, with its wide field of view and bright image, is used to acquire the object or image of interest. Second, the tracker camera image can be processed on board UVPI, if desired; the result can be used to control the gimballed mirror so that UVPI autonomously tracks the object of interest. Third, the tracker camera is calibrated so that it can acquire radiometric data within its bandpass.

The plume camera is also an intensified CCD camera that operates in the ultraviolet. The plume camera optical train contains a filter wheel that has four selectable filters with bandpasses in the 195 to 350 nm range. The overall response of the plume camera for each of these four filters is shown in detail in Fig. 2. The plume camera has a total field of view of 0.180 by 0.135°, with a correspondingly higher resolution than can be achieved by the tracker camera. Images over the full plume camera field of view can be recorded at a 5 Hz image rate. Like the tracker camera, the plume camera can also be operated in a mode where the field of view is restricted to the central 17% of the full field of view, and the image rate is increased to 30 Hz. The intensifier gain can be controlled to provide a radiometric dynamic range greater than  $10^6$ .

The primary function of the plume camera is to acquire images and radiometric data within the four selectable wavelength bands. UVPI was not designed to use the plume camera for tracking because of the relatively dim images expected in these wavelength bands.

In typical operation, the UVPI is programmed via ground command to point at the expected location of the plume or other object of interest. UVPI then enters a selected scan pattern until the desired object enters the field of view of the tracker camera. The tracker camera and control electronics on board UVPI then track the object, and both cameras gather image and radiometric

data. The plume camera filter can be changed as desired during this data collection to select wavelength bandpasses. If the plume or object of interest is temporarily lost because of a coasting phase between rocket stages or some other reason, UVPI can be commanded to enter various extrapolation or search modes.

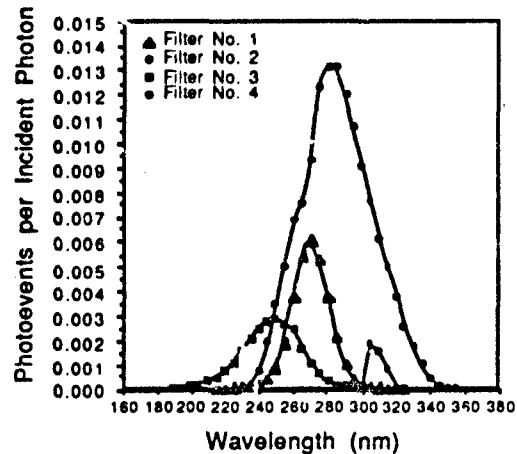


Fig. 2 - Plume camera: net quantum efficiency curves

### 1.2.2 Description of LACE Satellite

The Low-power Atmospheric Compensation Experiment (LACE) satellite was designed and built by the Naval Research Laboratory (NRL) in Washington, D.C. The satellite, Fig. 3, was launched on February 14, 1990, into a circular orbit at an altitude of 292 nmi and a  $43^\circ$  inclination. The spacecraft weighs 3175 lb. The body of the spacecraft is box-shaped, 4.5 ft by 4.5 ft and 8 ft high. Gravity gradient stabilization is provided by a 150-ft retractable boom with a 200-lb tip mass emerging from the top of the spacecraft. The LACE satellite has no orbit adjustment capability.

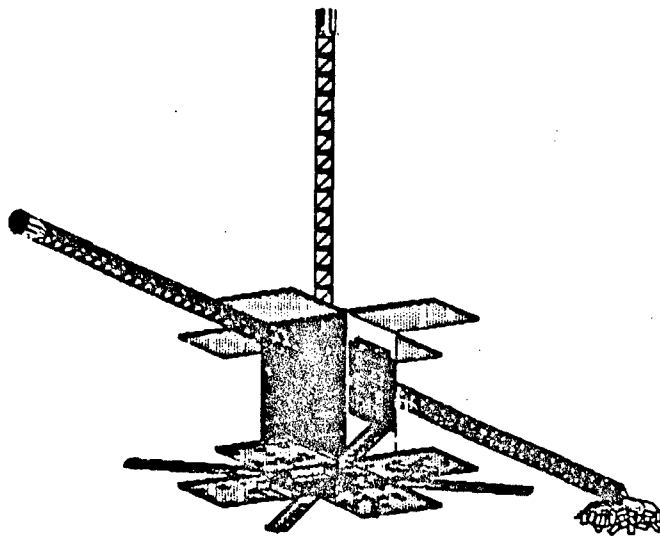


Fig. 3 - Schematic of LACE satellite

The satellite's primary purpose is to provide an orbiting instrumented target board capable of measuring the effects of active compensation of a ground-based laser beam propagated through the atmosphere. The LACE spacecraft was designed to support this experiment for 30 months. NRL operates three ground stations to communicate with and control the LACE satellite. Two of the three ground stations are transportable. Each transportable ground station (TGS) (built by NRL) is designed around two 18-ft truck trailers. One trailer houses the telemetry, command, and communications equipment; the other provides an uninterruptible power supply and work area. The third ground station is permanently located in Maryland. These stations provide all the command and communication links for the LACE spacecraft.

## 2.0 STRYPI MISSION PLAN

### 2.1 Scientific Objectives for UVPI

The primary goal of the Strypi mission [9,10] for UVPI was to collect spatially resolved, radiometric UV plume data for the second and third stages of the rocket. This was to be accomplished by using UVPI's capabilities for tracking and imaging a moving target at long range. The plume camera filters were cycled to vary the wavebands. Emphasis was placed on the solar-blind, mid-UV bands because this data can be obtained only from a space-based sensor, and it has the best potential for high signal-to-background contrast. Pointing accuracy was optimized because that simplifies registration of images when superposed (a necessary procedure for improving statistics). The UVPI observation was coordinated with ground observations that provided infrared and visible band data as important supplements to the UV data.

A secondary goal was to observe any serendipitous special events such as transients, puffs, chuffing, clouds, or contrails. The brightness, size, frequency, and persistence of such phenomena provide useful information.

Another secondary goal was to observe the bow shock, if any, associated with reentry of the Star 27 stage.

The specific objectives of the mission, related to UVPI data, are given in the following subsections. They revolve around a number of questions concerning plume radiance, spatial extent, temporal variability, and spectral shape of the UV emissions [5,10,11]. The objectives are grouped under headings reflecting these subjects.

#### 2.1.1 Radiometrics

The following four objectives are basic to those listed in the subsequent subsections.

- Obtain isoradiance contours for multiple plume camera bandpasses for the Antares and Star 27 plumes.
- Obtain radiant intensity measurements in multiple plume camera bandpasses for the Antares and Star 27 plumes based on the entire field of view of the plume camera and on a subregion corresponding approximately to a plume core.
- Compare radiometric measurements for Antares and Star 27 plumes with those generated by the CHARM 1.3 computer code.
- Provide radiometric measurements for nonplume, transient phenomena, if any.

#### 2.1.2 Spatial Features

- Obtain the length of each of the Antares and Star 27 plume central regions and investigate implications for cooling rate and emissivity of particles.
- Determine the shape of the shock boundary/mixing layer for different velocities of the rocket.
- Identify asymmetries in plume shape and investigate angle of attack and uneven burning as possible causes.

### 2.1.3 Temporal Features

- Identify temporal trends in radiometrics and investigate possible dependence on rocket velocity at fixed altitude.
- Investigate radiometric fluctuations to determine whether short-term variations in brightness are observed.
- Identify changes with time in the shape of the plumes' outer regions, if any, and investigate possible dependence on rocket velocity at fixed altitude.
- Identify persistence and cumulative effects, if any, in plumes or nonplume phenomena.

### 2.1.4 Spectral Features

- Compare the shape of the plume central region's emission spectrum from the multiple bandpass measurements with a reference spectral shape and spectral shape determinations based on other sensors.
- Relate tracker camera measurements to visible and infrared measurements made by other sensors.
- Characterize the emission spectrum for the plumes' outer regions, if any.

## 2.2 Strypi Description and Planned Trajectory

### 2.2.1 Strypi Description

A Strypi XI three-stage solid-propellant rocket system (Fig. 4) was chosen to be the target vehicle for this mission. Thrust, performance, cost, and quick availability were considerations in the choice. Strypi is approximately 13 m (43 ft) long and 0.787 m (31 in.) in diameter. Table 1 provides a summary of Strypi XI rocket motor characteristics.

The first stage was a Castor rocket motor. Its thrust was augmented by two strap-on Recruit boosters. The Recruits burned for about two seconds and were jettisoned seconds later.

The second stage was an Antares II rocket motor. It used a double-base propellant with 20.6% aluminum as fuel. The profile and characteristics of the Antares II rocket motor are shown in Fig. 5.

The third stage thrust was provided by a Star 27 rocket motor. The Star 27 motor used an aluminized composite propellant (ammonium perchlorate/aluminum). The profile and characteristics of the Star 27 rocket motor are shown in Fig. 6.

Instrumentation for the bow shock experiment [12,13] was contained inside a jettisonable shroud at the nose of the rocket. This instrumentation included 8 forward-viewing photometers, a spectrometer, a 130.4-nm atomic oxygen experiment, an electron microprobe, and a 121.6-nm hydrogen Lyman- $\alpha$  ionization chamber, all of which were mounted in the nose dome and took measurements through quartz windows. There were also 8 aft-viewing photometers and a spectrometer, which viewed the rocket motor plumes through periscopes. After the Star 27 burn, the periscopes were jettisoned, and these photometers viewed the bow shock directly through quartz windows.

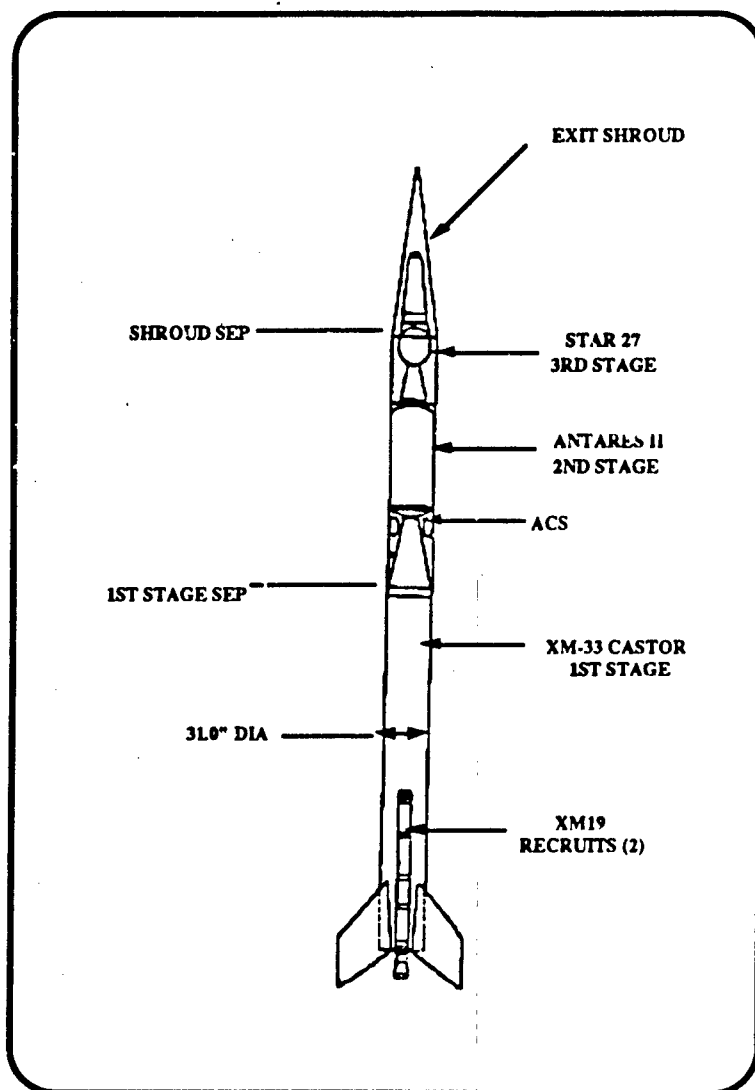


Fig. 4 - Strypi XI rocket\*

\*Figure reprinted from Ref. 14.

Table 1 - Strypi XI Rocket Motor Characteristics

Motor	Stage	Burn Time (s)	Avg Thrust (lb)	Total Impulse (lb-s)	Total Mass (lb-m)	Fuel Mass (lb-m)
Castor TX-33-39 S/N 726	1	40.74	61,750 (vac)	1,900,900	8,698	1,328
Recruit	1	2.16	34,800 (sl)	59,700	343	94
Antares II-A X259-A6 S/N YJ-02/0140	2	35.00	21,050 (vac)	71,200	2,820	224
Star 27 TE-M-616 S/N 42	3	41.35	5,900 (vac)	214,300	798	61

Note: vac = vacuum, sl = sea level.

Based on information from Ref. 14.

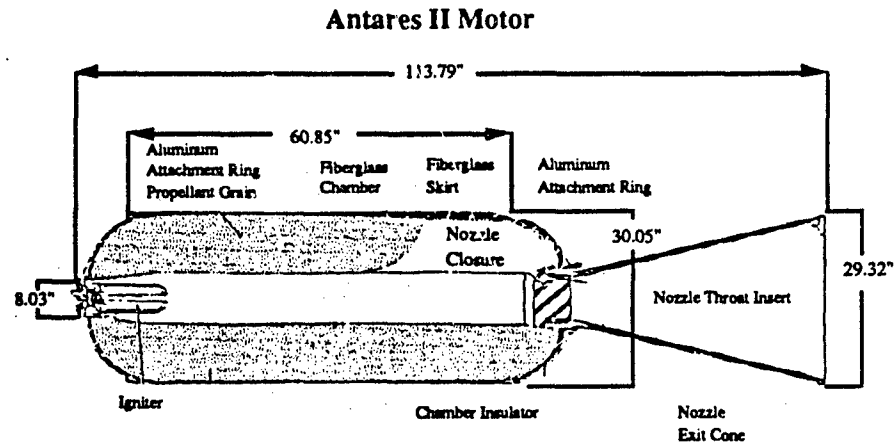
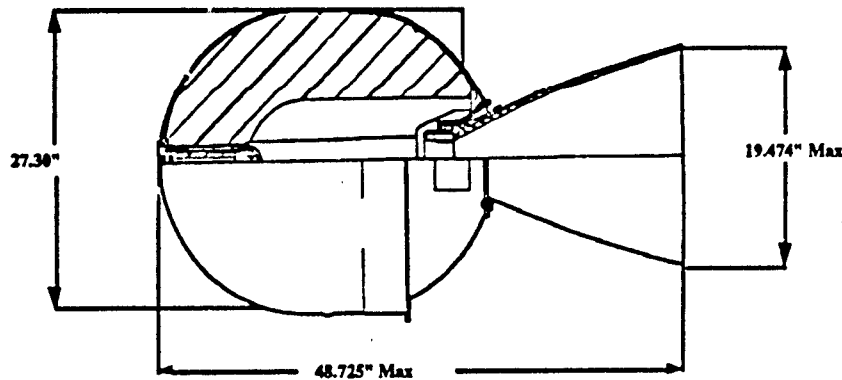


Fig. 5 - Antares II rocket motor\*

\*Figure reprinted from Ref. 14.

## Star 27 Motor



## Nozzle Characteristics

Initial throat diameter	2.74 in.
Final throat diameter	2.91 in.
Exit plane diameter	19.13 in.
Exit plane half-angle	15.0°
Effective cone half-angle	17.2°
Expansion ratio	45.94

## TP-H-3135C Propellant Constituents

	(wt %)
Ammonium perchlorate (oxidizer)	72.0
Carboxy-terminated polybutadiene (CTPB) (binder) (cured with epoxy resin and MAPO)	12.0
Aluminum (fuel)	16.0

## Typical Exhaust Gas Composition

	(mole fractions)
CO <sub>2</sub>	0.02621
CO	0.20851
H <sub>2</sub> O	0.17211
HCl	0.16619
H <sub>2</sub>	0.25477
N <sub>2</sub>	0.08471
Al <sub>2</sub> O <sub>3</sub> (solid)	0.08128

Fig. 6 - Star 27 rocket motor\*

\*Figure reprinted from Ref. 14.

## 2.2.2 Planned Strypi Trajectory

The planned trajectory of the Strypi XI test vehicle called for a launch from the Kauai Test Facility (KTF) at the U.S. Navy Pacific Missile Range Facility (PMRF), Barking Sands, Kauai, Hawaii. The Strypi trajectory was selected to provide maximum viewing time for UVPI and also for the sensors located at the Air Force Maui Optical Site (AMOS). These requirements resulted in a southbound trajectory running parallel to a descending LACE pass (Fig. 7). The nominal velocity and altitude profiles of the Strypi trajectory are shown in Fig. 8. The planned sequence of events for the Strypi flight is shown in Fig. 9.



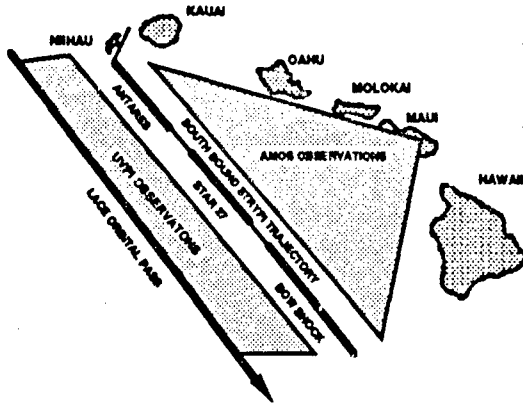


Fig. 7 - LACE trajectory relative to Strypi trajectory

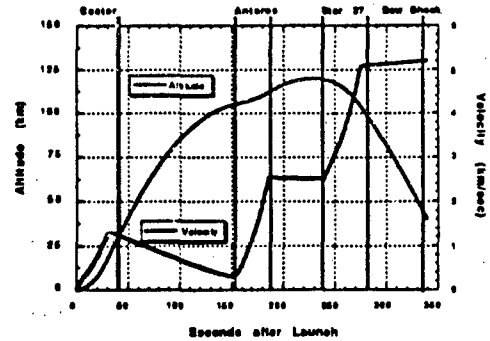


Fig. 8 - Strypi nominal altitude and velocity profiles

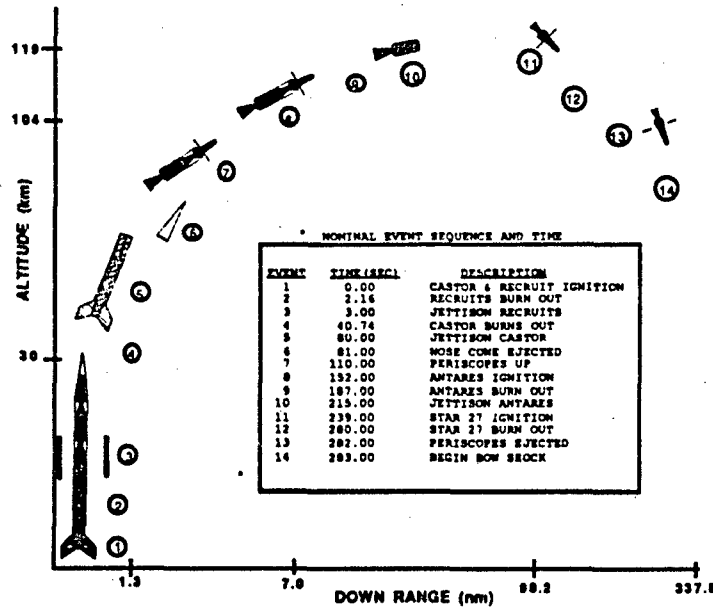


Fig. 9 - Planned sequence of events

Another choice involved the selection of a high or a low trajectory. The high trajectory, approximately 400-km peak, provided minimum range between UVPI and one of the three regions of interest (Antares burn, Star 27 burn, or bow shock). The low trajectory, 120-km peak, provided maximum viewing time for all three flight regions but at a greater range. The latter option was selected for its higher chance of success and the scientific community's desire to observe all three flight regions.

To meet range safety requirements, Strypi had to be launched to the southwest on an azimuth of approximately 208° to clear the Kauai area. Once the rocket was a safe distance from land, a dog-leg turn in the trajectory put Strypi on the planned azimuth (approximately 134°) for the encounter. Initially, this encounter portion of the trajectory ran parallel to the LACE orbit, but the resultant impact point was too close to the island of Hawaii. The azimuth was increased slightly to allow a wider safety margin at the impact point.

The missile was stabilized by fins and was unguided during the first-stage burn. The Castor fins were canted to  $0.75^\circ$  to impart a spin rate to the vehicle of approximately 2.4 revolutions per second at Castor burnout.

After Castor burnout, Strypi coasted until it was exoatmospheric, approximately at 70-km altitude. At this point, the expended Castor stage and the nose shroud were jettisoned. A cold-gas attitude-control system was then activated, and Strypi was reoriented to the proper attitude for Antares ignition. The vehicle was stabilized during the second-stage burn by the spin imparted by the first-stage fins.

Following Antares burnout, the attitude control system reoriented the vehicle for the firing of the third stage. This attitude was selected to provide a  $0^\circ$  angle of attack at 100-km altitude during reentry. The spin rate was reduced to approximately 2 revolutions per second prior to Star 27 ignition in order to be within that motor's certification range. Just prior to third-stage ignition, the expended second stage, which included the Antares rocket motor and the attitude control system, was jettisoned. The velocity of the third stage was predicted to be about 5 km/s at burnout. Reentry was expected to start about the time of third-stage burnout at an altitude of 100 km.

### 2.3 Planned Plume Observation

The Strypi launch and UVPI encounter were designed around a descending LACE pass over the TGS at Kihea, Maui. A brief summary of the planned encounter follows. The detailed plans are in Appendix C.

Upon the launch of the Strypi missile, the actual launch time, the modified Antares ignition time, and the trajectory type (i.e., nominal or dispersed) were to be incorporated into the real-time computation of the Antares pointing function, which would then be transmitted to the UVPI. Prior to Antares ignition, the UVPI was to point along the Strypi trajectory and attempt to acquire the rocket by using a circular scan, as described in Appendix C. Upon acquisition, the UVPI was to switch to its data acquisition mode. The four plume-camera filters were to be used in sequence during the 35-s Antares burn. After Antares burnout, the UVPI was to point along the predicted trajectory and, after Star 27 ignition, acquire this stage. Again, the UVPI was to switch to data acquisition mode, observing through 3 of the 4 plume-camera filters during the 41-s burn. The planned filter change sequence and filter observation durations are shown in Tables C2 and C3 in Appendix C.

The Strypi bow shock emission region was expected to start at the end of the Star 27 burn at 100-km altitude and end at an altitude of about 40 km, about 60 s after burnout. The UVPI would acquire data using plume-camera filters 2, 3, and 4. The tracking of the Strypi during the bow shock phase was uncertain because of the absence of a rocket plume, so a reacquisition procedure (described in Appendix C) was prescribed in the event of tracking loss.

### 2.4 Viewing Expectations

#### 2.4.1 Expected Geometry and Pointing

As described in Appendix C, the launch time was selected to optimize the viewing geometry between UVPI and Strypi during the critical flight regions. The highest priority was placed on viewing the Antares burn.

For the selected launch time of 14:18:35 GMT, the range between UVPI and Strypi on a nominal trajectory decreases from about 525 km to 450 km during the Antares burn, and the aspect angle between UVPI and the rocket spin axis decreases from  $108^\circ$  to  $84^\circ$  during the same period. The optimal aspect angle is  $90^\circ$ . During the Star 27 burn, the range increases from about 475 km to 550 km, and the aspect angle decreases from  $74^\circ$  to  $61^\circ$ . The range during the nominal bow shock emission increases from 550 km to 650 km, and the aspect angle decreases from  $61^\circ$  to  $54^\circ$ .

### 2.4.2 Expected Radiometrics (CHARM 1.3 Predictions)

The propellant in the Antares is a modified double-base composition, basically nitroglycerin and nitrocellulose, which has been enhanced with other additives including 7.5% ammonium perchlorate oxidizer and 20.6% powdered aluminum. The Star 27 rocket motor propellant is a composite with a composition of 72% ammonium perchlorate oxidizer and 16% powdered aluminum, with a small amount of hydrocarbon binder. The combustion products for both rocket motors are  $\text{Al}_2\text{O}_3$  particles,  $\text{H}_2\text{O}$ ,  $\text{CO}$ ,  $\text{CO}_2$ , and other gases. The temperature inside the rocket motor chamber is typically 3200 K, which is hot enough to melt the  $\text{Al}_2\text{O}_3$  (melting point = 2320 K) but not hot enough to vaporize it (boiling point = approximately 3700 K). As the exhaust exits the rocket nozzle it cools, and the  $\text{Al}_2\text{O}_3$  begins to solidify. The temperature of the exhaust decreases further as it moves away from the rocket [14].

In the ultraviolet, the emission from the plume central regions of these rocket motors is expected to be dominated by thermal emission from hot particles of  $\text{Al}_2\text{O}_3$ . In a simplified model, the temperature of the  $\text{Al}_2\text{O}_3$  particles is taken to be constant at the solidification temperature of 2320 K because the latent heat of fusion causes the temperature of the particles to pause momentarily at this point as they cool. In the outer region, other thermophysical processes can produce emission bands arising from exhaust gases or atmospheric constituents, and these will contribute to the spectrum.

Even in the simplified model, in which the  $\text{Al}_2\text{O}_3$  particles in the plume are assumed to be at a uniform temperature of 2320 K, the plume emission is different from a 2320 K blackbody for two primary reasons. First, the plume consists of a rather transparent cloud of particles, and the total emission from the cloud is substantially less than would be the case from a solid object the same size as the plume. Second, the  $\text{Al}_2\text{O}_3$  particles are typically a few microns in size and are inefficient emitters of visible and longer wavelengths. The effective emissivity for 2.3-micrometer ( $\mu\text{m}$ )  $\text{Al}_2\text{O}_3$  particles (as a function of wavelength) resulting from this effect is shown in Fig. 10.

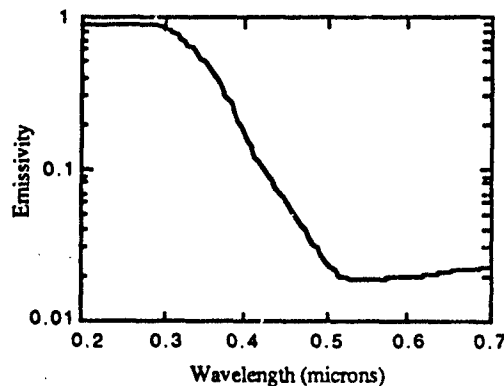


Fig. 10 - Effective emissivity of a 2.3- $\mu\text{m}$  alumina particle

Initially, a modified form of the code CHARM 1.2\* was used to model the response of the UVPI to the Antares and Star 27 rocket plumes to determine the relative risk of observation and to estimate the signal-to-noise ratio of each plume in the tracker camera [10]. As a result of this modeling, it was decided that the Antares plume would be the primary target because its stronger signal would provide the better chance of a successful observation.

\* The CHARM codes, CHARM 1.2 and CHARM 1.3 (a later version of the same code), are primarily infrared simulation codes and must be modified to extend their predictions to the ultraviolet.

Each rocket's emission was also modeled for all four filter bandpasses of the UVPI's plume camera. This information was used to determine the desired sequence of the plume-camera filters for the Antares and Star 27 burns. Filter PC-4 was selected to begin the observation of the Antares plume because its wider bandpass would provide the brightest signature. Filter PC-4 responds to wavelengths longer than 300 nm, which pass through the ozone layer, and its primary purpose would be to obtain a few seconds of data for comparison with that from ground-based and airborne sensors. Filters PC-1 and PC-3 observe wavelengths that do not pass through the ozone layer and, thus, cannot be observed from the ground. Use of these filters would provide unique data. Since the UVPI plume camera filters must be cycled in sequence, a few seconds of data using filter PC-2 would be collected to complete the data set, even though PC-2 passes wavelengths that can be observed from the ground. Therefore, the filter selection for the Antares burn should start with a few seconds of using filter PC-4, then switch to PC-3 for several seconds, then switch to PC-2 for a brief data collection opportunity, and end in PC-1 for several seconds of data prior to, and including, the burnout.

The filter sequence for the Star 27 burn should emphasize the use of filters PC-1 and PC-3 that pass wavelengths that are invisible from the ground. Therefore, the Star 27 observation should start with filter PC-1 for several seconds, then collect data for a few seconds using PC-2, and then switch to PC-3 and use that filter for the remainder of the Star 27 burn. This will allow collection of data from the burnout of the Star 27 in a band that is invisible to ground-based and airborne sensors.

A subsequent calculation of the radiometrics, (assuming a 500-km range) using CHARM 1.3 (a presumably more accurate code than CHARM 1.2) yielded the results shown in Tables 2 and 3 for the expected intensities of each stage and filter combination in units of W/sr [15]. [Conversion of W/sr to photoevents/frame was done by using the conversion factors for each filter shown in Table 17].

Table 2 - Expected Intensities for Antares Stage

Filter	W/sr	Photoevents/Frame
PC-1	66.7	70.1
PC-2	45.0	75.2
PC-3	17.4	13.9
PC-4	226.6	1,302.0
TC	1200.0	37,151.0

Table 3 - Expected Intensities for Star 27 Stage

Filter	W/sr	Photoevents/Frame
PC-1	11.4	11.9
PC-2	7.5	12.5
PC-3	2.9	2.3
PC-4	36.2	208.0
TC	181.3	5,613.0

The expected size and shape of the plumes, as predicted by CHARM 1.3, is given in more detail in Section 5.

### 3.0 STRYPI OBSERVATION

The Strypi XI vehicle was launched from Pad 1 at the Kauai Test Facility (KTF), which is located on the U.S. Navy Pacific Missile Range Facility (PMRF), Barking Sands, Kauai, Hawaii, at 14:18:35 GMT on 18 February 1991.

The weather at the time of launch was generally clear with scattered clouds. Neither LACE nor Strypi was illuminated by the sun or the moon at any time during the observation.

Figure 11 shows that the second-stage Antares rocket and the third-stage Star 27 rocket followed a southbound trajectory approximately parallel with the LACE satellite's descending pass over Hawaii. The sequence of events that occurred during the Strypi XI flight and the corresponding UVPI frame numbers are given in Table 4. The events refer to Fig. 9. A description of the nominal Strypi XI events is presented in Section 2.0.

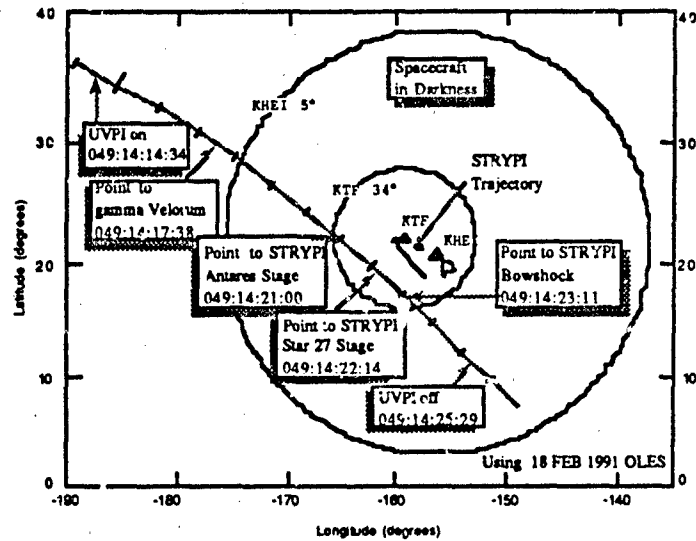


Fig. 11 - LACE ground track for orbit 5582 - 18 February 1991

Table 4 - Strypi Sequence of Events\*

Event	Frame	GMT	TALO (s)	Description
1	5700	14:18:35.0	0.0	Liftoff—castor & recruits ignition
2	5766	14:18:37.2	2.2	Recruits burnout
3	5790	14:18:38.3	3.0	Jettison recruits
4	6959	14:19:17.0	42.0	Castor burns out
5	8101	14:19:55.1	80.1	Jettison castor
6	8131	14:19:56.1	81.1	Eject nose cone
7	9000	14:20:25.1	110.1	Periscopes up
8	10352	14:21:10.2	155.2	Antares ignition
9	11425	14:21:46.0	191.0	Antares burns out
10	12147	14:22:10.1	215.1	Jettison antares
10a	12525	14:22:22.7	227.7	Antares bumps Star 27
11	12867	14:22:34.1	239.1	Star 27 ignition
12	13994	14:23:11.7	276.7	Star 27 burnout
13	14159	14:23:17.2	282.2	Eject periscopes
14	14183	14:23:18.0	283.0	Begin bow shock

\*The time of events was obtained from Sandia National Laboratories and is based on separation monitors, SANDAC monitors, and fire module capacitor voltages.

### 3.1 Strypi Performance

Strypi was launched on time and had close to nominal performance until the separation of the third stage resulted in some problems. This stage contained the Star 27 motor. Figure 12 shows the actual velocity and altitude profiles of Strypi as determined from onboard telemetry. Detailed tables of the Strypi trajectory parameters as a function of time are given in Appendix G. The first stage was less than  $1^\circ$  off in azimuth at burnout, which was closer to the planned nominal trajectory than to any of the preflight-defined dispersed trajectories. To compensate for first-stage trajectory anomalies, the Antares ignition time was changed from the nominal T+152 s to T+155.1 s. The onboard active guidance and control system of the second stage brought Strypi within about 2.5 km of the nominal target point for ignition of the third stage. However, it is believed that the Antares second-stage casing bumped the Star 27 stage just prior to the Star 27 ignition. This caused a third-stage coning with about a  $10^\circ$  half-angle during the Star 27 burn and caused a lofting of the trajectory. Star 27 burnout occurred at T+276.7 seconds, when Strypi was at an altitude of 112.3 km with a velocity of 5.04 km/s. The nominal values for Star 27 burnout are T+280 s, 99.4 km, and 5.09 km/s. The difference in altitude is important; it is believed to be the primary cause for failure to detect the bow shock emission with UVPI.

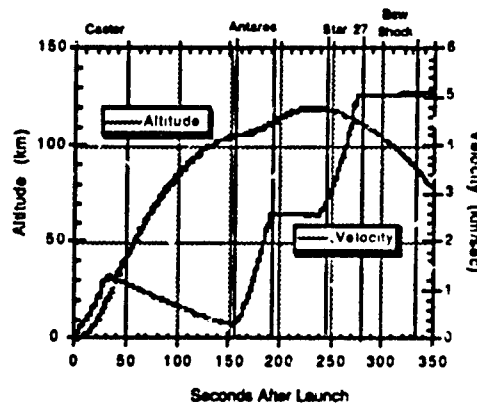


Fig. 12 - Strypi altitude and velocity profiles

The angle-of-attack and rocket motor chamber pressure profiles for the Antares and Star 27 burns, as determined from telemetry, are shown in Figs. 13 and 14, respectively.

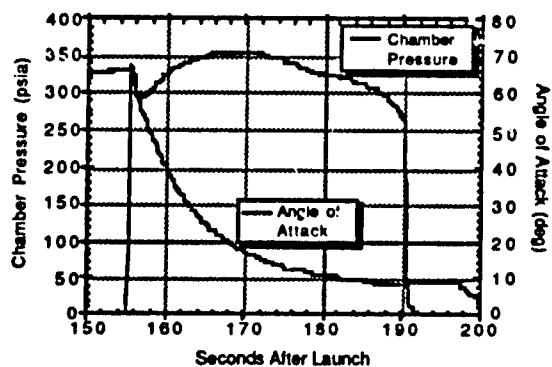


Fig. 13 - Antares chamber pressure and angle of attack

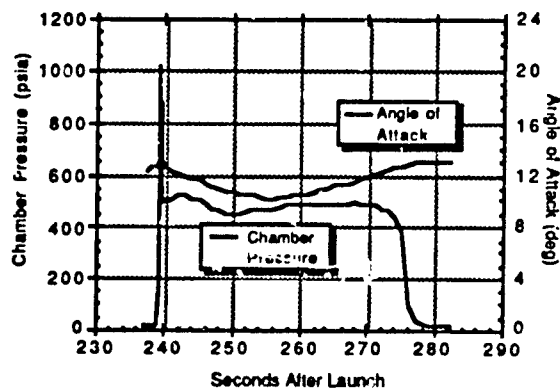


Fig. 14 - Star 27 chamber pressure and angle of attack

### 3.2 UVPI Operations, Actual Scenario

The actual UVPI events, delayed execution and real-time commands along with the corresponding time and UVPI frame numbers, are shown in Table 5. Boldface type denotes UVPI delayed execution commands, plain type denotes operator commands and ground events, and italic type denotes outside events beyond UVPI control (TALO is time after liftoff). The main events of the encounter are discussed in Section 2.2.2, Planned Strypi Trajectory.

Table 5 - Strypi Encounter List of Commands

Time (GMT)	TALO (s)	Frame	UVPI Delayed-Execution Commands	UVPI Real-Time Commands
14:14:50	-225.0		Turn UVPI on	
14:15:25	-190.0		Turn relays K1, K2 on	
14:15:45	-170.0		Set tracker max gain to 10	
14:15:50	-165.0		Initialize tracker	
14:16:00	-155.0		Set filter wheel position to 4	
14:16:08	-147.0		Load MASS AND INTENSITY run block	
14:16:39	-116.0		Turn off AGC, set track and plume gains to 0	
14:16:44	-111.0		Set extrapolate timeout to 5 s.	
14:16:45	-110.0		Set frame ratio to 1:15 (Plume: Tracker)	
14:16:51	-104.0		Open door to 51.24°	
14:17:11	-84.0		Turn on AGC	
14:17:12	-83.0	3212	Turn on tape recorder, tape unit A	
14:17:13	-82.0	3242	Swing gimbal to left (Az=-5.5°, El=+4.3°)	
14:17:18	-77.0	3392	Swing gimbal to right (Az=+5.0°, El=+1.4°)	
14:17:23	-72.0	3541	Turn off tape recorder	
14:17:24	-71.0	3571	Point to star (gamma Velorum) using FIXED STAR pointing function	
14:17:25	-70.0	3601	Set lost track function to FIXED STAR pointing function	Upload FIXED STAR pointing function (pred)
14:17:38	-57.0	3991		Point using FIXED STAR function (pred)
14:17:45	-50.0	4201	<i>KHEI AOS 5°</i>	
14:17:46	-49.0	4231		Open door one coarse step
14:17:55	-40.0	4501		Upload SCAN STAR function
14:18:08	-27.0	4890		Point using SCAN STAR function
14:18:15	-20.0	5100		Upload ANTARES function
14:18:20	-15.0	5250	<<<< GO/NO-GO Decision >>>>	
14:18:24	-11.0	5370		Upload ROCKET function
14:18:35	0.0	5700	<<<<<<<<<<STRYPI LAUNCH>>>>>>>>>>>>>>	Point using FIXED STAR function (pred)
14:18:52	17.0	6209		Upload FIXED STAR pointing function (calc)
14:19:04	29.0	6569		Point using FIXED STAR function (calc)
14:19:11	36.0	6779		Acquire using FIXED STAR function
14:19:17	42.0	6959	<i>Strypi Castor Burnout</i>	Turn zoom on
14:19:21	46.0	7078		Plume: Tracker frame ratio 8:2
14:19:29	54.0	7318		Filter wheel position 3
14:19:47	72.0	7858		Filter wheel position 2

Table 5 - Strypi Encounter List of Commands (Cont'd)

Time (GMT)	TALO (s)	Frame	UVPI Delayed-Execution Commands	UVPI Real-Time Commands
14:19:57	82.0	8158	<i>Update of Antares ignition time (±4 s)</i>	
14:20:02	87.0	8307		Filter wheel position 1
14:20:26	111.0	9027	Set filter wheel position to 4	
14:20:34	119.0	9267	Turn off zoom	
14:20:35	120.0	9297	Set frame ratio to 2:8 (Plume:Tracker)	
14:20:36	121.0	9327	Point to gimbal position 0,0	
14:20:37	122.0	9357	Open door fully for Strypi viewing	
14:20:38	123.0	9387	Initialize tracker	
14:20:42	127.0	9506		Upload ANTARES function
14:20:47	132.0	9656	Load MASS AND INTENSITY run block	
14:20:57	142.0	9956	Point to Strypi using ANTARES function	
14:20:58	143.0	9986	Set lost track function to ANTARES function	
14:21:00	145.0	10046		Acquire using ANTARES function
14:21:02	147.0	10106	Turn on tape recorder, tape unit A	
14:21:10	155.2	10352	<i>Strypi Antares Ignition</i>	
14:21:14	159.0	10466		Turn zoom on, etc.
14:21:26	171.0	10825		Filter wheel position 2
14:21:35	180.0	11095		Filter wheel position 1
14:21:46	191.0	11425	<i>Strypi Antares Burnout</i>	
14:21:49	194.0	11515	Turn off zoom	
14:21:50	195.0	11545	Set frame ratio to 2:8 (Plume:Tracker)	
14:21:56	201.0	11725	Turn off tape recorder	
14:22:03	208.0	11934		Upload ROCKET function
14:22:14	219.0	12264		Point using ROCKET function
14:22:24	229.0	12564	Turn on tape recorder, tape unit A	
14:22:28	233.0	12684	Point to Strypi using ROCKET function	
14:22:29	234.0	12714	Set lost track function to ROCKET function	Acquire using ROCKET function
14:22:30	235.0	12744		
14:22:34	239.1	12867	<i>Strypi Star 27 Ignition</i>	
14:22:36	241.0	12924		Turn zoom on
14:22:41	246.0	13073		Plume:Tracker frame ratio 8:2
14:22:48	253.0	13283		Filter wheel position 2
14:22:56	261.0	13523		Filter wheel position 3
14:23:03	268.0	13733		Upload BOW SHOCK function
14:23:10	275.0	13943	Set extrapolate timeout to 10 s.	
14:23:10	275.0	13943	Set tracker max gain to 11	
14:23:11	276.0	13973		Point using BOW SHOCK function
14:23:12	276.7	13994	<i>Strypi Star 27 Burnout</i>	
14:23:18	283.0	14183	<i>Strypi Bow Shock Start</i>	
14:23:22	287.0	14302		Turn zoom on
14:23:26	291.0	14422		Turn zoom off



Table 5 - Strypi Encounter List of Commands (Cont'd)

Time (GMT)	TALO (s)	Frame	UVPI Delayed-Execution Commands	UVPI Real-Time Commands
14:23:34	299.0	14662		Plume:Tracker frame ratio 2:8
14:23:40	305.0	14842		GSIP froze
14:23:43	308.0	14932		Filter wheel position 4
14:23:48	313.0	15082		Activate joystick
14:24:13	338.0	15831	<i>Strypi LOS (40 km)</i>	
14:24:23	348.0	16131	Turn off AGC	
14:24:24	349.0	16161	Set track and plume MCP gains to 0	
14:24:24	349.0	16161	Park gimbal mirror	
14:24:24	349.0	16161	Turn off tape recorder	
14:24:25	350.0	16191	Close door fully	
14:24:55	380.0	17090	Start Dark Field Data Test	
14:24:57	382.0	17150	Turn on tape recorder, tape unit A	
14:25:18	403.0	17780	Turn off tape recorder	
14:25:29	414.0			Command UVPI shutdown
14:27:26	531.0		Command UVPI shutdown	
14:27:26	531.0		<i>KHEI LOS 5°</i>	

Figure 15 correlates the telemetry frame numbers with the time after liftoff. The linear equation for this is given as:

$$\text{TALO} = (\text{FRAME} - 5700.1) / 29.975$$

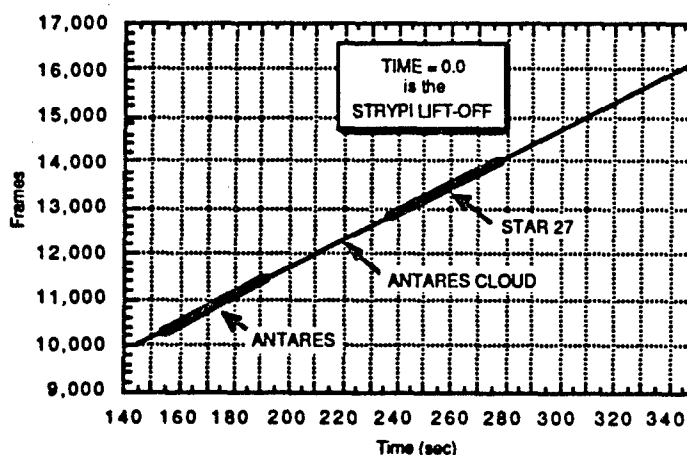


Fig. 15 - Telemetry frame vs time after liftoff

### 3.2.1 UVPI Pre-Encounter Activities

When Maui TGS acquired the telemetry signal at 14:17:19 GMT, UVPI's status was nominal. The target star, gamma Velorum, appeared to be in a good position, so UVPI was declared ready for Strypi launch at 14:18:03, 17 s before the required time. The target star was then used to compute the yaw attitude of the spacecraft. The computed yaw appeared to give better results than the predicted yaw, so the computed yaw value was selected for subsequent use.

After yaw determination and verification were completed, gamma Velorum was acquired. Calibration data were then collected for this star in all four plume-camera filter positions.

### 3.2.2 Antares Plume Observation

At 14:18:35.0 GMT, Strypi was launched, and the launch time was announced and confirmed.

At 14:20:10, the revised Antares ignition time (155.1 s) and Strypi trajectory type (nominal) were announced, verified, and incorporated into the real-time software. The trajectory was actually dispersed slightly left of nominal, but a nominal trajectory was called in accordance with guidelines set before the mission.

About 23 s prior to Antares ignition, the new Antares pointing function was successfully transmitted. UVPI started scanning along the nominal trajectory with a  $0.65^\circ$  radius circle at 14:20:57. The acquire command was sent about 10 s prior to Antares ignition, which occurred at about 14:21:11.

About 1 s after Antares ignition, part of the rocket plume was seen on the top edge of the tracker camera screen on the left side. The plume central region was just out of view. The tracker immediately centered and locked onto the Antares plume at 14:21:14, about 2 s after the initial sighting of the plume. Immediately after acquisition, the command was sent to initiate the sequence to select zoom image transmission rate, change the plume-to-tracker image ratio to 8:2, and change to filter PC-3. Filter PC-3 was in place at 14:21:19, about 2 s later than planned. During the change of the filter wheel from PC-4 to PC-3, the tracker momentarily lost lock for about 2 s but then reacquired and kept steady lock for the remainder of the burn. Filter PC-2 was commanded and in place at 14:21:31, about 2 s later than planned, and the switch to filter PC-1 occurred at 14:21:40, about 6 s late. The tracker camera gain was 7 during most of the Antares burn but changed to a value of 6 about 5 s prior to burnout.

After Antares burnout, which occurred at 14:21:46, zoom image transmission rate was turned off by a delayed execution command. At that time, a large, persistent plume trail was seen by the tracker camera. The tracker acquired this trail and locked back along the trail to near the Antares ignition point. It held lock there at a tracker camera gain of 10 for about 30 s until it was commanded by the ground station, at 14:22:18, to point back to Strypi in readiness for the Star 27 burn.

### 3.2.3 Star 27 Plume Observation

At 14:22:29 GMT, 5 s prior to Star 27 ignition, the acquire command was sent. Star 27 ignition occurred at 14:22:34, and the rocket plume appeared a second later close above the radar cursor on the tracker-camera screen. Within a second, the tracker locked onto the Star 27 plume. UVPI was commanded to zoom image transmission rate, and the plume-to-tracker image ratio was changed to 8:2. The planned filter sequence was commanded. Filter PC-2 took effect at 14:22:53, about 2 s late, and filter PC-3 was in place at 14:23:01, about 2 s early. The tracker camera gain was limited to a maximum of 10 through most of the Star 27 burn until the maximum was raised to 11 near the end.

The burnout of Star 27 occurred at 14:23:12, about 3 s earlier than expected. There is a 3-s trailoff included in the burn time, so the burnout actually started at the time observed.

### 3.2.4 Bow Shock Observation

Just preceding Star 27 burnout, a dim trail was seen by the tracker camera for a few frames. An image of this dim trail can be seen at the end of Section 8. The commands to point with the bow shock pointing function, turn zoom image transmission rate off, switch to a plume-to-tracker image ratio of 2:8, switch to filter PC-4, and activate the joystick were given at this time.

When zoom image transmission rate was turned off, nothing identifiable was seen by the tracker camera; the radar cursor indicated that Strypi was out of the field of view off the top edge of the screen. At 14:23:40, about 8 s before the command to activate the joystick was sent, a ground station computer failed and had to be restarted. Although the ground station was still able to receive camera images and send commands by using the control keyboard, the UVPI data screen was not being updated; also, joystick commands could not be sent. By the time the computer was restarted, the bow shock period was over.

One reason that UVPI was unable to observe the bow shock is that Strypi had deviated several kilometers from its nominal trajectory. By the end of the Star 27 burn, its altitude was too high for the bow shock emission to start. By the time the bow shock emission started, at 100-km altitude, UVPI had automatically reverted to pointing to the nominal trajectory, which put Strypi out of the tracker camera's field of view.

The command to turn off UVPI was sent on time at 14:26:13 GMT.

### 3.3 Encounter Geometry

The range and aspect angles between UVPI and Strypi (Fig. 16) were calculated by using the position and attitude of Strypi as determined from the processed Strypi telemetry data. The aspect angle is defined as the angle between the line-of-sight (LOS) vector from UVPI to the target point and the longitudinal axis of the rocket. Zero degree aspect angle means UVPI is looking at the rocket's nose, and 180° means looking up the nozzle. The oscillations in aspect angle, starting just prior to the Star 27 ignition, are due to the coning of Strypi.

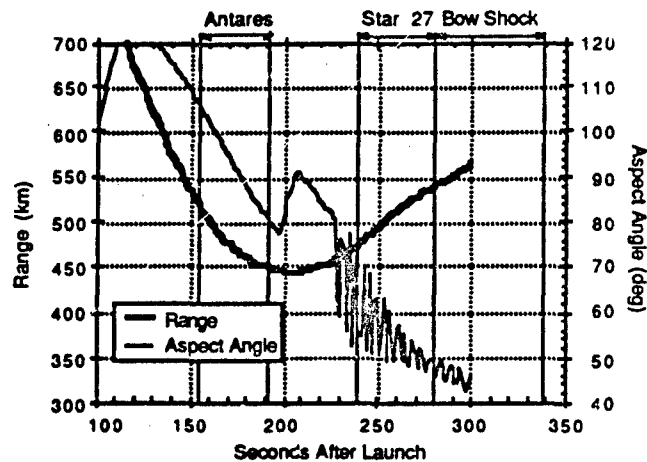


Fig. 16 - Strypi/UVPI encounter geometry

The range for the Antares burn was from about 512 km at ignition to about 450 km at burnout. The range for the Star 27 burn was from about 475 km at ignition to about 540 km at burnout. The minimum range, 446 km, occurred during the coast period shortly after Antares burnout. This was the result of a compromise in the encounter design to obtain the best possible geometry for both rocket burns but with more emphasis on the Antares burn.

Figure 17 shows the percent vignetting of the UVPI image and the orientation angle of the rocket body in the tracker camera's field of view. At Antares ignition, there was only 2% vignetting that decreased to 0% by the time UVPI had locked onto it. It remained at 0% for the remainder of the burn. The vignetting stayed at 0% for the first 12 s of the Star 27 burn then increased to a maximum of about 5.2% by burnout.

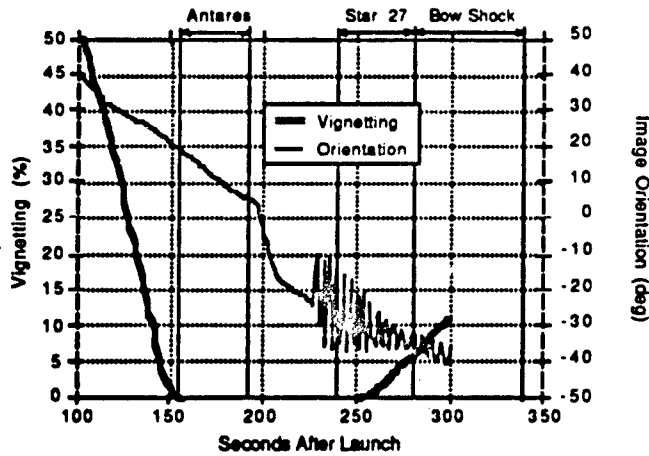


Fig. 17 - Strypi/UVPI image factors

The orientation angle shown in Fig. 17 is used to assist with the radiometric analysis of the plume. This angle is defined as the angle between the tracker camera's horizontal axis and the projection of the rocket body onto the focal plane of the tracker camera, with counter-clockwise positive.

3.4 Pointing and Tracking Overview

3.4.1 Mode Sequence

The tracker was commanded to the Mass and Intensity Centroid track mode throughout the Strypi XI observation. Figure 18 shows the timing of the various mission modes during the observations. The Antares rocket burned for 45 s. The acquisition sequence moved the gimbals in the POINT mode until the target was in the field of view and then transitioned to the ACQUIRE mode. When the tracker locked onto the target, the mission mode transitioned to the TRACK mode. The initial acquisition of the Antares rocket lost track because the rocket plume was at the edge of the tracker camera's field of view. This resulted in the tracker jumping between the TRACK and the ACQUIRE modes. During the Antares burn, the tracker momentarily lost track because of changes in the size and intensity of the rocket plume. After the Antares rocket burned out, the tracker locked onto the trailing cloud left behind the Antares rocket. At the start of the Star 27 burn, the acquisition sequence was repeated by sequencing through the POINT, ACQUIRE, and TRACK mission modes. The Star 27 rocket burned for 41 s.

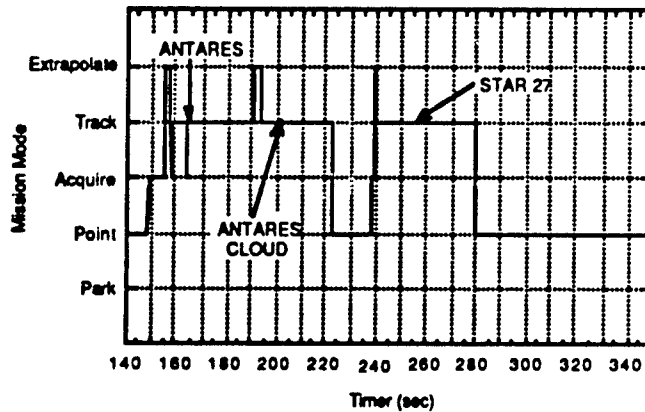


Fig. 18 - Mission mode vs time after launch

### 3.4.2 Gimbal Angles

Figures 19 and 20 show the azimuth and elevation gimbal angles, respectively, as a function of time. The LACE satellite's ground track was descending in a southeast direction and paralleled the Antares and Star 27 rocket burns. The Strypi XI trajectory was to the left of the spacecraft, thereby resulting in a slightly positive elevation gimbal angle. Initially, the Antares was in front of the spacecraft, as shown by a negative azimuth gimbal angle. By the end of the Star 27 burn, the spacecraft was in front of the Star 27 rocket, thereby resulting in a positive azimuth gimbal angle. The elevation gimbal angle remained between  $13^\circ$  and  $15^\circ$  throughout the encounter, while the azimuth gimbal angle moved from  $-20^\circ$  to  $+20^\circ$ . The azimuth and elevation gimbal rates are calculated to be  $2.6^\circ/\text{s}$  and  $0.1^\circ/\text{s}$ , respectively, which are well within specifications. The dashed lines in these plots represent the SC-1 computer-commanded gimbal angles. At the beginning of the encounter, the SC-1 commanded the gimbal angles while the mission mode was set to the POINT mode or the ACQUIRE mode. This continued until the tracker locked onto the target image. At that time, the mission mode was set to TRACK. Note that the SC-1-commanded gimbal angles remain fixed to the last commanded value. There was a noticeable transient as the tracker brought the tracking errors to zero. This transient response is discussed in Appendix D, Section D.1.0 where it is shown to be consistent with earlier laboratory tests and other encounters. When the tracker loses the target, the SC-1 extrapolates the previous gimbal angles according to their previous gimbal rates. The gimbal motion then exhibits a transient that is a result of the extrapolation function implementation.

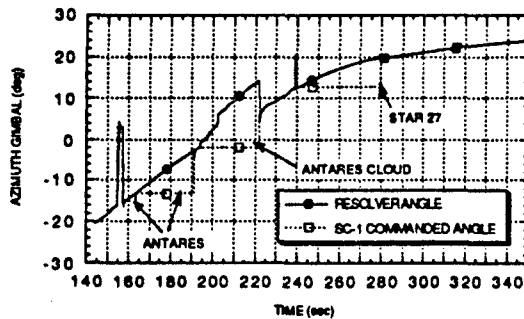


Fig. 19 - Azimuth gimbal angles vs time after launch

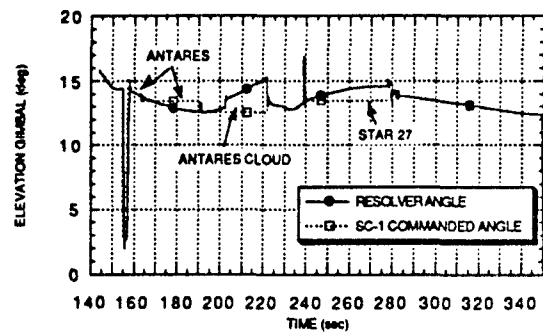


Fig. 20 - Elevation gimbal angles vs time after launch

### 3.5 Tracker Performance Summary

Table 6 shows the seven data intervals for which the performance of the tracker was analyzed. These intervals do not include initial acquisition of the Antares or Star 27, Antares momentary loss of track, or the Antares cloud. Rather, these intervals are representative of the nominal tracking while collecting plume signatures in the plume camera.

Table 6 - Antares and Star 27 Tracking Analysis Intervals

Data Interval	Telemetry Frames	TALO (s)	Rocket Stage
1	10,536 - 10,549	161.3 - 161.8	Antares
2	10,656 - 10,913	165.3 - 173.9	Antares
3	10,963 - 11,190	175.6 - 183.2	Antares
4	11,286 - 11,413	186.4 - 190.6	Antares
5	13,142 - 13,239	248.3 - 251.5	Star 27
6	13,489 - 13,599	259.8 - 263.5	Star 27
7	13,677 - 13,928	266.1 - 274.5	Star 27

### 3.5.1 Tracking Jitter During Antares Burn

Data intervals 1 through 4 from Table 6 were chosen for analysis of tracker performance during the Antares burn. Appendix D.2.1 provides a detailed analysis of the tracking errors during these intervals. Table 7 summarizes the statistics associated with tracking errors for each of these intervals. The standard deviation is the RMS value about the mean. Hence, the x RMS tracking error varies between 7 and 10 microradians ( $\mu\text{rad}$ ) while the y RMS tracking error varies between 6 and 13  $\mu\text{rad}$ . These jitter values are within the tracker specification of 15  $\mu\text{rad}$  RMS.

Table 7 - Tracking Error Statistics During Antares Burn

Interval	Telemetry Frames	Parameter	Tracking Error X ( $\mu\text{rad}$ )	Tracking Error Y ( $\mu\text{rad}$ )
1	10,536 to 10,549	Minimum	-20.6	-58.1
		Maximum	5.6	-35.8
		Mean	-3.4	-47.6
		Std deviation*	7.2	6.0
		Points	14	14
2	10,656 to 10,913	Minimum	-43.1	-80.5
		Maximum	18.8	-35.8
		Mean	-0.4	-55.2
		Std deviation*	9.1	9.7
		Points	257	257
3	10,963 to 11,190	Minimum	-24.4	-71.5
		Maximum	31.9	-35.8
		Mean	3.3	-48.2
		Std deviation*	10.3	7.2
		Points	228	228
4	11,286 to 11,413	Minimum	-28.1	-143
		Maximum	30	-40.2
		Mean	-2.0	-62.1
		Std deviation*	7.1	12.9
		Points	130	130

\*RMS Jitter

### 3.5.2 Tracking Jitter During Star 27 Burn

Intervals 5, 6, and 7 were chosen for analysis of tracker performance during the Star 27 burn. Appendix D.2.2 provides a detailed analysis of the tracking errors during these intervals. Table 8 summarizes the statistics associated with tracking errors for each of these intervals. Note that the x RMS tracking error varies between 16 and 187  $\mu\text{rad}$  and the y RMS tracking error varies between 18 and 167  $\mu\text{rad}$ . These jitter values are larger than the tracker specification of 15  $\mu\text{rad}$  RMS. Hence, the tracker did not track the Star 27 rocket within the design specifications, and the operation resulted in larger-than-expected jitter in the plume camera. The poor tracking results are primarily attributed to the weak signal from the Star 27. See Appendix D for details.

### 3.5.3 Comparison with Previous Encounters

A comparison with tracking errors for previous encounters, Nihka and Starbird, is given in Table 9.

Table 8 - Tracking Error Statistics During Star 27 Burn

Interval	Telemetry Frames	Parameter	Tracking Error X ( $\mu$ rad)	Tracking Error Y ( $\mu$ rad)
5	13,142 to 13,239	Minimum	-556.9	-370.94
		Maximum	103.1	169.9
		Mean	-19.9	-50.8
		Std deviation*	83.4	61.0
		Points	105	105
6	13,489 to 13,599	Minimum	-43.1	-93.8
		Maximum	37.5	-4.4
		Mean	-2.9	-45.5
		Std deviation*	15.9	17.9
		Points	112	112
7	13,677 to 13,928	Minimum	-1455	-670.4
		Maximum	1241.3	1707.1
		Mean	-1.0	-54.3
		Std deviation*	187.3	166.6
		Points	252	252

\*RMS Jitter

Table 9 - Tracking Error Comparison

Rocket Encounter	Mean Tracking Error		RMS Jitter	
	X ( $\mu$ rad)	Y ( $\mu$ rad)	X ( $\mu$ rad)	Y ( $\mu$ rad)
Antares	-3 to 3	-47 to -62	7 to 10	6 to 13
Star 27	-1 to -19	-45 to -54	16 to 187	18 to 167
Nihka	2	-67	13	10
Starbird Third Stage	-15	67	13	7
Starbird Fourth Stage	-15	67	13	7

This table shows that the tracking jitter has remained consistent and within specifications for the Nihka, Starbird, and Antares observations. These exhibited approximately 100% peak video value. The one exception is the tracking of the Star 27 rocket. It did not track within jitter specifications, less than 15  $\mu$ rad RMS, because the tracker camera gain level was held to a low limit. This resulted in a low percentage of peak video value in the presence of a weak plume signature and yielded poor tracking stability.

#### 4.0 PLUME IMAGES

In this section the observed plume image data are presented. The data intervals used in this report are defined in 4.1, and a discussion of the calibration procedure is presented in 4.2. Examples of single plume camera images are given in 4.3, and the averages of images over the defined data intervals for the plume and tracker cameras are presented in 4.4 and 4.5, respectively. Subsection 4.6 discusses the error in the radiometric observations. The concluding subsection, 4.7, discusses the noise-equivalent radiance for the UVPI.

##### 4.1 Definition of Data Intervals

###### 4.1.1 Camera Parameters

Table 10 summarizes the Antares and Star 27 data intervals used in this report, along with the number of plume-camera images and tracker-camera images analyzed in each interval. Table 11

reports important calibration parameters associated with the intervals. The UVPI-Strypi range is used to determine source radiant intensity, as discussed in 4.2. The image angle variation associated with a sequence of frames is a measure of the variation in plume image axis orientation with respect to TV lines in the image display. This parameter is relevant to the spatial analysis presented in Section 5.0. The data intervals listed in Table 10 are identical to those used in the UVPI tracking analysis and listed in Table 6.

Table 10 - Definitions of Data Intervals

Data Interval	Strypi Stage	GMT	TALO (s)	Plume Camera Filter	Telemetry Frame Range	No. of Plume Images	No. of Tracker Images
1	Antares	14:21:16.33 - 14:21:16.76	61.3 - 151.8	PC-4	10536- 10549	12	2
2	Antares	14:21:20.33 - 14:21:28.91	165.3 - 173.9	PC-3	10656- 10913	207	50
3	Antares	14:21:30.58 - 14:21:38.14	175.6 - 183.2	PC-2	10963- 11190	157	40
4	Antares	14:21:41.34 - 14:21:45.59	186.4 - 190.6	PC-1	11286- 11413	104	26
5	Star 27	14:22:43.27 - 14:22:46.51	248.3 - 251.5	PC-1	13142- 13239	44	31
6	Star 27	14:22:54.84 - 14:22:58.52	259.8 - 263.5	PC-2	13489- 13599	89	23
7	Star 27	14:23:01.12 - 14:23:09.49	266.1 - 274.5	PC-3	13677- 13928	171	41

Table 11 - Parameters Associated with Data Intervals

Data Interval	Strypi Stage	Plume Camera Filter	Bandpass (nm)	Plume-to-Tracker Ratio	UVPI-Strypi Range (km)	Image Angle Variation (deg)
1	Antares	PC-4	235-350	2:8	496	0
2	Antares	PC-3	195-295	8:2	477	3.4
3	Antares	PC-2	300-320	8:2	462	2.9
4	Antares	PC-1	220-320	8:2	452	0.6
5	Star 27	PC-1	220-320	2:8 & 8:2	495	12.6
6	Star 27	PC-2	300-320	8:2	515	8.6
7	Star 27	PC-3	195-295	8:2	529	6.4

Appendix E provides basic camera parameters pertinent to the radiometric calibration of the data for all frames during which the Antares and Star 27 stages were observed. Parameters provided include time, telemetry frame number, gain level for both cameras, and exposure time for both cameras. Changes in gain levels are indicated along with other comments. The plume camera has a constant  $1/30$ th of a second exposure time for each frame. The tracker camera has an electronic gate that can vary the exposure time to a maximum of  $1/30$ th of a second. Figure 21 shows the camera gain levels for both tracker and plume cameras. Figure 22 shows exposure time for both cameras as a function of telemetry frame number. In these figures, the data intervals are depicted as horizontal, bold, solid lines.

The Antares plume was first observed in the plume camera around frame 10457. Because of gain changes and ensuing transients in the plume camera, data analysis was limited to intervals 1 through 4 of Table 10. Approximately 0.5 s of filter 4 data, 8.6 s of filter 3 data, 6.5 s of filter 2 data,



and 4.3 s of filter 1 data were collected during this time. Analysis of tracker camera data is restricted to these same intervals.

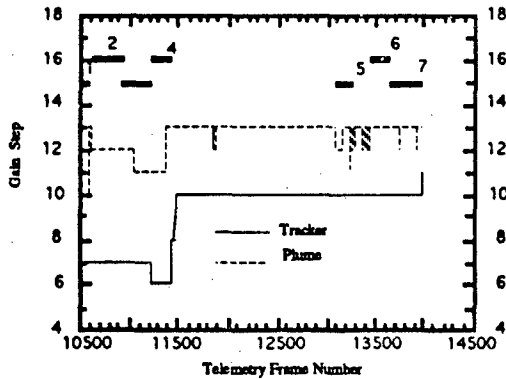


Fig. 21 - Tracker and plume camera gain

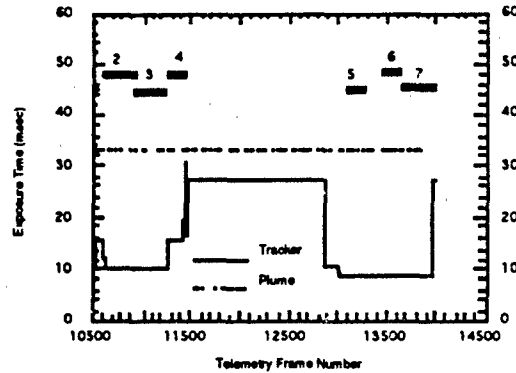


Fig. 22 - Tracker and plume camera exposure times

The Star 27 plume was first observed in the plume camera around frame 12987. Because of gain changes and ensuing transients in the plume camera, analysis of both tracker and plume camera data was limited to intervals 5 through 7 of Table 10. Approximately 7.1 s of filter 3 data, 3.7 s of filter 2 data, and 2.4 s of filter 1 data were collected during this time.

In addition to the Antares and Star 27 plumes, a large cloud trail was observed. The cloud was initially observed in the tracker camera in frames 10438 through 10564, approximate GMT interval 14:21:13.0 through 14:21:17.3. This initial cloud was associated with Antares stage ignition. The cloud was again observed in the tracker camera in frames 11490 through 12344 (approximate time range 14:21:48.1 through 14:22:16.6) after the Antares stage had burned out. The cloud is described in detail in Section 8.

## 4.2 UVPI Data Analysis Methodology

The data analysis procedure for the UVPI cameras can be divided into two stages: the data values reported by the CCD array electronics are converted to photoevent counts, and the photoevent counts must be translated into radiometric quantities. In addition, the point spread function of the individual cameras must be considered when interpreting the data. The following sections deal with each of these in turn.

### 4.2.1 Photoevent Calculation

The raw image data transmitted from the satellite is in the form of arrays of 8-bit binary numbers  $Q_k$  representing the intensity of light falling on the  $k$ th pixel of the CCD. These  $Q_k$  are converted into the number of photoevents  $P_k$  occurring at the corresponding photocathode location during the image frame:

$$P_k = (1/G_g)(Q_k - D_k)/U_k, \quad (1)$$

where

$G_g$  is gain conversion factor for gain step  $g$ , i.e., the value of  $Q_k$  for a single photoevent, assumed to be the same for all pixels  $k$ ;

$D_k$  is the dark value for the  $k$ th pixel; and

$U_k$  is the gain nonuniformity correction factor for the  $k$ th pixel.

The pulse height distribution of the image intensifier will cause noninteger values for  $P_k$ . The conversion of CCD response peaks to integral photoevent counts is possible only on the weakest images, because of the overlap of photoevent images. Hence,  $P_k$  values are treated as continuous variables. The  $G_g$ ,  $D_k$ , and  $U_k$  factors are summarized in Appendix B. An additional processing step, in which a statistical decision threshold is determined for each calibrated image, is discussed in the addendum at the end of this report.

#### 4.2.2 Extraction of Radiometric Quantities

Three levels of data reduction are useful for any radiometric experiment. In the first level, data merely are reduced to instrument readings or counts; in the second level, instrument readings are converted by instrument-specific conversion factors into approximate measures of physical quantities with no assumed spectral model of the phenomenon being measured; and in the third level of reduction, a spectral model of the phenomenon is used to reduce data and present it. In reducing the data for the Strypi, one must begin by understanding the meaning of the instrument readings. The UVPI gives readings in the form of photoevents.

##### 4.2.2.1 Relation of Photoevents to Spectral Radiance

The general expression [16] for the number of photoevents  $P_k$  at pixel  $k$  due to an extended source of spectral radiance  $L(\lambda)$ , with units of, e.g.,  $W/cm^2\text{-}\mu\text{m}\text{-sr}$ , is given by:

$$P_k = (A_c \Omega \tau / hc) \int \lambda Q(\lambda) L(\lambda) d\lambda, \quad (2)$$

where

- $A_c$  is system aperture area,
- $\Omega$  is pixel field of view,
- $\tau$  is exposure time,
- $h$  is Planck's constant,
- $c$  is speed of light, and
- $Q(\lambda)$  is wavelength-dependent photoelectronic conversion efficiency, or net quantum efficiency, of the optics and detector.

The factor  $\lambda/hc$  in Eq. (2) is required to convert  $Q(\lambda)$  to the optical efficiency ordinarily incorporated in the optical transfer equation, or equivalently, to convert the spectral radiance  $L(\lambda)$  to a photon radiance [photons/s- $cm^2\text{-}\mu\text{m}\text{-sr}$ ]. The system aperture area is  $78 \text{ cm}^2$ . The exposure time  $\tau$  is 1/30th second for the plume camera and variable to a maximum of 1/30th second for the tracker camera. The pixel field of view  $\Omega$  is  $12.5 \times 9.8 \mu\text{rad} = 1.22 \times 10^{-10} \text{ sr}$  for the plume camera and  $182 \times 143 \mu\text{rad} = 2.6 \times 10^{-8} \text{ sr}$  for the tracker camera. At the typical range of 500 km, these pixel fields of view correspond to 6.2 by 4.9 m and 91 by 72 m, respectively.

Some information about the spectral distribution function must be known to extract accurate values for the source radiometric parameters. Given a model spectral distribution function  $R(\lambda)$  of some arbitrary amplitude, the photoevent count  $P_k'$  that would be observed from a source with this distribution is

$$P_k' = (A_c \Omega \tau / hc) \int \lambda Q(\lambda) R(\lambda) d\lambda. \quad (3)$$

If we assume that  $L(\lambda)$  and  $R(\lambda)$  are related by a multiplicative constant  $\alpha$  over one of the filter bands, then the estimated spectral radiance within that band can be written as

$$L(\lambda) = \alpha R(\lambda) \quad (4)$$

or, more specifically,

$$L(\lambda) = \left( P_k / P_k' \right) R(\lambda). \quad (5)$$

The second level of data reduction assumes little or no knowledge about the source spectrum, whereas in the third level an approximate model for the spectrum is assumed to exist.

#### 4.2.2.2 Peak Normalized Radiance

The second level of data reduction is to use the instrument and filter acceptance band-specific conversion factors to obtain measures of physical quantities. This process is begun by defining the integral of spectral radiance over the detector passband in terms of  $P_k$ .

$$\int \lambda Q(\lambda) L(\lambda) d\lambda = P_k hc / (A_c \Omega \tau) \quad (6)$$

To define a measure of in-band radiance, the wavelength of peak net quantum efficiency is defined as  $\lambda_m$ , and the integral is normalized over the detector passband to define a peak normalized radiance, in accord with standard practice:

$$L_{pn} = \int \lambda Q(\lambda) L(\lambda) d\lambda / \lambda_m Q(\lambda_m) \quad (7)$$

or, in terms of the data in  $P_k$

$$L_{pn} = (P_k / \tau) (hc / (A_c \Omega \lambda_m Q(\lambda_m))) \quad (8)$$

where the quantity  $hc / A_c \Omega = 2.11 \cdot 10^{-4} J - nm / m^2 - sr$ .

The values of  $\lambda_m$  and  $Q(\lambda_m)$  for each of the filters are given in Table 12.

Table 12 - Camera Filter, Wavelength of Peak Quantum Efficiency, and Peak Quantum Efficiency

Filter	$\lambda_m$ (nm)	$Q(\lambda_m)$	$\lambda_m Q(\lambda_m)$ (nm)
Plume PC-1	270	.00606	1.64
Plume PC-2	305	.00182	.555
Plume PC-3	250	.00284	.710
Plume PC-4	280	.0131	3.67
Tracker	355	.0200	7.10

For the brightest pixel  $P_k$ , the peak normalized radiance measured for each filter is given in Table 13. These values are for the Antares motor.

Table 13 - Photoevents Per Second and Peak Normalized Radiance for the Brightest Pixel in the Plume Camera Filter Bands

Filter	$P_k/\tau$ (photoevents/s)	$L_{pn}$ $\mu\text{W}/\text{sr}\cdot\text{cm}^2$
Plume PC-1	26.3	.517
Plume PC-2	10.6	.377
Plume PC-3	6.79	.188
Plume PC-4	158	.821

The peak normalized spectral radiance is merely an approximate measure of the total radiance in the passband of the filter. It would only give the true radiance if the plume spectrum were a narrow line spectrum peaking at  $\lambda_m$  for each filter. Thus, the peak normalized spectrum is mathematically equivalent to the choice of a model spectral distribution function:  $R(\lambda)$  that is a monochromatic source that peaks at  $\lambda_m$ .

$$R(\lambda) = R_0 \delta(\lambda - \lambda_m). \quad (9)$$

This is, of course, not a good approximation to the spectra of the Strypi plumes seen by UVPI. These spectra are actually broad continuum spectra roughly resembling blackbody spectra. To find any better estimates of spectral radiance in-band and total radiance in-band, there must be a reliable model for the shape of the spectrum of the plume.

#### 4.2.2.3 Formulation and Comparison of a Model Plume Spectrum

The third level of data reduction requires a reliable model of the phenomenon being measured to use as a reference. In the case of Strypi radiometric data, a model spectral shape is needed. Such a spectral shape can be found by considering the physics of UV emission from solid-fuel rocket plumes.

Both the rocket motors for the Antares and the Star 27 contain powdered aluminum in their propellant. This aluminum oxidizes and emerges as an incandescent mist in the rocket exhaust. It is this mist of oxidized aluminum particles that emits much of the UV radiation seen by UVPI in the plume central region. The mist is optically thin, that is, when one sees the plume one is not seeing a solid object but mostly empty space. The plumes are thus nearly transparent. The spectrum produced by the plume central region in the UV is typically that of a nearly transparent cloud of micron-sized  $\text{Al}_2\text{O}_3$  particles at the melting point, 2320 K. This resembles a scaled blackbody curve for wavelengths below 300 nm but is much depressed below a blackbody at longer wavelengths. Because the heat of fusion for alumina is very high, the particles should remain at roughly this temperature throughout the plume as it expands and dims. That is, most of the light in the plume will be from isothermal alumina at 2320 K. This means that most of the bright plume particles will have the same spectrum throughout the detector field of view.

The spectrum that is used to model the brightest parts of the plume [17] is that of a blackbody times an emissivity function  $e_{\text{Al}}(\lambda)$  (Fig. 10). This emissivity curve is basically characteristic of hot alumina particles found in rocket exhaust plumes. The spectral shape compared to a blackbody spectral shape is shown in Fig. 23. (The bandpasses of the tracker camera and the four plume-camera filters are also indicated in Fig. 23).

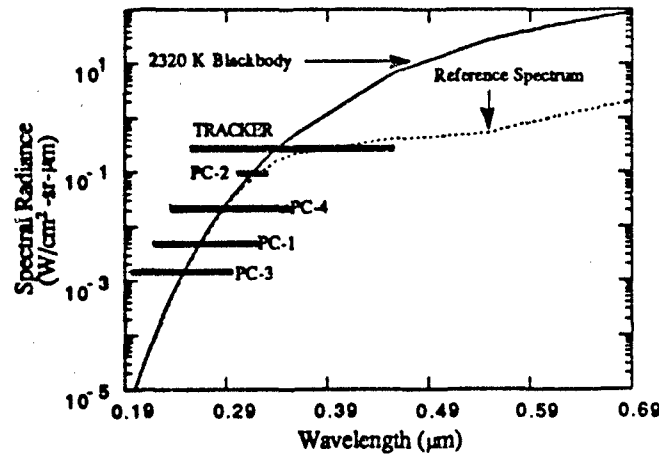


Fig. 23 - Spectral shape function based on reference spectrum model

The normalized spectral shape is fairly generic to all solid-fueled boosters with aluminum-loaded fuel and are termed the reference spectrum  $R(\lambda)$ . Mathematically,

$$R(\lambda) = e_{Al}(\lambda)L_{BB}(\lambda), \quad (10)$$

where  $L_{BB}$  is the 2320 K blackbody spectrum.

The simplest comparison of  $R(\lambda)$  to the actual plume spectrum data is to calculate  $P_k'$  by using Eq. (3):

$$P_k' = (A_c \Omega \tau / hc) \int \lambda Q(\lambda) R(\lambda) d\lambda, \quad (11)$$

then, dividing Eq. (2) by Eq. (11) and using Eq. (4) to get:

$$\frac{P_k}{P_k'} = \frac{\int \lambda Q(\lambda) L(\lambda) d\lambda}{\int \lambda Q(\lambda) R(\lambda) d\lambda} = \frac{\alpha \int \lambda Q(\lambda) R(\lambda) d\lambda}{\int \lambda Q(\lambda) R(\lambda) d\lambda} = \alpha. \quad (12)$$

Therefore,  $\alpha$  can be calculated for each passband and for each pixel by calculating  $P_k'$  and comparing it to the measured value of  $P_k$ . The values of  $P_k/\tau$  and  $P_k'/\tau$  obtained as average for the brightest pixel over several images for the Antares plume in the various filter bands are given in Table 14. The ratio of  $P_k$  to  $P_k'$  are all within a factor of 4. The reference spectrum varies over more than 3 orders of magnitude in the region of the filter bands. This agreement in the value of  $\alpha$  for the four filter bandpasses is quite good. This suggests that the reference spectrum is an acceptable approximation to the actual plume spectrum.

Since the reference spectral shape should be generic to rockets with aluminum-loaded fuel, the Star 27 spectrum should also have this approximate shape because it also contains aluminum. Hence, the reference spectrum can be used for radiometric interpretation of plume data for both rockets.

Table 14 - Photoevents Per Second from Antares Plume and Reference Spectrum Model For Brightest Pixel and Ratios of These Values

Filter	$P_k/\tau$	$P_k'\tau$	$P_k/P_k'$
Plume PC-1	26.3	1864	.0141
Plume PC-2	10.6	1950	.0054
Plume PC-3	6.79	365.7	.0186
Plume PC-4	158	27930.	.0057

#### 4.2.3 Specific Radiometric Values

All the radiometric values to be presented in the data summary can be obtained from the scaled source function  $L(\lambda)$  equal to  $\alpha R(\lambda)$ .

##### 4.2.3.1 Spectral Radiance

The procedure above yields a function  $L(\lambda)$  that describes the amplitude of the spectral shape corresponding to the observed number of photoevents. Describing this function with a single numerical value is difficult because of the extremely rapid variation of the spectral radiances evident in Fig. 23. Despite this rapid variation, single numerical values of plume spectral radiance and spectral radiant intensity can be obtained. These values were obtained by taking  $L(\lambda)$  at a specific characteristic wavelength  $\lambda_c$  for each filter passband. This might have been selected to be the center of each filter passband, but this choice would neglect the shift in the effective response that results from the spectrally varying source. A response centroid wavelength, weighted by the reference spectral function, was defined:

$$\lambda_c \equiv \int \lambda^2 R(\lambda) Q(\lambda) d\lambda / \int \lambda R(\lambda) Q(\lambda) d\lambda. \quad (13)$$

This describes the wavelength of average contribution to the UVPI response for each filter. These centroid wavelengths were computed for the reference spectral shape and are shown in Table 15. In this table, the integrals of Eq. (13) have been evaluated as discrete summations over the range of nonnegligible  $Q(\lambda)$ .

This is simply a means of selecting a nominal, characteristic wavelength for describing the outcome of the fitting of the spectral shape to the instrument measurement as single numerical values. Other procedures might have been used to select a reference wavelength describing the spectral radiance function. One might, for example, have taken the central wavelength for each filter and cited the numerical value of the fit function at those wavelengths. This would yield different values for the nominal spectral radiances without changing the function  $L(\lambda)$  at all. In short, these single numerical values for the rapidly varying spectral radiometric parameters must be treated with caution.

Table 15 - Plume Camera Filter Bandpass Limits, Full-Width-Half-Maximum, Central Wavelength, and Reference Spectrum-Weighted Centroid Wavelength

Camera/Filter	Nominal Bandpass	FWHM Bandpass	Central $\lambda$ (nm)	Centroid $\lambda$ Reference Spectrum
Plume PC-1	220-320	25	270	280
Plume PC-2	300-320	10	305	310
Plume PC-3	195-295	50	250	265
Plume PC-4	235-350	56	280	305
Tracker	255-450	150	355	390

#### 4.2.3.2 Radiance

Once the spectral radiance is known, the spectral integrals can be evaluated to obtain values for the radiance:

$$L_e = \int_{\lambda_i}^{\lambda_v} L(\lambda) d\lambda = L(\lambda_c) \int_{\lambda_i}^{\lambda_v} R(\lambda) d\lambda / R(\lambda_c). \quad (14)$$

The units of  $L_e$  are (power)/(area)(solid angle), or  $W/m^2\text{-sr}$ . The evaluation of these integrals is limited to the nominal bandwidth of the pertinent filter. Note that the integrand of Eq. (14) does not include the response function  $Q(\lambda)$  and, therefore, does not become small outside the filter passbands. The values obtained for  $L_e$  will depend very strongly on the limits of integration.

#### 4.2.3.3 Radiant Intensity and Spectral Radiant Intensity

Radiance and spectral radiance are most useful for comparing the observed signals with backgrounds of distributed emission, e.g., airglow, scattered sunlight, or scattered moonlight. For some purposes, such as model prediction comparison, the radiant intensity and spectral radiant intensity are useful. In the case of the tracker camera, only the latter values are meaningful since this instrument cannot resolve the plume, and the source must be treated as a point source rather than as a distributed source.

This conversion can be achieved from the preceding expressions by multiplying by the projected area of the detector  $R^2\Omega$ , where  $R$  is the range to the source and  $\Omega$  is the detector field of view. This is equivalent to summing the apparent radiance and spectral radiance over the projected pixel area and attributing it to a point source within the field of view of the pixel. The spectral radiant intensity  $I(\lambda)$  and the radiant intensity  $I_e$  can be obtained directly from the corresponding expressions for the spectral radiance and radiance, Eqs. (5) and (14), respectively:

$$I(\lambda) = \left( \frac{P_t}{P_r} \right) R(\lambda) R^2 \Omega = R^2 \Omega L(\lambda), \quad (15)$$

and

$$I_e = \int_{\lambda_i}^{\lambda_v} I(\lambda) d\lambda = R^2 \Omega L_e \quad (16)$$

The units of  $I(\lambda)$  are (power)/(spectral bandwidth)(solid angle), or  $W/nm\text{-sr}$ , and the units of  $I_e$  are (power)/(solid angle), or  $W/\text{sr}$ . As before, the radiant intensity in this sense is an integral across a limited portion of the spectrum defined by the nominal filter edges. The value so obtained is far smaller than would be obtained for the full-spectrum radiant intensity and will also be very sensitive to the range of integration chosen for Eq. (16).

#### 4.2.4 Point Spread Function Effects

The full-width-half-maximum (FWHM) of the plume camera point spread function is about  $90 \mu\text{rad}$  (9 pixels). That of the tracker camera is about  $230 \mu\text{rad}$  (1.5 pixels). The plume length is expected to be 30 m or less, which corresponds to  $67 \mu\text{rad}$  at a 450-km range. The effect of the point spread is to blur a small source image over an increased image area, reducing its apparent source radiance as well as increasing its apparent dimensions.

The amount of the reduction of the apparent source radiance depends on the true dimensions of the source. The ratio of the true radiance to the apparent radiance is on the order of the ratio of the area of the point spread function to the true source area. For example, if the true plume length is

30 m, and the 9-pixel diameter at a 450-km range amounts to 40 m, then this reduction in the apparent source radiance will be about 2.8:1 for the plume camera and 12:1 for the tracker camera. This effect may therefore be significant in a comparison of the apparent radiance values presented in the image and contour plots with predicted plume values. In the absence of independent determination of the source dimensions, the apparent radiance values cannot be corrected for this effect.

#### 4.2.5 Radiometric Data Analysis Summary and Conversion Values

The essence of the data analysis procedure is the determination of the amplitude of the reference spectral shape that would yield the observed photoevent count. Should some emission phenomenon be discovered that features a different emission spectral shape, the analyses would necessarily change, yielding different values for the nominal spectral radiance of the source. This is a well-known and unavoidable problem in the interpretation of radiance measurements.

The principal result of the analysis is the source spectral radiance function  $L(\lambda)$  and the spectral radiant intensity function  $I(\lambda)$ . These functions may vary rapidly with wavelength.

Nominal spectral radiance values needed for displays of the measurements are obtained by specifying a reference wavelength for each filter, taken to be the centroid wavelength in this report, and calculating the spectral radiance at that wavelength with the scaled spectral shape function. Changing the reference wavelengths would change the nominal values, without changing the radiance source.

Radiance and radiant intensity values are obtained by integrating the scaled source spectral shape function between specified limits. Those chosen here are the zero-response limits of the various filters. Any change in these limits will correspondingly change the values, even though the source spectrum and strength are unchanged. These numbers are very sensitive to the limits of integration and can be compared to any other numbers only if the other values are based on identical spectral limits.

Finally, the specific conversion coefficients for photoevents to radiometric values may be useful. Any revised spectral shape assumption will lead to a different set of conversion coefficients. Table 16 lists the radiometric values for single photoevents. All values assume an exposure time of 1/30th second; the radiant intensity values refer to a range of 500 km. The spectral radiance  $L(\lambda_c)$  and the radiance  $L_e$  values are applied to single photoevents per pixel. That is, the number of photoevents measured in a particular pixel is multiplied by the value in the table to determine the radiance of the source in that pixel's field of view. The spectral radiant intensity  $I(\lambda_c)$  and radiant intensity  $I_e$  values are normally applied to the total number of photoevents measured in the plume image.

Table 16 - Radiometric Values Corresponding to Single Photoevents

Filter	$L(\lambda_c)$ ( $\mu\text{W}/\text{m}^2\text{-nm}\text{-sr}$ )	$L_e$ ( $\text{W}/\text{m}^2\text{-sr}$ )	$I(\lambda_c)$ ( $\text{W}/\text{nm}\text{-sr}$ )	$I_e$ ( $\text{W}/\text{sr}$ )
PC-1	$2.07 \times 10^2$	$3.11 \times 10^{-2}$	$6.34 \times 10^{-3}$	$9.51 \times 10^{-1}$
PC-2	$9.55 \times 10^2$	$1.95 \times 10^{-2}$	$2.93 \times 10^{-2}$	$5.98 \times 10^{-1}$
PC-3	$3.91 \times 10^2$	$4.08 \times 10^{-2}$	$1.19 \times 10^{-2}$	$1.25 \times 10^0$
PC-4	$5.38 \times 10^1$	$5.68 \times 10^{-3}$	$1.65 \times 10^{-3}$	$1.74 \times 10^{-1}$
TR	$3.96 \times 10^{-2}$	$4.96 \times 10^{-6}$	$2.58 \times 10^{-4}$	$3.23 \times 10^{-2}$



### 4.3 Examples of Single Plume Camera Images

This subsection presents raw plume image data. Given the characteristics of the UVPI cameras, e.g., exposure time, optics aperture, and the rocket plume radiant intensity, the number of photoevents that are registered within the focal plane array of a camera can be individually counted as isolated events. In this respect, UVPI can be used as a photon-counting instrument.

Figure 24 shows single images, in zoom image transmission rate, of the Antares burn for the different filters. The image in the upper left corner is frame 10542, PC-4; the upper right corner is frame 10671, PC-3; the lower left corner is frame 10987, PC-2; and the lower right corner is frame 11307, PC-1. Pixel radiance is encoded as image brightness, where dark and bright are, respectively, relatively smaller and larger radiance. The images show that the shape of the plume central region and outer region is not necessarily clearly delineated in a single frame.

Every bright spot on the image corresponds to one or more photoevents that pile up at that particular pixel during the exposure time of the camera. Figure 25 illustrates the number of photoevents per second measured at each pixel location in the center 64 by 64 pixels of the lower-left-corner image shown in Fig. 24. The z axis corresponds to the number of photoevents per second while the x and y axes correspond to row and column indices. The actual procedure used to compute the number of photoevents from the measured digital number in the UVPI telemetry stream was discussed in the previous subsection. Figure 25 is also representative of single images during the Star 27 burn.

### 4.4 Calibrated Plume Camera Images

In this subsection calibrated plume camera images are presented that show the spatial distribution of the time-averaged plume radiance. The calibrated images are composite images formed while observing the Antares or Star 27 stages during the seven data intervals listed in Table 10. As explained in Section 4.2, the reference emission spectrum is assumed to convert UVPI measurements into units of radiance ( $\text{Watts}/\text{sr}\cdot\text{cm}^2$ ) for both the Antares and the Star 27 data. Within each interval the plume-to-tracker image ratio is primarily 8:2, and the exposure time for each individual plume camera image is 1/30th of a second. Many individual images are superposed to form each composite image.

The limiting resolution of the UVPI cameras is described by the point spread function. Observation of a ground-based beacon, a source less than 5-m across, shows that the full-width-half-maximum of the point source response in the plume camera is about 9 pixels, or about 90  $\mu\text{rad}$ , which is equivalent to 40 m at a 450-km range. Figure 26 shows a plume-camera image of the beacon on the same scale as the Strypi plume images, which follow. This is representative of the plume camera's point spread function.

The Antares stage was observed with the four plume-camera filters; the Star 27 was observed with only three of the four filters. Figures 27 through 33 show the resulting calibrated composite images for the seven data intervals. In these images the radiant intensity has been mapped to a false color scale, with black representing the highest intensity, yellow the middle intensity, and white the lowest intensity. A horizontal color bar depicting the mapping of radiant intensity into colors is shown on the lower left corner of each image. A histogram of the image intensity values is shown above the color bar in the form of white dots.

With each picture or plot a companion summary table provides relevant information for the quantitative interpretation of the image or plot. The parameters presented in these tables are described in Table 17.

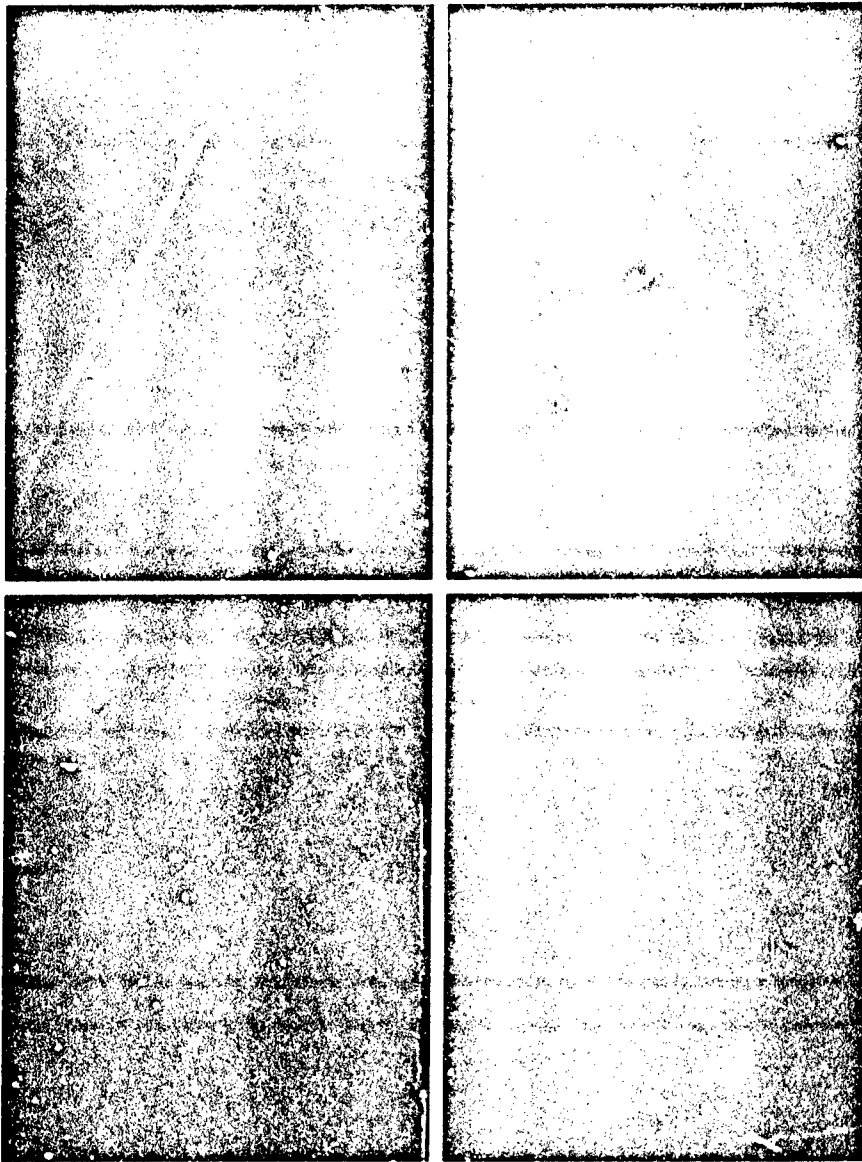


Fig. 24 - Single unprocessed plume camera images of Antares plume

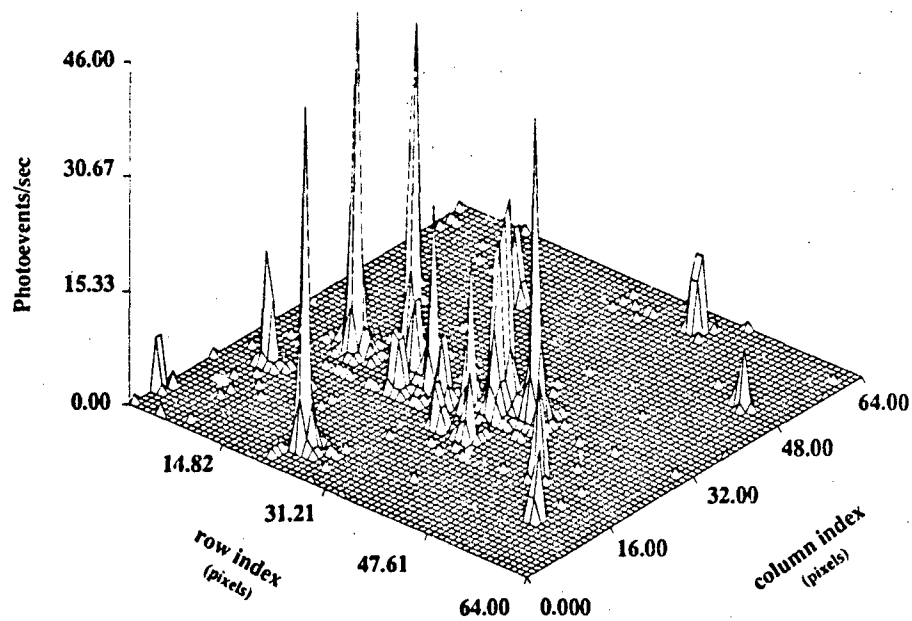


Fig. 25 - Single image of Antares plume

Table 17 - Description of Basic Parameters

Aspect angle	Angle, in degrees, between the LOS and the rocket body longitudinal vector
Average range	Average distance, in kilometers, between UVPI and the plume target
Camera	Camera used, either tracker or plume
Displayed image size	Size in pixels (picture elements) of the image being displayed
Number of superposed images	Number of images averaged together to generate the composite image. Due to the tracker-to-plume image ratio, this number is not equal to the number of frames in the range
Pixel footprint	Projected pixel dimensions, in meters, at target range. This number does not account for any spreading introduced by the optics or jitter since it incorporates only the instantaneous field of view
Range of frames used	Range of frames containing the set of tracker or plume camera images superposed
Spectral band	Spectral band, in nanometers, covered by all images within the set. This band includes more than 99% of the net quantum efficiency response curve
Target observed	Either the Antares or the Star 27 stage
Total photoevents/s	Sum of all photoevent-per-second pixel values over the specified region of the focal plane
Total radiant intensity (W/sr)	Radiant intensity associated with the total photoevents per second
Total spectral radiant intensity (W/sr- $\mu\text{m}$ )	Spectral radiant intensity at the specified centroid wavelength associated with the total photoevents per second
Apparent peak radiance ( $\mu\text{W}/\text{sr}\text{-cm}^2$ )	Apparent radiance measured at the brightest pixel in an image. Because of the size and structure of UVPI's point spread function, the value given is not likely to be a good measure of the true peak radiance at the source. The value is useful for rough comparisons and order-of-magnitude estimates.
Apparent peak spectral radiance ( $\mu\text{W}/\text{sr}\text{-cm}^2\text{-}\mu\text{m}$ )	Apparent spectral radiance at the specified centroid wavelength measured at the brightest pixel in an image. Because of the size and structure of UVPI's point spread function, the value given is not likely to be a good measure of the true peak spectral radiance at the source. The value is useful for rough comparisons and order-of-magnitude estimates.
Error (%)	Total error associated with the above radiometric values. This error includes gain conversion factor error and the error attributable to photon shot noise and detector noise. The error estimate is based on the total number of images superposed. See Section 4.6 for in-depth discussion.

Note that the number of images superposed in each data interval can be significantly different. For example, only 12 images were used for interval 1, and 207 were used for interval 2. For each interval, as many images as possible were superposed.

During the Antares stage, the outer region is more evident in the last three filter wheel positions, i.e., PC-3, PC-2, and PC-1. This may be because there were only 12 superposed images of PC-4 data, compared with more than 100 images for each of the other filters.

Because of the relatively long observation time, the apparent rocket velocity vector changes from interval to interval. The velocity is directed out of the page towards the viewer at an angle that is the complement of the aspect angle shown in Fig. 16. Over the period of observation, the direction of the rocket velocity vector projected on the image plane changes significantly. Table 18 summarizes the direction of the velocity vector projected on the image plane.

Table 18 - Apparent Velocity Vector Direction for Each Interval

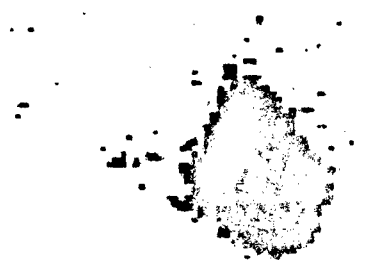
Interval	Stage	Filter	Direction of Motion Relative to Tracker Camera X Axis (deg)
1	Antares	PC-4	16.3
2	Antares	PC-3	13.6
3	Antares	PC-2	9.1
4	Antares	PC-1	6.1
5	Star 27	PC-1	-29.1
6	Star 27	PC-2	-31.7
7	Star 27	PC-3	-33.4

During the Star 27 stage, the number of images superposed for filters 1, 2, and 3, are respectively, 44, 89, 171. For this stage, the plume shape is not as clearly defined as for the Antares stage. This is the result of a weaker signal, which affected the tracking performance.



**Observing sensor:** UVPI  
**Target observed:** UVPI Ground-Based Beacon  
**Orbit number:** 1173  
**Range of frames used:** 12778-12778  
**Camera:** Plume  
**Displayed image size (pixels):** 112 (vertical) x 91 (horizontal)  
**Average range (km):** 450

Fig. 26 - Plume camera image of ground-based beacon illustrating the point spread function



<b>Observing sensor:</b>	UVPI (Feb. 18, 1991)
<b>Target observed:</b>	Strypi, Antares stage
<b>Range of frames used:</b>	10536-10549
<b>Number of superposed images:</b>	12
<b>Camera:</b>	Plume
<b>Spectral band (nm):</b>	235-350 (PC-4)
<b>Displayed image size (pixe's):</b>	112 (vertical) x 91 (horizontal)
<b>Average range (km):</b>	496
<b>Pixel footprint (m) @ range:</b>	4.86 (vertical) x 6.20 (horizontal)
<b>Aspect angle (deg):</b>	100
<b>*Total photoevents/s:</b>	$1.46 \times 10^4$
<b>*Total radiant intensity (W/sr):</b>	$8.31 \times 10^1$
<b>*Total spectral radiant intensity @ 305 nm (W/sr-<math>\mu\text{m}</math>):</b>	$7.87 \times 10^2$
<b>*Error (%):</b>	At least 13.5 (more frames needed)

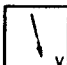


\*For full image.

Fig. 27 - Composite plume camera image for interval 1





Observing sensor:	UVPI (Feb. 18, 1991)	
Target observed:	Strypi, Antares stage	
Range of frames used:	10556-10913	
Number of superposed images:	207	
Camera:	Plume	
Spectral band (nm):	195-295 (PC-3)	
Displayed image size (pixels):	112 (vertical) x 91 (horizontal)	
Average range (km):	477	
Pixel footprint (m) @ range:	4.67 (vertical) x 5.96 (horizontal)	
Aspect angle (deg):	94	
*Total photoevents/s:	$9.75 \times 10^2$	
*Total radiant intensity (W/sr):	$3.69 \times 10^1$	
*Total spectral radiant intensity @ 265 nm (W/sr- $\mu\text{m}$ ):	$3.53 \times 10^2$	
*Error (%):	10.3	

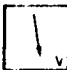
\*For full image.

Fig. 28 - Composite plume camera image for interval 2



1  
2  
3  
4  
5  
6  
7  
8  
9  
10  
11  
12  
13  
14  
15  
16  
17  
18  
19  
20  
21  
22  
23  
24  
25  
26  
27  
28  
29  
30  
31  
32  
33  
34  
35  
36  
37  
38  
39  
40  
41  
42

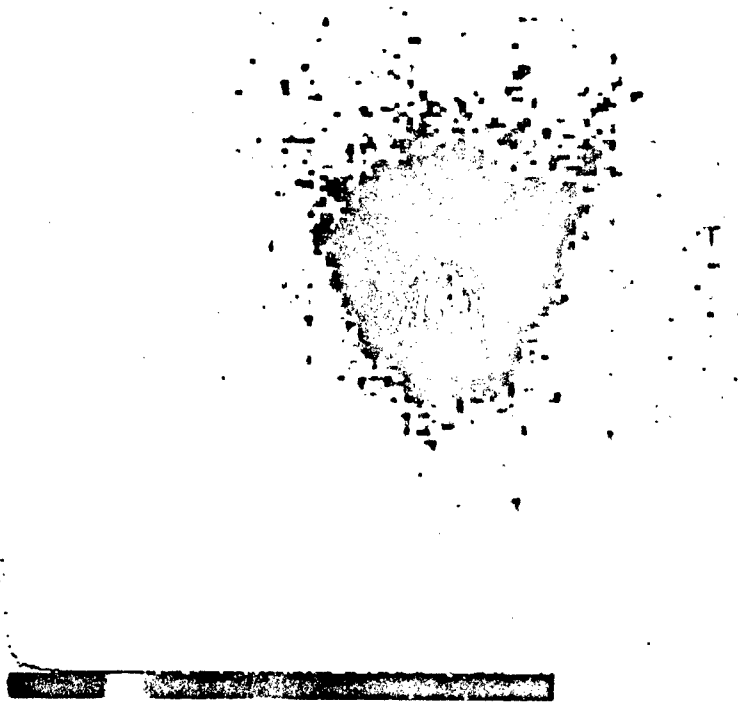



Observing sensor:	UVPI (Feb 18, 1991)	
Target observed:	Strypi, Antares stage	
Range of frames used:	10963-11190	
Number of superposed images:	157	
Camera:	Plume	
Spectral band (nm):	300-320 (PC-2)	
Displayed image size (pixels):	112 (vertical) x 91 (horizontal)	
Average range (km):	462	
Pixel footprint (m) @ range:	4.53 (vertical) x 5.78 (horizontal)	
Aspect angle (deg):	90	
*Total photoevents/s:	$1.91 \times 10^3$	
*Total radiant intensity (W/sr):	$3.24 \times 10^1$	
*Total spectral radiant intensity @ 310 nm (W/sr- $\mu\text{m}$ ):	$1.59 \times 10^3$	
*Error (%):	16.0	

\*For full image.

Fig. 29 - Composite plume camera image for interval 3



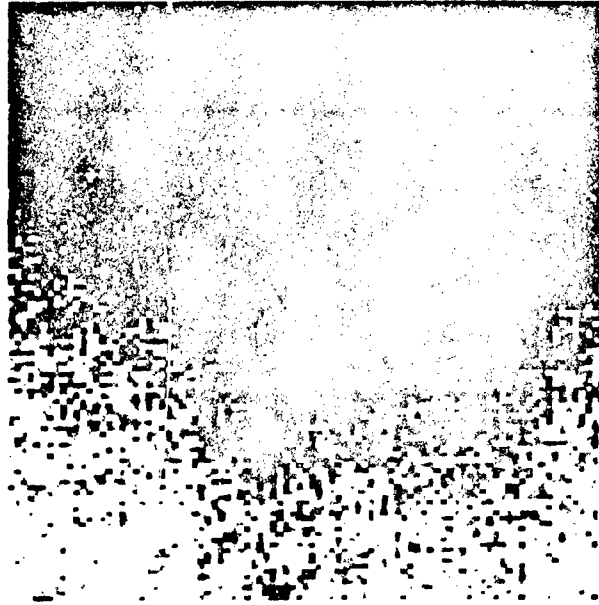



Observing sensor:	UVPI (Feb 18, 1991)	
Target observed:	Strypi, Antares stage	
Range of frames used:	11284-11413	
Number of superposed images:	104	
Camera:	Plume	
Spectral band (nm):	220-320 (PC-1)	
Displayed image size (pixels):	112 (vertical) x 91 (horizontal)	
Average range (km):	452	
Pixel footprint (m) @ range:	4.43 (vertical) x 5.65 (horizontal)	
Aspect angle (deg):	81	
*Total photoevents/s:	$3.52 \times 10^3$	
*Total radiant intensity (W/sr):	$9.11 \times 10^1$	
*Total spectral radiant intensity		
@ 280 nm (W/sr- $\mu\text{m}$ ):	$6.07 \times 10^2$	
*Error (%):	11.1	

\*For full image.

Fig. 30 - Composite plume camera image for interval 4





Observing sensor:	UVPI (Feb. 18, 1991)	
Target observed:	Strypi, Star 27 stage	
Range of frames used:	13142-13239	
Number of superposed images:	44	
Camera:	Plume	
Spectral band (nm):	220-320 (PC-1)	
Displayed image size (pixels):	112 (vertical) x 91 (horizontal)	
Average range (km):	495	
Pixel footprint (m) @ range:	4.85 (vertical) x 7.19 (horizontal)	
Aspect angle (deg):	56	
*Total photoevents/s:	$4.58 \times 10^2$	
*Total radiant intensity (W/sr):	$1.42 \times 10^1$	
*Total spectral radiant intensity		
@ 280 nm (W/sr- $\mu\text{m}$ ):	$9.49 \times 10^1$	
*Error (%):	12.2	

\*For full image.

Fig. 31 - Composite plume camera image for interval 5





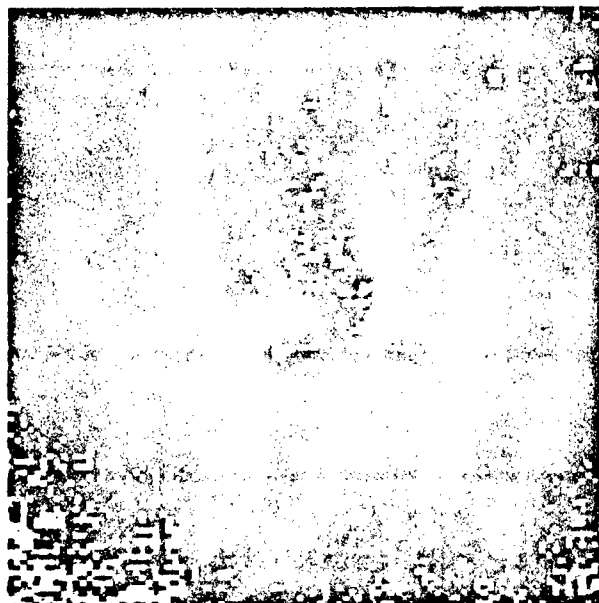
Observing sensor:	UVPI (Feb. 18, 1991)	
Target observed:	Strypi, Star 27 stage	
Range of frames used:	13489-13599	
Number of superposed images:	89	
Camera:	Plume	
Spectral band (nm):	300-320 (PC-2)	
Displayed image size (pixels):	112 (vertical) x 91 (horizontal)	
Average range (km):	515	
Pixel footprint (m) @ range:	5.05 (vertical) x 6.43 (horizontal)	
Aspect angle (deg):	53	
*Total photoevents/s:	$2.17 \times 10^2$	
*Total radiant intensity (W/sr):	4.59	
*Total spectral radiant intensity @ 310 nm (W/sr- $\mu\text{m}$ ):	$2.25 \times 10^2$	
*Error (%):	17.7	

\*For full image.

Fig. 32 - Composite plume camera image for interval 6







Observing sensor:	UVPI (Feb. 18, 1991)	
Target observed:	Strypi, Star 27 stage	
Range of frames used:	13677-13928	
Number of superposed images:	171	
Camera:	Plume	
Spectral band (nm):	195-295 (PC-3)	
Displayed image size (pixels):	112 (vertical) x 91 (horizontal)	
Average range (km):	529	
Pixel footprint (m) @ range:	5.18 (vertical) x 6.61 (horizontal)	
Aspect angle (deg):	50	
*Total photoevents/s:	$2.76 \times 10^2$	
*Total radiant intensity (W/sr):	$1.29 \times 10^1$	
*Total spectral radiant intensity @ 265 nm (W/sr- $\mu\text{m}$ ):	$1.23 \times 10^2$	
*Error (%):	11.3	

\*For full image.

Fig 33 - Composite plume camera image for interval 7



#### 4.4.1 Registration of Plume Camera Images

The composite images presented in this report are formed by adding values for corresponding pixels over all the images in the data interval. This has the effect of increasing the signal-to-noise ratio (SNR). The impact of superposing the plume camera images with no frame registration was assessed by computing the average centroid position and the standard deviation of the centroid position over all the images in an interval. Table 19 summarizes the centroid position for the plume camera for each of the data intervals. The intensity centroid for each image was computed after setting to zero all those pixels with amplitude below 5% of the peak pixel amplitude. The data indicate that maximum RMS jitter for the Antares intervals was 7.1 pixels; for the Star 27 intervals it was 13.8 pixels.

Table 19 - Centroid Statistics for Plume-Camera Images

Data Interval	Images Superposed	Angle Variation (deg.)	Centroid RMS Jitter (pixels)	Average Centroid Position (row, col)
1	12	0	1.1	(55.6,41.2)
2	207	3.4	7.1	(48.8,40.4)
3	157	2.9	6.8	(52.5,42.5)
4	104	0.6	3.1	(52.8,42.4)
5	44	12.6	10.1	(49.8,47.3)
6	89	8.6	3.2	(45.6,47.0)
7	171	6.5	13.8	(45.1,48.8)

Although the superposed images presented in this report do not take into consideration frame registration, preliminary analysis indicates that the improvement obtained by using frame registration is not highly noticeable. For example, Fig. 34 illustrates the effect of frame registration for interval 2. The left image is obtained by using direct superposition, while the right image is the result using frame registration. Given the image aspect angle and the centroid position for an interval, frame registration was done by rotating the consecutive images around the centroid point before they were superposed. The amount of rotation used was obtained from the same source used to generate Fig. 16. Similarly, Fig. 35 illustrates the effects of frame registration for data interval 5.

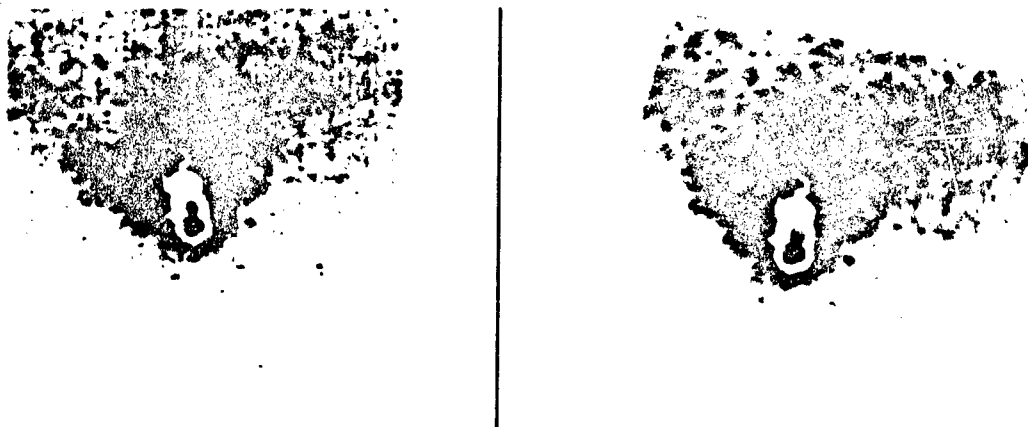


Fig. 34 - Comparison of image superposition methods for data interval 2. Left image uses direct superposition; right image uses frame registration



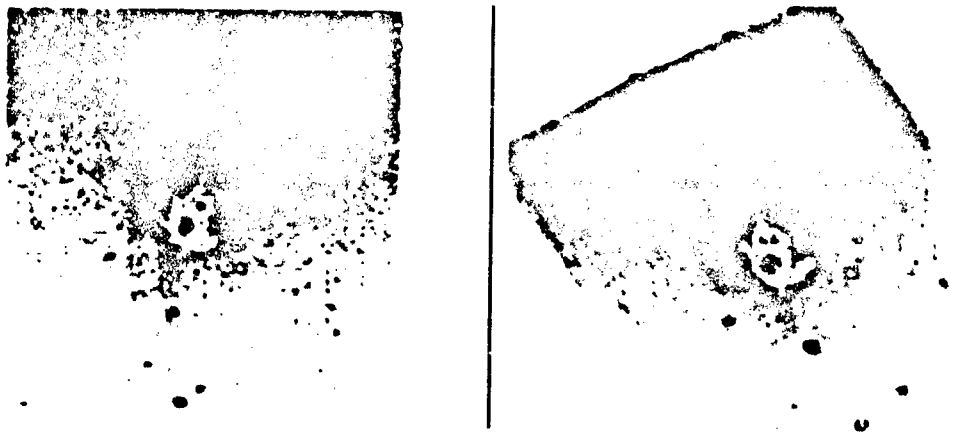


Fig. 35 - Comparison of image superposition methods for data interval 5.  
Left image uses direct superposition; right image uses frame registration

#### 4.5 Calibrated Tracker-Camera Images

While the plume camera gathered rocket plume images, the tracker camera gathered plume images at a lower rate because of the plume-to-tracker image ratio. The tracker camera's exposure time varied over the data intervals (Table 20).

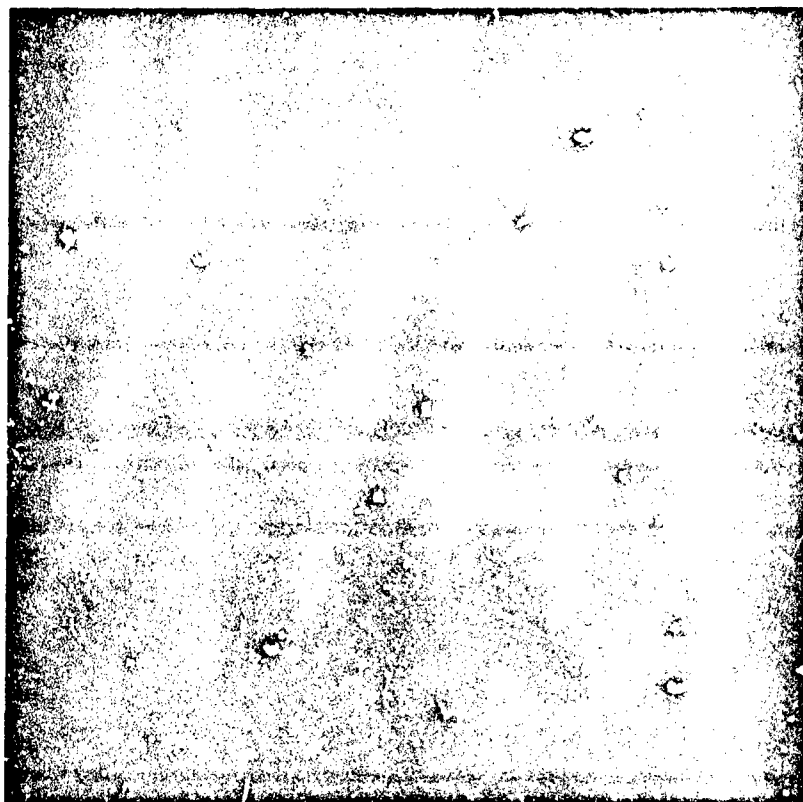
Table 20 - Tracker Camera Exposure Time

Data Interval	Tracker Camera Exposure Time (ms)
1	15.40
2	9.66
3	9.66
4	15.40
5	8.60
6	8.60
7	8.60

The limiting resolution of the UVPI cameras is described by the point spread function. Observation of the ground-based beacon, a source less than 5 m across, showed that the full-width-half-maximum of the point source response in the tracker camera is about 1.5 pixels, or about 230  $\mu$ rad. This is equivalent to 104 m at a 450-km range. Figure 36 shows a tracker-camera image of the ground-based beacon on the same scale as the Strypi tracker-camera images that follow. This is representative of the tracker camera's point spread function.

The corresponding composite tracker camera images for each of the seven data intervals are shown in Figs. 37 - 43. In this section the pseudo-color scale used for mapping the radiant intensity into colors was inverted to allow the subtle outer region to be observed. The outer region in the tracker camera was more evident during the Antares stage, especially during intervals 1 and 4. The Star 27 stage did not show much evidence of an outer region in the tracker camera.



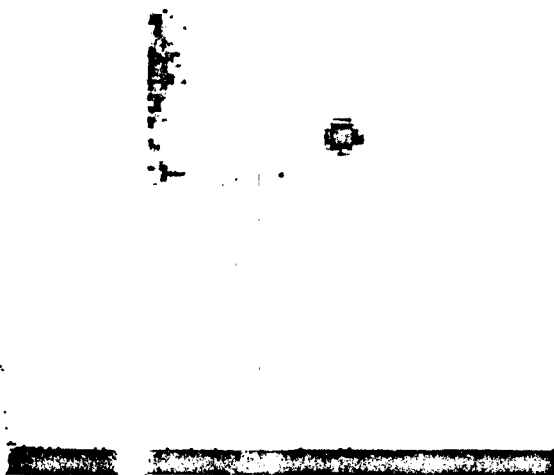



<b>Observing sensor:</b>	UVPI
<b>Target observed:</b>	UVPI Ground-Based Beacon
<b>Orbit number:</b>	1173
<b>Range of frames used:</b>	12772-12772
<b>Camera:</b>	Tracker
<b>Displayed image size (pixels):</b>	112 (vertical) x 91 (horizontal)
<b>Average range (km):</b>	450

Fig. 36 - Tracker-camera image of ground-based beacon illustrating the point spread function








Observing sensor:	UVPI (Feb. 18, 1991)	
Target observed:	Strypi, Antares stage	
Range of frames used:	10536 - 10549	
Number of superposed images:	2	
Camera:	Tracker	
Spectral band (nm):	255 - 450	
Displayed image size (pixels):	112 (vertical) x 91 (horizontal)	
Average range (km):	496	
Pixel footprint (m) @ range:	70.9 (vertical) x 90.2 (horizontal)	
Aspect angle (deg):	100	
*Total photoevents/s:	$2.76 \times 10^5$	
*Total radiant intensity (W/sr):	$2.93 \times 10^2$	
*Total spectral radiant intensity		
@ 390 nm (W/sr- $\mu\text{m}$ ):	$2.34 \times 10^3$	
*Error (%):	15.6	

\*For central 19 x 19 pixels.

Fig. 37 - Composite tracker camera image for interval 1





Observing sensor:	UVPI (Feb. 18, 1991)	
Target observed:	Strypi, Antares stage	
Range of frames used:	10656 - 10913	
Number of superposed images:	50	
Camera:	Tracker	
Spectral band (nm):	255 - 450	
Displayed image size (pixels):	112 (vertical) x 91 (horizontal)	
Average range (km):	477	
Pixel footprint (m) @ range:	68.2 (vertical) x 86.8 (horizontal)	
Aspect angle (deg):	94	
*Total photoevents/s:	$5.13 \times 10^5$	
*Total radiant intensity (W/sr):	$5.04 \times 10^2$	
*Total spectral radiant intensity		
@ 390 nm (W/sr- $\mu\text{m}$ ):	$4.02 \times 10^3$	
*Error (%):	15.6	

\*For central 19 x 19 pixels.

Fig. 38 - Composite tracker-camera image for interval 2



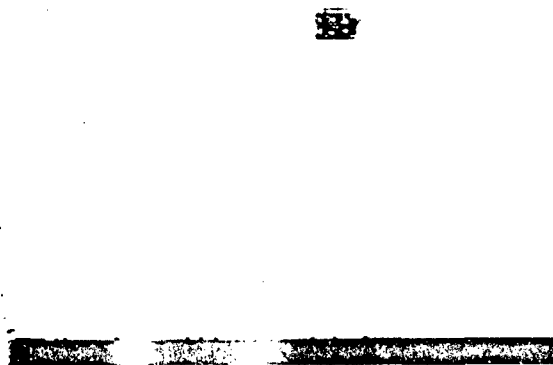


Observing sensor:	UVPI (Feb. 18, 1991)	
Target observed:	Strypi, Antares stage	
Range of frames used:	10963 - 11190	
Number of superposed images:	40	
Camera:	Tracker	
Spectral band (nm):	255 - 450	
Displayed image size (pixels):	112 (vertical) x 91 (horizontal)	
Average range (km):	462	
Pixel footprint (m) @ range:	66.0 (vertical) x 84 (horizontal)	
Aspect angle (deg):	90	
*Total photoevents/s:	$5.78 \times 10^5$	
*Total radiant intensity (W/sr):	$5.32 \times 10^2$	
*Total spectral radiant intensity		
@ 390 nm (W/sr- $\mu\text{m}$ ):	$4.24 \times 10^3$	
*Error (%):	15.6	

\*For central 19 x 19 pixels.

Fig. 39 - Composite tracker-camera image for interval 3





Observing sensor:	UVPI (Feb. 18, 1991)	
Target observed:	Strypi, Antares stage	
Range of frames used:	11286 - 11413	
Number of superposed images:	26	
Camera:	Tracker	
Spectral band (nm):	255 - 450	
Displayed image size (pixels):	112 (vertical) x 91 (horizontal)	
Average range (km):	452	
Pixel footprint (m) @ range:	64.6 (vertical) x 82.2 (horizontal)	
Aspect angle (deg):	81	
*Total photoevents/s:	$4.22 \times 10^5$	
*Total radiant intensity (W/sr):	$3.71 \times 10^2$	
*Total spectral radiant intensity		
@ 390 nm (W/sr- $\mu\text{m}$ ):	$2.96 \times 10^3$	
*Error (%):	15.6	


\*For central 19 x 19 pixels.

Fig. 40 - Composite tracker-camera image for interval 4








Observing sensor:	UVPI (Feb. 18, 1991)	
Target observed:	Strypi, Star 27 stage	
Range of frames used:	13142 - 13239	
Number of superposed images:	31	
Camera:	Tracker	
Spectral band (nm):	255 - 450	
Displayed image size (pixels):	112 (vertical) x 91 (horizontal)	
Average range (km):	495	
Pixel footprint (m) @ range:	70.7 (vertical) x 90.0 (horizontal)	
Aspect angle (deg):	56	
*Total photoevents/s:	$5.32 \times 10^4$	
*Total radiant intensity (W/sr):	$5.62 \times 10^1$	
*Total spectral radiant intensity		
@ 390 nm (W/sr- $\mu\text{m}$ ):	$4.48 \times 10^2$	
*Error (%):	15.6	

\*For central 19 x 19 pixels.

Fig. 41 - Composite tracker-camera image for interval 5





Observing sensor:	UVPI (Feb. 18, 1991)	
Target observed:	Strypi, Star 27 stage	
Range of frames used:	13489 - 13599	
Number of superposed images:	23	
Camera:	Tracker	
Spectral band (nm):	255 - 450	
Displayed image size (pixels):	112 (vertical) x 91 (horizontal)	
Average range (km):	515	
Pixel footprint (m) @ range:	73.6 (vertical) x 93.7 (horizontal)	
Aspect angle (deg):	53	
*Total photoevents/s:	$5.37 \times 10^4$	
*Total radiant intensity (W/sr):	$6.14 \times 10^1$	
*Total spectral radiant intensity		
@ 390 nm (W/sr- $\mu\text{m}$ ):	$4.90 \times 10^2$	
*Error (%):	15.6	

\*For central 19 x 19 pixels.

Fig. 42 - Composite tracker-camera image for interval 6





Observing sensor:	UVPI (Feb. 18, 1991)	
Target observed:	Strypi, 27 stage	
Range of frames used:	13677 - 13928	
Number of superposed images:	41	
Camera:	Tracker	
Spectral band (nm):	255 - 350	
Displayed image size (pixels):	112 (vertical) x 91 (horizontal)	
Average range (km):	529	
Pixel footprint (m) @ range:	75.6 (vertical) x 96.2 (horizontal)	
Aspect angle (deg):	50	
*Total photoevents/s:	$4.57 \times 10^4$	
*Total radiant intensity (W/sr):	$5.52 \times 10^1$	
*Total spectral radiant intensity @ 390 nm (W/sr- $\mu\text{m}$ ):	$4.40 \times 10^2$	
*Error (%):	15.6	

\*For central 19 x 19 pixels.

Fig. 43 - Composite tracker-camera image for interval 7

With each picture or plot a companion summary table provides relevant information for the quantitative interpretation of the image or plot. The parameters presented in these tables are described in Table 17. Radiometric values reported in the table accompanying each figure are for the central 19 by 19 pixels of the tracker camera. This field of view approximately matches the total field of view of the plume camera. This field of view contains plume central region and a portion of the outer region. Therefore, it cannot reliably be converted to radiant intensity or spectral radiant intensity. However, to provide estimates of the radiant intensity and spectral radiant intensity, values based on reference spectral energy distribution assumptions are reported for the tracker camera observations. These results have been reduced by 16.3% to account for red leakage in the tracker camera filter.

Note that the number of images superposed in each data interval can be significantly different. For example, only 2 images were used for interval 1, and 50 were used for interval 2. For each interval, as many images as possible were superposed.

#### 4.6 Error Analysis for Radiometric Observations

The complete estimate of the error in determining radiometric values from the digital numbers reported by the UVPI cameras observing a rocket plume is composed of two components: measurement noise, addressed in Section 4.6.1, which includes photon shot noise and other intrinsic sensor noise sources, and calibration error, discussed in Section 4.6.2, which is the error contained in the gain conversion factor. Section 4.6.3 discusses the calculation of the total error based on the error components presented in 4.6.1 and 4.6.2.

##### 4.6.1 Error Due to Measurement Noise

Because of photon shot noise, the error in the calculated number of photoevents changes as a function of the plume radiant intensity, which could change as a function of time. Since the Antares and Star 27 thrust curves have a slow variation with time (Figs. 13 and 14), the plume radiance was assumed to be locally constant. That is, the radiant intensity statistics are not affected by a small shift in time. A window size of 15 consecutive images was selected for the statistical analysis of the plume-camera data, and a window of 9 consecutive images was selected for the tracker-camera analysis. A larger time window could be used with the risk of making the locally constant assumption invalid.

Given the number of photoevents as a function of image, the following quantities are defined:

- $M$  is number of images in data interval,
- $N$  is number of images used within the window,
- $\mu_i$  is local mean over  $N$  images around  $i$ th image,
- $\sigma_i$  is local standard deviation around  $i$ th image,
- $t_i$  is  $3.1\sigma_i + \mu_i$ , detection threshold,
- $\epsilon_i$  is  $\sigma_i/\mu_i$ , local error around the  $i$ th image,
- $G_g$  is gain conversion factor for gain step  $g$ , in units of sensor output per photoevent,
- $\epsilon_{1/G}$  is error in  $1/G_g$ ,
- $\epsilon_N$  is average local error in the measured number,

$$\epsilon_N = \frac{1}{M} \sum_i \left( \frac{\sigma_i}{\mu_i} \right), \text{ and} \quad (17)$$

- $\epsilon_u$  is upper bound error in the measured number for the case of  $M$  averaged images,

$$\epsilon_u = \frac{\max(\epsilon_i)}{\sqrt{M}}, \text{ over all } i. \quad (18)$$

To prevent extreme values from affecting the local statistics, the maximum and minimum values within the  $N$  window samples were rejected. That is, only  $N-2$  images were used for computing the local mean and local standard deviation. Under the assumption that the mean radiant intensity is high enough for the radiant intensity fluctuations to be modeled by a gaussian distribution, the probability of exceeding the above-defined threshold,  $t_i$ , is no more than 0.001.

Table 21 lists  $M$ , the number of images averaged in each data interval, and  $\epsilon_N$ , the error due to measurement in the values averaged over the window that consists of  $N$  images. There are three columns of  $\epsilon_N$  values corresponding to plume-camera central region measurements, plume-camera central region plus outer region, and tracker-camera 19 by 19 pixel field of view. The 19 by 19 tracker-camera pixels approximately cover the full field of view of the plume camera. The central region and outer region as used in this report are defined in Section 5.1.

Table 21 - Percent Error per Image Due to Measurement Noise,  $\epsilon_N$

Interval	Images ( $M$ )	Plume-Camera Central Region	Plume-Camera Central Region + Outer Region	Tracker Camera (19 x 19)
1	12	—	—	—
2	207	33.8	24.8	3.4
3	157	28.3	18.4	4.5
4	104	17.4	17.4	6.3
5	44	44.7	32.9	6.0
6	89	87.1	55.5	6.2
7	171	58.6	48.9	6.0

#### 4.6.2 Error in Gain Conversion Factor

The gain conversion factor  $G_g$ , derived from on-orbit calibration as discussed in Appendix B.4.0, is based on calibration star measurements. The mean and standard deviation of  $G_g$ , based on measurements of several calibration stars over the full set of UVPI camera gains, can be obtained for each camera configuration by calculating the deviations of individual calibration star measurements about a mean calibration curve.

Table 22 tabulates the error associated with the gain conversion factor for the plume and tracker cameras. The values reported are the average deviations of calibration star measurements about the mean calibration curve.

Table 22 - Average Error in  $1/G_g$  for Tracker and Plume Cameras

Camera/Filter	Average Deviation from Mean Calibration Curve (%)
Tracker	15.6
Plume, PC-1	10.5
Plume, PC-2	15.9
Plume, PC-3	9.9
Plume, PC-4	13.5

#### 4.6.3 Calculation of Total Error

The estimated total calibration error depends on the number of images averaged together,  $M$ . In this report, the total error is defined as the ratio of the standard deviations of the number of photoevents to the mean value of the number of photoevents. Assuming that the digital number



reported by UVPI for a calibration star and the gain conversion factor  $G_g$  are uncorrelated, or weakly correlated, then the total error per image  $\epsilon_F$  can be obtained [18] from:

$$\epsilon_F = \sqrt{\epsilon_N^2 \cdot \epsilon_{1/G}^2 + \epsilon_N^2 + \epsilon_{1/G}^2}, \quad (19)$$

where  $\epsilon_N$  is the average local error in the number of measured photoevents presented in Table 21, and  $\epsilon_{1/G}$  is the error in the gain conversion factor tabulated in Table 22.

For the case of  $M$ -averaged images, an upper bound estimate of the total error is given by

$$\epsilon_T = \sqrt{\epsilon_N^2 \cdot \epsilon_{1/G}^2 + \epsilon_N^2 + \epsilon_{1/G}^2}. \quad (20)$$

Notice that  $\epsilon_T$  can never be smaller than  $\epsilon_{1/G}$  no matter how many images are averaged together.

Table 23 summarizes the overall error analysis results for the plume central region radiant intensities for each of the data intervals. The first column identifies the data interval. The second column contains the number of images within the data interval. The column under the  $K$  heading contains the ratio of the average standard deviation of photoevents to the square root of the average number of photoevents, i.e.,

$$K = \frac{1}{N} \sum_i \left( \frac{\sigma_i}{\sqrt{\mu_i}} \right). \quad (21)$$

Table 23 - Plume Central Region Radiometric Percent Errors for Plume Camera

Interval	$M$	$K$	$\epsilon_F$	$\epsilon_T$
1	12	-	-	-
2	207	1.381	35.4	10.7
3	157	1.465	32.8	16.2
4	104	1.468	20.4	11.1
5	44	1.302	46.2	13.4
6	89	1.370	89.6	20.6
7	171	1.445	59.7	12.2

Under the assumption that the signal is not changing rapidly in time,  $K$  relates the measured noise to the theoretical performance of a background limited system, where the dominant source of noise is shot noise. A ratio of  $K=1$  implies pure background-limited performance. Hence, the values obtained indicate that although UVPI is close to background-limited performance, other sources of sensor noise are present.

The fourth and fifth columns show, respectively, the total percent error on an image by image basis and the total percent error resulting after averaging all  $M$  images available within the appropriate data interval. Data interval number 1 did not have enough images to compute  $\epsilon_N$ .

Similar to Table 23, Tables 24 and 25 show, respectively, the radiant intensity errors for the total plume-camera field of view and those for the 19 by 19 tracker-camera pixels that overlay the plume-camera field of view.

Table 24 - Central Region Plus Outer Region Radiometric Percent Errors for Plume Camera

Interval	M	K	$\epsilon_F$	$\epsilon_T$
1	12	—	—	—
2	207	1.40	26.8	10.3
3	157	1.45	24.5	16.0
4	104	1.89	20.4	11.1
5	44	1.24	34.7	12.2
6	89	1.44	58.4	17.7
7	171	1.43	50.2	11.3

Table 25 - Radiometric Percent Errors: Tracker Camera Over 19 x 19 Pixel Window

Interval	M	K	$\epsilon_F$	$\epsilon_T$
1	2	—	—	—
2	50	2.59	16.0	15.6
3	40	3.64	16.3	15.6
4	26	5.54	16.8	15.6
5	31	1.39	16.7	15.6
6	23	1.45	16.8	15.6
7	41	1.30	16.7	15.6

Table 26 lists  $\epsilon_T$  for each of the seven data intervals: the plume camera observing the central region only, the plume camera observing the central region and the outer region, and the 19 by 19 pixel field in the tracker camera that corresponds to the full plume-camera field of view.

Table 26 - Total Radiometric Percent Errors,  $\epsilon_T$ 

Interval	Plume Camera Central Region	Plume Camera Central Region + Outer Region	Tracker Camera 19 x 19
1	—	—	—
2	10.7	10.3	15.6
3	16.2	16.0	15.6
4	11.1	11.1	15.6
5	13.4	12.2	15.6
6	20.6	17.7	15.6
7	12.2	11.3	15.6

#### 4.7 Noise Equivalent Radiance

Following the noise equivalent radiance (NER) definition given in the Infrared Handbook [19], the UVPI NER is defined as the source radiance level that will result in a signal-to-noise ratio of 1 at the output of a single pixel. The NER can be interpreted as the sensitivity limit for an imaging system. For UVPI, a single NER number does not fully characterize the sensitivity of the system since this is a function of integration time, spectral filter, camera gain level, number of images superposed, and the assumed source spectrum.

The following discussion is based on empirical estimates of the signal and noise within the UVPI cameras as opposed to a theoretical discussion. A theoretical expression for the signal power to noise power ratio applicable to the microchannel plate image intensifier of the UVPI can be found in Ref. 20. A single pixel in the plume or tracker camera can be treated as a photoevent counting device. The signal-to-noise ratio (SNR) definition from which the empirical UVPI NER is derived is

$$(SNR)^2 = M^2 \cdot S^2 / (M \cdot N^2 + M \cdot N_s^2), \quad (22)$$

where

- $M$  is the number of images superposed. This affects the effective integration time.
- $S$  is the mean number of signal-related photoevents collected in a pixel during the integration time.
- $N$  is the signal independent noise standard deviation for a single pixel expressed in photoevents/image. This noise source is constant. When expressed in photoevents/image, its level depends on the camera gain setting used.
- $N_s$  is the signal dependent photon shot noise standard deviation expressed in photoevents/image. Based on extensive measurements made on UVPI data, the signal-dependent noise can be expressed in terms of the mean number of signal-related photoevents by using

$$N_s = 2S^{1/2} \quad (23)$$

Note that this is two times higher than the photon shot noise prediction.

From the SNR expression above, the mean number of signal-related photoevents/image in a pixel that will result in a SNR of 1 is

$$S' = 2[1 + (1 + M \cdot N^2 / 4)^{1/2}] / M. \quad (24)$$

Notice that for the case of only one superposed image,  $M = 1$ , and a negligible level of sensor noise  $N$ , the resulting sensitivity limit is 4 photoevents/image. The NER is related to  $S'$  by a multiplicative constant  $K$ , i.e.,

$$NER = K \cdot S' = 2K[1 + (1 + M \cdot N^2 / 4)^{1/2}]M, \quad (25)$$

where  $K$  is the radiometric calibration constant that converts from photoevents/image to  $\mu\text{W}/\text{sr}\cdot\text{cm}^2$ .  $K$  is a function of the spectral filter used, the single-image exposure time, and the assumed source spectrum.

The radiometric sensitivity could also be improved by performing spatial averaging at the expense of a lower spatial resolution.

Table 27 summarizes the estimated NERs, or sensitivity levels, for the seven data intervals for the plume camera, under the assumption of the reference spectrum. Since, for the plume camera, the signal-independent noise is negligible compared to the signal-dependent noise, image superposition provides an increase in sensitivity that is linear with the number of superposed images.

Table 27 - Plume Camera NER Per Pixel for Data Intervals

Data Interval	Stage	Filter	UVPI Gain Step	NER for Single Image (W/sr-cm <sup>2</sup> )	Number of Images Superposed	NER for Data Interval (W/sr-cm <sup>2</sup> )
1	Antares	PC-4	10	$2.3 \times 10^{-6}$	12	$1.9 \times 10^{-7}$
2	Antares	PC-3	12	$1.6 \times 10^{-5}$	207	$7.9 \times 10^{-8}$
3	Antares	PC-2	11	$7.8 \times 10^{-6}$	157	$5.0 \times 10^{-8}$
4	Antares	PC-1	11	$1.2 \times 10^{-5}$	104	$1.2 \times 10^{-7}$
5	Star 27	PC-1	12	$1.2 \times 10^{-5}$	44	$2.8 \times 10^{-7}$
6	Star 27	PC-2	13	$7.8 \times 10^{-6}$	89	$8.8 \times 10^{-8}$
7	Star 27	PC-3	13	$1.6 \times 10^{-5}$	171	$9.5 \times 10^{-8}$

Table 28 summarizes the estimated NERs, or sensitivity levels, for the seven data intervals for the tracker camera under the assumption of the reference spectrum. The last column expresses the sensitivity level in photoevents/s. As opposed to the plume camera, in the tracker camera the signal-independent noise is not negligible, and the improvement in sensitivity is not linear with the number of images superposed.

Table 28 - Tracker Camera NER Per Pixel for Data Intervals

Data Interval	Stage	NER for Single Image (W/sr-cm <sup>2</sup> )	Number of Images Superposed	UVPI Gain Step	NER for Data Interval (W/sr-cm <sup>2</sup> )	Minimum Detectable Number of Photoevents/S for Superposed Images
1	Antares	$1.1 \times 10^{-8}$	2	7	$7.3 \times 10^{-9}$	44
2	Antares	$1.8 \times 10^{-8}$	50	7	$2.0 \times 10^{-9}$	120
3	Antares	$1.8 \times 10^{-8}$	40	7	$2.3 \times 10^{-9}$	140
4	Antares	$1.8 \times 10^{-8}$	26	6	$3.2 \times 10^{-9}$	190
5	Star 27	$8.2 \times 10^{-9}$	31	10	$4.9 \times 10^{-10}$	29
6	Star 27	$8.2 \times 10^{-9}$	23	10	$6.0 \times 10^{-10}$	36
7	Star 27	$8.2 \times 10^{-9}$	41	10	$4.1 \times 10^{-11}$	24

## 5.0 SPATIAL FEATURES

This section concentrates on the spatial characterization of the measured plumes. First, definitions for the plume central region and outer region are presented. Second, contour plots for each of the seven data intervals are presented for the plume camera, followed by contour plots for the tracker camera. Third, the plume's spatial extent is discussed with consideration for the UVPI's point spread function (PSF). Finally, the observed plume is compared to the CHARM 1.3 model predictions.

### 5.1 Delineation of Plume Central and Outer Regions

Because of the generally low signal statistics in a single image, an accurate delineation of the plume central or outer region is not possible from a single image. Hence, an average of superposed images (a composite image) is used to define the plume central region extent for each of the seven intervals.

Definition of the central region was begun by selecting all pixels in the composite image for which the radiance was at least 25% of the brightest pixel radiance. The resulting region was

expanded further by performing a dilation with a square window of 5 by 5 pixels. By using this criterion, the region defining the plume central region is depicted in Figs. 44 and 45. The images on the left are the composite images, and in the images on the right, the corresponding central region is overlaid as a completely white region. Figure 44 shows the four intervals for the Antares burn, and Fig. 45 shows the three intervals for the Star 27 burn.

Table 29 summarizes the central region extent in pixels for each of the seven data intervals considered. Figure 45 shows that for the Star 27 stage during filter positions 1 and 3, intervals 5 and 7, the resulting central region is not contiguous and includes a large number of pixels. This is the result of the weak signal that affected the tracker performance, compounded by the coning that took place during the Star 27 stage. Therefore, no values for central region extent are reported for these two intervals.

For the tracker camera, the central region is defined as all those pixels that overlap the plume camera field of view. Hence, in this report, the central region for the tracker camera is not defined over the same area as for the plume camera.

From the point of view of phenomenology, an argument can be made that the central region definition above does not fully contain the plume core. To validate the definition of the plume central region, additional consecutive dilation operations were performed to force the defined central region to become larger. Figures 46 through 49 show the number of photoevents per image in the central and outer regions as a function of central region size for the Antares stage data intervals. A vertical dashed line is used to illustrate the central region size used in this report. These plots can be used to scale the results presented in the report if a different central region size is desired.

## 5.2 Calibrated Plume Contours

Figure 50 shows the contour plot for the ground beacon, a point source, on the same scale as Figs. 51 through 57, discussed below. This figure indicates the resolution of the plume-camera contour plots due to the point spread function.

Figures 51 through 57 show the contour plots for the seven data intervals, starting with filter 4 in the Antares stage and ending with filter 3 in the Star 27 stage. With each picture or plot a companion summary table provides relevant information for the quantitative interpretation of the image or plot. The parameters presented in these tables are described in Table 17.

The black, blue, and red contours represent, respectively, plume radiance contours at 0.95, 0.5, and 0.095 of the maximum radiance in the image. The radiance units are watts per steradian per square centimeter, and the horizontal and vertical axes are scaled in meters.

Because of the UVPI's dynamic range of 256 levels in the analog to digital converter, it is difficult to get well defined plume contours at levels below 0.095 of the maximum radiance unless a large number of images are superposed.

Table 30 contains the value of the maximum apparent pixel radiance measured for the brightest pixel for the plume camera as a function of data interval. The table also shows apparent peak spectral radiance reported at the specified centroid wavelength. As expected, the Star 27 stage results in weaker radiance values than the Antares stage. The PC-1 and PC-3 peak radiance values during the Star 27 stage are uncertain because of the low signal-to-noise ratio. Because of the size and structure of UVPI's point spread function, the values given are primarily useful for rough comparisons and order-of-magnitude estimates. Estimates of true source peak radiance require further analysis. A comparison of UVPI apparent peak radiance measurements with reference spectrum predictions is presented in Section 5.5.

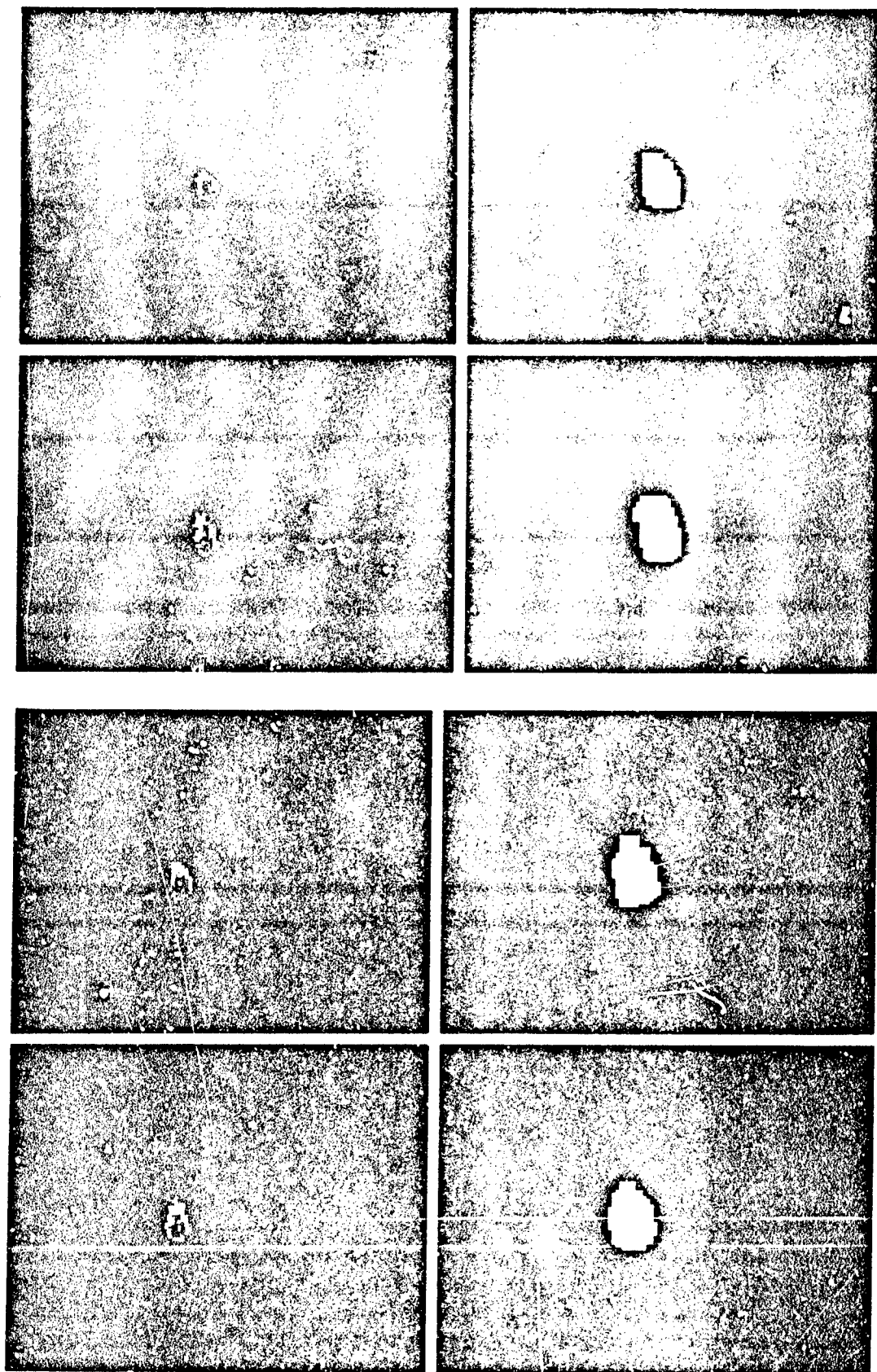


Fig. 44 - Highlighted plume central regions for Antares



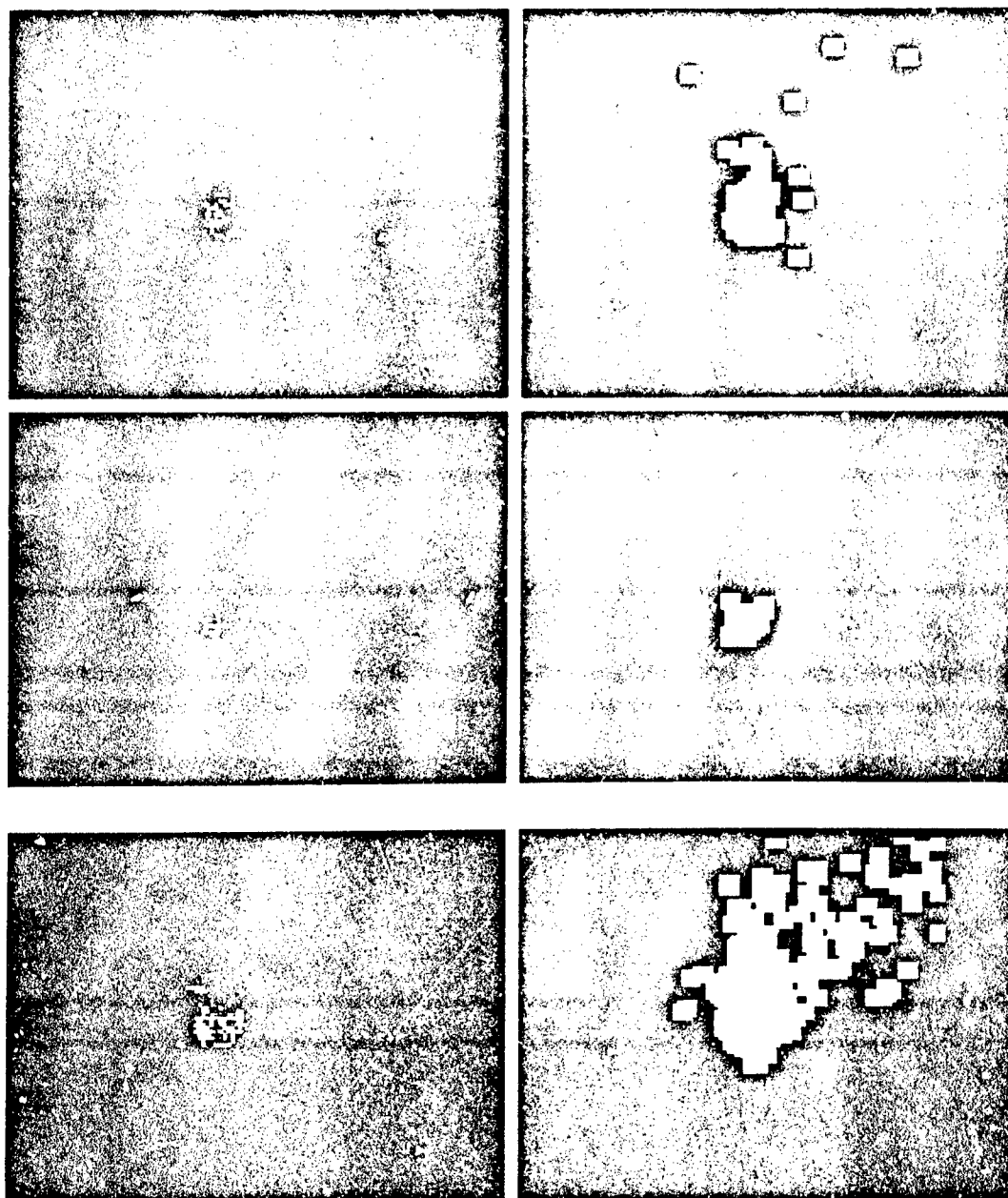


Fig. 45 - Highlighted plume central regions for Star 27

Table 29 - Central Region Extent in Plume Camera

Interval	Stage	Filter	Central Region Extent (pixels)	Central Region Extent (m <sup>2</sup> )
1	Antares	PC-4	182	5435
2	Antares	PC-3	265	7336
3	Antares	PC-2	272	7112
4	Antares	PC-1	268	6707
5	Star 27	PC-1	—	—
6	Star 27	PC-2	172	5588
7	Star 27	PC-3	—	—



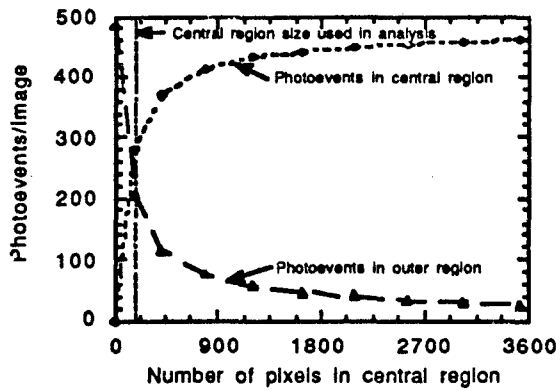


Fig. 46 - Photoevents as a function of defined central region size, Antares interval 1

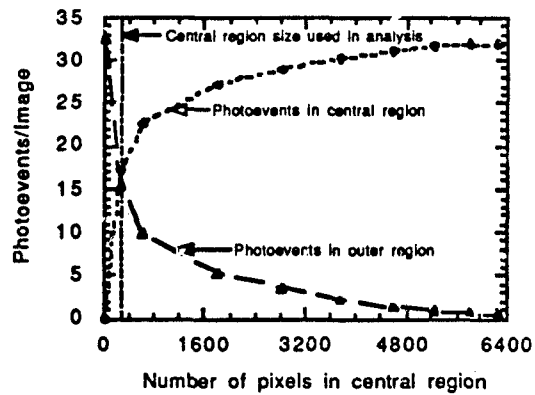


Fig. 47 - Photoevents as a function of defined central region size, Antares interval 2

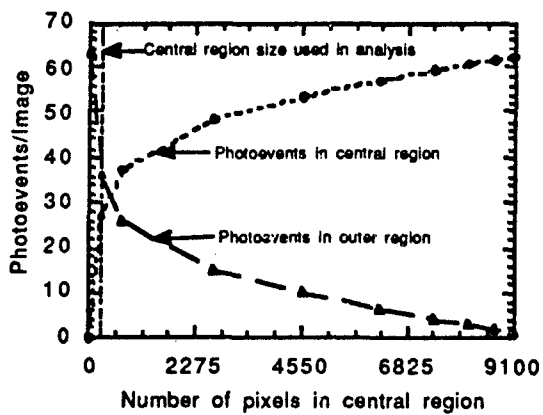


Fig. 48 - Photoevents as a function of defined central region size, Antares interval 3

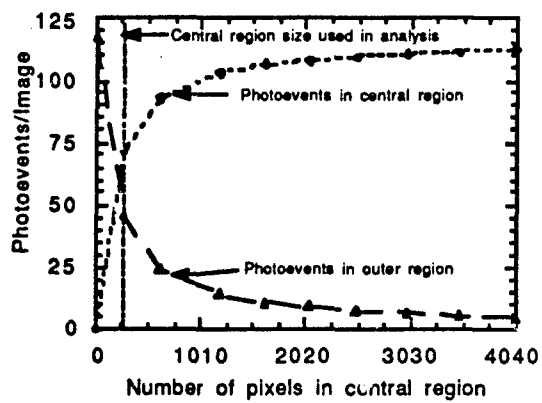
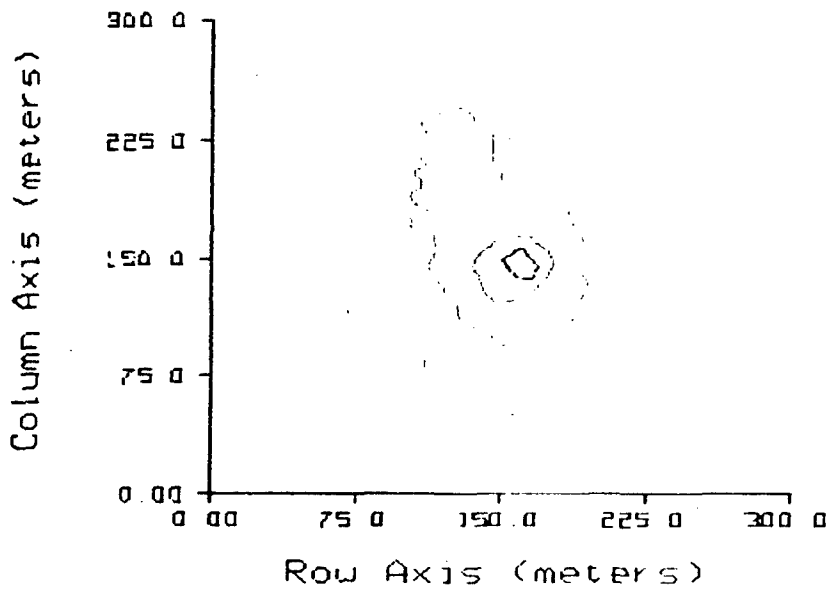


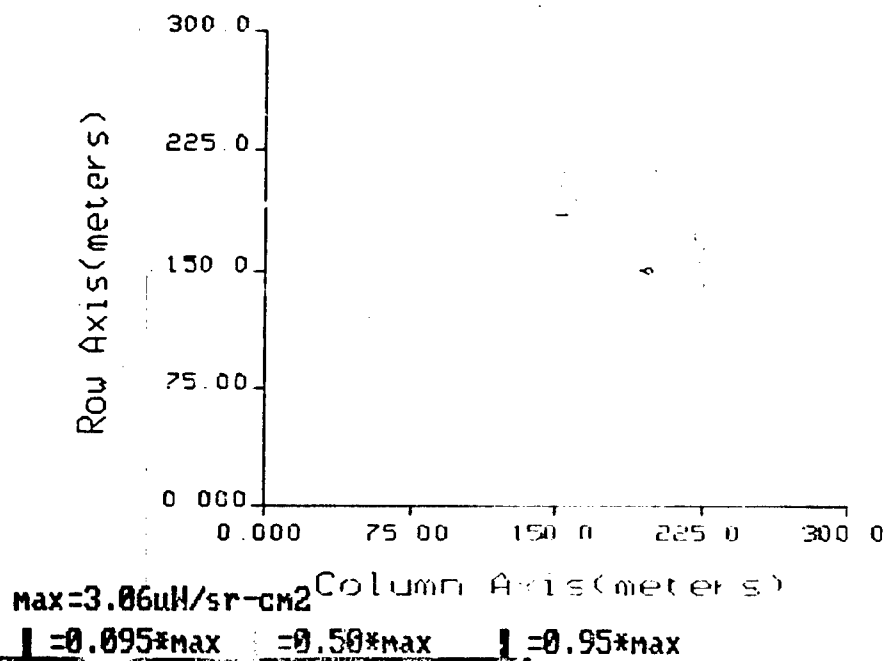
Fig. 49 - Photoevents as a function of defined central region size, Antares interval 4



Observing sensor:	UVPI
Target observed:	UVPI ground-based beacon
Orbit:	1173
Range of frames used:	12778-12778
Camera:	Plume
Average range (km):	450

Fig. 50 Plume-camera contour plot for ground-based beacon



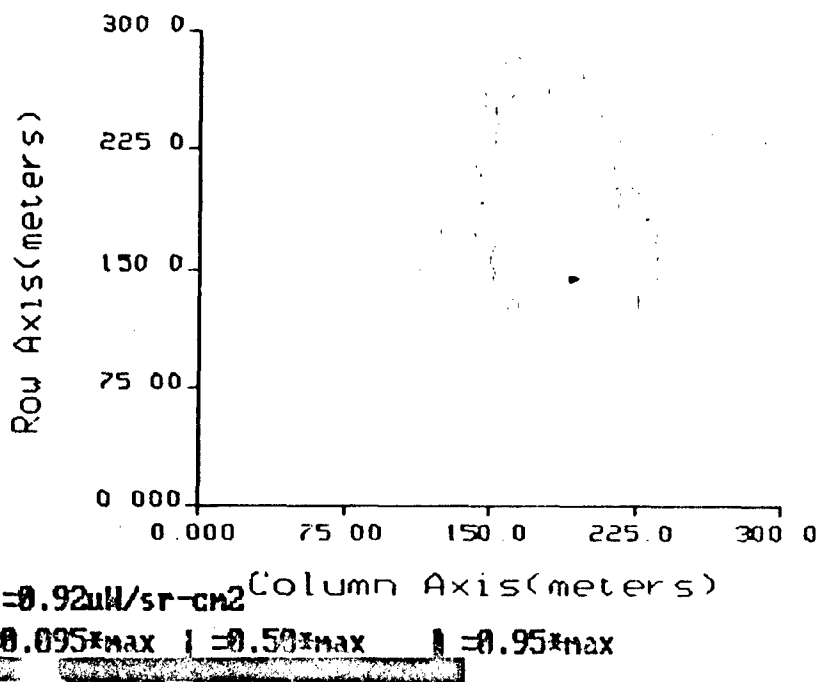


Observing sensor:	UVPI (Feb. 18, 1991)
Target observed:	Strypi, Antares stage
Range of frames used:	10536-10549
Number of superposed images:	12
Camera:	Plume
Spectral band (nm):	235-350 (PC-4)
Displayed image size (pixels):	41.15 (vertical) x 32.26 (horizontal)
Average range (km):	496
Pixel footprint (m) @ range:	4.86 (vertical) x 6.20 (horizontal)
Aspect angle (deg):	100
*Photoevents/s:	1.58 x 10 <sup>2</sup>
*Apparent peak radiance ( $\mu$ W/sr-cm <sup>2</sup> ):	2.99
*Apparent peak spectral radiance @ 305 nm ( $\mu$ W/sr-cm <sup>2</sup> - $\mu$ m):	2.83 x 10 <sup>1</sup>

\*For brightest pixel

Fig. 51 - Plume camera contour plot for interval 1



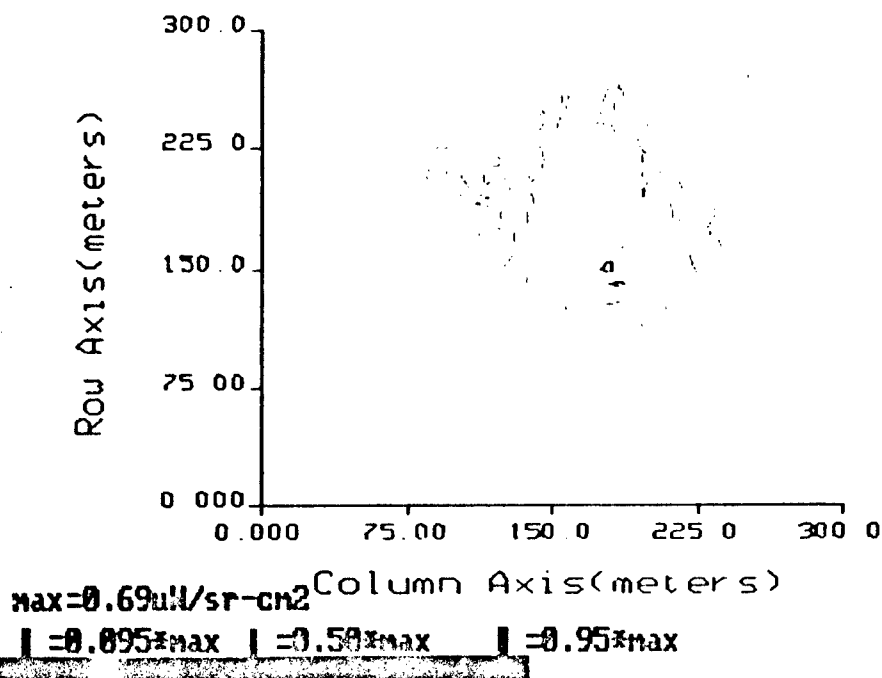


Observing sensor:	UVPI (Feb. 18, 1991)
Target observed:	Strypi, Antares stage
Range of frames used:	10656-10913
Number of superposed images:	207
Camera:	Plume
Spectral band (nm):	195-295 (PC-3)
Displayed image size (pixels):	42.82 (vertical) x 33.56 (horizontal)
Average range (km):	477
Pixel footprint (m) @ range:	4.67 (vertical) x 5.96 (horizontal)
Aspect angle (deg):	94
*Photoevents/s:	6.79
*Apparent peak radiance ( $\mu\text{W}/\text{sr}\cdot\text{cm}^2$ ):	$9.23 \times 10^{-1}$
*Apparent peak spectral radiance @ 265 nm ( $\mu\text{W}/\text{sr}\cdot\text{cm}^2\cdot\mu\text{m}$ ):	8.84

\*For brightest pixel

Fig. 52 - Plume-camera contour plot for interval 2





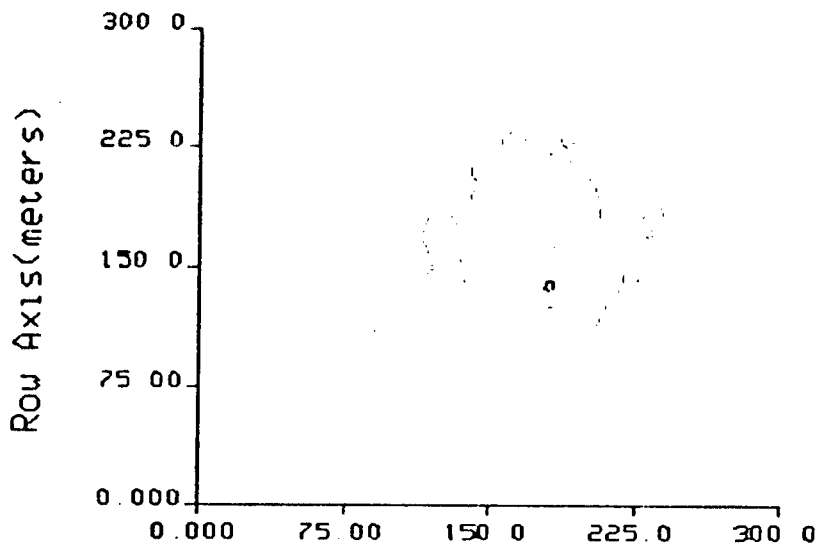
Observing sensor:	UVPI (Feb. 18, 1991)
Target observed:	Strypi, Antares stage
Range of frames used:	10963-11190
Number of superposed images:	157
Camera:	Plume
Spectral band (nm):	300-320 (PC-2)
Displayed image size (pixels):	44.15 (vertical) x 34.60 (horizontal)
Average range (km):	462
Pixel footprint (m) @ range:	4.53 (vertical) x 5.78 (horizontal)
Aspect angle (deg):	90
*Photoevents/s:	1.06x10 <sup>1</sup>
*Apparent peak radiance (μW/sr-cm <sup>2</sup> ):	6.92x10 <sup>-1</sup>
*Apparent peak spectral radiance @ 310 nm (μW/sr-cm <sup>2</sup> -μm):	3.39x10 <sup>1</sup>

\*For brightest pixel

Fig. 53 - Plume-camera contour plot for interval 3







max=2.73 $\mu$ W/sr-cm<sup>2</sup> Column Axis (meters)

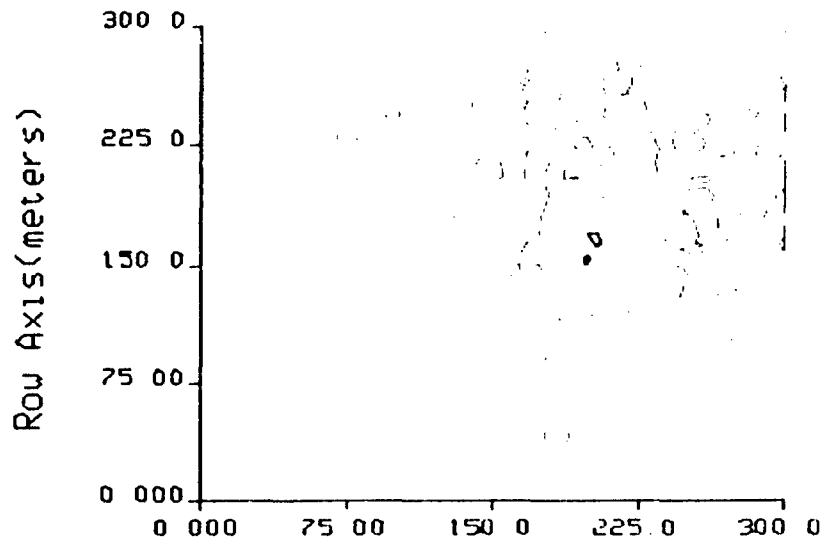
| =0.095\*max | =0.50\*max | =0.95\*max

Observing sensor:	UVPI (Feb. 18, 1991)
Target observed:	Strypi, Antares stage
Range of frames used:	1:284-11413
Number of superposed images:	104
Camera:	Plume
Spectral band (nm):	220-320 (PC-1)
Displayed image size (pixels):	45.15 (vertical) x 35.40 (horizontal)
Average range (km):	452
Pixel footprint (m) @ range:	4.43 (vertical) x 5.65 (horizontal)
Aspect angle (deg):	81
*Photoevents/s:	2.63x10 <sup>1</sup>
*Apparent peak radiance ( $\mu$ W/sr-cm <sup>2</sup> ):	2.72
*Apparent peak spectral radiance @ 280 nm ( $\mu$ W/sr-cm <sup>2</sup> - $\mu$ m):	1.81x10 <sup>1</sup>

\*For brightest pixel

Fig. 54 - Plume-camera contour plot for interval 4





max=0.38  $\mu\text{W}/\text{sr}\cdot\text{cm}^2$  Column Axis (meters)

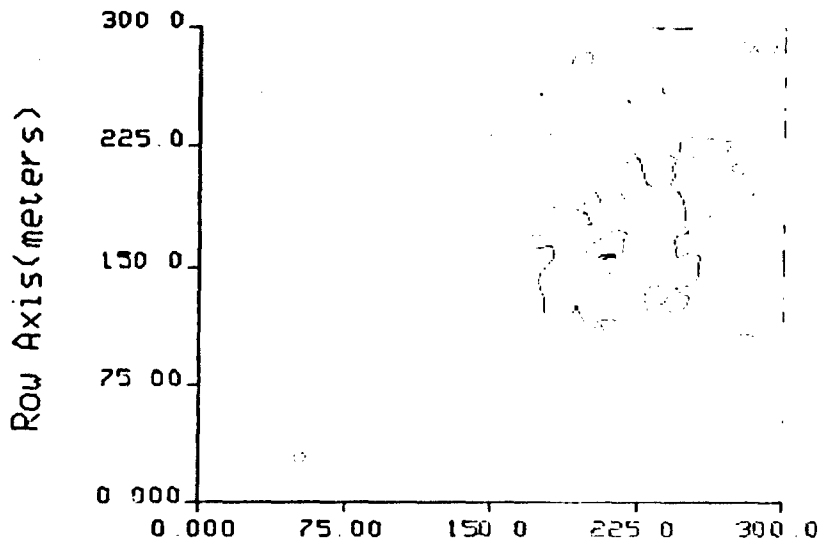
$I = 0.095 \times \text{max}$   $I = 0.50 \times \text{max}$   $I = 0.95 \times \text{max}$

Observing sensor:	UVPI (Feb. 18, 1991)
Target observed:	Strypi, Star 27 stage
Range of frames used:	13142-13239
Number of superposed images:	44
Camera:	Plume
Spectral band (nm):	220-320 (PC-1)
Displayed image size (pixels):	41.24 (vertical) x 27.82 (horizontal)
Average range (km):	495
Pixel footprint (m) @ range:	4.85 (vertical) x 7.19 (horizontal)
Aspect angle (deg):	56
*Photoevents/s:	3.82
*Apparent peak radiance ( $\mu\text{W}/\text{sr}\cdot\text{cm}^2$ ):	Uncertain
*Apparent peak spectral radiance @ 280 nm ( $\mu\text{W}/\text{sr}\cdot\text{cm}^2\cdot\mu\text{m}$ ):	Uncertain

\*For brightest pixel

Fig. 55 - Plume-camera contour plot for interval 5





max=0.18 $\mu$ W/sr-cm<sup>2</sup> Column Axis (meters)

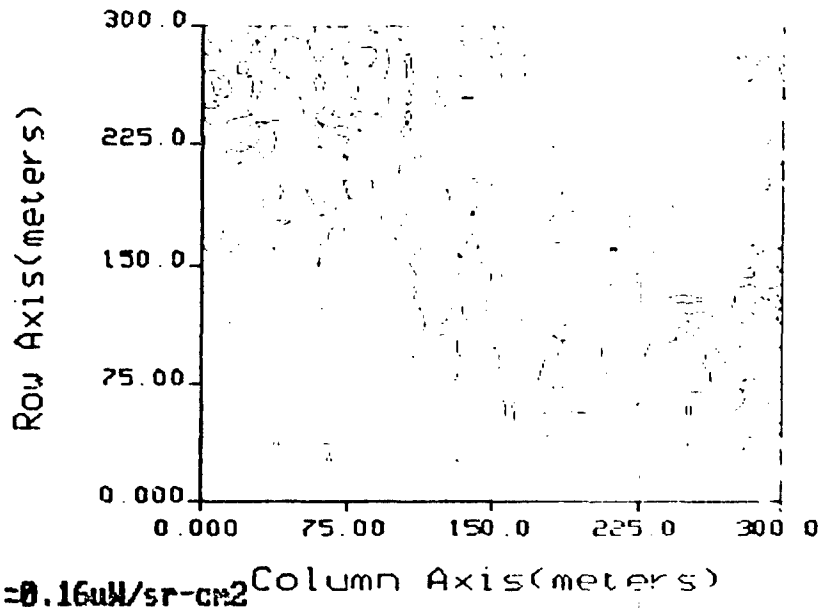
█ =0.095\*max █ =0.50\*max █ =0.95\*max

Observing sensor:	UVPI (Feb. 18, 1991)
Target observed:	Strypi, Star 27 stage
Range of frames used:	13489-13599
Number of superposed images:	89
Camera:	Plume
Spectral band (nm):	300-320 (PC-2)
Displayed image size (pixels):	39.60 (vertical) x 31.10 (horizontal)
Average range (km):	515
Pixel footprint (m) @ range:	5.05 (vertical) x 6.43 (horizontal)
Aspect angle (deg):	5.3
*Photoevents/s:	2.75
*Apparent peak radiance ( $\mu$ W/sr-cm <sup>2</sup> ):	$1.79 \times 10^{-1}$
*Apparent peak spectral radiance @ 310 nm ( $\mu$ W/sr-cm <sup>2</sup> - $\mu$ m):	8.77

\*For brightest pixel

Fig. 56 - Plume-camera contour plot for interval 6





Observing sensor:	UVPI (Feb. 18, 1991)
Target observed:	Strypi, Star 27 stage
Range of frames used:	13677-13928
Number of superposed images:	171
Camera:	Plume
Spectral band (nm):	195-295 (PC-3)
Displayed image size (pixels):	38.61 (vertical) x 30.26 (horizontal)
Average range (km):	529
Pixel footprint (m) @ range:	5.18 (vertical) x 6.61 (horizontal)
Aspect angle (deg):	50
*Photoevents/s:	1.13
*Apparent peak radiance ( $\mu\text{W}/\text{sr}\cdot\text{cm}^2$ ):	Uncertain
*Apparent peak spectral radiance @ 265 nm ( $\mu\text{W}/\text{sr}\cdot\text{cm}^2\cdot\mu\text{m}$ ):	Uncertain

\*For brightest pixel

Fig. 57 - Plume-camera contour plot for interval 7



Table 30 - Plume Camera Apparent Peak Radiometric Value

Interval	Stage	Filter	Apparent Peak Radiance ( $\mu\text{W}/\text{sr}\cdot\text{cm}^2$ )	Apparent Peak Spectra <sup>l</sup> Radiance ( $\mu\text{W}/\text{sr}\cdot\text{cm}^2\cdot\mu\text{m}$ )	$\lambda$ Centroid Wavelength (nm)
1	Antares	PC-4	2.99	$2.83 \times 10^1$	305
2	Antares	PC-3	$9.23 \times 10^{-1}$	8.84	265
3	Antares	PC-2	$6.92 \times 10^{-1}$	$3.39 \times 10^1$	310
4	Antares	PC-1	2.72	$1.81 \times 10^1$	280
5	Star 27	PC-1	—	—	280
6	Star 27	PC-2	$1.79 \times 10^{-1}$	8.77	310
7	Star 27	PC-3	—	—	265

### 5.3 Calibrated Tracker-Camera Spatial Features

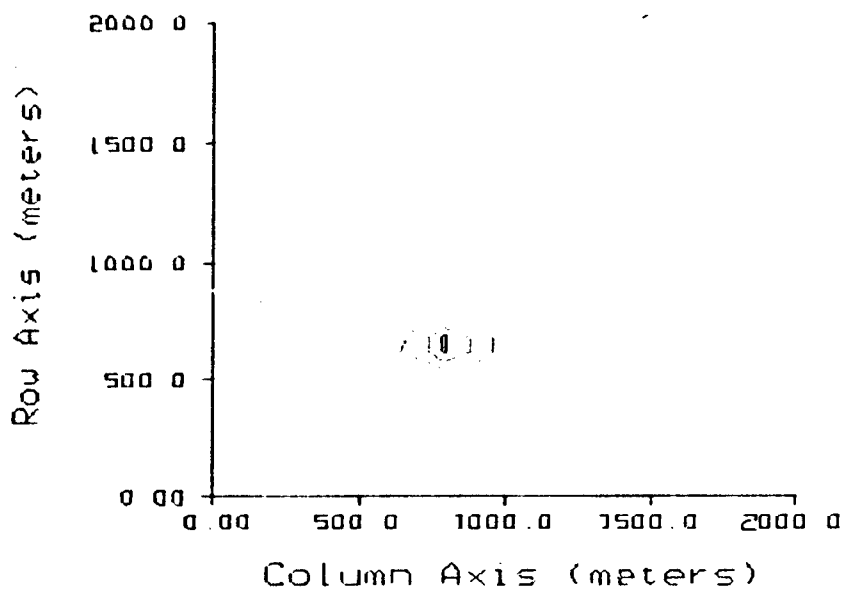
The resolution of the tracker camera, as limited by the point spread function, is approximately 230  $\mu\text{rad}$ . At a 450 to 500-km range, this is equivalent to about 110 m. Since the Antares and Star 27 plumes are expected to be only 15 to 40 m long, the tracker camera cannot resolve the plume. Likewise, the tracker camera cannot resolve the luminous structure within the plume. This is consistent with the primary role of the tracker camera as a plume acquisition and tracking instrument in support of the higher resolution plume camera.

However, the tracker camera is a radiometrically calibrated instrument and is, within its resolution limits, capable of quantitative plume radiometric measurements. Some examples of the images obtained by the tracker camera and the apparent radiances of the plume sources are given. Since the plumes are well below the camera resolution limit, the images essentially show the point spread function of the tracker camera.

Figure 58 shows the tracker-camera contour plot for the ground beacon, a point source. This figure indicates the resolution of the tracker-camera contour plots resulting from the point spread function. Figures 59 and 60 are tracker-camera contour plots for the Antares and Star 27 burns, respectively. The contour plots for other intervals are essentially the same.

The apparent radiance values correspond to spreading the plume source over the area defined by the tracker-camera's resolution limit. Since this area is as much as 85 times the plume area, the apparent radiance values are well below the true plume radiances. Furthermore, since the true plume area is not well known, it is not possible to adjust these apparent radiance values for the limited camera resolution. The apparent radiance values listed with the plume images are shown only as indications of the tracker camera results and are not to be taken as valid measures of the plume radiance.

The Antares and Star 27 plumes, at these ranges, must be treated as point sources that yield radiant intensity values. The radiant intensity measurements by the tracker camera are shown in Section 6.

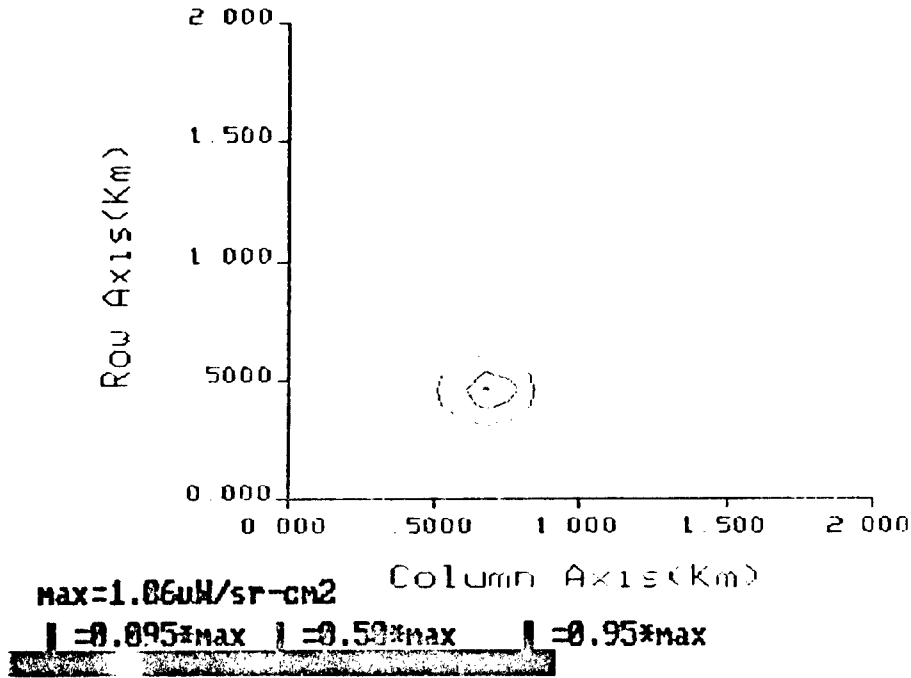


**I = 0.095\*max    I = 0.50\*max    I = 0.95\*max**

Observing sensor:	UVPI
Target observed:	UVPI ground-based beacon
Orbit number:	1173
Range of frames used:	12772 - 12772
Camera:	Tracker
Displayed image size (km):	2 (vertical) x 2 (horizontal)
Average range (km):	480

Fig. 58 - Tracker-camera centour plot for ground-based beacon



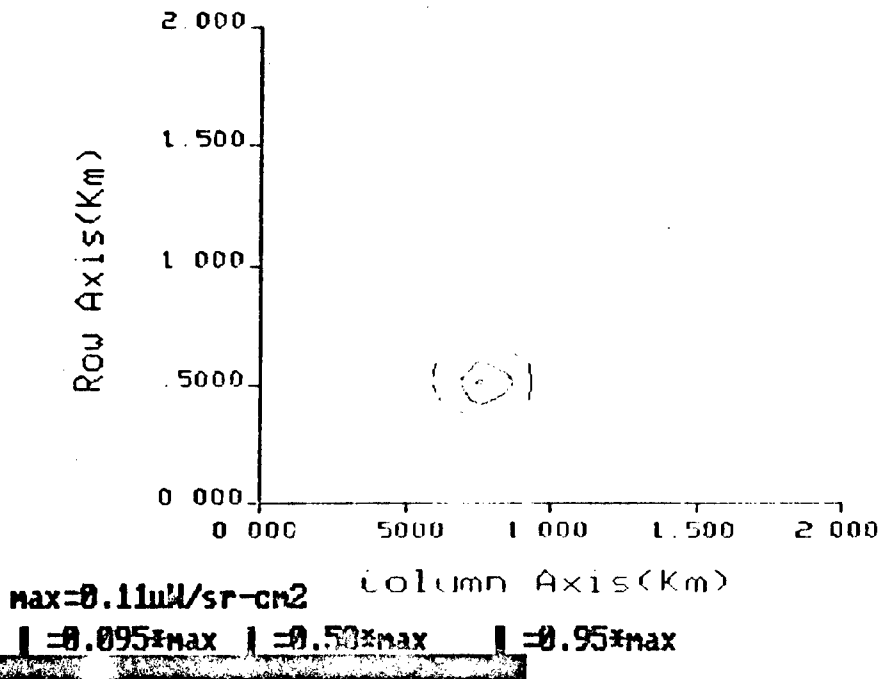


Observing sensor:	UVPI (Feb. 18, 1991)
Target observed:	STRYPI, Antares stage
Range of frames used:	10963 - 11190
Number of superposed images:	40
Camera:	Tracker
Spectral band (nm):	255 - 450
Displayed image size (km):	2 (vertical) x 2 (horizontal)
Average range (km):	462
Pixel footprint (m) @ range:	66.0 (vertical) x 84 (horizontal)
Aspect angle (deg):	90
*Photoevents/s:	$6.42 \times 10^4$
*Apparent peak radiance ( $\mu\text{W}/\text{sr}\cdot\text{cm}^2$ ):	1.06
*Apparent peak spectral radiance @ 390 nm ( $\mu\text{W}/\text{sr}\cdot\text{cm}^2\cdot\mu\text{m}$ ):	8.49

\*For brightest pixel

Fig 59 - Tracker-camera contour plot for interval 3





Observing sensor:	UVPI (Feb. 18, 1991)
Target observed:	STRYPI, Star 27 stage
Range of frames used:	13489 - 13509
Number of superposed images:	23
Camera:	Tracker
Spectral band (nm):	255 - 450
Displayed image size (km):	2 (vertical) x 2 (horizontal)
Average range (km):	515
Pixel footprint (m) @ range:	73.6 (vertical) x 33.7 (horizontal)
Aspect angle (deg):	53
*Photoevents/s:	6.78x10 <sup>3</sup>
*Apparent peak radiance ( $\mu$ W/sr-cm <sup>2</sup> ):	1.12x10 <sup>-1</sup>
*Apparent peak spectral radiance @ 390 nm ( $\mu$ W/sr-cm <sup>2</sup> - $\mu$ m):	8.96x10 <sup>-1</sup>

\*For brightest pixel

Fig. 60 Tracker camera contour plot for interval 6

Even though the plume central region looked like a point source to the tracker camera, a low-intensity trail, extending beyond the field of view of the tracker camera, was observed in the tracker camera during the Antares stage.

For example, Fig. 61 shows a three-dimensional plot of the superposed image that results from data interval 1 during the Antares burn. The z axis corresponds to the plume source amplitude, in photoevents/s, as a function of position over a 64 by 64 pixel region. A reduced pseudo-color image of the same region is overlaid on the upper right-hand corner of this figure. Notice the presence of a faint trail to the left of the central region. Figure 62 is identical to Fig. 61, except that the data were clipped to 20% of the peak amplitude in Fig. 61. This was done to emphasize the presence of the trail. The radiometric values of the trail are higher than the minimum detectable number of photoevents/second, reported in Section 4.7, for the tracker camera during interval 1. Hence, the trail is believed to be real. Figures 63 - 68 show similar results for intervals 2, 3, and 4.

During the Star 27 burn, no extended trail was observed in the tracker camera. Notice, from Figs. 69 and 70, that the Star 27 peak signal level on PC-1, interval 5, is about an order of magnitude smaller than the Antares peak signal level on PC-1, interval 4. On the other hand, the minimum detectable number of photoevents/s during interval 5 is about 15 times smaller than the corresponding value during interval 4. Hence, one can conclude that during the Star 27 burn no detectable trail was observed even though the relative sensitivity was better. The trail was not observed in data intervals 6 or 7 either.

The trail observed in the tracker camera during the Antares burn is the same cloud that the UVPI tracked after the Antares burnout, which is discussed in Section 8.

NRL/BENDIX STRYPI Observation  
Tracker Set=1 255-450nm

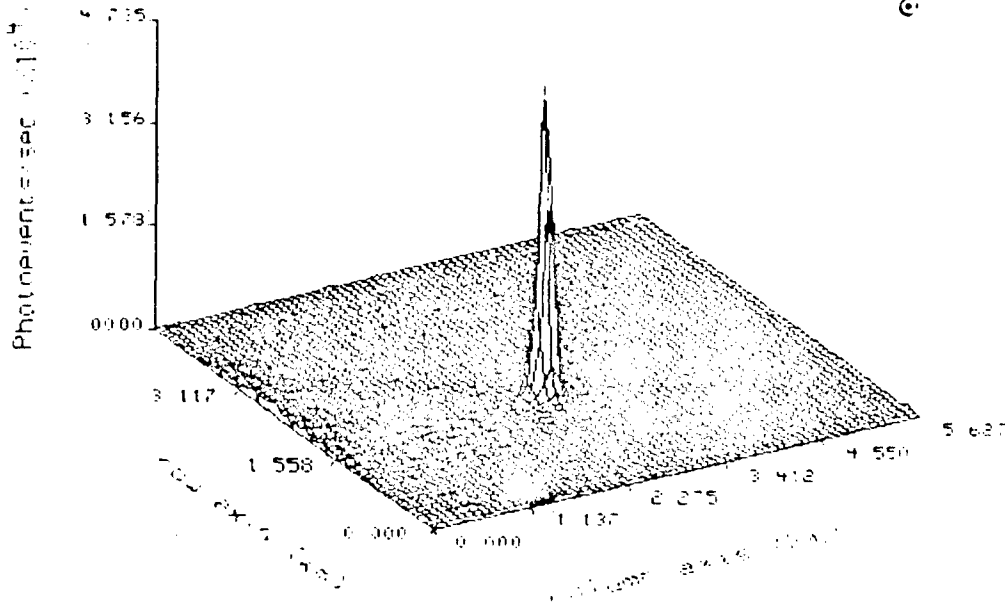


Fig. 61 - Tracker-camera response over a 64 by 64 pixel region, interval 1

NRL/BENDIX STRYPI Observation  
Tracker Set=1 255-450nm

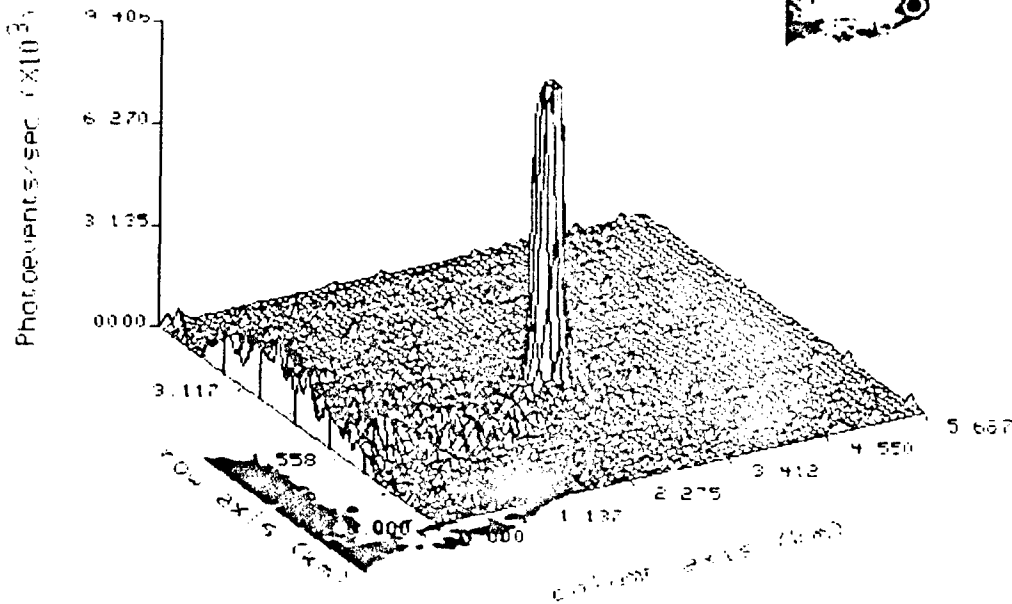


Fig. 62 - Clipped tracker-camera response over a 64 by 64 pixel region, interval 1





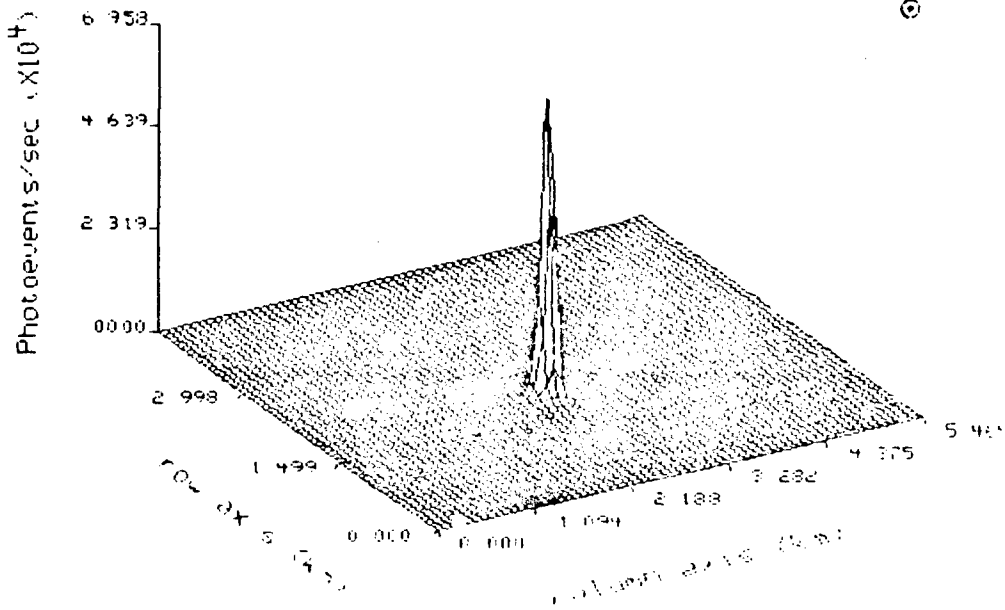


Fig. 63 - Tracker camera response over a 64 by 64 pixel region, interval 2

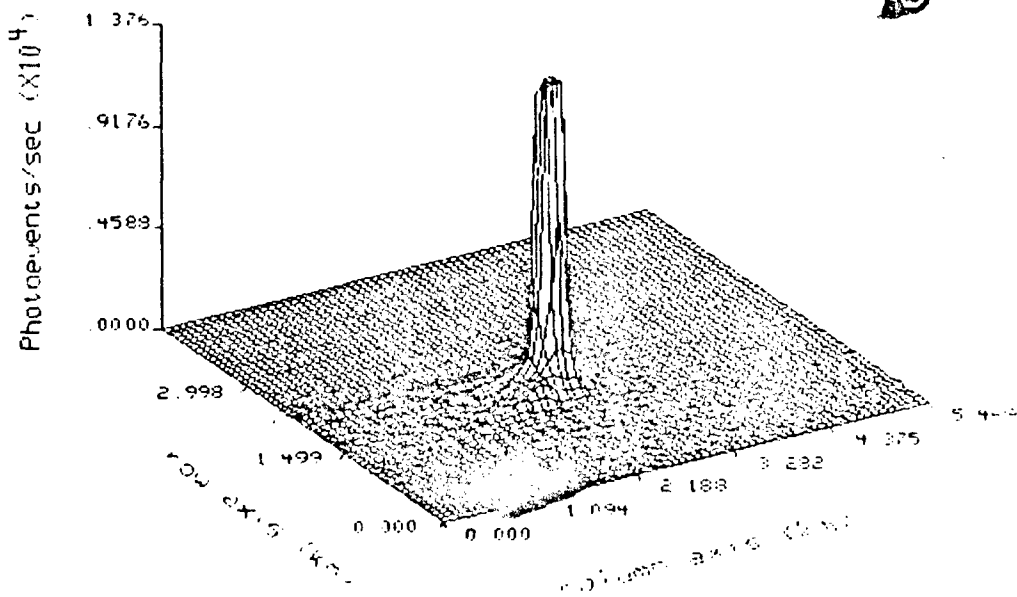


Fig. 64 - Clipped tracker-camera response over a 64 by 64 pixel region, interval 2



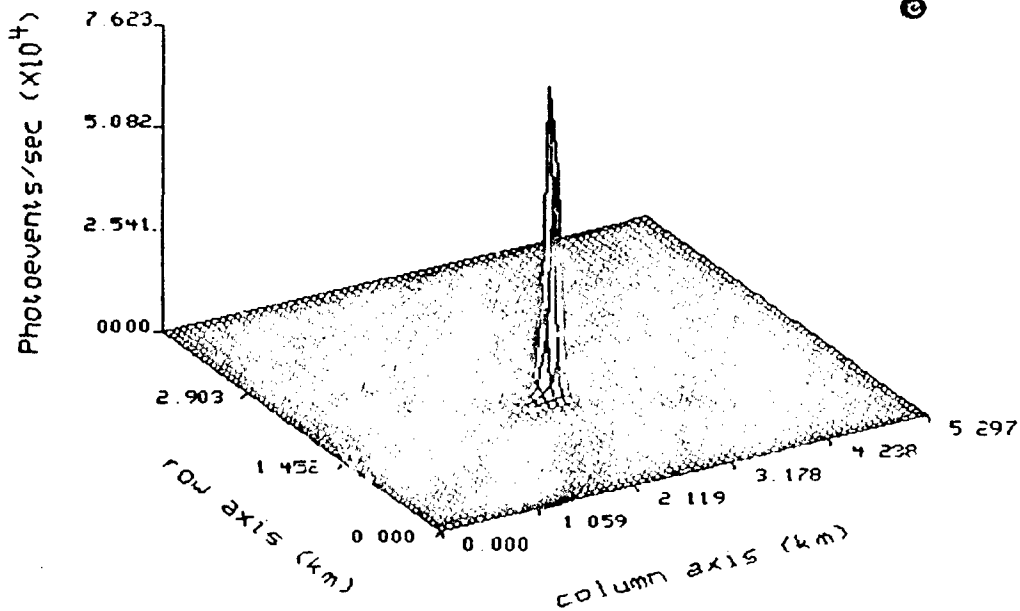


Fig. 65 - Tracker-camera response over a 64 by 64 pixel region, interval 3

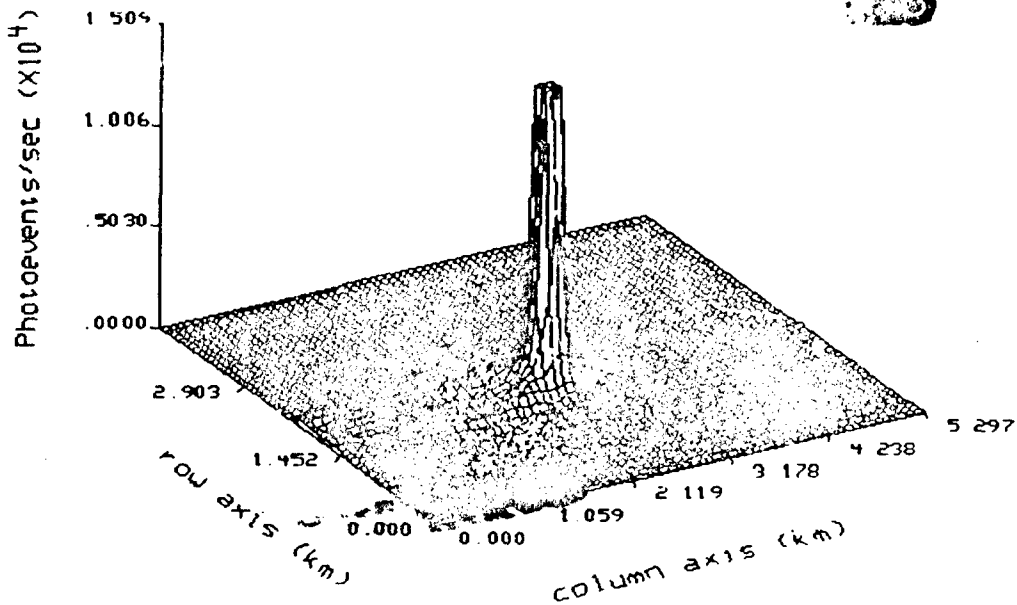


Fig. 66 - Clipped tracker-camera response over a 64 by 64 pixel region, interval 3



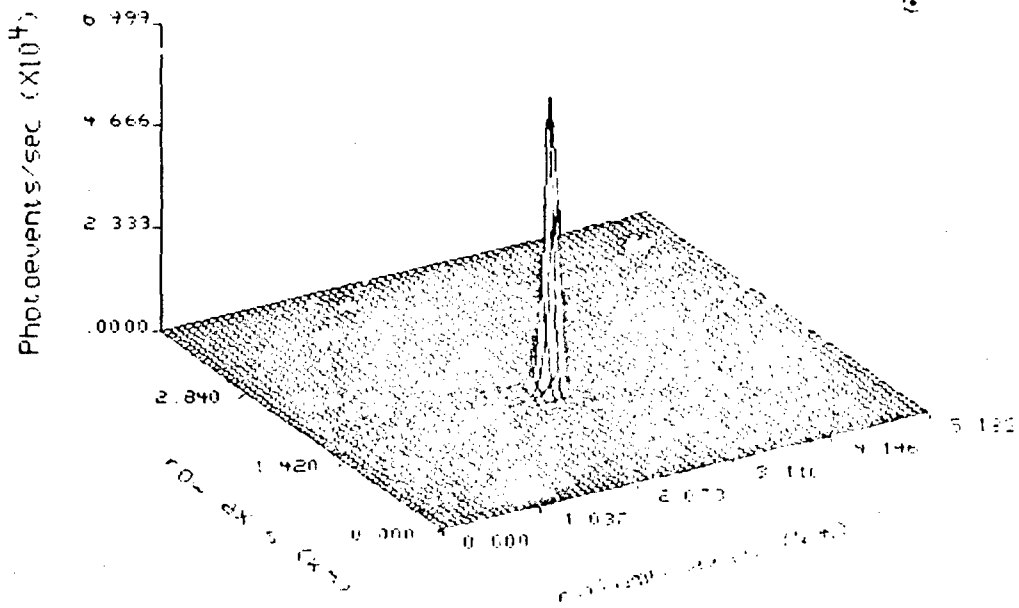


Fig. 67 - Tracker-camera response over a 64 by 64 pixel region, interval 4

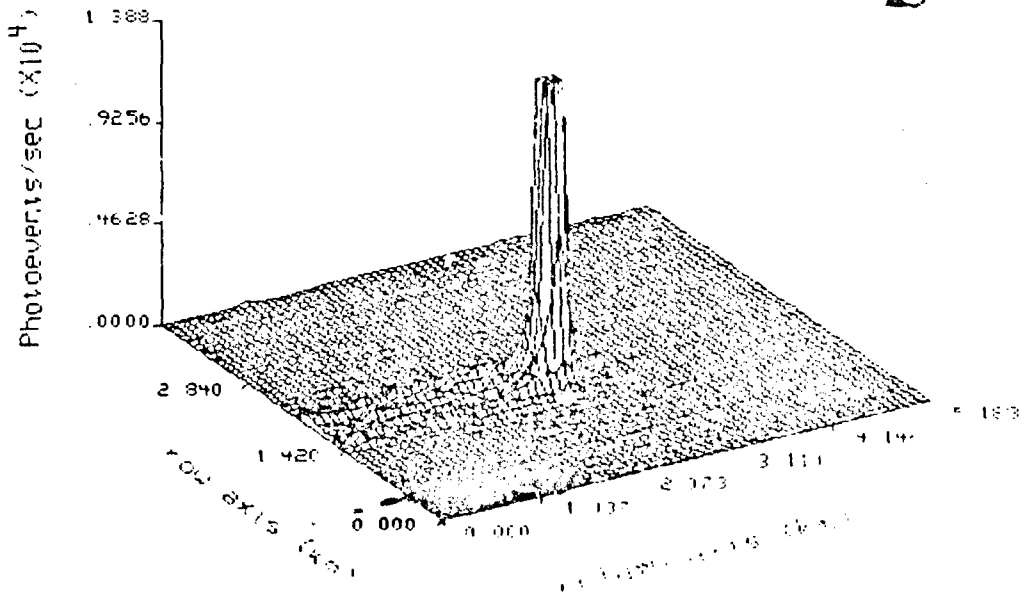


Fig. 68 - Clipped tracker-camera response over a 64 by 64 pixel region, interval 4



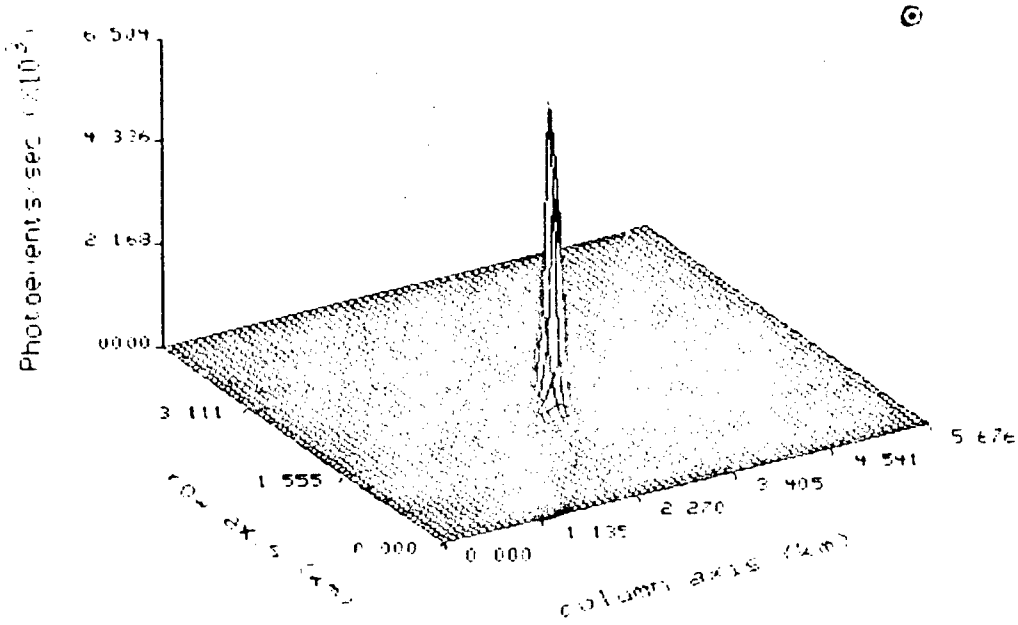


Fig. 69 - Tracker-camera response over a 64 by 64 pixel region, interval 5

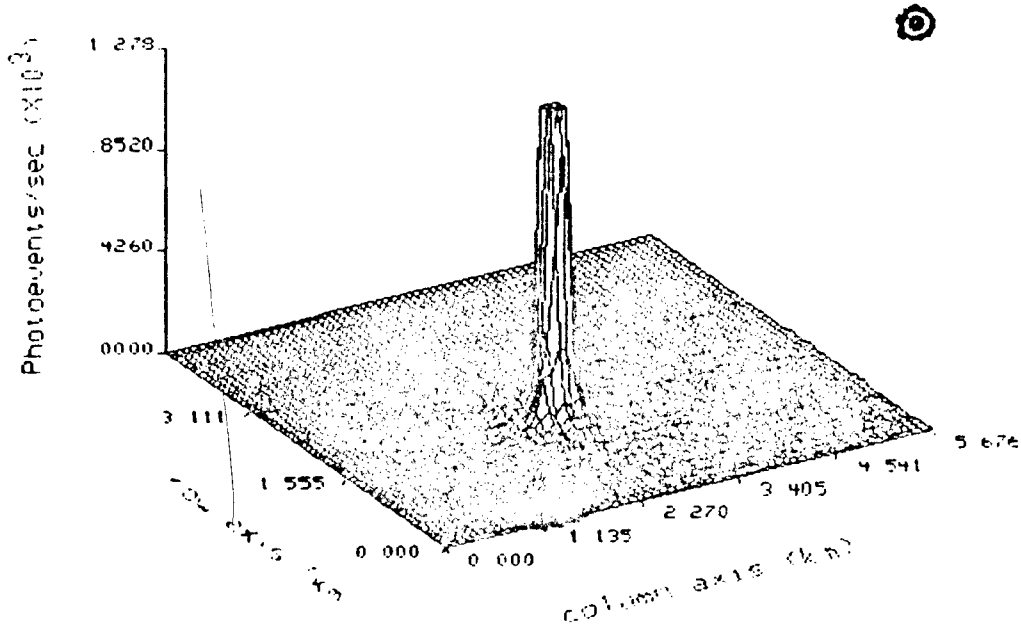


Fig. 70 - Clipped tracker-camera response over a 64 by 64 pixel region, interval 5





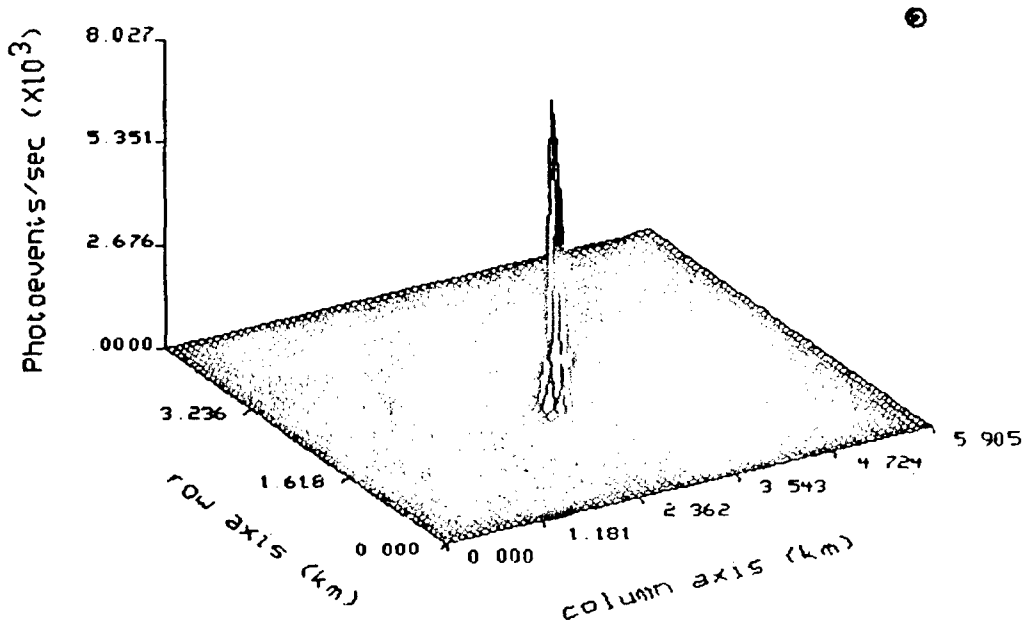


Fig. 71 - Tracker-camera response over a 64 by 64 pixel region, interval 6

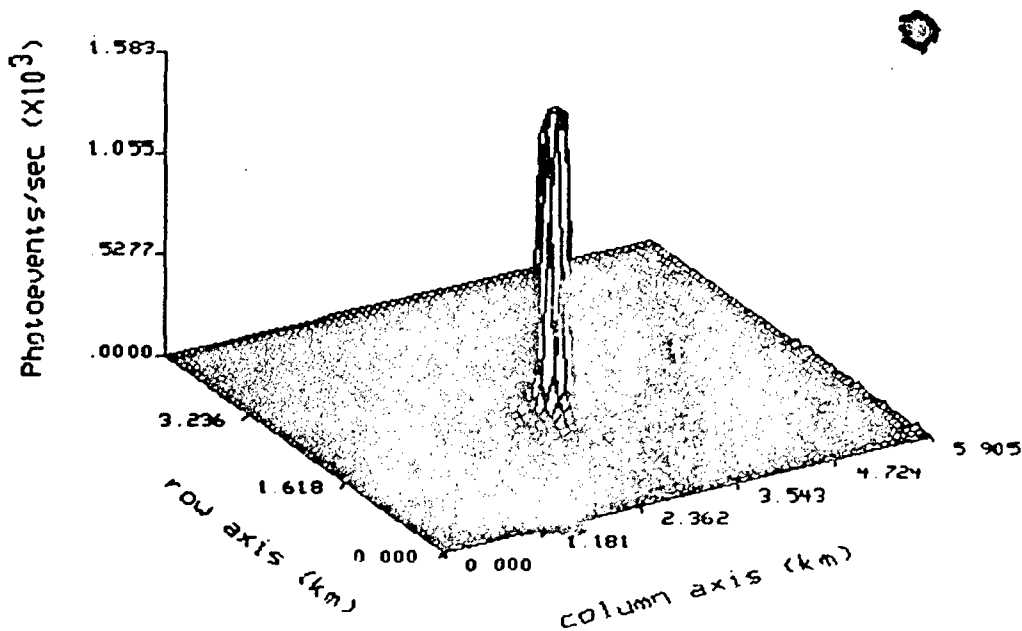


Fig. 72 - Clipped tracker-camera response over a 64 by 64 pixel region, interval 5



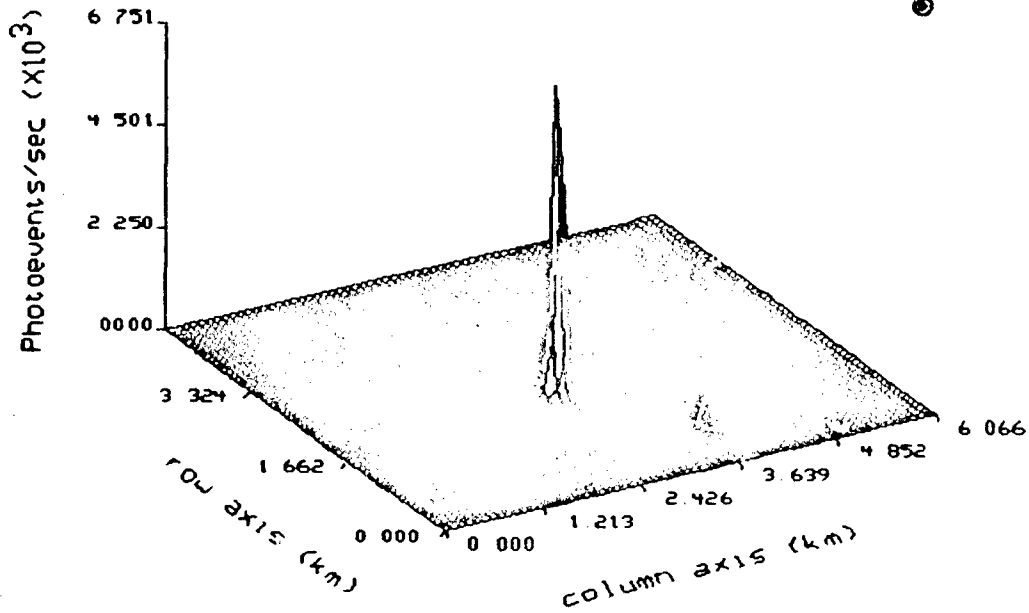


Fig. 73 - Tracker-camera response over a 64 by 64 pixel region, interval 7

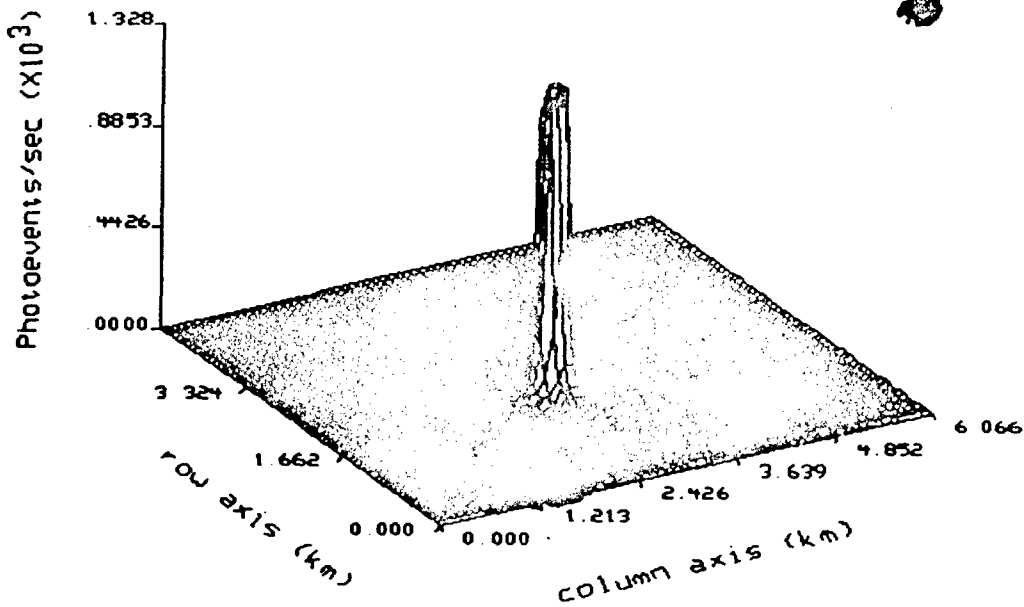


Fig. 74 - Clipped tracker-camera response over a 64 by 64 pixel region, interval 7

#### 5.4 Plume Extent and Point Spread Function

The effective UVPI point spread function (PSF) is defined as the response of the instrument to a point source, e.g., a star or a ground-based beacon. An understanding of the UVPI plume camera's PSF is critical in establishing the maximum size of the observed Antares and Star 27 plumes. Table 31 summarizes the estimated plume central region axial length for each data interval during the Antares burn. The observed plume length during the Antares and Star 27 burns, from peak to 50% of peak, is about 35 m. These plume length estimates do not incorporate corrections for the aspect angle or for the plume camera's PSF. The plume length observed during the Star 27 burn is not shown because of the significant amount of tracking jitter that took place during this burn

Table 31 - Observed Axial Length of Plume Central Region

Interval	Stage	Filter	Peak to 50% Maximum (m)	Peak to 10% Maximum (m)
1	Antares	PC-4	35	100
2	Antares	PC-3	38	105
3	Antares	PC-2	35	105
4	Antares	PC-1	35	93

Based on review of UVPI data from many observations, one may conclude that the plume camera's PSF depends on the observation modality, i.e., downward looking versus sideward looking. Sideward looking observations use the door-mounted mirror but downward looking observations do not. The observation of the Antares and Star 27 plumes did not use the door-mounted mirror. The existing data for point sources indicate that the PSF is less circularly symmetric when using the door-mounted mirror. This could be the result of jitter in the door mirror.

Figure 26 shows a plume-camera image of a ground-based beacon. A scaled version of the plume camera's PSF for the beacon is presented in Table E6. The intensity values were scaled such that the brightest pixel will map to 1. Figure 75 shows a three-dimensional plot of the PSF that results from observation of the ground-based beacon. For the ground-based beacon, the axial length of the PSF from peak to 50% of the peak along the major axis is about 20 m at a range of 450 km, as shown in Fig. 76. The FWHM is about 40 m. In conjunction with the discussion in Section 5.5, this suggests that the actual axial length of the Antares plume, as measured by peak to 50% of maximum (in the data waveband), is no more than 15 m. This is in agreement with CHARM 1.3 predictions (see Section 5.5).

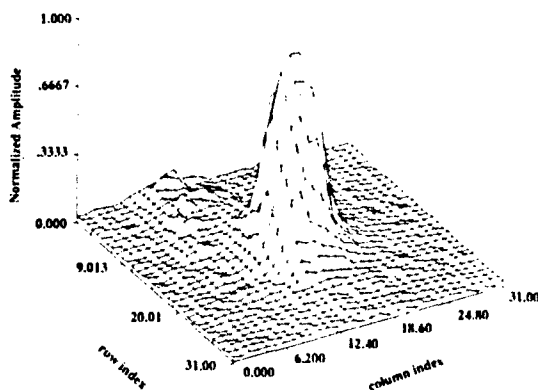


Fig. 75 - Plume-camera PSF for ground-based beacon

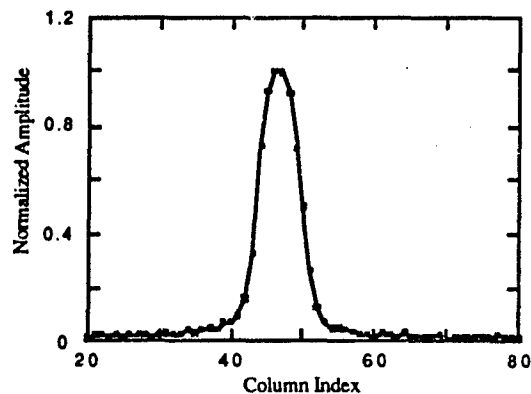


Fig. 76 - Axial profile through plume-camera PSF for ground-based beacon

Figures 77 through 83 show profiles of the radiance along the major axis of the plume, measured by the plume camera, for each of the data intervals. The horizontal line in each figure corresponds to the NER sensitivity limit after image superposition. It is evident from these figures that, after image superposition, a good SNR was achieved for all filters during the Antares burn, and a marginal SNR was achieved during the Star 27 burn.

Figure 36 shows a tracker-camera image of a ground-based beacon. A scaled version of the tracker camera's PSF for the beacon is presented in Table E7. The intensity values were scaled such that the brightest pixel will map to 1. Figure 84 shows a three-dimensional plot of the PSF that results from observation of the ground-based beacon, and Fig. 85 is an axial profile of the beacon as seen by the tracker camera.

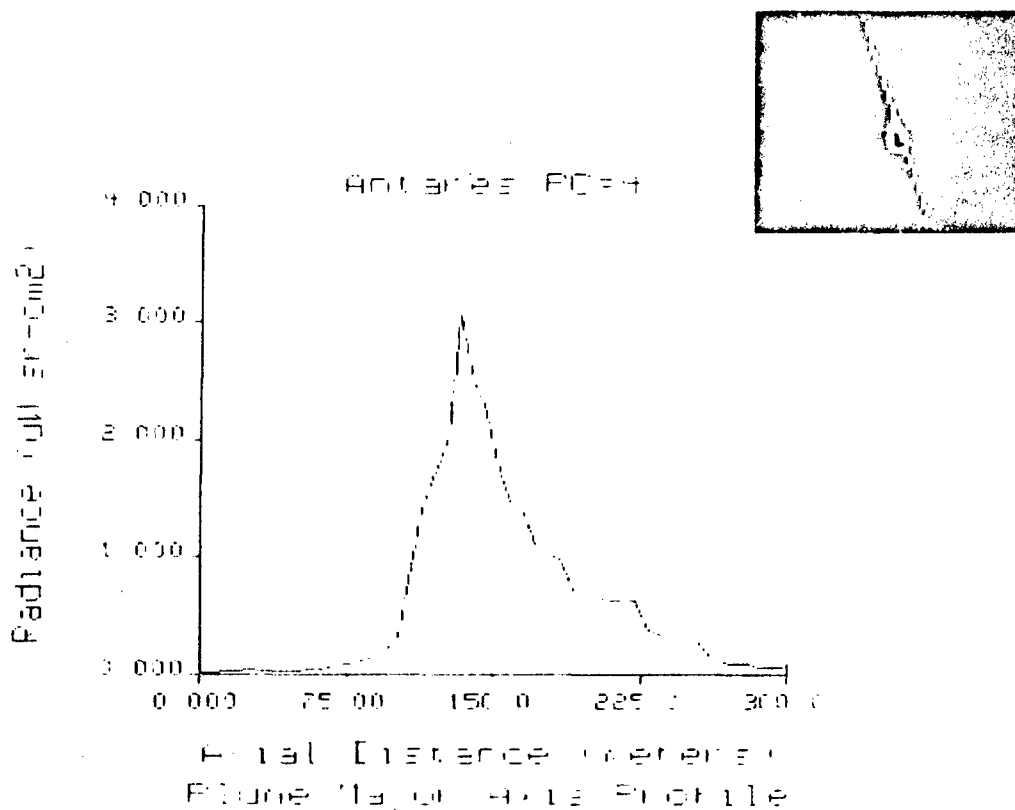


Fig. 77 Axial profile along plume central region for data interval 1, plume camera



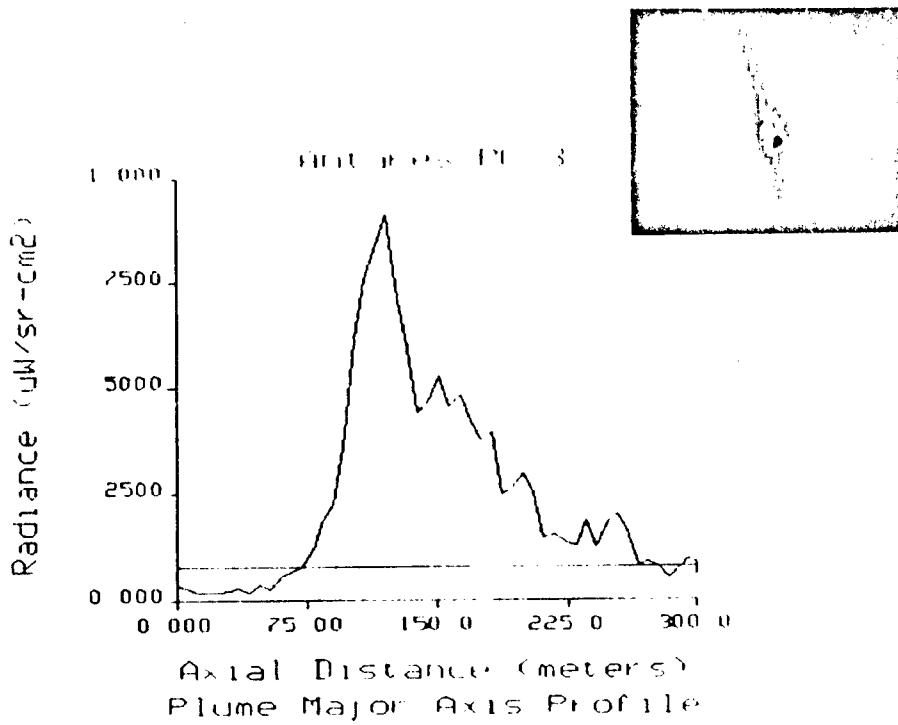


Fig. 78 - Axial profile along plume central region for data interval 2, plume camera

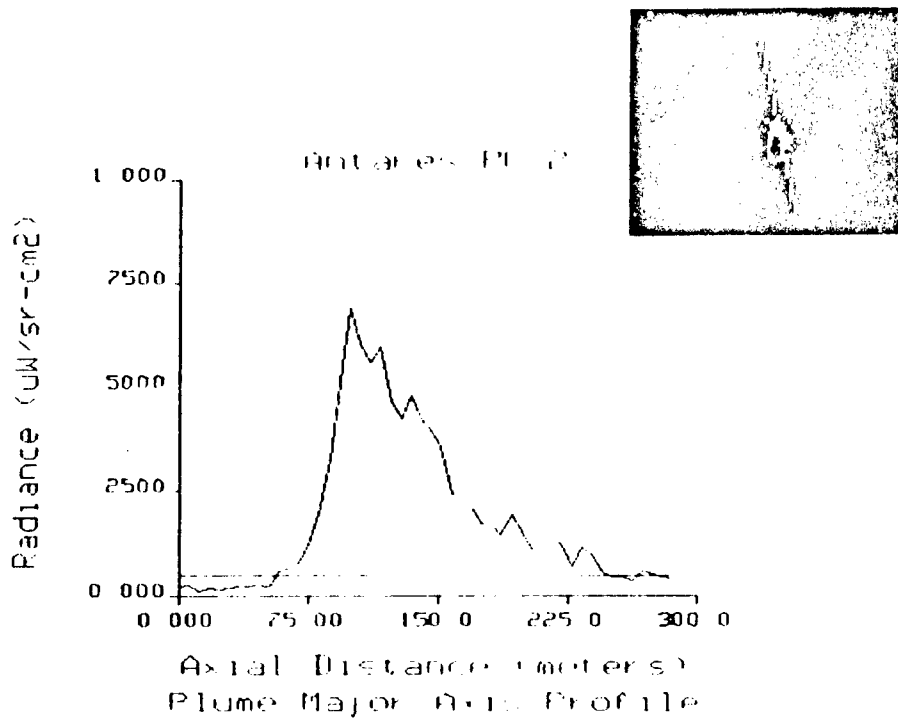


Fig. 79 - Axial profile along plume central region for data interval 3, plume camera





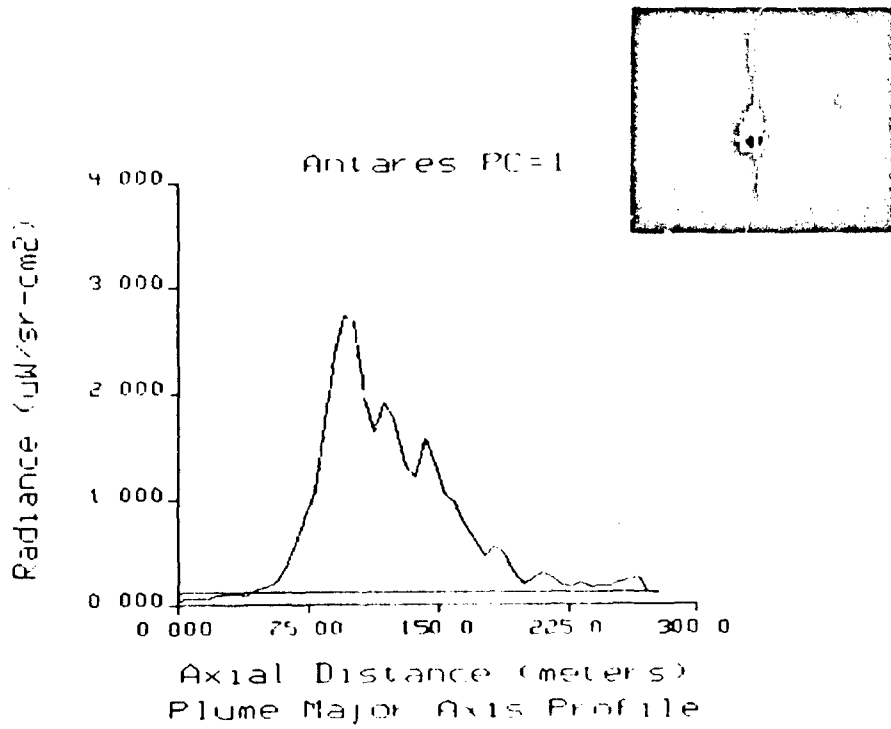


Fig. 80 - Axial profile along plume central region for data interval 4, plume camera

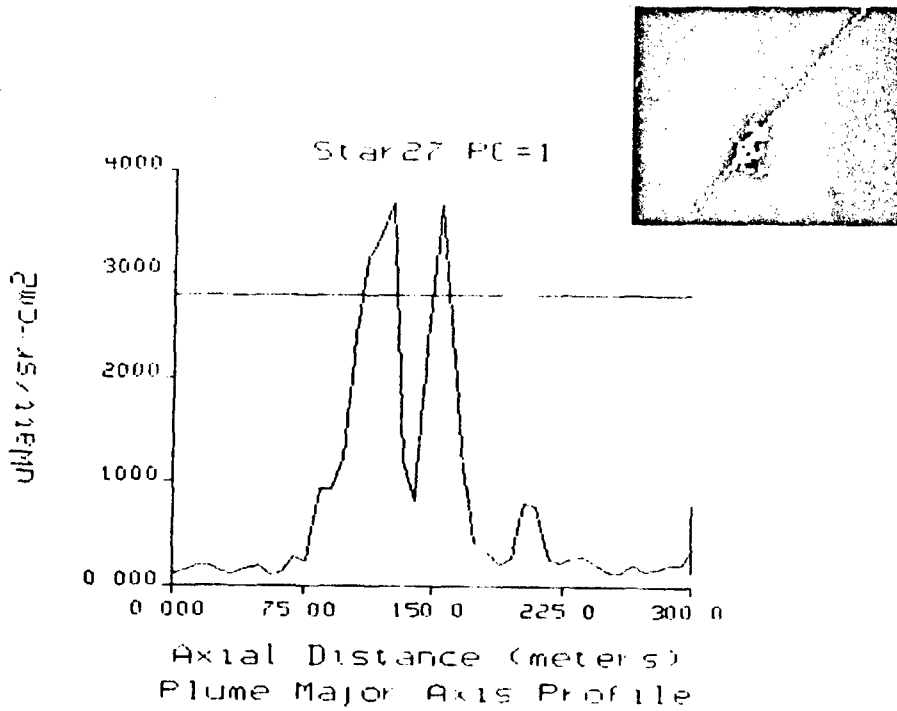


Fig. 81 - Axial profile along plume central region for data interval 5, plume camera



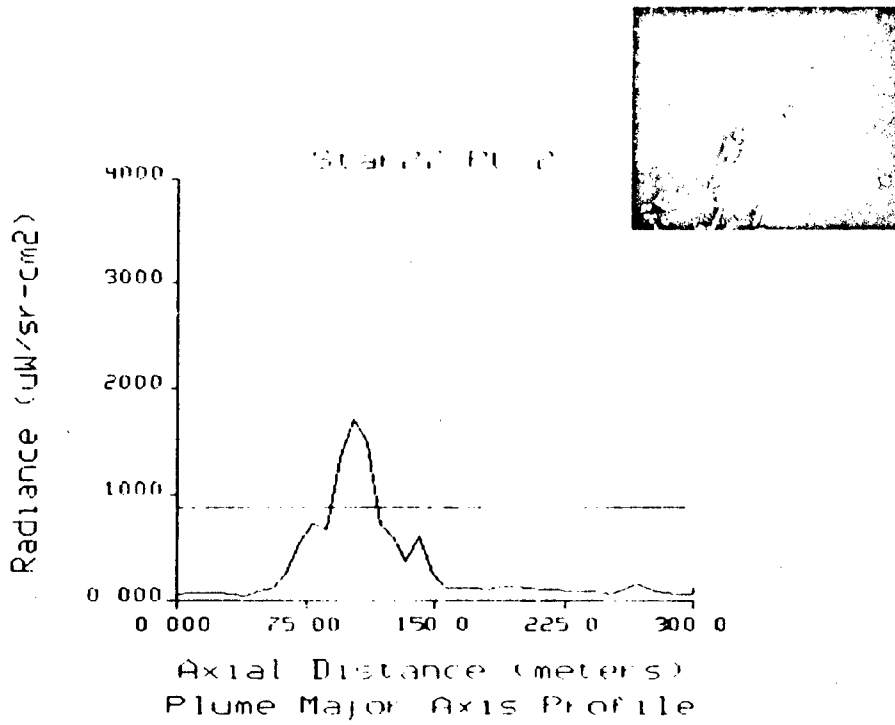


Fig. 82 - Axial profile along plume central region for data interval 6, plume camera

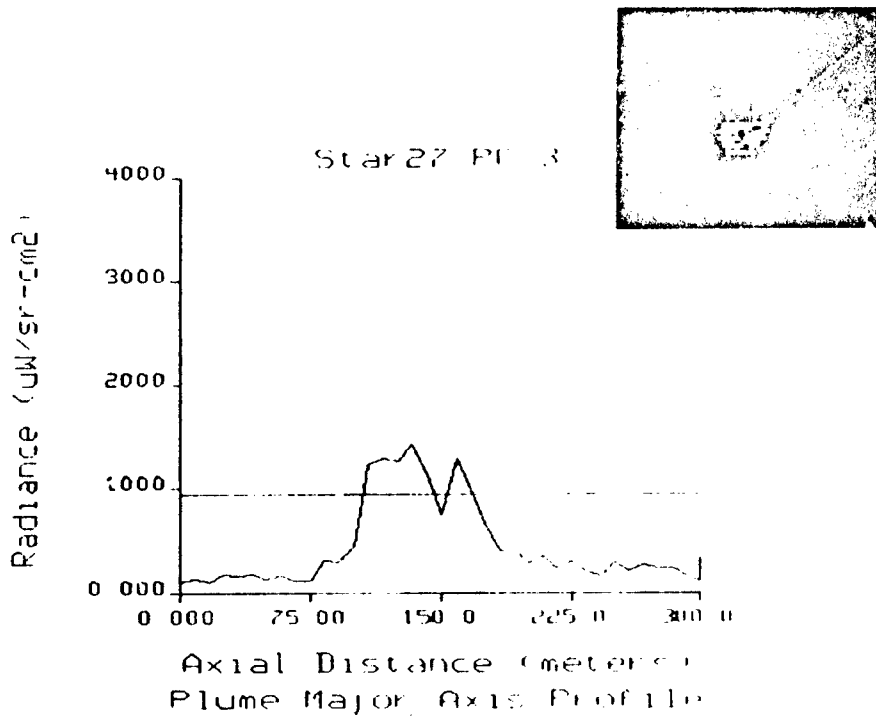


Fig. 83 - Axial profile along plume central region for data interval 7, plume camera

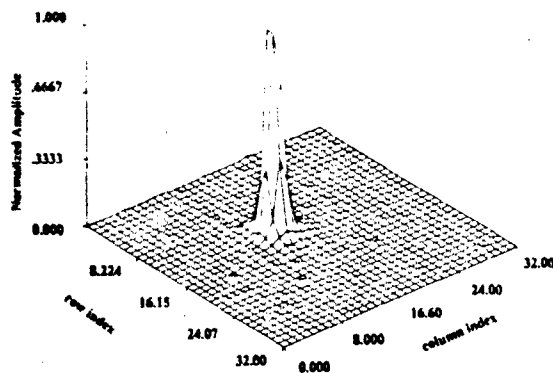


Fig. 84 - Tracker-camera PSF for ground-based beacon

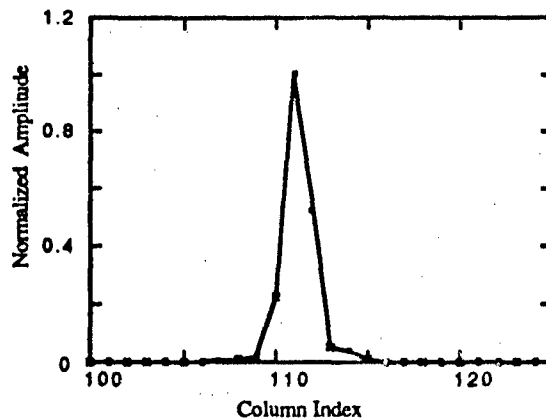


Fig. 85 - Axial profile through tracker-camera PSF for ground-based beacon

### 5.5 Comparison of Results to CHARM 1.3 Predictions

This subsection compares the UVPI measurements to the predictions provided by a theoretical plume model. The Institute for Defense Analyses (IDA) generated a number of CHARM 1.3 runs in which both the Antares and Star 27 stages were modeled [10,15], using each of the UVPI's plume-camera filter bandpasses. The following parameters were common to all the runs:

Model:	CHARM 1.3
Object modeled:	Intrinsic core
Aspect:	90°
Horizontal resolution:	5.0 m
Vertical resolution:	5.0 m

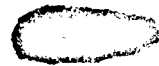
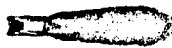
In all of IDA's runs, a 5 by 5-m pixel resolution was used. To get a comparison between the CHARM 1.3 predictions and the UVPI measurement, the CHARM 1.3 predictions were convolved with an estimate of the UVPI's PSF. A normalized version of the ground beacon image, Frame 12778, Orbit 1173, was used as the best UVPI plume-camera PSF estimate.

Figures 86 and 87 show an example of the CHARM 1.3 prediction convolved with the UVPI point spread function (PSF). The left image in Fig. 86 shows a false-color CHARM 1.3 image prediction with 5-m resolution for the Antares stage, assuming it is being observed with PC-4. The right image shows the same CHARM 1.3 prediction, except that it is convolved with the UVPI point spread function. Figure 87 is the corresponding contour plot for the image prediction, again assuming UVPI PC-4 and convolution with UVPI PSF. The CHARM 1.3 Antares plume predictions and contour plots for the other UVPI filter positions, as well as those for the Star 27 stage, are qualitatively similar to those shown in Figs. 86 and 87.

For each of the seven data intervals, Figs. 88 through 94 show: the CHARM 1.3 high-resolution prediction of the plume radiance as a function of axial distance; the CHARM 1.3 prediction convolved with the UVPI plume camera PSF; and a horizontal line depicting the noise equivalent radiance (NER) of the plume camera. For the Antares stage, intervals 1 through 4, the data interval NER, i.e., the NER obtained after image superposition, is too low to appear on the graph. For the Star 27 stage, the predicted plume signal is marginally over the data interval NER and well below the single-image NER. This explains the spatially nonhomogeneous aspect of the processed images for the Star 27 stage.

CHARM1.3 Prediction  
Using 5 Meter Resolution

Charm1.3 Prediction  
Using UVPI's PSF

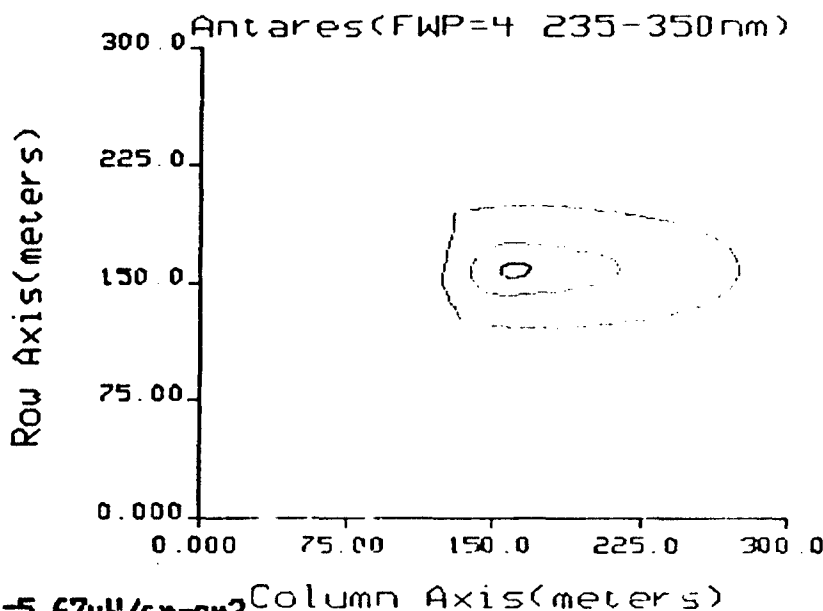


max=18uW/sr-cm<sup>2</sup>

                     =0.095\*max                         =0.50\*max                         =0.95\*max

NRL/ACT 8/13/91

Fig. 86 - High-resolution and PSF-convolved CHARM 1.3 image prediction of UVPI's Antares observation using PC-4



max=5.67uW/sr-cm<sup>2</sup>

                     =0.095\*max                         =0.50\*max                         =0.95\*max

NRL/ACT 6/3/91

Fig. 87 - PSF convolved CHARM 1.3 contour plot prediction of UVPI's Antares observation using PC-4

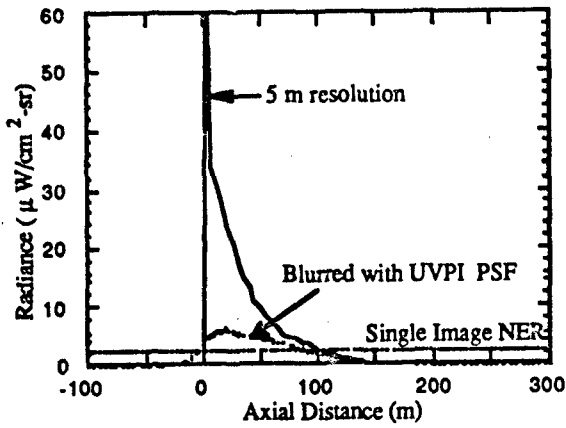


Fig. 88 - CHARM 1.3 predicted axial profile along plume for data interval 1, plume camera

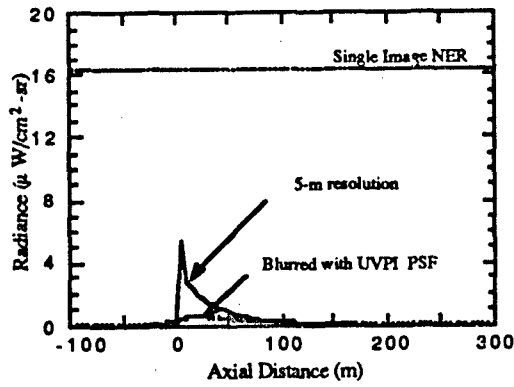


Fig. 89 - CHARM 1.3 predicted axial profile along plume for data interval 2, plume camera

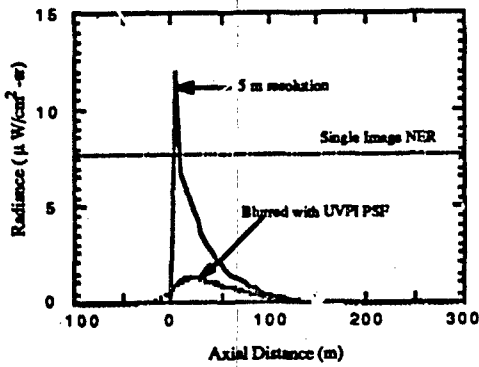


Fig. 90 - CHARM 1.3 predicted axial profile along plume for data interval 3, plume camera

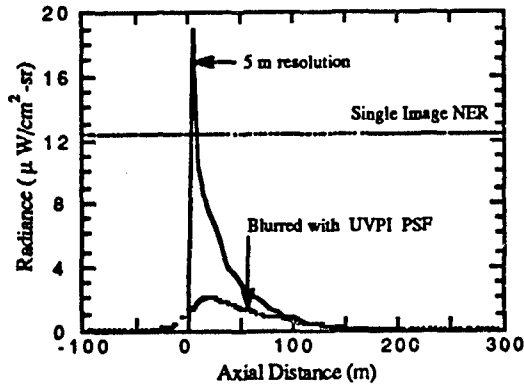


Fig. 91 - CHARM 1.3 predicted axial profile along plume for data interval 4, plume camera

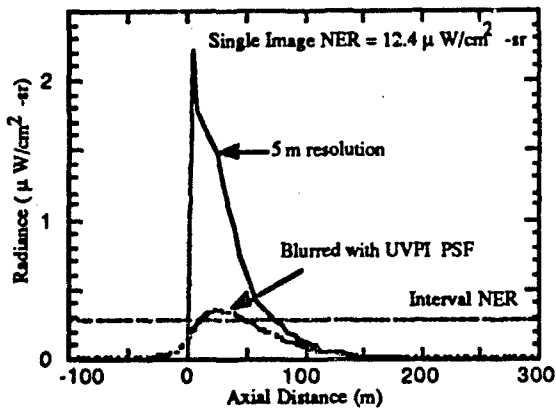


Fig. 92 - CHARM 1.3 predicted axial profile along plume for data interval 5, plume camera

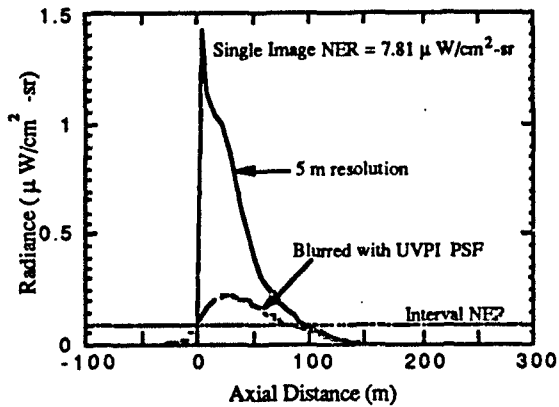


Fig. 93 - CHARM 1.3 predicted axial profile along plume for data interval 6, plume camera

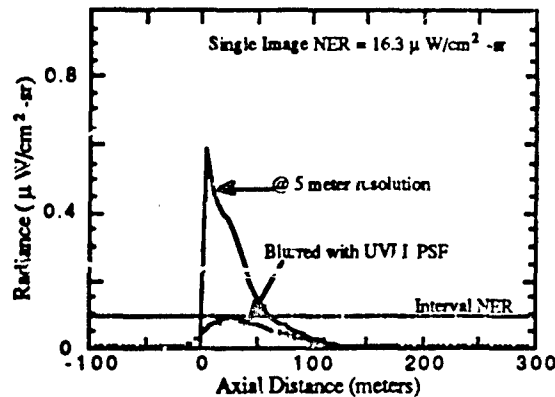


Fig. 94 - CHARM 1.3 predicted axial profile along plume for data interval 7, plume camera

An effect of the UVPI PSF is to reduce the peak signal level. Based on the prediction shown in Fig. 88, one may note that even after introducing the effect of the UVPI PSF, a single image in interval 1, using PC-4, could provide a strong signal well above the UVPI radiometric sensitivity. This is in strong agreement with the observation. On the other hand, the single-image radiance in interval 2, PC-3, would be below UVPI's radiometric sensitivity level. However, since more than 200 images were averaged in interval 2, the effective sensitivity was lowered to the point where high SNR per pixel was achieved. Table 32 provides a qualitative estimate, based on CHARM 1.3 and convolution with the UVPI PSF, of the data quality in each interval.

Table 32 - Strypi Data Quality Estimate

Data Interval	Single Image	Superposed Images	SNR Comment
1	Good (above NER)	Excellent	High
2	Poor (below NER)	Good	Good after processing
3	Marginal	Good	Good after processing
4	Marginal	Good	Good after processing
5	Very poor	Marginally useful	Marginal after processing
6	Very poor	Useful	Marginal after processing
7	Very poor	Marginally useful	Marginal after processing

The close agreement between data quality estimates and the observations suggests that the high-resolution CHARM 1.3 predictions and the UVPI sensor characterization information can be used in planning an observation to guarantee adequate SNR.

The peak radiances and the plume lengths for the CHARM 1.3 image predictions are listed in Tables 33 and 34. These tables list computed results for both the Antares and Star 27 stages and for UVPI filters used for the observation of these stages.

In Table 34 measured plume lengths are not reported for the Star 27 stage. A reliable estimate of the plume length of the Star 27 could not be made because of inadequate tracking and signal level during its burn. However, one may observe that the predicted CHARM 1.3 plume length is independent of the spectral band being modeled. The resulting CHARM 1.3 predicted length modified by UVPI's PSF for the Antares stage is in good agreement with the observed Antares plume length.



Table 33 - Peak Radiance Comparison

Interval	Stage	Filter	CHARM 1.3 @ 5-m Resolution Peak Radiance ( $\mu\text{W}/\text{sr}\text{-cm}^2$ )	CHARM 1.3 Convolved Peak Radiance ( $\mu\text{W}/\text{sr}\text{-cm}^2$ )	UVPI Measured Peak Radiance ( $\mu\text{W}/\text{sr}\text{-cm}^2$ )
1	Antares	PC-4	61.50	6.3	2.99
2	Antares	PC-3	5.28	0.52	0.92
3	Antares	PC-2	11.98	1.3	0.69
4	Antares	PC-1	18.9	2.0	2.72
5	Star 27	PC-1	2.21	0.36	—
6	Star 27	PC-2	1.42	0.23	0.18
7	Star 27	PC-3	0.583	0.09	—

Table 34 - Comparison of Measured to Predicted Plume Length

Interval	Stage	Filter	Plume Length (m) Peak to 50% and Peak to 10%					
			CHARM 1.3 @ 5-m Resolution		CHARM 1.3 Using UVPI's PSF		UVPI Measured	
			50%	10%	50%	10%	50%	10%
1	Antares	PC-4	8.5	63	52	110	35	100
2	Antares	PC-3	8.5	63	52	110	38	105
3	Antares	PC-2	8.5	63	52	110	35	105
4	Antares	PC-1	8.5	63	52	110	35	93
5	Star 27	PC-1	30	78	44	100	—	—
6	Star 27	PC-2	30	78	44	100	—	—
7	Star 27	PC-3	30	78	44	100	—	—

The data for interval 6 and the false-color image of the plume imply a compact plume of approximately 15 m from peak to 50% of maximum. This is smaller than the point spread function of the plume camera. This result can be explained by comparing the detectability threshold with the CHARM 1.3 prediction of axial length.

Figure 93 shows: the CHARM 1.3 high-resolution prediction of the plume intensity as a function of axial distance; the CHARM 1.3 prediction convolved with the UVPI plume camera point spread function; and a horizontal line at the noise-equivalent radiance based on the superposed images. Only a small portion of the plume is above the detectability threshold because of the low signal level; therefore, the measured plume length is reduced.

## 6.0 TEMPORAL FEATURES

This section presents calibrated photoevents per image and radiant intensity values for each of the seven data intervals selected. The calibration procedure used is described in Section 4.2. The conversion to radiant intensity is performed by using a reference emission spectrum for incandescent alumina particles that is typical of the emission spectrum produced by solid-fuel rocket motors containing ammonium perchlorate/aluminum. The latter is similar to the model used in the CHARM 1.3 code. The bandpasses of each of the plume camera filters are also shown in Appendix B. Section 6.1 presents the plume camera observations, and 6.2 presents the tracker-camera observations.

As a quick overview, Figs. 95 and 96 show plume-camera long-term trends in the central region spectral radiant intensity for the Antares and Star 27 stages, respectively. The values plotted were derived by assuming the reference spectral shape. Figures 97 and 98 show similar results for the tracker camera's Antares and Star 27 observations, respectively. In Figs. 97 and 98, each interval shows two curves, one assuming a reference spectral shape and the other assuming a flat spectral shape. Although the actual spectral shape is certainly variable over the 19 by 19 pixel region reported for the tracker camera, one can assume that the mean spectral radiant intensity falls somewhere in the range spanned by the two curves. Notice that the tracker-camera mean changes from interval to interval. Consequently, part of the difference among measurements taken with the four filters of the plume camera is attributable to long-term temporal variations rather than to spectral differences.

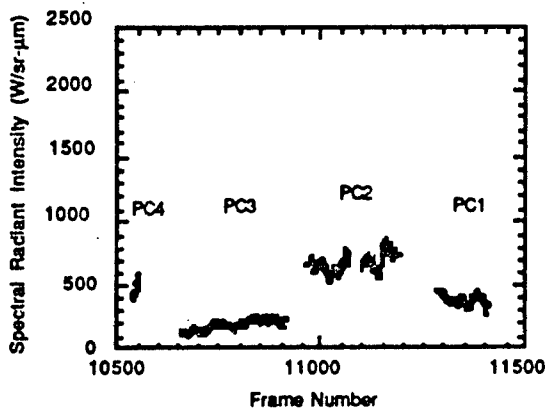


Fig. 95 - Mean central region spectral radiant intensity, plume camera, Antares stage

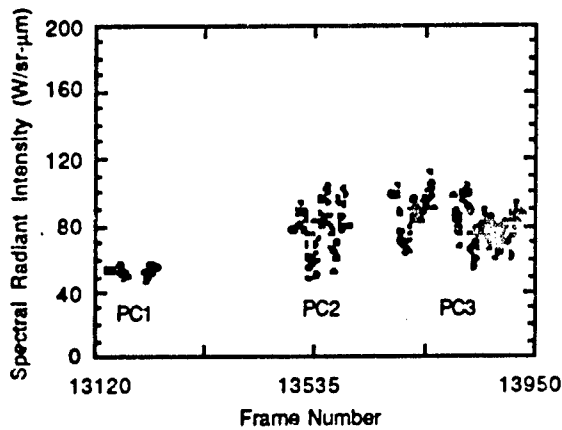


Fig. 96 - Mean central region spectral radiant intensity, plume camera, Star 27 stage

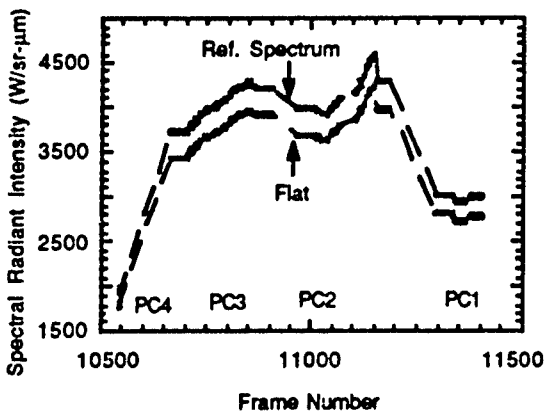


Fig. 97 - Mean spectral radiant intensity, tracker camera, Antares stage

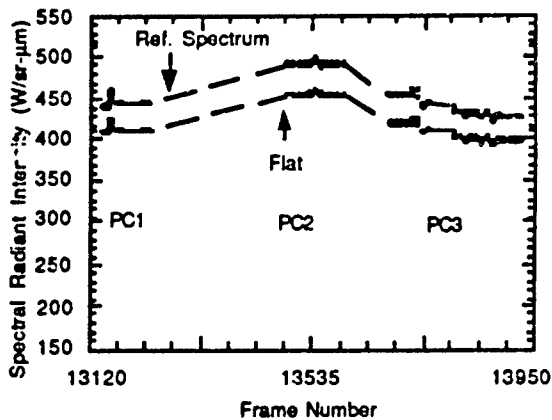


Fig. 98 - Mean spectral radiant intensity, tracker camera, Star 27 stage

Figures 99 and 100 show outer region results for the Antares and Star 27 stages, respectively. The curves shown for each interval correspond to two spectral shape assumptions: flat and reference. Although the actual spectral shape of outer region emissions is not known, it can be assumed that the actual spectral radiant intensity falls somewhere in the range spanned by the two curves. Note that, in general, the centroid wavelength at which spectral radiant intensity is normally reported depends on

the spectral shape assumption made. For these figures, all curves specify spectral radiant intensity at the reference centroid wavelength for each interval.

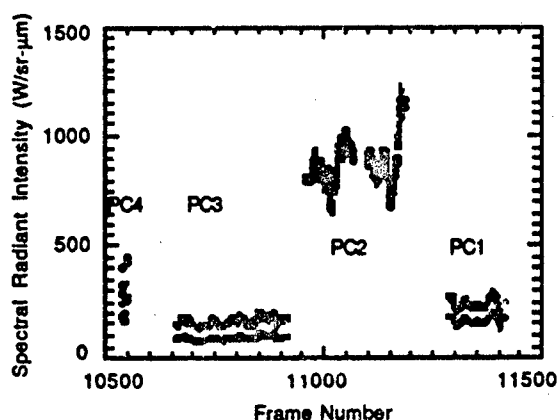


Fig. 99 - Mean outer region spectral radiant intensity, plume camera, Antares stage

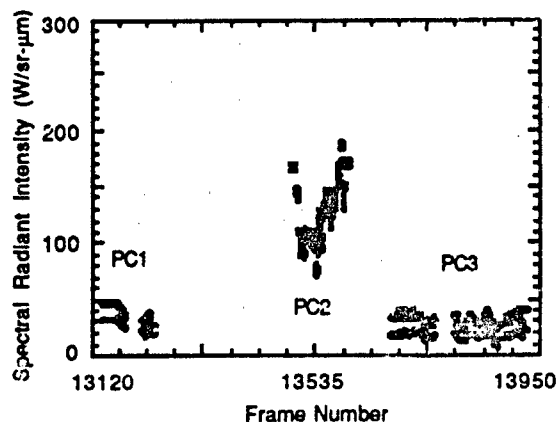


Fig. 100 - Mean outer region spectral radiant intensity, plume camera, Star 27 stage

### 6.1 Plume Camera Radiant Intensity Plots

This section presents the number of photoevents observed in the plume camera for each image of the seven analyzed data intervals. Table 35 lists the figures contained in this section. For intervals 1 through 4, in addition to the total number of photoevents per image, there are plots of the number of photoevents per image in the central and outer regions. The poor quality of the Star 27 tracking did not allow separation into central and outer regions for the Star 27 stage images.

Table 35 - Radiant Intensity Figures

Interval	Stage	Total	Central Region	Outer Region
1	Antares	100	101	102
2	Antares	103	104	105
3	Antares	106	107	108
4	Antares	109	110	111
5	Star 27	112	—	—
6	Star 27	113	—	—
7	Star 27	114	—	—

The plume central region figures also report radiant intensity that is calculated by using a reference source spectral shape. Because of the difficulty of selecting an accurate source spectral shape for the outer region, the conversion of photoevents to radiant intensity was carried out for the outer region component by using two different spectral shapes. The values are reported in Tables 36 and 37 but are not included in the figures.

The separation into plume central and outer regions is described in Section 5.1. During the telemetry frame ranges depicted in each plot, the plume-to-tracker image ratio was primarily 8:2. Consequently, the plots show repeated groups that consist of eight consecutive plume-camera images followed by a gap where the two tracker-camera images occurred.

In addition to the intensities, the figures include: the estimated local mean, which is a running average of the intensity, and a threshold of 3.1 standard deviations above the local mean, which flags intensity values that are highly unlikely (probability less than 0.001) based on local statistics. The

outer region plots, which are computed as the difference between the total and the central region, do not have the threshold. The local statistics are computed by using a running window of 15 frames for plume-camera data. A more complete discussion of the computations of local statistics is contained in Section 4.6.

Figures 101 through 115 convey information useful for:

- indexing those frames or times at which a significant statistical deviation in the intensity is observed, based on the local statistics;
- obtaining a 1:1 comparison between number of photoevents/image and  $W/sr/image$  under the assumption of a reference model; and
- showing the intensity variation over both the plume central region and the plume outer region.

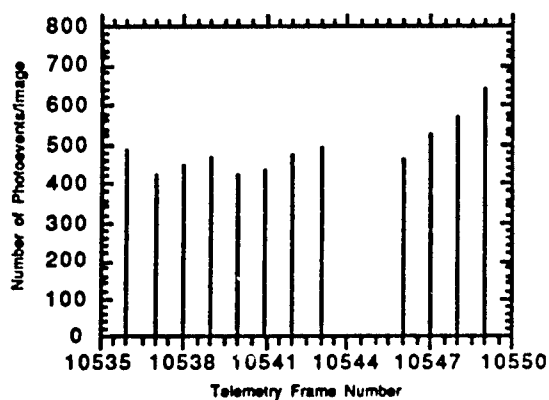


Fig. 101 - Antares, plume camera, total intensity for interval 1

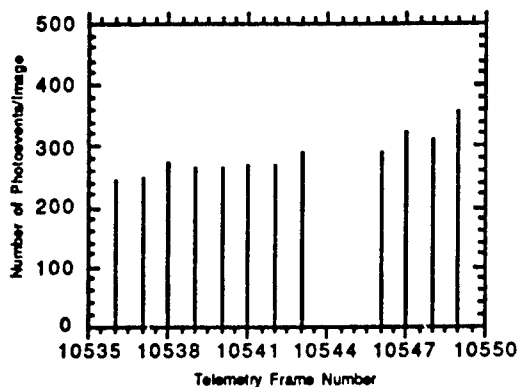


Fig. 102 - Antares, plume camera, central region intensity for interval 1

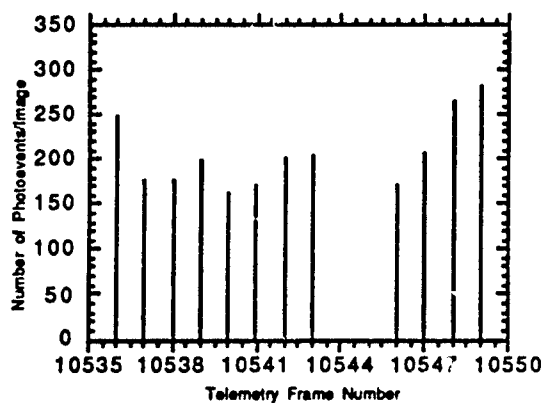


Fig. 103 - Antares, plume camera, outer region intensity for interval 1

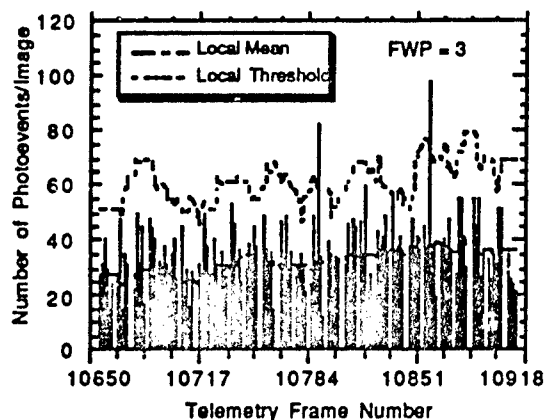


Fig. 104 - Antares, plume camera, total intensity for interval 2

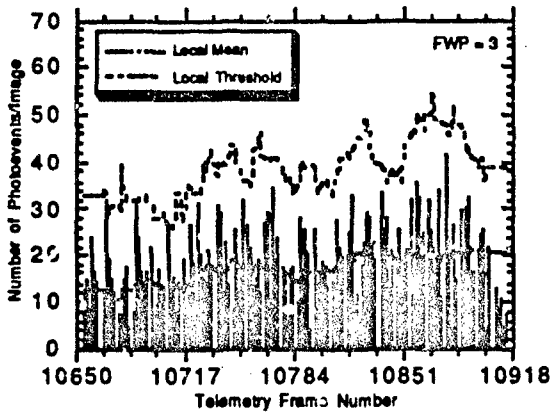


Fig. 105 - Antares, plume camera, central region intensity for interval 2

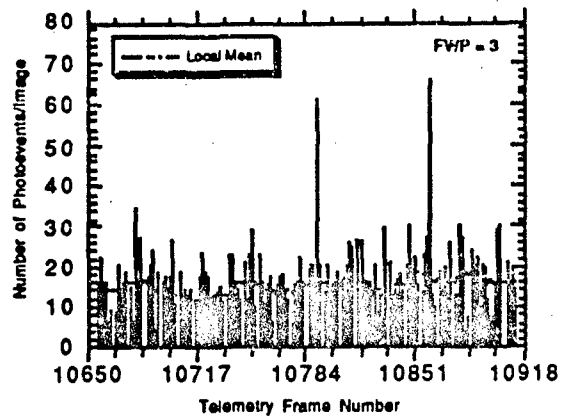


Fig. 106 - Antares, plume camera, outer region intensity for interval 2

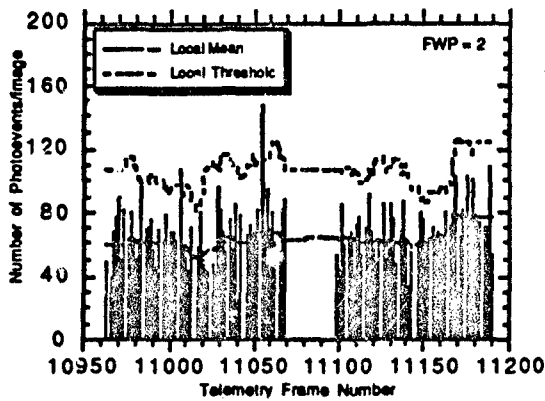


Fig. 107 - Antares, plume camera, total intensity for interval 3

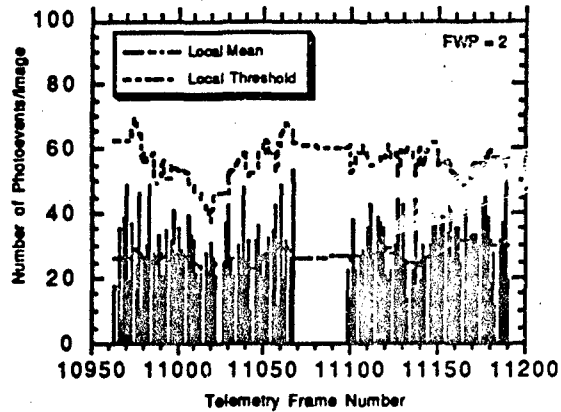


Fig. 108 - Antares, plume camera, central region intensity for interval 3

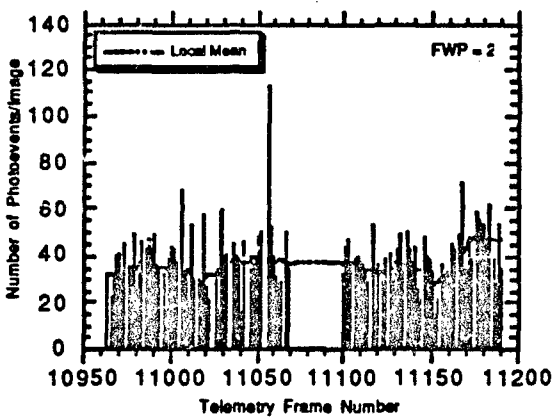


Fig. 109 - Antares, plume camera, outer region intensity for interval 3

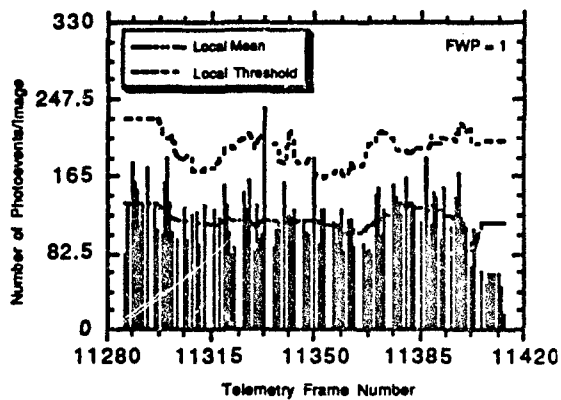


Fig. 110 - Antares, plume camera, total intensity for interval 4

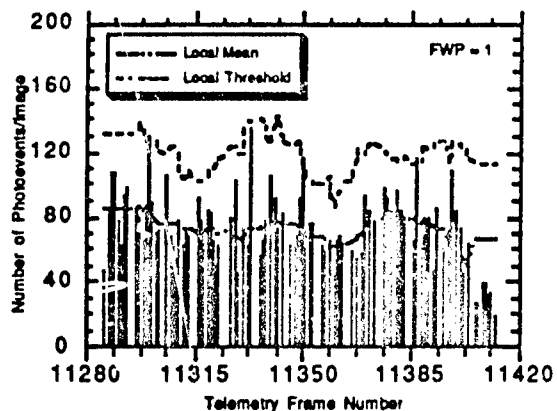


Fig. 111 - Antares, plume camera, central region intensity for interval 4

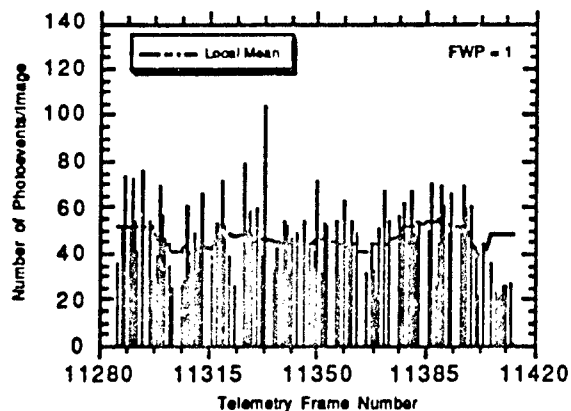


Fig. 112 - Antares, plume camera, outer region intensity for interval 4

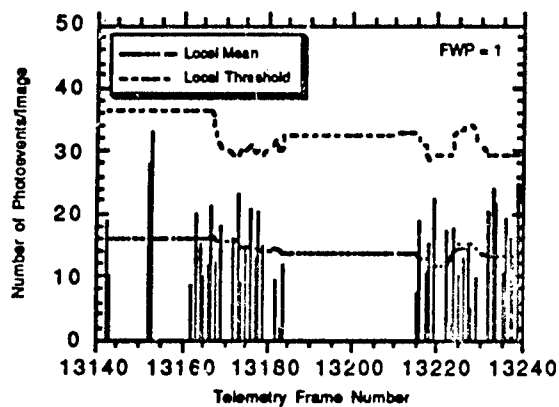


Fig. 113 - Star 27, plume camera, total intensity for interval 5

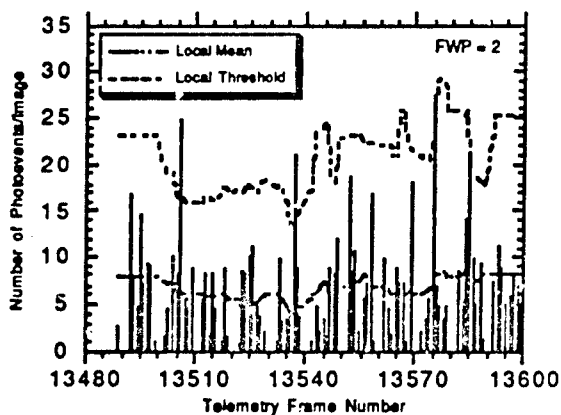


Fig. 114 - Star 27, plume camera, total intensity for interval 6

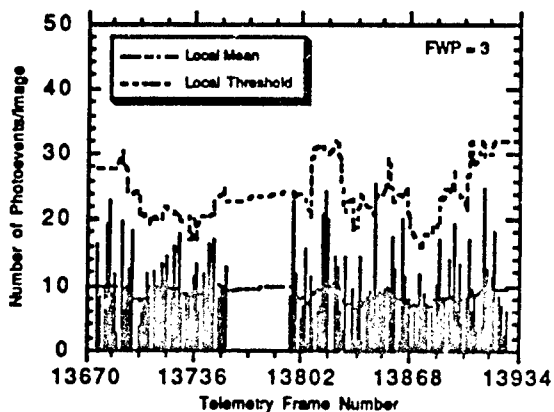


Fig. 115 - Star 27, plume camera, total intensity for interval 7

The first data interval, depicted by Figs. 101 through 103, did not have enough sample points to compute the local mean as a function of frame number.

Figure 104 shows two instances in which the measured number of photoevents exceeds the local mean by more than 3.1 standard deviations. The probability of such an event is less than 0.001. Therefore, all instances in which the measured number of photoevents exceeded the threshold were investigated in great detail. No reason was found to disregard any of these data points.

Tables 36 and 37 summarize the average radiant intensities (ARI) for the plume-camera observations over the seven data intervals. The central region average radiant intensity reported for each of the data intervals is based on the reference spectral energy distribution assumption. It represents the average of all images in the interval. The outer region ARI values reported in Table 36 are based on the reference spectral energy distribution assumption; the outer region ARI values reported in Table 37 are based on the flat spectral energy distribution. Table 36 includes reference spectrum predictions of ARI for the sake of completeness. How to compare the predictions to the experimentally determined values is not obvious because of different fields of view and complexities with regard to central and outer region mechanisms. Values of total spectral radiant intensity were not computed for Table 37, where the central and outer regions are analyzed by using different spectral shapes. For Star 27, no values are reported because a flat spectral assumption for the central region is completely unjustified. The totals are computed as the sum of central and outer region.

Table 36 - Summary of Plume Camera Average Radiant Intensities Using Reference Spectral Response

Interval	Filter	Band (nm)	Measured ARI*			Measured ASRI**		Reference Model
			Central Region ARI (W/sr)	Outer Region ARI (W/sr)	Total (W/sr)	$\lambda$ Centroid Wavelength (nm)	Total Spectral Radiant Intensity (W/sr- $\mu$ m)	Predicted ARI (W/sr)
1	PC-4	235-350	48.2	34.9	83.1	305	787	226.6
2	PC-3	195-295	19.4	17.5	36.9	265	353	17.4
3	PC-2	300-320	13.9	18.5	32.4	310	1588	45.0
4	PC-1	220-320	55.4	35.7	91.1	280	607	66.7
5	PC-1	220-320	—	—	14.2	280	95.9	11.4
6	PC-2	300-320	—	—	4.59	310	225	7.5
7	PC-3	195-295	—	—	12.9	265	123	2.9

\* ARI - Average radiant intensity

\*\*ASRI - Average spectral radiant intensity

Table 37 - Summary of Plume Camera Average Radiant Intensities Using Flat Spectral Response for the Outer Region

Interval	Filter	Band (nm)	Measured ARI*		
			Central Region ARI† (W/sr)	Outer Region ARI (W/sr)	Total (W/sr)
1	PC-4	235-350	48.2	22.0	70.2
2	PC-3	195-295	19.4	9.09	28.5
3	PC-2	300-320	13.9	17.6	31.5
4	PC-1	220-320	55.4	16.6	72.0

\* ARI - Average radiant intensity

† Central region calculation assumes reference spectral response

Recall that the quoted central region radiant intensity values during the Star 27 stage are questionable because of the tracking performance.

When operating in the zoom image transmission rate, each telemetry frame contains one image.

## 6.2 Tracker Camera Intensity Plots

Figures 116 through 122 present total photoevents per image for the seven data intervals analyzed throughout this report. The figures in this section are based on a 19 by 19 pixel section of the tracker camera, which corresponds approximately to the total field of view of the plume camera. This field of view contains plume central region and a portion of the outer region and, therefore, cannot reliably be converted to radiant intensity. However, to provide an estimate of the average radiant intensity, values based on reference spectral energy distribution assumptions are reported in Table 38 for the tracker-camera observations. These results have been reduced by 16.3% to account for red leakage in the tracker-camera filter.

Figures 116 through 122 are primarily intended to show image-to-image variations in the number of photoevents per image. Although temporal increases and decreases in the mean number of photoevents per image are evident in the figures, these trends are shown much more clearly in Figs. 97 and 98.

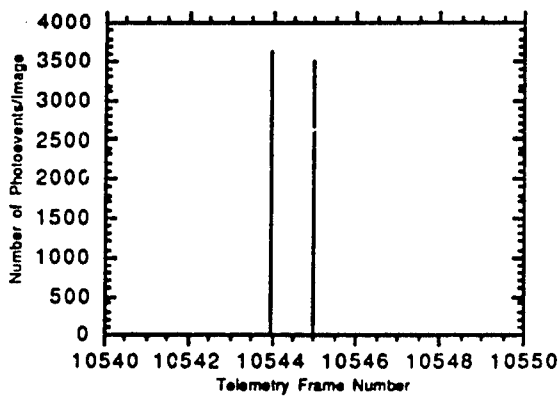


Fig. 116 - Antares, tracker camera total intensity for interval 1

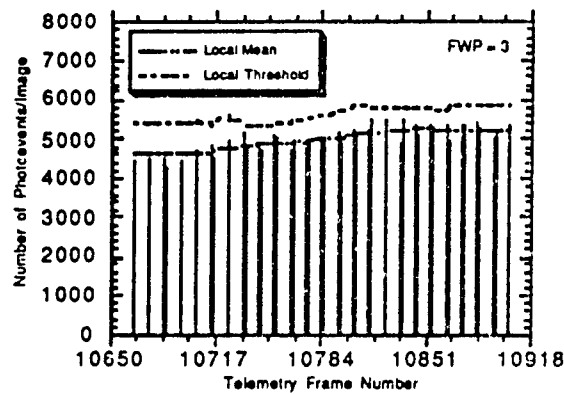


Fig. 117 - Antares, tracker camera total intensity for interval 2

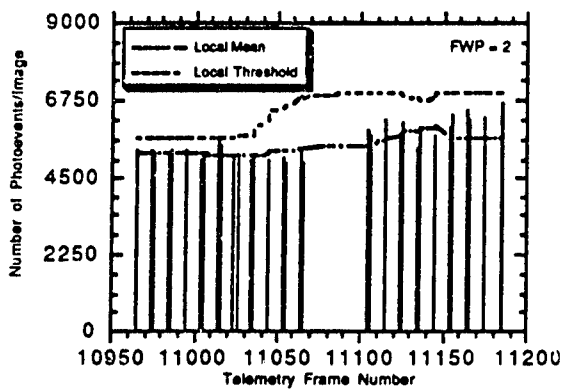


Fig. 118 - Antares, tracker camera total intensity for interval 3

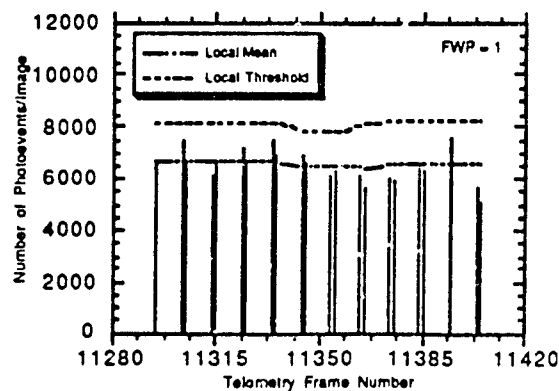


Fig. 119 - Antares, tracker camera total intensity for interval 4



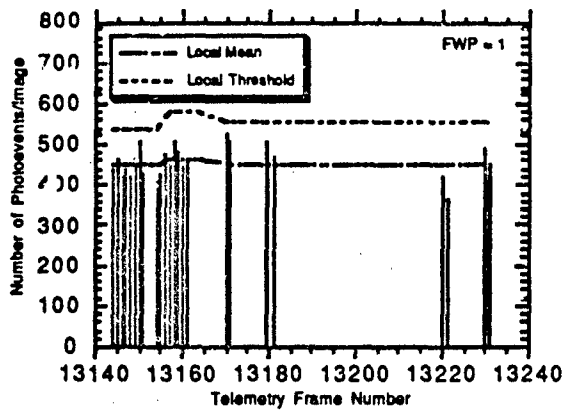


Fig. 120 - Star 27, tracker camera total intensity for interval 5

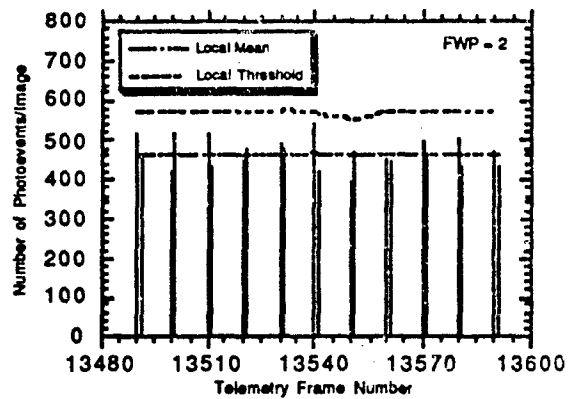


Fig. 121 - Star 27, tracker camera total intensity for interval 6

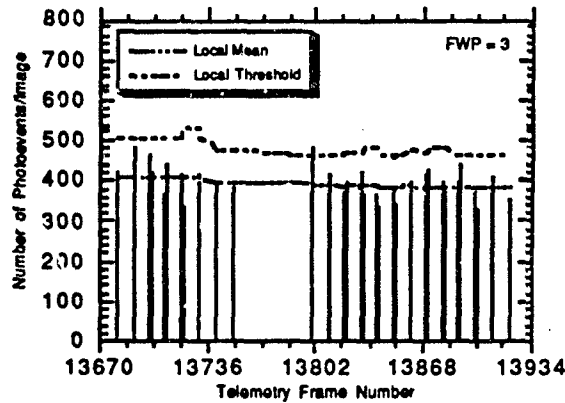


Fig. 122 - Star 27, tracker camera total intensity for interval 7

Table 38 - Summary of Tracker-Camera Average Radiant Intensities

Interval	Stage	Filter	Band (nm)	ARI* in 19 x 19 Pixel Region (W/sr)	ASRI** in 19 x 19 Pixel Region @ 390 nm (W/sr- $\mu$ m)
1	Antares	PC-4	255-450	293	2340
2	Antares	PC-3	255-450	504	4020
3	Antares	PC-2	255-450	532	4240
4	Antares	PC-1	255-450	371	2960
5	Star 27	PC-1	255-450	56.2	448
6	Star 27	PC-2	255-450	61.4	490
7	Star 27	PC-3	255-450	55.2	440

\* Average radiant intensity

\*\* Average spectral radiant intensity

The separation into plume central region and outer region is described in Section 5.1. For the telemetry frame ranges depicted in each plot, the plume-to-tracker image ratio was primarily 8:2. Consequently, the plots show repeated groups consisting of two consecutive tracker-camera images followed by a gap where the eight plume-camera images occurred.

In addition to the intensities, the figures include: the estimated local mean, which is a running average of the intensity, and a threshold of 3.1 standard deviations above the local mean, which flags intensity values that are highly unlikely (probability less than .001) based on the local statistics. The local statistics are computed by using a running window of 9 frames for tracker camera data. A more complete discussion of the computations of local statistics is contained in Section 4.6. The greater than 3.1 standard deviation events appear uncorrelated between the plume and tracker cameras, suggesting that if they represent real events they last less than  $1/30$ th of a second.

## 7.0 SPECTRAL ANALYSIS OF PLUMES

This section presents the spectral analysis of the total emission from the plume central region and from the outer region. As discussed in Section 2, the UVPI plume and tracker cameras observed the Antares and Star 27 stages at a range of approximately 500 km by using a sequence of bandpasses. The figures and tables in this section show the computed spectral radiant intensity in  $W/sr-\mu m$  of the plume central region of the Antares stage and the spectral radiant intensity measured over the entire plume-camera field of view for both the Antares and Star 27 stages. The results from the UVPI observations of the central region of the Antares plume show that the ratio of the spectral radiant intensity at the longer wavelengths, relative to the spectral radiant intensity at the shorter wavelengths, is smaller than predicted by the reference spectrum. The results for the entire plume-camera field of view for both stages show a similar relative deficit at the longer wavelengths.

### 7.1 Observed Spectral Radiant Intensities

The conversion of the plume and tracker camera data to radiometric values requires the assumption of a source spectrum, as described in Section 4.2. The reference spectral shape has been used in the analysis of the camera data presented in this section. The wavelength for which the spectral radiant intensity is reported for each filter bandpass is the centroid wavelength when the assumed source spectrum is convolved with the UVPI net quantum efficiency function, as described in Section 4.2.

#### 7.1.1 Antares Observation

The plume camera observations of the Antares stage were made between 162 and 191 s after liftoff. The range from UVPI to the rocket was between 452 and 496 km over this time period. The spectral radiant intensities of the plume central region, as measured by UVPI in the plume-camera bands, are plotted in Fig. 123. In addition, Fig. 123 shows the reference spectral shape, scaled arbitrarily to pass through the data points, and for comparison shows a blackbody spectrum chosen to coincide with the reference spectral shape at short wavelengths. The data and scaled reference based values are listed in Table 39.

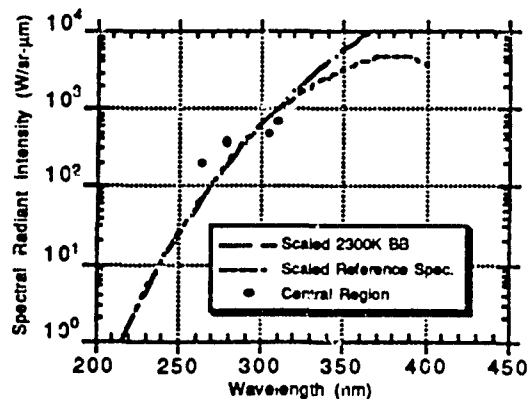


Fig. 123 - Measured spectral radiant intensity for the Antares central region

Table 39 - Measured and Scaled Spectral Radiant Intensity in Units of W/sr- $\mu$ m for Antares

Wavelength (nm)	Filter	Observed Central Region	Plume-Camera Field of View	Scaled Reference Comparison
265	PC-3	$1.86 \times 10^2$	$3.53 \times 10^2$	$7.64 \times 10^1$
280	PC-1	$3.69 \times 10^2$	$6.07 \times 10^2$	$2.06 \times 10^2$
305	PC-4	$4.56 \times 10^2$	$7.87 \times 10^2$	$8.00 \times 10^2$
310	PC-2	$6.81 \times 10^2$	$1.59 \times 10^3$	$9.84 \times 10^2$
390	TC	—	$3.39 \times 10^3$	$4.63 \times 10^3$

Figure 123 shows that the ratio of the spectral radiant intensity measured by UVPI for the Antares central region at the shorter wavelengths, relative to that at the longer wavelengths, is larger than predicted by the reference spectral shape. The relative intensity increase for the 265- and 280-nm data points is a factor of three to five, well beyond the instrument uncertainty.

The spectral radiant intensity measured by UVPI over the entire plume camera field of view is shown in Fig. 124. These measurements were made by the plume camera operating in the plume-camera bands and by the tracker camera. Note that the tracker camera pixels analyzed in this section correspond to the full field of view of the plume camera. Figure 124 also shows the same reference spectral shape and blackbody spectrum used in Fig. 123. The data and scaled reference based values are listed in Table 40.

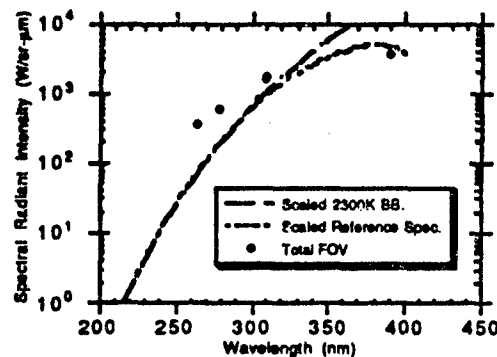


Fig. 124 - Measured spectral radiant intensity for the plume camera field of view for Antares

Figure 124 shows that the reference spectral shape is in good agreement with the 305 to 390-nm trend. It also shows that the reference model predicts a more rapid decrease with decreasing wavelength below 300 nm than the data show. These results are similar to those found for the Antares plume central region analysis.

### 7.1.2 Star 27 Observation

The third stage of Strypi, a Star 27 rocket motor, was also observed by the plume and tracker cameras. In the plume camera, only filters PC-1, PC-2, and PC-3 were used for the observation. These observations were made between 249 and 275 s after liftoff, during which time the range to the Star 27 was between 495 and 549 km. The spectral radiant intensities of the total field of view of the plume camera were measured by UVPI, and these results are presented in Fig. 125. Figure 125 also shows the reference spectral shape and a blackbody spectrum chosen to coincide with the reference prediction at short wavelengths. The data and reference based values are in Table 40. Note that values for the plume central region alone are not given for the Star 27 stage because of the relatively poor tracking of this stage.

As in the Antares stage, the spectral radiant intensities computed from the UVPI Star 27 data show an excess at the shorter wavelengths, relative to the longer wavelengths, than predicted by the reference spectrum.

Table 40 - Measured and Scaled Spectral Radiant Intensity in Units of  $W/sr \mu m$  for Star 27

Wavelength (nm)	Filter	Plume-Camera Field of View	Scaled Reference Comparison
265	PC-3	$1.23 \times 10^2$	$7.6^4$
280	PC-1	$9.49 \times 10^1$	$2.05 \times 10^1$
310	PC-2	$2.25 \times 10^2$	$9.84 \times 10^1$
390	TC	$4.59 \times 10^2$	$4.63 \times 10^2$

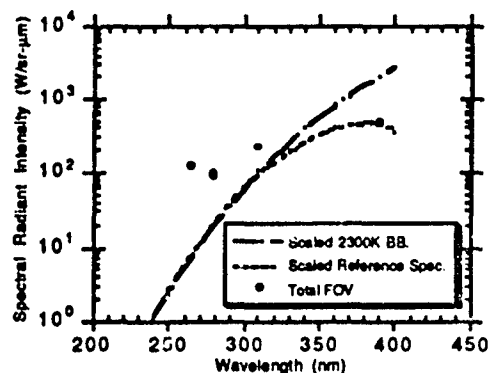


Fig. 125 - Measured spectral radiant intensity for the plume camera field of view for Star 27

## 7.2 Discussion

The reference model hypothesizes that the principal source of UV radiation is thermal emission from alumina particles at the fusion temperature of alumina, 2320 K. The spectral shape departs from that of a blackbody because of the decreasing effective emissivity of the particles with increasing wavelength. No obvious modification to this model will yield the UV enhancement evident in the UVPI data. A plausible hypothesis is that an additional emission mechanism is producing the excess UV emission. Spectral line emission by exhaust gases and by the mesospheric atmosphere disturbed by the rocket, e.g., NO<sub>y</sub> bands are possible sources.

## 8.0 TRAILING CLOUD OBSERVATIONS

### 8.1 Initial Transient

Just prior to Antares ignition, the UVPI gimbals were directed in a scan pattern designed to compensate for uncertainties in the Antares trajectory. At Antares ignition, the Antares rocket plume was on the edge of the tracker camera's field of view. In addition, Fig. 126 shows that the target was extremely large. Poor tracking occurred until about 158 s when the target reduced to a reasonable size in the tracker camera's focal plane. Ground-based cameras tracking the Antares ignition showed a huge cloud expelled from the Antares nozzle. Initial UVPI tracking locked onto this cloud. However, since the tracker was in the Mass and Intensity Centroid mode, the bright signal of the rocket plume near the engine nozzle dominated the tracking centroid after the cloud began to dissipate.

#### 8.1.1 Size and Radiometrics of Initial Cloud

Figure 127 shows a tracker camera image of the initial cloud at 158.9 s. The cloud is at a range of 496 km and is approximately  $3 \times 10^6$  m<sup>2</sup> in projected area. For comparison, the plume central region has a projected area of approximately  $5.4 \times 10^3$  m<sup>2</sup>. By using the reference spectral shape assumption, the apparent peak radiance (that measured at the brightest pixel in the tracker-camera cloud image) is calculated to be  $2.3 \times 10^{-8}$  W/sr-cm<sup>2</sup>. The cloud radiance in the plume

camera PC-4 passband is well below the single-frame noise-equivalent radiance of  $2.3 \times 10^{-6}$  W/sr-cm<sup>2</sup>.

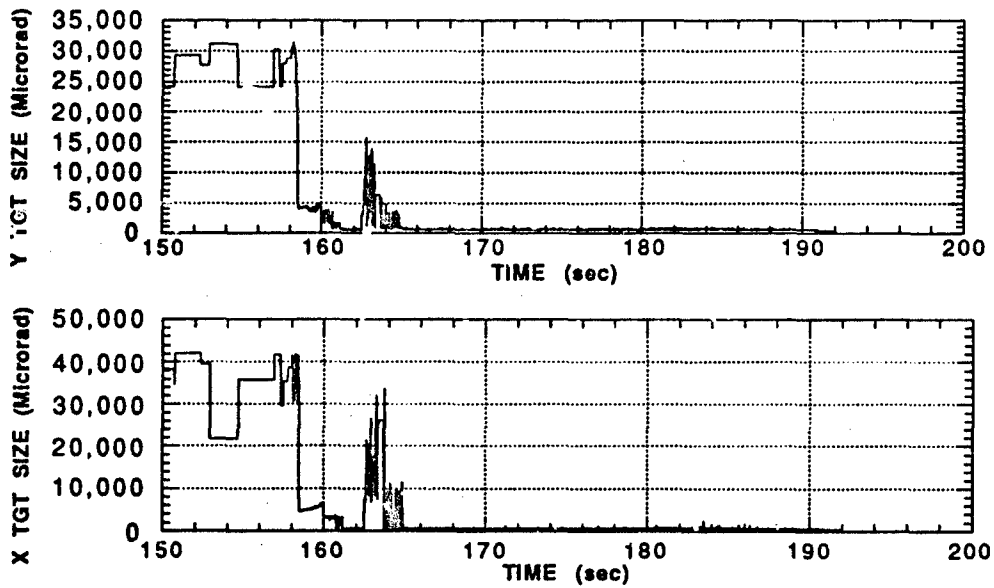


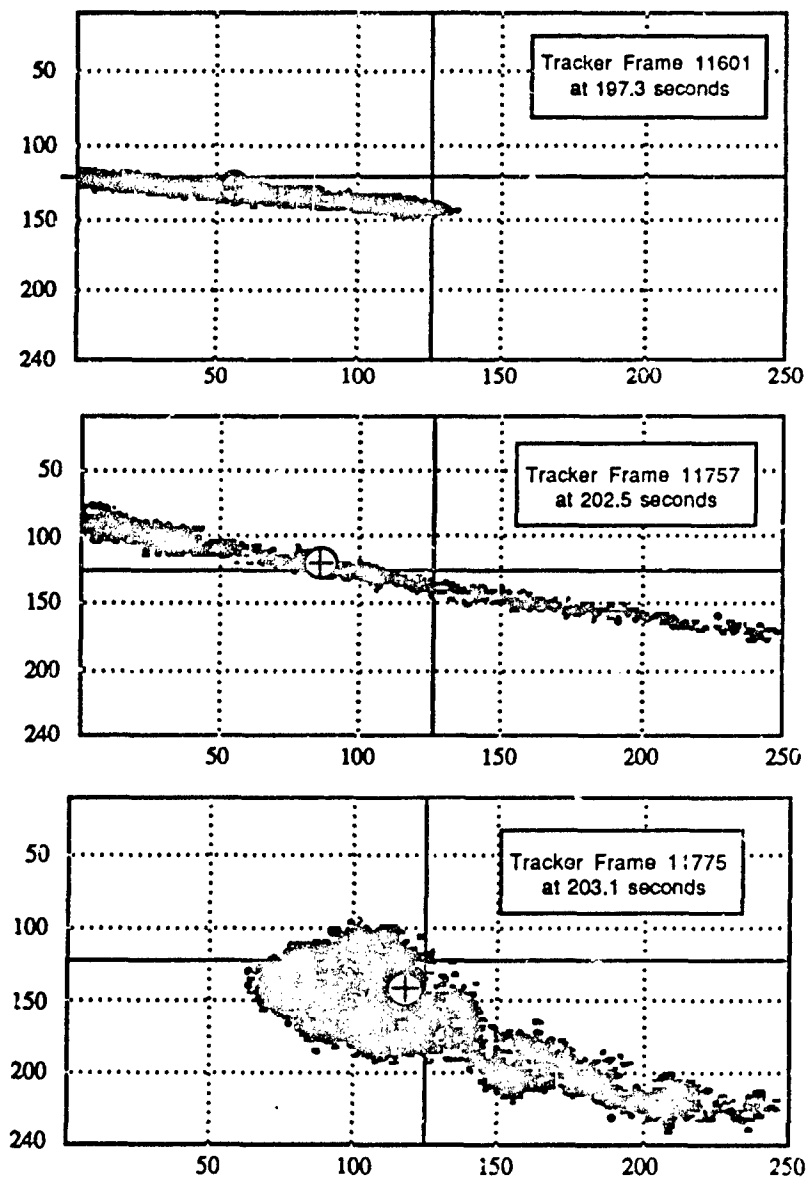
Fig. 126 - X target and Y target size during the Antares burn



Fig. 127 - Initial cloud imaged by tracker camera at 158.9 seconds

## 8.2 Antares Cloud Trail

During the Antares burn, a large trailing cloud formed behind the rocket. Figure 128 is a sequence of images of this trailing cloud as seen by the tracker camera. The top image was made immediately after the Antares burned out. Initially, the tracker locked onto the tip of the cloud for 2 to 3 s. Then the tracking centroid shifted to the point shown by a cross within a circle. Note that it is biased to the left side of the camera's focal plane. The middle image shows how the cloud looked to the tracker camera pointed toward the midpoint of the cloud. Again, the centroid is biased to the left. The bottom image shows the end of the Antares cloud trail, which corresponds to the ignition point of the Antares motor. The tracker continued to track this spot until commanded to point for the Star 27 ignition.



Relative Frame Coordinates

Fig. 128 - Tracker camera images of Antares cloud trail

### 8.2.1 Size and Radiometrics of the Cloud Trail

Figure 129 is a pseudocolor mosaic of three tracker camera images, 11565, 11757, and 11799, close in time to the three shown in Fig. 128. Figure 130 shows a profile generated by summing along columns using the same three images. This profile shows that during the 6.4 s between acquisition of images 11565 and 11757, the radiant intensity of the cloud segment shown in 11565 dropped by approximately a factor of two, suggesting rapid cooling. This temporal change in radiant intensity is not reflected in the mosaic because the three images were scaled to approximately match each other at the boundaries in the pseudocolor representation.

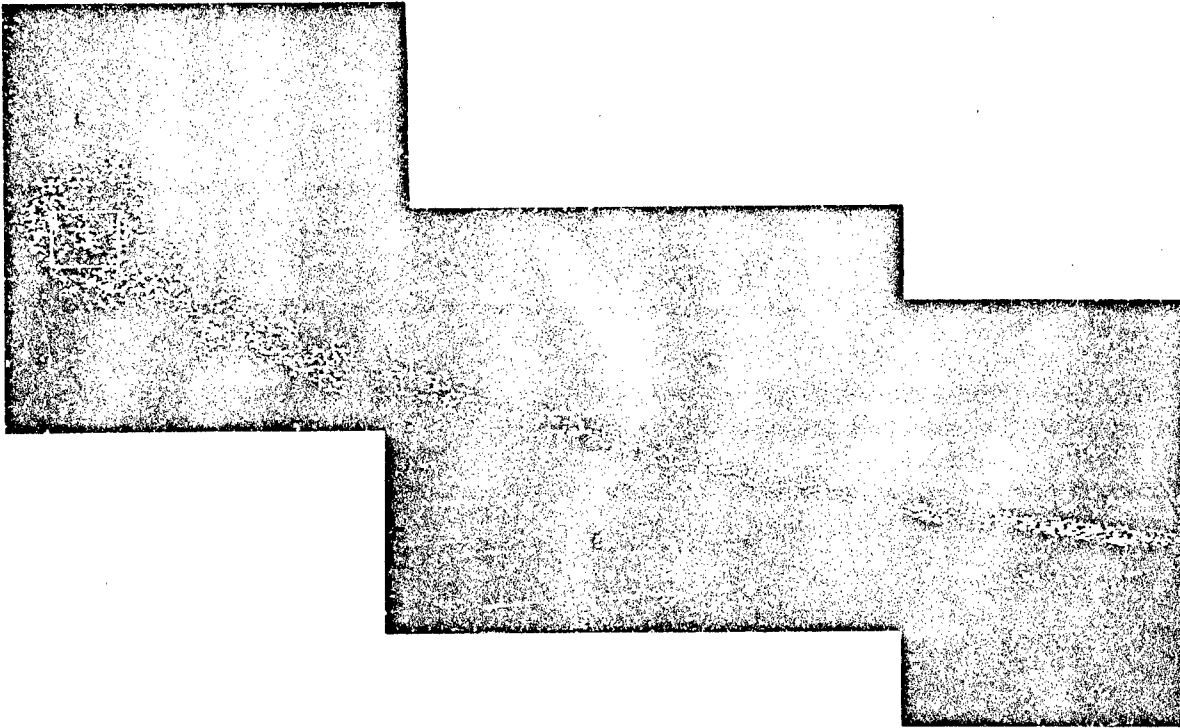


Fig. 129 - Color mosaic of Antares cloud trail

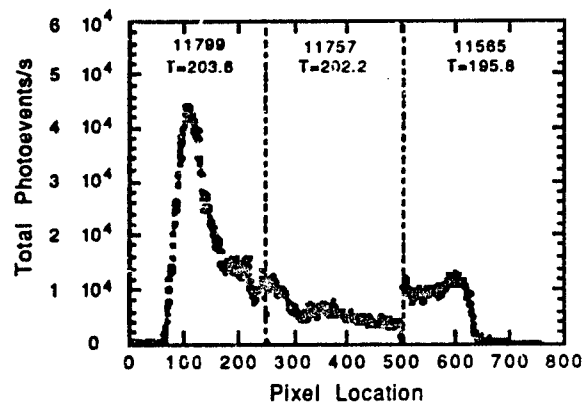


Fig. 130 - Antares cloud trail profile

By using absolute position vectors for the Antares ignition and burnout, the cloud length is calculated to be approximately 42.9 km. Based on an analysis of UVPI gimbal angles, it is clear that the end of the cloud trail shown in the mosaic is: at the same position as the initial cloud discussed in Section 8.1, and has grown to approximately 16 times the projected area of the initial cloud. The brightest portion of the cloud trail at the time of tracker camera image 11799 is shown in Fig. 129 within the indicated rectangular region. It has an apparent peak radiance of  $\sim 1.7 \times 10^{-8}$  W/sr-cm<sup>2</sup>, which is 70% of the apparent peak radiance measured in the tracker-camera passband for the initial cloud immediately following Antares ignition. This suggests that there may be a very long time constant associated with the processes, producing radiance in the brightest region of the cloud trail. For comparison, the apparent peak radiance measured in the tracker-camera passband at the tip of the cloud trail imaged during frame 11565 is approximately  $2.5 \times 10^{-8}$  W/sr-cm<sup>2</sup>. During the time the cloud trail was being tracked, the radiance measured by the plume camera in the PC-1 passband was well below the single-frame noise-equivalent radiance of  $1.2 \times 10^{-5}$  W/sr-cm<sup>2</sup>.

### 8.3 The Star 27 Dim Trail

Four frames of UVPI tracker camera data show a dim trail behind the Star 27 stage within the last second prior to burnout. There is no indication of a Star 27 trail prior to these images, and there is no evidence of the trail in the plume-camera images. One of the tracker images, frame number 14000, can be seen in Fig. 131.



Fig. 131 - Star 27 dim trail



## 9.0 SUMMARY AND CONCLUSIONS

### 9.1 Summary

The goal of the Strypi mission was the acquisition from space of radiometric UV plume data by using the UVPI on board the LACE satellite. The UVPI plume camera is an imaging radiometer with four filters, centered at 250, 270, 280, and 305 nm (Table 12). This instrument was designed to obtain radiometric data in a spectral region that is especially favorable for missile detection because of the very low solar background. Operation from space is necessary because the atmosphere is practically opaque to wavelengths below 300 nm. From a 500-km range, the plume camera has a resolution of approximately 45 m.

The Strypi XI, a three-stage solid-propellant missile system, was obtained for this observation. The first stage, a Castor motor with two Recruit boosters, operated at too low an altitude to be observed from space. The mission was designed for observing the second (Antares) and third (Star 27) stage plumes, as well as the possible bow shock from the reentry of the third stage. The rocket trajectory was selected to permit simultaneous observation from the LACE satellite and from the Air Force Maui Optical Site (AMOS).

The Strypi was launched from the U.S. Navy Pacific Missile Range Facility before sunrise on 18 February 1991. The Antares and Star 27 stages were successfully tracked by the UVPI camera from a range of 450 to 550 km. The Antares plume was tracked for about 30 s, and plume data were acquired with all four plume-camera filters. The weaker plume from the Star 27 stage was tracked, but this was accompanied by a large amount of jitter that was attributed to the weaker rocket plume. The jitter prevented stable imaging of this stage with the plume-camera. Plume data of variable quality were obtained with three of the four plume-camera filters. The observation intervals are summarized in Tables 10 and 11.

The 480 images of the Antares plume were of sufficient quality and tracking accuracy to permit the superposition of images for increased radiometric accuracy. The weak signal of the Star 27 stage yielded radiometry of significantly lower reliability.

The superposed images were analyzed to obtain the spectral radiance, evaluating the plume as a spatially resolved source, and the spectral radiant intensity, summing over space to treat the plume as a point source. The radiometric analysis requires a model spectral shape, for which a reference model was taken. The analysis procedure is described in Section 4.2. The spectral values were also integrated over the nominal filter bandwidths to obtain radiance and radiant intensity values.

Figures 27 through 33 are false-color maps of the spatial distributions of the time-averaged radiant intensities of the Antares and Star 27 plumes. Contour plots of the plume radiance were also generated from the superposed images, and are presented in Figs. 51 through 57.

Figure 26 shows the image and Fig. 50 the contour plot of the NRL ground-based UV beacon. A point source is well represented by the contour plots under these conditions. This image indicates the resolution limit of the instrument at a 450-km range. The lengths of the rocket plumes observed during this mission are less than or comparable to the 45-m resolution limit (Table 34). The consequent smearing of the source over an increased effective area significantly reduces the observed peak radiance of the plumes. The observed radiances are denoted "apparent" values. This is to distinguish between the observed radiance values and those that would be obtained from an instrument having higher spatial resolution. An adjustment of the CHARM predicted peak radiances for this effect yields factor-of-two agreement between prediction and observation (Table 33).

Radiant intensity values, obtained by summing over the plume central region and over the plume camera field of view, are not affected by this resolution effect. The plume central region was defined for these computations as the region in which the radiance exceeded 25% of the peak apparent value plus the area defined by a 5 by 5 pixel dilation of this region. The projected area of the central region so defined was approximately 6500 m<sup>2</sup> (Table 29). The remainder of the plume-

camera images is denoted the outer region. The reference spectral shape is unlikely to be an accurate model for the radiometry of the outer region. This region was analyzed by using a flat spectral shape as well as the reference spectral shape to obtain reasonable bounds for the true radiometric values. The central region and outer region radiant intensities are summarized in Tables 36 and 37. The temporal behavior of the plume central region, outer region, and total radiant intensities is shown in Figs. 101 through 115.

The radiant intensity (the total radiated power) of the observed outer region is comparable to that of the plume central region. The outer region's radiance is low compared to the plume central region but its area is much greater. A comparison of the outer region images with other nadir images, e.g., the plume-camera images of the ground beacon, show no such radiance in the outer region. The outer region emission is clearly associated with the missile. However, the mechanism of the outer region radiance has not been established.

The UVPI tracker camera provides wideband data, 255 to 450 nm, that may complement the plume-camera data. The wide field of view of the tracker camera clearly prevents resolution of the plume, but radiant intensity values can be obtained. A 19 by 19 pixel region of the tracker camera images, matching the total field of view of the plume camera, was used for computing radiant intensities. The values so obtained are summarized in Table 38, and the time variations illustrated in Figs. 116 through 122.

The spectral radiant intensities deduced from the UVPI observations can be compared to the reference model of plume emission. The plume-central region spectral radiant intensities show a reference-spectrum-like dependence over the 250 to 300-nm range. The data suggest that the 250 to 270-nm values are higher relative to the 280 to 300-nm values than the reference spectrum predicts (Fig. 123). The spectral radiant intensities summed over the plume-camera field of view show a similar ultraviolet excess. The full field values from the plume camera can be complemented by the tracker-camera data over the same area. The 390-nm value obtained adds support to the tentative conclusion that the decrease in plume spectral radiant intensity as the wavelength decreases below 300 nm is less than expected on the basis of the reference model (Fig. 124).

The Strypi trajectory was planned in coordination with the LACE orbit to permit a search for evidence of bow shock photoemission. However, the Antares and Star 27 stages apparently collided at separation, causing the Star 27 to loft above its planned altitude and burn out at 112 km instead of 99 km. This delayed the onset of the putative bow shock, which was not expected to be seen above 100-km altitude. The burnout of the plume terminated automatic plume tracking, and the Star 27 stage was lost from the instrument field of view before it reached bow shock altitude.

A very large cloud of bright material was observed just prior to Antares ignition. The apparent area of this initial cloud was several hundred times the area of the Antares plume. The cloud was observed again following the Antares motor burn (Fig. 128) and was sufficiently bright to interfere with tracking of the missile stages. The cloud occurred behind the missile stage and is not believed to be responsible for the outer region emission observed to the sides of the missile.

## 9.2 Achievement of Objectives

The results of the UVPI observation of the Strypi missile can be compared to the objectives listed in Section 2.1.

### 9.2.1 General Objectives

- *Obtain isoradiance contours for the Antares and Star 27 plumes.* Spatially resolved images of the Antares and Star 27 plumes were obtained for seven data intervals. These corresponded to imaging with all four plume-camera filters for the Antares and three of the four filters for the Star 27 stage. These images were scaled to spectral radiance maps and contours, as illustrated in Sections 4 and 5.
- *Obtain radiant intensity measurements based on the entire field of view of the plume camera and on a subregion corresponding approximately to a plume core.* Radiant intensity measurements for the plume camera FOV and for a

- plume central region defined in Section 5.1 were extracted from the images for the seven data intervals. These results are presented in Section 6.
- *Compare radiometric measurements for the Antares and Star 27 plumes with those generated by the CHARM 1.3 computer code.* The preliminary comparison undertaken here suggests that the UVPI data represent a spectral shape somewhat different from that of the reference spectrum. The experimental results indicate that the emission at wavelengths shorter than 300 nm is greater, relative to the emission at longer wavelengths, than is predicted by the reference model. These results are described in Section 7. The detailed comparison of CHARM predictions to the UVPI observations is a task for the modelers.
- *Provide radiometric measurements for nonplume, transient phenomena, if any.* An initial cloud at Antares ignition was observed, and its radiance was measured with the tracker camera. The cloud, which was seen to extend behind the plume, was again observed by the tracker camera following Antares stage burnout. These observations are described in Section 8.

### 9.2.2 Spatial Features

- *Obtain the length of the Antares and Star 27 plume central regions.* The resolution limit of the UVPI corresponds, at this range, to about 45 m, which is comparable to the expected plume length. Thus, a close measurement of the plume length was not possible, but (as described in Section 5.5) the observations are consistent with the predicted plume length.
- *Determine the shape of the shock boundary/mixing layer for different rocket velocities.* Despite the very weak radiance of the outer region, the boundary layer was detectable from the multiple-image superpositions. The shape is evident from Figs. 44 (Antares) and 45 (Star 27) and may be correlated with the rocket velocity (Fig. 12), which varied from 0.5 to 5.0 km/s.
- *Identify asymmetries in plume shape and investigate possible causes.* No plume shape asymmetries were observed. The resolution limit of the UVPI at this range is such that only large asymmetries could have been detected.

### 9.2.3 Temporal Features

- *Identify temporal trends in radiometrics and investigate possible dependence on rocket velocity.* The time behavior of the radiant intensity of the Antares and Star 27 plumes is described in Section 6. No obvious correlation with rocket velocity was observed.
- *Investigate radiometric fluctuations to determine whether short-term variations in brightness are observed.* The statistics of the variations in plume radiant intensity are described in Section 6. Several peaks beyond the range of statistical likelihood were observed. The data were carefully analyzed and no reason was found to reject them.
- *Identify changes with time in the shape of the plumes' outer region.* The shape of the outer regions, and the variation with time, can be observed in Figs. 44 and 45.
- *Identify persistence and cumulative effects, if any, in plumes or nonplume phenomena.* A large cloud was observed behind the Antares plume (Section 8). The cloud was observed twice, once immediately following Antares ignition and once following Antares burnout. The apparent peak radiance of the portion of the cloud observed immediately after ignition was seen to decrease by only 30% during the period of Antares burn.

### 9.2.4 Spectral Features

- *Compare the shape of the plume central region's emission spectrum with the reference spectral shape, which is that of micron-sized alumina particles at the melting point, and spectral shape determinations based on other sensors.* As described in Section 7, the UVPI data indicate that the decrease in spectral radiance and radiant intensity as the wavelength decreases below 300 nm is less

- than indicated by the reference model. A comparison of the UVPI data with data acquired by other sensors is currently in progress.
- *Relate tracker camera measurement to visible and infrared measurements made by other sensors.* The UVPI acquired plume radiometric data to 450-nm wavelength. These radiant intensity values can be compared to data at longer wavelengths from other sensors as those data become available.
  - *Characterize the emission spectrum for the plumes' outer regions, if any.* Outer region spectral shape information can be extracted from the central region and total image data, by using the values tabulated in Section 7. However, the result is subject to large uncertainties because of the imprecision in distinguishing between central region and outer region, compounded by the uncertainties in the determination of the central region radiometric values. The data suggest a stronger far UV,  $\lambda < 300$  nm, component in the outer region radiance than is seen in the central region.

It is clear from the above that most of the task objectives were achieved, but the instrumental limitations in resolution and signal strength, as well as the uncertainty in the reference spectral shape, complicate the extraction of precise values.

### 9.3 Conclusions

The UVPI observation of the Strypi launch demonstrates the capability of the instrument for tracking and imaging missiles in flight from a 500-km range. The brighter plume of the Antares stage was successfully tracked throughout its burn, despite the interference of an ignition cloud. The fainter plume of the Star 27 stage was tracked with a relatively large amount of jitter.

The Antares stage was acquired for a total of 480 camera images distributed over all four UVPI filters. The Star 27 was tracked for a total of 304 images, and data were obtained for three of the four filters. The spectral radiance and spectral radiant intensities were extracted from these images. Absolute values are necessarily obtained on the basis of an assumed spectral shape; namely, the reference spectrum. A comparison of the results for the four UVPI filters indicates that the reference shape is not inaccurate, but the new data indicate a stronger component in the far UV,  $\lambda < 300$  nm, than the model predicts.

The images reveal not only a radiant plume but an extensive outer region with a passband-integrated radiant intensity comparable to that of the plume central region. The far-UV component of this outer region appeared to be even stronger, relative to the near-UV component, than that of the central region. The mechanism of excitation of this outer region has not been established. Although spectral radiant intensity values for the outer region were estimated by calculations based on both the reference spectral shape and a spectrally flat model, these values must be considered tentative until a reliable spectral model for the outer region is available.

The time dependence of the plume central region radiant intensity within each filter interval showed no pronounced trends or variations. Momentary, single-frame peaks exceeding the range of normal statistical variation were detected. Whether these can be correlated with missile-engine events or other sensors remains to be seen.

The tracker camera obtained radiant intensity data in the 255 to 450-nm wavelength range. These data, taken with the plume camera data in the 195 to 350-nm range, support the following conclusion: The central region spectrum is quite close to the reference model with an enhancement of the emission in the far-UV between 250 and 280 nm.

The third stage of the missile rose to a higher altitude than planned and burned out before descending to altitudes where a bow shock might occur. The tracker lost track when the missile ceased firing and could not follow the third stage to lower altitudes. Thus the experiment did not yield a test of the existence of a luminous bow shock.

A very large, persistent cloud trail from the Antares stage was observed. This 43-km trail was sufficiently bright and persistent that it did briefly confuse the UVPI tracker.

The data base of UV radiometric information, yielding refined interpretations and evaluations, will be a foundation for further analysis. Comparison with models and with data from sensors on other platforms will also yield improved radiometric results and an enhanced phenomenological understanding of UV emission by solid-fuel rocket motors in the upper atmosphere.

#### ACKNOWLEDGMENTS

The successful observation of the Strypi rocket plumes by the Ultraviolet Plume Instrument and preparation of the data were due to the efforts of many. Within the NRL LACE Program, engineering and testing personnel carefully prepared and repeatedly tested the command sequence specified by the UVPI Encounter Manager (Dr. Trevor Sorensen). Then they successfully executed the sequence to obtain the Strypi data. LACE satellite operations personnel coordinated the transmission of the delayed execution commands and pointing functions, the overall satellite operations during the observation, and the transmission of the data stored in the UVPI's memory. Data processing personnel then verified the quality of the transmitted data and prepared it for the image processing team.

Dr. William Jeffrey, then with the Institute for Defense Analyses, served as the SDIO Science Manager for this observation. As such, he identified the SDIO's objectives for this mission, helped define the trajectory for the Strypi rocket, and helped the UVPI Encounter Manager specify the command sequence to achieve the SDIO's objectives. Dr. Jeffrey also provided CHARM-based plume intensity predictions for use in planning the UVPI observation and for comparison with the resulting UVPI data.

The purchase and launch of the Strypi XI rocket were funded by the Directed Energy Directorate of the Strategic Defense Initiative Organization (SDIC/TND), which also sponsors the NRL LACE Program and the UVPI. Observation of the Strypi plumes by the UVPI was a primary objective of the Strypi launch and, therefore, the launch was precisely phased with a LACE satellite overpass.

Sandia National Laboratories successfully integrated and launched the Strypi XI rocket under a contract with Fairchild Space Company. It is noteworthy that the entire integration and launch effort was compressed into approximately six months. The diligent efforts of Sandia and Fairchild in this accomplishment are commendable.

The Navy Space Surveillance Center (NAVSPASUR) made special calculations of precision ephemeris for the LACE satellite needed for successful pointing of the UVPI.

Finally, the outstanding efforts of many NRL and contractor personnel who designed, built, and tested the LACE satellite are acknowledged.

#### REFERENCES

1. G. N. Freeman, D. R. Crow, W. Malkmus, K. H. Wilson, and P. D. Thomas, "Composite High Altitude Radiation Model (CHARM)," AFAL TR-87-019, Photon Research Associates, Inc., La Jolla, CA, Sept. 1987.
2. "Probe-1 First Report (U)," UCRC-15892, Photon Research Associates, Inc., La Jolla, CA, prepared for Lawrence Livermore National Laboratory, Jan. 1987 (SECRET).
3. J. F. Carbery and C. I. Meng, "Delta 181 Mission Quick Look Science Report (U)," JHU/APL SDO-8676, Johns Hopkins University Applied Physics Laboratory, Laurel, MD, Feb. 1988 (SECRET).

4. J. F. Carbary and C. I. Meng, "Delta 181 Mission Performance Quick Look Report (U)," DRC #EAS-800-085, Johns Hopkins University Applied Physics Laboratory, Laurel, MD, Feb. 1988 (SECRET).
5. J. A. Marqusee, "The State of Knowledge of UV/V Boost and Post-Boost-Phase Phenomenology and a Preliminary Assessment of Its Utility to SDI, (U)," IDA Paper P-2232, Institute for Defense Analyses, Alexandria, VA, July 1989.
6. J. T. Wright, "Ultraviolet Plume Instrument (UVPI) Subsystem Users Manual," SDRL 068, Loral EOS Document No. 3731, Loral Electro Optical Systems, Pasadena, CA, Jan. 1989.
7. H. W. Smathers, D. M. Horan, L. H. Reynolds, W. Ramsey, and H. D. Wolpert, "Design and Description of the Ultraviolet Plume Instrument (UVPI)," *Proc. SPIE* 1158, 196 (Aug. 1989).
8. H. W. Smathers, G. R. Carruthers, W. Ramsey, G. Steiner, and W. Louissant, "Calibration and Performance of the Ultraviolet Plume Instrument (UVPI)," *Proc. SPIE* 1158, 212 (Aug. 1989).
9. J. Nicholas, "Experiment Requirements Document for UVPI Observations of SDIO Special Projects (SPFE) Launches Rev 3," The Analytic Sciences Corporation, Arlington, VA, Aug. 1990.
10. W. Jeffrey, and R. R. Strunce, Jr., "Experiment Requirements Document for UVPI Observations of Strypi XI," Institute for Defense Analyses and Star Technologies Corporation, Feb. 1991.
11. R. A. Reed and V. S. Calia, "Review of Rocket Particle Properties Research," AEDC-TR-89-11, Final Report, Arnold Engineering Development Center, Tullahoma, TN, Nov. 1989.
12. D. A. Levin, L. H. Caveny, D. M. Mann, R. J. Collins, C. Howlett, P. Epsy, P. Erdman, and E. Zipf, "Ultraviolet Emissions from In-Flight Plume and Hardbody Flowfields," Proceedings of the 19th JANNAF Exhaust Plume Technology Subcommittee Meeting, Chemical Propulsion Institute of American, (CPIA)-568, p. 117, May 1991.
13. D. A. Levin, R. T. Loda, and R. S. Collins, "Instrumentation Consideration for a Bow Shock Radiation Experiment," *Proc. SPIE* 1059, 226 (1989).
14. L. W. Lathrop, "SP4/Strypi XI Development," Report SAND 88-2178, Sandia National Laboratories, Albuquerque, NM, 1988.
15. "Radiometric Calculations for Strypi Mission," Memorandum to H.W. Smathers, NRL, from W. Jeffrey, Institute for Defense Analyses, Alexandria, VA, May 1991.
16. C. L. Wyatt, *Radiometric System Design* (Macmillan, New York, 1987).
17. J. A. Marqusee, Institute for Defense Analyses (private communication, 14 March 1991).
18. A. Papoulis, *Probability, Random Variables, and Stochastic Processes*. 2nd ed. (McGraw Hill, New York, 1984).
19. W. L. Wolfe and G. J. Zissis, eds., *The Infrared Handbook* (Environmental Research Institute of Michigan, 1978).
20. R. H. Kingston, *Detection of Optical and Infrared Radiation* (Springer-Verlag, New York, 1978), pp 43-51.
21. Sonneborn et al., "IUE Observing Guide," *IUE NASA Newsletter* No. 32, 1987, p. 1.

22. A. D. Code, A. V. Holm, and R. L. Bottemiller "Ultraviolet Photometry from the Orbiting Astronomical Observatory XXXIV, Filter Photometry of 531 Stars of Diverse Types," *Astrophys. J. Suppl.*, 43, 501 (1980).
23. M. Breger, "Catalog of Spectrophotometric Scans of Stars," *Astrophys. J. Suppl.*, 32, 7-87 (Sept. 1976).
24. K. Fukunaga, "Introduction to Statistical Pattern Recognition," Academic Press, 1972.

## Appendix A THE ULTRAVIOLET PLUME INSTRUMENT

### A.1.0 UVPI DESCRIPTION AND BLOCK DIAGRAM

The Ultraviolet Plume Instrument (UVPI), designed and built by Loral Electro Optical Systems [6,7], comprises six subassemblies (Fig. A1) ranging in size from 4.4 to 0.3 ft<sup>3</sup>. The six subassemblies are sensor head assembly, electronics interface assembly, camera frame controller, digital tape recorder, power supply, and tracker assembly. The total weight is about 170 lb, and the operating power consumption averages about 170 W.

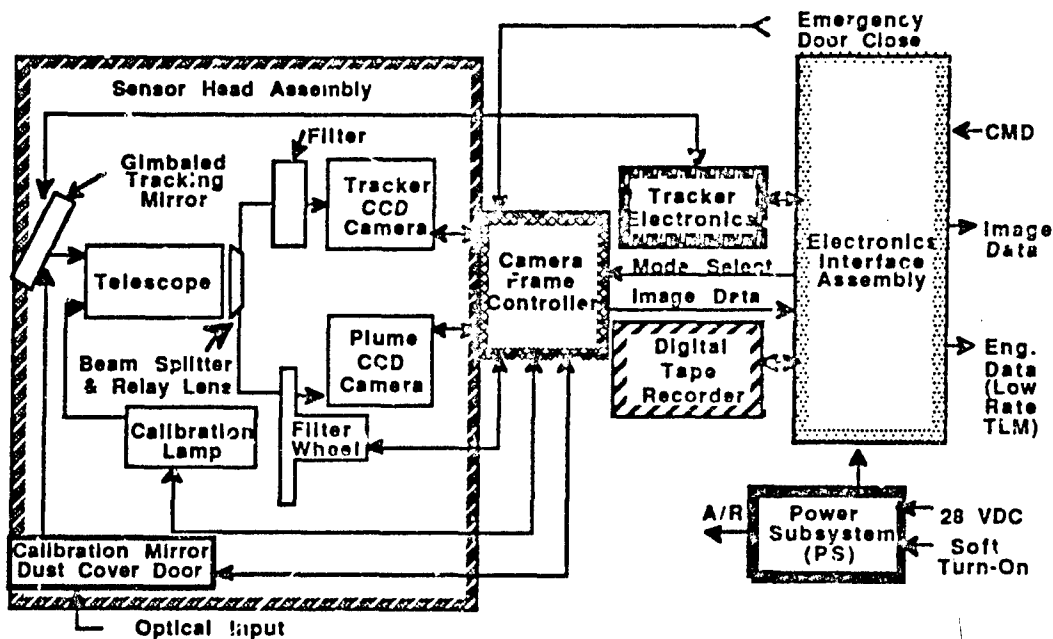


Fig. A1 - UVPI block diagram

There are two intensified charge-coupled-device (ICCD) cameras, the tracker camera and the plume camera, which are boresighted and share a common optical telescope. The tracker camera is used to locate, acquire, and track a target; the plume camera collects target images in the rear and mid-ultraviolet wavelengths. The camera images are digitized and transmitted to the ground or are recorded onboard for later transmission. Figure A2 is a diagram of the flow of commands and data within the UVPI.

The instrument was designed to transmit or store images in a selectable normal or high image rate mode because of the limited telemetry data rate, 3.125 Mbps. In the high image rate, or zoom mode, only the central portion of the image is retained. This allows a 30 Hz image rate while using the same bandwidth. The normal image transmission rate is 5 Hz. The photometric range and



sensitivity of the UVPI cameras were selected for nighttime operations. That is, the UVPI was designed to view and track relatively bright targets against a dark background.

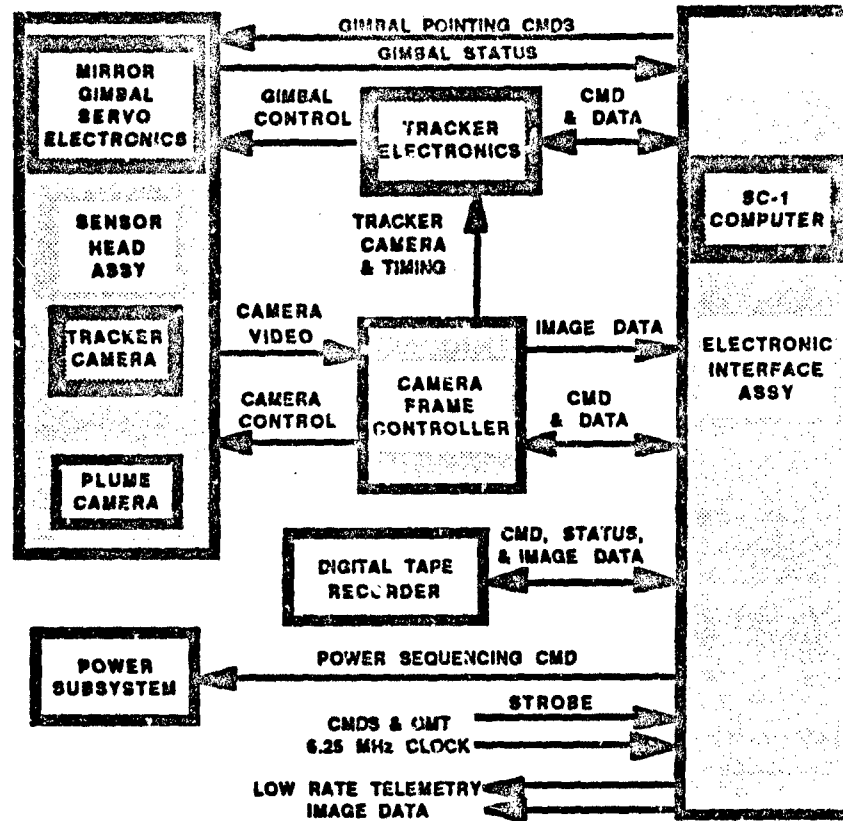


Fig. A2 - Command and data flow within the UVPI

The UVPI is mounted within the satellite and looks through an aperture in the Earth-oriented panel. A gimballed mirror provides UVPI with a field of regard of a  $50^\circ$  half-angle cone about the satellite's nadir. When the UVPI is not in use, a door covers the aperture. Attached to the inside of this door is a flat mirror that allows the UVPI cameras to view celestial objects or the Earth's limb when the door is partially opened.

#### A.1.1 Sensor Head Assembly

The sensor head assembly shown in Fig. A3 houses the UVPI optical components and the two intensified video cameras. The two major sections are the optical bench and the gimbal frame. The optical bench contains the telescope, calibration lamp, tracker and plume cameras, power regulator, filter wheel for the plume camera, filter drive motor, plume-camera folding mirror, relay optics, beam splitter, and the filter for the tracker camera. The optical bench is attached to the gimbal frame that also accommodates the gimbals and resolvers, gimballed mirror, gimbal caging mechanism, calibration mirror, the door, and the door drive motor.

The telescope shown in Fig. A4 is a Cassegrain configuration with refractor corrector plate. The circular aperture is 10 cm in diameter, yielding a  $78 \text{ cm}^2$  gross collecting area. A beam splitter allows the two cameras to share the beam and the forward telescope optics. The effective collecting area, which accounts for beam reduction caused by central blocking and the beam splitter, is used in calculating the net quantum efficiency reported in Appendix E. The focal length for the tracker

camera is 60 cm, which gives an  $f$  number of 6 and a field of view of  $2.62^\circ$  by  $1.97^\circ$ . The plume camera uses a relay lens of magnification 10.3, which provides a focal length of 600 cm, an  $f$  number of 60, and a field of view of  $.180^\circ$  by  $.135^\circ$ .

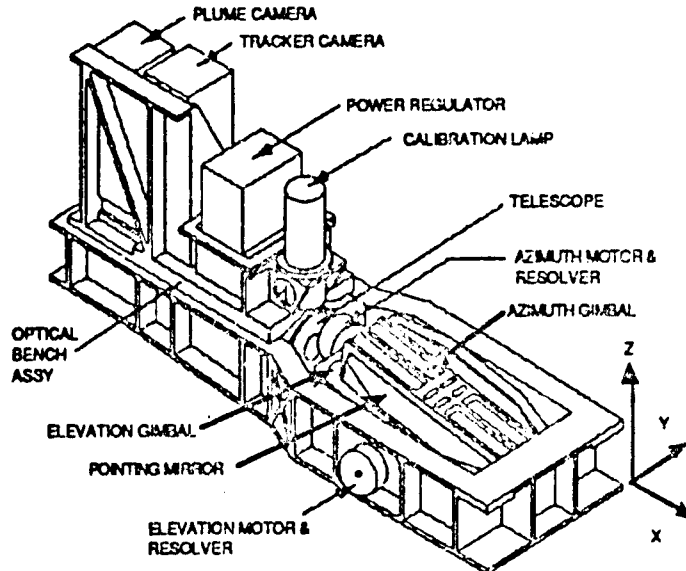


Fig. A3 - UVPI sensor head assembly diagram

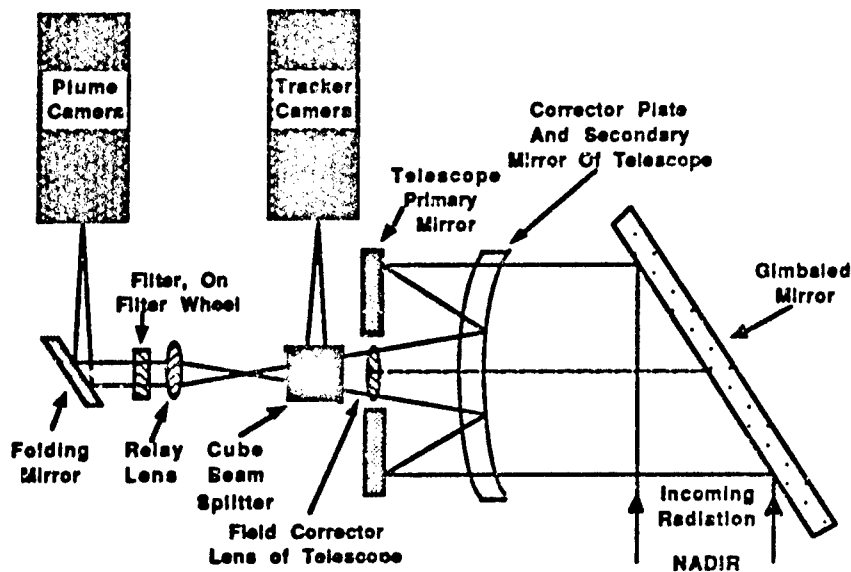
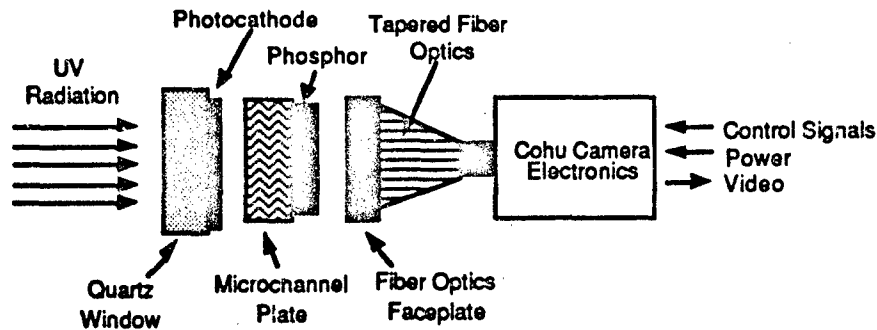


Fig. A4 - UVPI sensor head assembly optics

The intensified cameras shown in Fig. A5 consist of an image intensifier followed by a fiber-optic reducer and a CCD television camera. The intensifiers, which were made by ITT, convert incoming ultraviolet photons into outgoing green photons, giving a large increase in intensity while preserving the spatial characteristics of the image.



### ITT Image Intensifier

- Photocathode
  - CsTe (plume) - 25 mm dia.
  - Bialkali (tracker) - 40 mm dia.
- Microchannel plate
  - 2 Stage (plume)
  - 2 Stage (tracker)
- P 20 phosphor output

### Cohu Camera Characteristics

- RS-170 output - 30 frames/s
- 754 pixel x 240 line array [TI 241 chip set]
- Array has 11-mm diagonal

### Control - Telemetry

- MCP Gain
- Camera Temperature

Fig. A5 - Schematic of intensified CCD camera

The intensifier is a vacuum-sealed cylinder containing circular quartz windows in front and back. The photocathode material, which converts incoming ultraviolet photons to electrons, is a semi-transparent coating on the inside of the front window. The P20 phosphor, which converts electrons to green photons, is a coating on the inside of the back window. The electrons are multiplied as they pass from front to back through a dual-chevron microchannel plate (MCP) that has electron gains of approximately  $10^5$  at high gain settings. The electron energy is increased by the phosphor's anode potential. The overall net gain provides about  $10^7$  green photons per ultraviolet photon.

The tapered fiber optic provides a size reduction of the image to match the intensifier output to the CCD chip input. The CCD chip is a Texas Instrument 241C with a well-transfer function of 1.2 microvolts/electron.

#### A.1.2 Camera Frame Controller

The primary function of the UVPI Camera Frame Controller (CFC) is to receive RS-170 video signals from the plume and tracker cameras, digitize them, and supply them to the electronics interface assembly. The received analog video signals are restored, multiplexed, digitized, and summed by internal CFC circuits. The tracker camera's video signal is buffered and made available to the tracker electronics for target centroid calculations and for determination of the gimbaled mirror pointing commands. Camera telemetry data from the CFC and engineering telemetry data from the electronics interface assembly are added to the digitized video frames and telemetered by the LACE spacecraft for later analysis.

The secondary functions of the CFC are automatic gain control of the exposure of each camera, normal/zoom image rate selection, plume-to-tracker ratio selection, camera telemetry data generation for post-mission reconstruction of the acquired images, filter wheel control, door position control, calibration lamp on/off control, gimbal cage/uncage control, and providing telemetry status data to the electronics interface assembly.

Horizontal and vertical control signals are supplied to both cameras by the CFC for synchronization. An on-board microcontroller allows communication with the electronics interface assembly for receiving commands and periodically sending status information.

The CFC camera frame and field definitions are shown in Fig. A6. The focal plane for each camera is an array of 754 vertical by 480 horizontal pixels. Each video frame is composed of two 754 by 240 pixel fields. The fields from the tracker camera are sent to the tracker electronics at a 60 Hz rate. To form plume- or tracker-camera images for telemetering or onboard storage, three pixels are averaged to form a superpixel, and two fields are then averaged. The result is the 251 vertical by 240 horizontal array of pixels at 30 Hz.

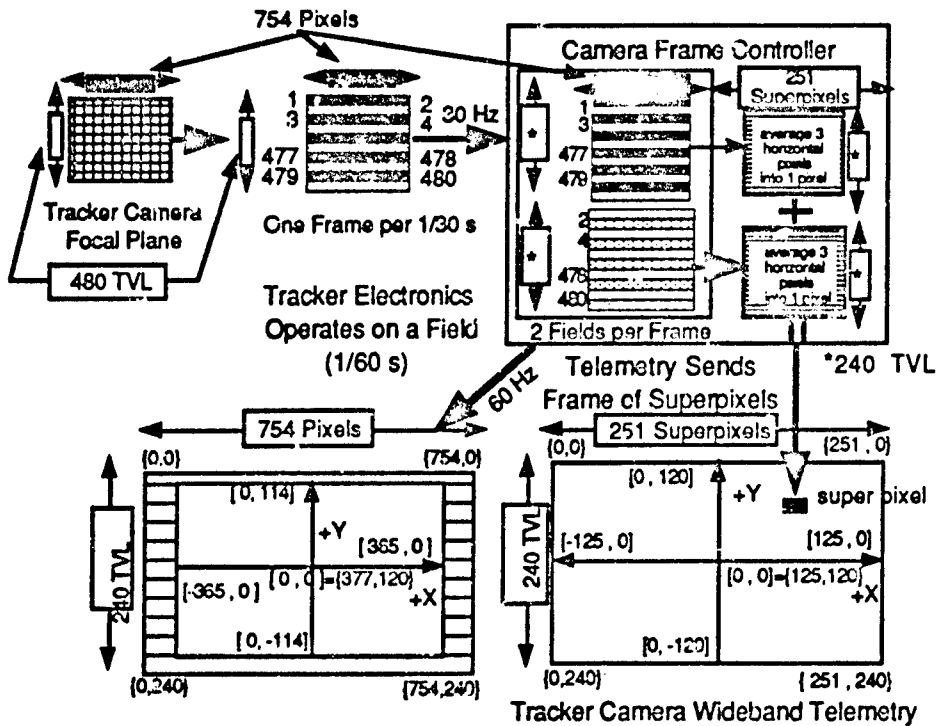


Fig. A6 - UVPI camera frame and field definitions

### A.1.3 Electronics Interface Assembly

The electronics interface assembly (EIA) is the UVPI system controller. Its function is to receive commands and timing information from the spacecraft and distribute reformatted command and timing to the UVPI subsystems. In addition, the EIA collects video camera data from both cameras and status information from the subsystems for delivery to the high and low speed telemetry spacecraft ports.

The heart of the EIA is the SC-1 control computer, also referred to as the instrument control computer (ICC). This is an environmentally ruggedized, general-purpose, 16-bit computer based on a common 8086-type processor. The computer is fabricated in CMOS, and operates at a 5 MHz clock rate.

The SC-1 provides two main on-board input and output links. The first is a serial data channel, RS-232 format, which communicates with the tracker electronics. This interface is software configurable and operates at a 9600-baud data rate. The second link is an extension of the main CPU bus of the SC-1 and is used for communication within the electronics interface assembly.

Pointing the gimballed mirror is possible in either open-loop or closed-loop modes. In the open-loop mode, the SC-1 computer uses a pointing function to calculate a sequence of desired azimuth and elevation angles for the gimbals. The gimbal servo then adjusts the gimbal until the gimbal angle readouts match the desired angles. The pointing function, which calculates the desired

angles, consists of two segmented polynomials, each of the same order ranging from three to six. Up to 255 pointing functions can be transmitted and stored in the SC-1 computer, and the desired function can be selected by command.

In the closed-loop mode, the tracker electronics determine the tracking error by measuring the angular displacement between a target centroid and the center of the tracker-camera's field of view. The gimballed mirror is then moved under control of the tracker electronics to bring the target centroid to the center of the tracker camera's field of view.

The open-loop pointing is used in the POINT mission mode shown in Fig. A7. This mode is used to move the mirror through a scan pattern in order to find the target if it is beyond the tracker-camera's field of view. Once the target is seen in the tracker camera by the ground station operator, the ACQUIRE mode is commanded. This enables the tracker to take control after it has locked onto the target. When this occurs, the mission mode is changed to TRACK. If the target image is lost while it is being tracked, the tracker electronics will enter the EXTRAPOLATE mission mode. Accordingly, the SC-1 computer will point the gimballed mirror by using a second-order polynomial extrapolation function based on the recent gimbal angle history. If the target reappears during the extrapolated pointing, the tracker electronics will go back into the TRACK mode and regain control of the gimbal.

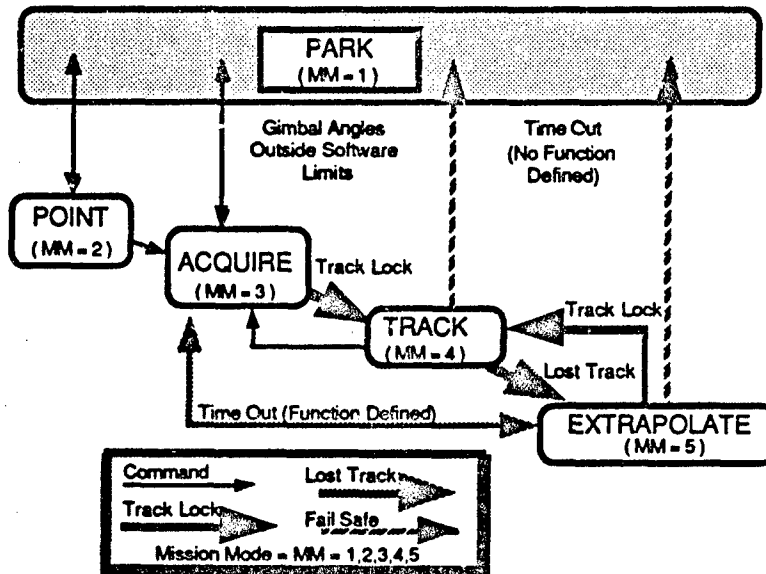


Fig. A7 - Allowable mission mode transitions

#### A.1.4 Power Subsystem

The power subsystem provides all of the input power needed by the UVPI at various voltage levels and provides electromagnetic interference protection for the UVPI. To aid LACE's tight power budget, the power subsystem is designed so that lower power levels can be used when mission requirements warrant. This would occur, for example, when only commands are being loaded or when only the tape recorder playback function needs to be actuated. Primary power is received from the LACE spacecraft at 28 volts DC. Maximum power used by the UVPI is 218 W (normal is 157 W).

#### A.1.5 Digital Tape Recorder

The digital tape recorder is a NASA standard magnetic tape recorder used for storing digitized video and engineering data. The unit, designed and manufactured by RCA, can store approximately 7 min. of data at 2.7 Mbps.

## A.1.6 UVPI Tracking Subsystem

### A.1.6.1 Tracker Camera

The UVPI is mounted within the satellite and looks through an aperture in the Earth-oriented panel. By using a gimbaled mirror, the UVPI has a field of regard (FOR) of a  $50^\circ$  half-angle cone about the satellite's nadir (Fig. A8). The tracker camera's field of view (FOV) is  $2.62^\circ$  by  $1.97^\circ$ , which corresponds to approximately 22 km by 16 km on the ground at nadir. The tracker camera characteristics are shown in Table A1. The tracking subsystem specification requirements and performance are shown in Table A2.

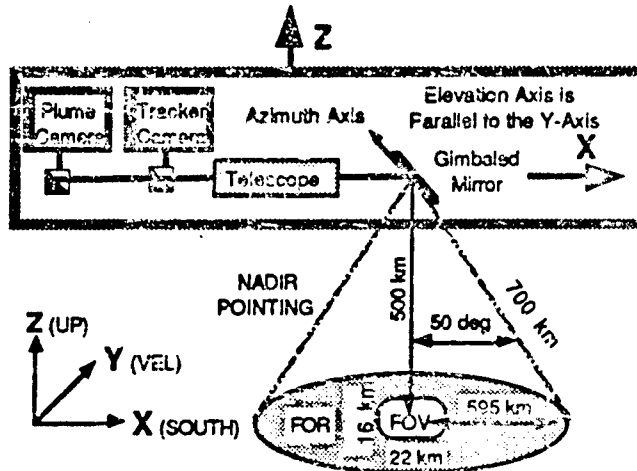


Fig. A8 - Tracker-camera FOV and FOR

Table A1 - Plume and Tracker Camera Characteristics

Parameter	Tracker Camera	Plume Camera
Spectral region	255-450 nm	195-350 nm
Number of filters	1	4
Time for filter change	n/a	1.7 s
Image rate: Normal	5/s	5/s
Zoom*	30/s	30/s
Pixels: Normal	251 x 240	251 x 240
Zoom	91 x 112	91 x 112
Digitization	8 bits/pixel	8 bits/pixel
Image data rate	2.5 Mbps	2.5 Mbps
Field of view	$2.62 \times 1.97$ deg	$.180 \times .135$ deg
Field of regard	$100 \times 97$ deg	$100 \times 97$ deg
Pixel footprint	$182 \times 143$ $\mu$ rad	$12.5 \times 9.8$ $\mu$ rad
System resolution	220 to 250 $\mu$ rad	80 to 100 $\mu$ rad
Pixel exposure time	0.16 to 33.3 ms	33 ms
Frames integrated	n/a	1 - 6
Exposure range	$>10^6$	$>10^6$
Noise equivalent radiance	See Section 4.7 for detailed discussion. NER depends on gain setting and filter selected.	

\*Reduced field of view.

Table A2 - Tracking Subsystem Requirements and Performance

Specifications	Requirements	Measured Performance
Position loop bandwidth	5 Hz	5 Hz
Pointing error	400 $\mu$ rad RMS	96 $\mu$ rad RMS
Tracking jitter	15 $\mu$ rad RMS	6 $\mu$ rad RMS
Tracking velocity	1 deg/s	7 deg/s
Tracking acceleration	0.05 deg/s <sup>2</sup>	5 deg/s <sup>2</sup>

## A.1.6.2 Tracker Electronics

Figure A9 shows the functions of the tracker electronics. The tracker camera's video signal is received from the camera frame controller on a RS-170 link at 60 fields per second. The video signal is first passed through the spot remover that removes the effects of sensor blemishes and optical system obstructions, and removes background clutter on a field-to-field basis. The spot remover contains two video memories to map spot locations. One memory stores the short-term map for background clutter subtraction, and the other memory stores the map of longer lasting blemishes. The correction for blemishes is achieved by substituting a predetermined video level for the blemished location.

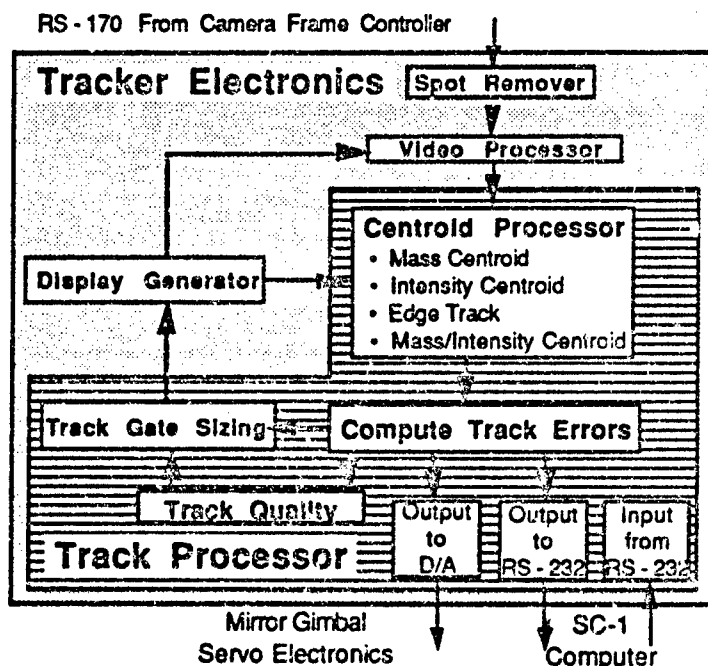


Fig. A9 - Functions of tracker electronics

After passing through the spot remover, the video signal enters the video processor. The video processor also receives the horizontal and vertical control signals and a clock signal to control synchronization and data sampling. The video processor also determines the target size.

A tracking window, or track gate, bounds the subarray of pixels that are identified as part of the target. The size of the tracking window can be directly controlled by the SC-1 computer or by the track gate sizing portion of the tracker electronics as a ratio with the target size.

The data from the pixels within the tracking window are sent to the centroid processor, which can use one of several algorithms to determine the location of the target in the tracker camera's focal plane.

Algorithm choices include mass centroid, which spatially averages all pixels above threshold with equal weighting; intensity centroid, which weights each pixel by the intensity of its response; and mass and intensity centroid. For mass and intensity centroid tracking, the intensity centroid algorithm is used to determine the target position within the field of view and the mass centroid algorithm is used to calculate the target size and target validity.

Figure A10 shows the definitions associated with the tracker camera's focal plane that the tracker electronics use in determining the target location in the focal plane. The tracking error is used to command the gimbal servo electronics to drive the tracking error to zero as described in Appendix D. The gimbal commands are converted to analog signals and transmitted to the gimbal servo electronics at 60 Hz. The tracker electronics transmits data to the SC-1 computer in a command-response sequence except during the TRACK mode, when the output data are transmitted at 30 Hz.

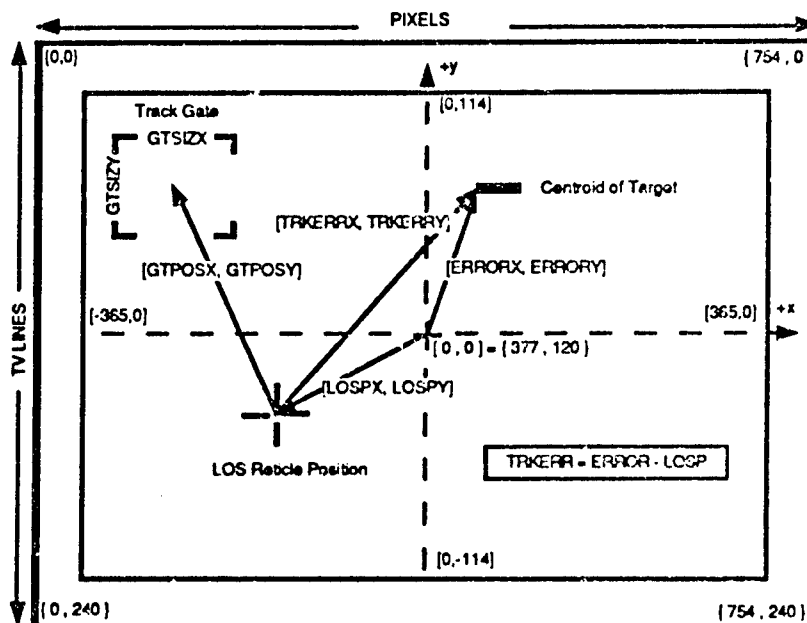


Fig. A10 - Definitions associated with tracker-camera's focal plane





## Appendix B

### UVPI CHARACTERIZATION AND CALIBRATION

This appendix discusses the characterization and calibration of the UVPI plume and tracker cameras. Section B.1.0 discusses the spectral response of the cameras and the conversion from incident photons to photoevents detected by the UVPI. Section B.2.0 details the conversion from photoevents to the digital number reported in the UVPI data stream. The method for converting UVPI data to radiant intensity and spectral radiant intensity units is detailed in Section B.3.0. Section B.4.0 shows the results of on-orbit calibration of the instrument by observing known stars.

#### B.1.0 UVPI SPECTRAL RESPONSE

The UVPI plume and tracker cameras are described in detail in Appendix A. The optical paths for both the plume and tracker cameras can be divided into two parts. The first part of each camera system consists of the telescope, a bandpass filter to select the observation wavelength, and the photocathode of a microchannel plate (MCP) image intensifier. For the plume camera, one of four bandpass filters can be selected, and the photocathode material is CsTe. For the tracker camera, only one bandpass filter is available, and the photocathode material is bialkali. The second part of each camera system consists of the remaining elements of the image intensifier, the CCD imager, and the CCD control electronics that convert the pixel response to a digital number. The gain of each image intensifier is selectable, and the exposure time of the tracker camera is selectable by strobing the intensifier high voltage. The response of the UVPI cameras can be divided into the gains of the two parts described above.

The first component of the response for each camera is the net quantum efficiency, which is the probability that a photon incident on the UVPI telescope will produce a photoevent (PE). A photoevent is defined as a photoelectron at the photocathode that is collected and amplified by the MCP. This component of the response is wavelength-dependent. It corresponds primarily to the filter bandpasses but also includes the wavelength dependence of the optics and photocathodes. The collection efficiency of the MCP is incorporated into this component.

The second component of the response for each camera is the conversion ratio between photoevents and the digital number reported by the CCD control electronics. This digital number is the one that is reported for each pixel in the telemetry stream. This component is not wavelength dependent; it takes into account MCP gain and phosphor and CCD efficiencies.

The net quantum efficiencies for the plume and tracker cameras are shown in this section. The conversion of photoevents per pixel to a digital number in telemetry is discussed in Section B.2.0.

##### B.1.1 Ultraviolet Response

The response of the UVPI plume and tracker cameras as a function of wavelength in the ultraviolet was carefully measured before launch. The net quantum efficiency of the plume camera for each of the four bandpass filters is shown in Fig. B1. The net quantum efficiency of the tracker camera is shown in Fig. B2. The values of net quantum efficiency plotted in these figures are tabulated in Appendix E.

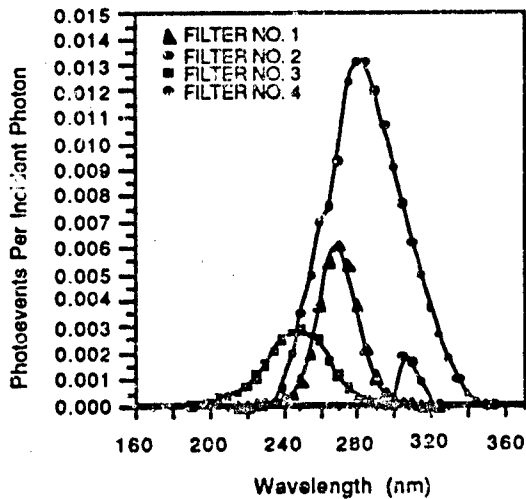


Fig. B1 - Plume camera net quantum efficiency curves

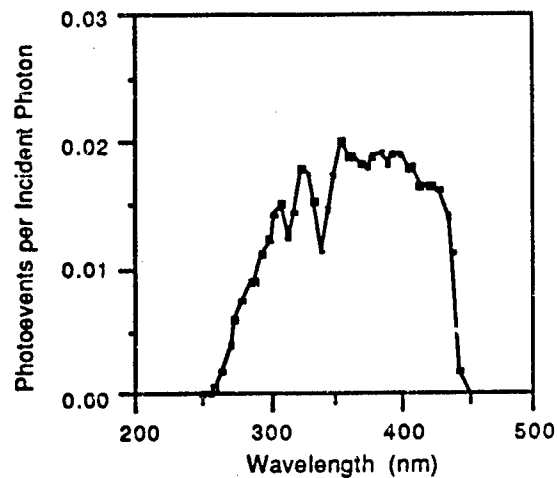


Fig. B2 - Tracker camera net quantum efficiency curve

### B.1.2 UVPI Extended Response

Some sources observed by the UVPI, such as rocket plumes, are much brighter in the visible and near-infrared wavelengths than in the ultraviolet. Therefore, even a strongly attenuated response of UVPI to these wavelengths could significantly affect the data. A combination of very conservative estimates and laboratory measurements were made to characterize the response of the UVPI into the visible and near-infrared; the results are shown in this section. It should be emphasized that the readings presented here are worst-case values and represent an upper bound on the long-wavelength response of UVPI. Tests and analysis are in progress to better characterize the long-wavelength response.

Analysis shows that only the plume camera with filter 4 and the tracker camera have the possibility of significant response to long wavelengths when observing a source such as a plume. The plume camera with filters 1, 2, or 3 does not have significant long-wavelength response. The estimated worst-case net quantum efficiency extended to long wavelengths for the plume camera is shown in Figs. B3 through B6. Similarly, the estimated worst-case net quantum efficiency for the tracker camera is shown in Fig. B7.

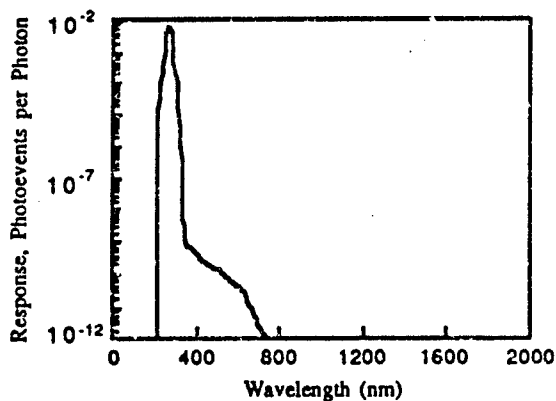


Fig. B3 - Plume camera extended net quantum efficiency, filter 1

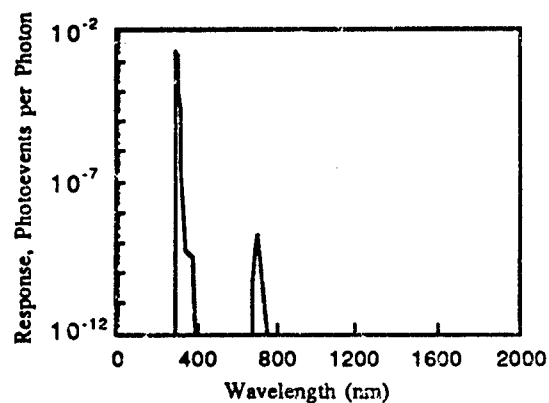


Fig. B4 - Plume camera extended net quantum efficiency, filter 2

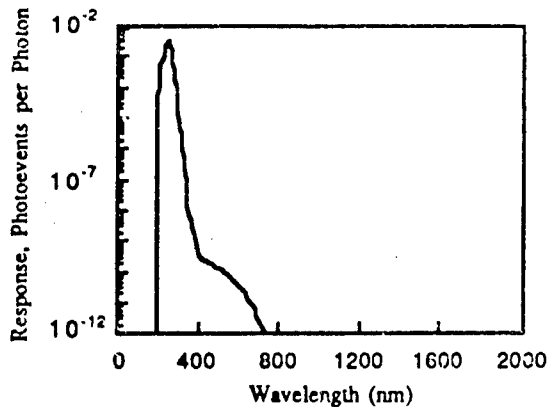


Fig. B5 - Plume camera extended net quantum efficiency, filter 3

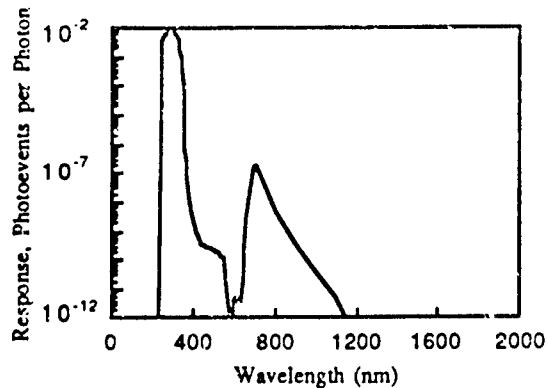


Fig. B6 - Plume camera extended net quantum efficiency, filter 4

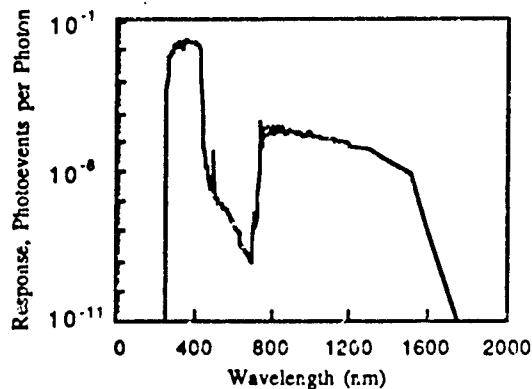


Fig. B7 - Tracker camera extended net quantum efficiency

To estimate the possible effects of long-wavelength response when observing a thermal source, analysis was carried out to determine the percentage of photoevents detected by UVPI that would arise from out-of-band radiation with wavelengths longer than the nominal bandpasses shown in Figs. B1 and B2. This analysis assumes the worst-case estimates for long-wavelength UVPI response shown in Figs. B3 through B7, and a thermal source with the reference spectral shape. By using these conservative assumptions, the analysis shows that less than one percent of the photoevents recorded by the plume camera arise from long-wavelength radiation. Because the potential effect of the long-wavelength response is negligible, the plume camera data reported in this document have not been adjusted for the potential long-wavelength response. The analysis for the tracker camera, using the same assumptions, shows that no more than 14% of the photoevents reported by the tracker camera arise from photons with wavelengths longer than the nominal tracker bandpass. The data reported in this document for the tracker camera have been adjusted to account for this effect by dividing the total number of photoevents recorded by the tracker camera by 1.14.

## B.2.0 CONVERSION FROM DIGITAL NUMBER TO PHOTOEVENTS PER PIXEL

### B.2.1 Gain Conversion Factor $G_g$

It is assumed that the net quantum efficiency curves shown in Section B.1.0 remain constant under all measurement conditions. Therefore, variations in the responsiveness of the instrument are taken into account in the gain conversion factor  $G_g$  for the  $g$ th gain step. The values of  $G_g$  are not

dependent on wavelength but are dependent primarily on microchannel plate gain step. To a lesser extent, the  $G_g$  values depend on phosphor efficiency, CCD efficiency, sensor temperature, and possibly pass-specific parameters. The values of  $G_g$  are shown for the tracker camera in Fig. B8, and for the plume camera in Fig. B9. The values of  $G_g$  for both cameras are tabulated in Appendix E. The units for  $G_g$  are digital number per photoevent.

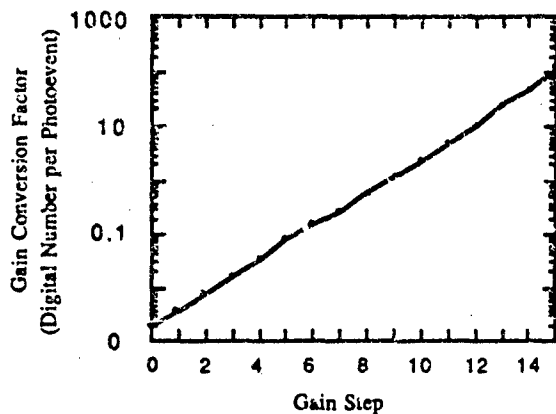


Fig. B8 -  $G_g$  vs gain step for tracker camera

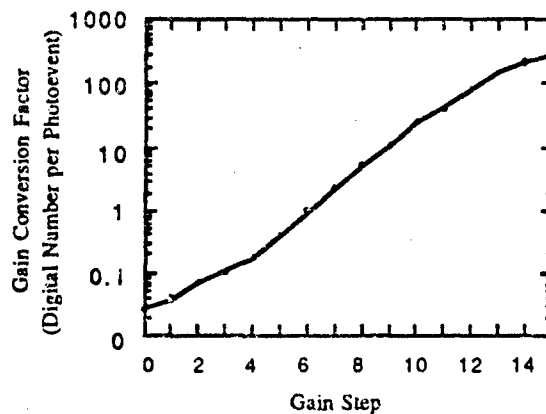


Fig. B9 -  $G_g$  vs gain step for plume camera

The values of  $G_g$  for all gain steps were measured before launch. In addition, the value for gain step 15 was determined by using sparse-field data for which single, isolated photoevents are generated from dark-noise or illumination. The values for all pixels associated with each isolated photoevent are summed, and the resulting sum is the  $G_g$  value for this step. Finally, on-orbit calibrations for all plume and tracker camera bandpasses were performed. These are discussed in Section B.4. The on-orbit calibrations agreed well with the laboratory calibrations and are used as the primary instrument calibration.

### B.2.2 Dark Field

Dark field images are collected with the UVPI door closed. The pixel brightness results from two sources: dark current in the photocathode, microchannel plate, and charge-coupled device; and a fixed bias voltage on the readout line. The dark current component has fixed pattern spatial variations that can be determined accurately by averaging a large number of frames. The bias voltage component contributes some spatially and temporally random noise.

The dark field average used for calibration of the Strypi data was generated from data collected during the Strypi observation pass immediately following the plume observation. This allowed generation of  $D_k$ , the dark value for the  $k$ th pixel. Previous analysis showed that, as expected, average dark field values do not depend on microchannel plate gain step. However, at high gain steps, occasional responses due to cosmic rays or thermally generated electrons from the photocathode are present.

For the tracker camera, 139 dark field images were averaged. The spatial mean of the temporal mean pixel values is 19.6, and the spatial mean of the temporal standard deviation in pixel values is 1.6. For the plume camera, 27 images were averaged. The spatial mean of the temporal mean pixel values is 9.3, and the spatial mean of the temporal standard deviation in pixel values is 1.0.

### B.2.3 Spatial Nonuniformity

Tracker and plume camera nonuniformity matrices were generated by using several images looking down at the ocean. This allowed generation of  $U_k$ , the gain nonuniformity correction factor for the  $k$ th pixel. For the tracker camera, the images of small moving clouds were removed by selecting the minimum value in a temporal sequence of images on a pixel-by-pixel basis. For the plume camera, a sequence of images (taken with filter 4, 235 to 350 nm bandpass), were averaged. No clouds crossed the plume camera's field of view during the sequence.

For the central 91 by 112 pixels transmitted by using the zoom image transmission rate, overall nonuniformity is less than 5%.

### B.3.0 UVPI DATA ANALYSIS METHODOLOGY

#### B.3.1 An Example

The derivation of radiometric values from the observed photoevent numbers was described in Section 4.2. An example here illustrates the procedure and clarifies the significance of the values presented in the body of the report.

Some reference spectral function must be assumed to convert the photoevent counts to radiometric values. The reference function  $R(\lambda)$  is generally taken here to be the most likely representation of the plume emission available. The amplitude of the reference function is arbitrary and is conveniently set by tying the function to the Planck blackbody function below 300 nm. The essence of the radiometric analysis is the determination of the amplitude of this reference function that will yield the observed photoevent counts.

Suppose, for this example, that the observed photoevent count is 1.0 for a single plume-camera pixel with plume-camera filter 4. Then the amplitude of the reference function is calculated by integrating the assumed reference function across the instrument response curve, according to Eq. (3) in Section 4.2.2.1, such that this photoevent count would be observed. Figs. B10 shows this amplitude-scaled reference function with the UVPI instrument response using filter 4 with center wavelength 280 nm, full-width-half-maximum 56 nm, and nominal full bandpass 235 to 350 nm.

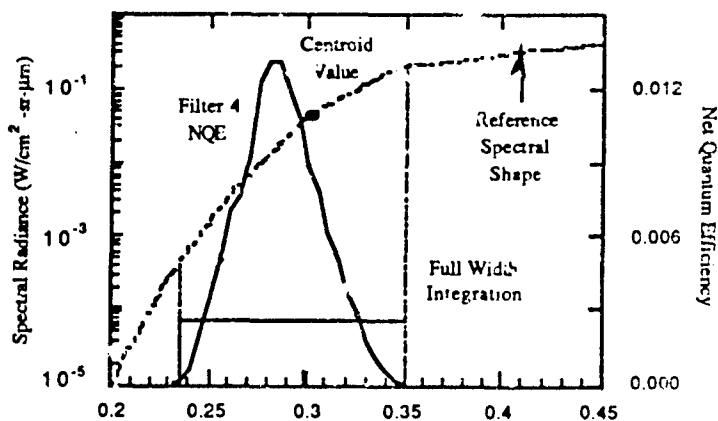


Fig B10 - Scaled reference function  $L(\lambda)$  and centroid location assuming reference spectrum.

This scaled reference curve is essentially the complete answer,  $L(\lambda)$ , to the question of the radiometric value of the source. This curve cannot unambiguously be specified as a single number, as is needed for tabulation and for graphing against other variables, e.g., time. A simple means of specifying the curve is to specify its value at a selected wavelength. The most representative

wavelength was taken to be the centroid of the instrument response as weighted by the reference shape, according to Eq. (13) in Section 4.2.3.1. The reference shape is so strongly variable in wavelength that this centroid differs substantially from the center wavelength of the instrument response, as illustrated in Fig. B10. One could choose a different wavelength for specification of the reference function and thereby change the tabulated spectral radiance without changing the solution function  $L(\lambda)$  at all. If one chose to specify the spectral radiance at the filter peak instead of the response centroid, for example, the nominal spectral radiance would be changed by almost a factor of two. This change would be a matter of numeric specification, not a real change to the spectral radiance solution.

Some users have requested that the observations be stated as radiances, rather than as spectral radiances. Radiance values are obtained by integrating across the portion of the reference function specified by the full width of the instrument response (the full width integration shown in Fig. B10). Again, one could justifiably redefine the spectral width of the integration, such as taking the full-width-half-maximum points instead of the full-width endpoints, and change the quoted radiance value substantially. Such a change would be an artifact of the radiance definition and would not imply any real change to the reference function determined from the data. Comparisons of radiance numbers must be based on identical integration ranges to be valid. Similar considerations apply to spectral radiant intensity and radiant intensity calculations.

The foundation of the data analysis is the assumed source spectral shape  $R(\lambda)$ . A change in the assumed source spectral shape will necessarily change all the numerical results. This is an unavoidable and well-known difficulty in the analysis of radiometric data from practical instruments.

#### B.4.0 ON-ORBIT CALIBRATION OF UVPI

The radiometric calibration constants for the UVPI have been confirmed on orbit. This was done by measuring the sensor output for a star and comparing it with the predicted number of photoevents based on the star's spectrum and brightness. The ratio of these two quantities is the gain conversion factor  $G_g$  for the gain step used in the measurement. The predictions of the number of photoevents from a star are based on measured stellar emission spectra obtained by the International Ultraviolet Explorer (IUE) and Orbiting Astrophysical Observatory (OAO) satellites [21,22]. Spectral information spanning the Balmer discontinuity and extending to longer wavelengths was obtained from atmosphere-corrected ground-based measurements [23].

Figures B11 and B12 show calibration results for the plume camera and tracker camera, respectively. Figure B11 shows calibration points for all four plume-camera filters. The solid curve shown in each figure is very close to that measured before launch, and these star measurements are the primary calibration for the UVPI. The stars used for calibration are mostly type B stars of sufficiently high temperature that they are strong emitters in the ultraviolet and make any long-wavelength response of the UVPI insignificant. The on-orbit calibration measurements indicate that the UVPI responsiveness has remained constant during the first year following launch. Section 4.6 addresses the error in the gain conversion factor and the sources of error that affect the data analyses.

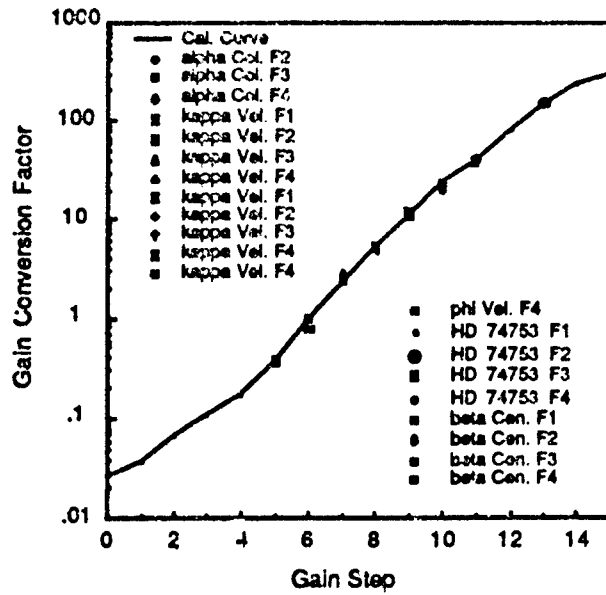


Fig. B11 - Star measurements for plume camera

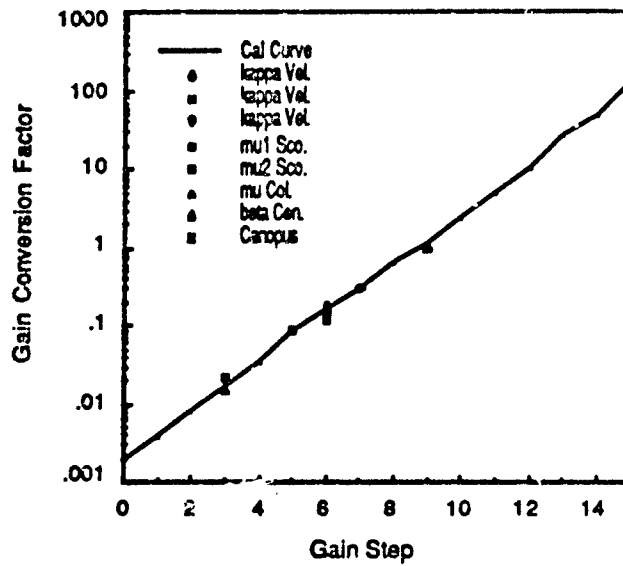


Fig. B12 - Star measurements for tracker camera





## Appendix C PREFLIGHT PLANNING

Preflight planning consisted of determining the optimal launch window and developing the details of the encounter scenario. These are discussed in detail in sections C.1.0 and C.2.0 below.

### C.1.0 LAUNCH WINDOW AND LAUNCH TIME SELECTION

Based on the predicted Strypi trajectory, the launch window was calculated to provide favorable geometry for UVPI viewing of the Strypi flight and to meet the constraints of the various experiments. These constraints included: darkness on both the LACE spacecraft and the Strypi vehicle, and the moon not appearing within view of the bow shock sensors within the nose of the missile.

Figure C1 shows the trajectory visibility plot for the observation on 18 February 1991, based on the planned nominal Strypi trajectory and LACE orbital elements used during the observation. The x axis of the plot shows the possible launch time, in seconds, after the reference GMT of 14:15:00. The y axis shows the time into the trajectory after launch. A visibility envelope is defined by the triangle marked (Time First Seen) and square marked (Time Last Seen) lines. A point within the envelope means that if Strypi was launched at the time corresponding to the x axis value, then Strypi is visible to UVPI at the time in the trajectory denoted by the y axis value. The visibility limit was based on the 50° from nadir field of regard for UVPI.

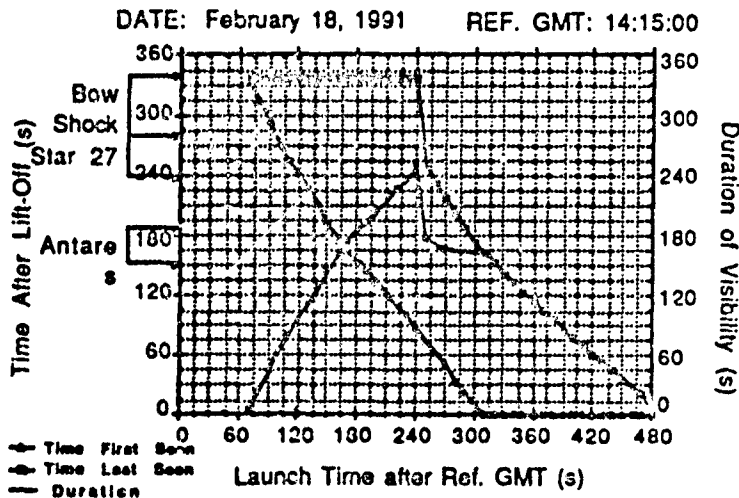


Fig. C1 - Strypi trajectory visibility plot

The following is an example based on Fig. C1. If Strypi was launched at 14:18:00, 180 s after the reference GMT, then UVPI would first be able to view Strypi at 154 s after liftoff, which is just after the nominal Antares ignition time of 152 s. UVPI would be able to keep Strypi in view at least until 338 s after launch, which is the point where the planning trajectory ended.

An acceptable launch window must meet the mission requirements of viewing the Antares and Star 27 burns and the bow shock region. By using Fig. C1, the launch window was determined to be from about 185 s to 240 s after the Reference GMT, i.e., from 14:18:05 to 14:19:00.

Within the launch window, a launch time was selected to optimize viewing geometry of the highest priority portions of the flight in terms of range between UVPI and Strypi, aspect angle, and vignetting of the UVPI camera image. The selected launch time was then checked to ensure that it fit in with the UVPI encounter activities without jeopardizing a successful observation. This was especially important for the launch opportunity on 18 February 1991, since there were only a few seconds between expected acquisition of signal from LACE and the deadline for stopping the launch. The optimum launch time was determined to be 14:18:35 GMT based upon the aforementioned factors. The nominal encounter geometry for this selected launch time is shown in Fig. C2.

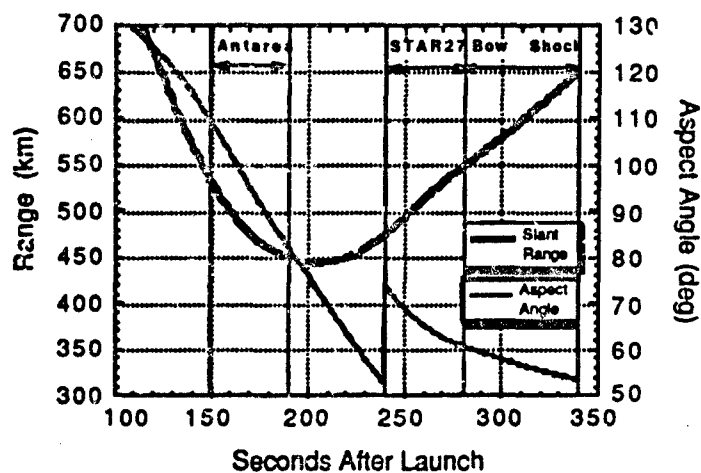


Fig. C2 - Strypi/UVPI planned encounter geometry for launch at 14:18:35 GMT on 18 February 1991

## C.2.0 ENCOUNTER PREPARATIONS

Preparations for the UVPI-Strypi encounter required development of a detailed sequence of delayed-execution commands to be transmitted to the spacecraft prior to the encounter. Since the encounter time was so short, most of the commands had to be preloaded to operate the instrument automatically with only a few select commands left to be sent by the ground crew in real time. Preparations also involved verification of the command sequence through both ground simulation and flight rehearsals. Initial command sequence verification was done by testing the delayed-execution commands along with the real-time commands and pointing functions by using the LACE Operational Test Bed (LOTB), a complete simulator including a preprogrammed target trajectory. Finally, to test the entire system and encounter timeline in actual operation, three rehearsals were conducted with the spacecraft observing UV ground beacons as simulated plume targets at the appropriate time of day on each of several days just prior to launch.

### C.2.1 Planned Plume Observation Scenario

This is the detailed scenario as planned for the encounter. Table C1 is the timeline of events for the Strypi-UVPI encounter. Boldface denotes UVPI delayed-execution commands, plain text denotes real-time commands or ground events, and italics denote outside events beyond UVPI control.

Table C1 - Timeline of Events for the Strypi Observation

Time (GMT)	Time-Launch	Delayed Execution Commands	Ground Operations	Real-Time Commands
4:21	-9:57:35	VAFB5576		Primary upload
4:31	-9:47:35	PGSS5576	Update KPY file	Backup #1 upload
6:01	-8:17:35	VAFB5577	Update Yaw_ampl.dat	Backup #2 upload; BSM monitor
12:37	-1:41:35	KHEL5581	Prepare uvecs file (Run UVECS_5582.COM)	BSM monitor
14:14:50	-0:03:45	Turn UVPI on		
14:15:25	-0:03:10	Turn k1, k2 on		
14:15:45	-0:02:50	Set tracker max gain to 10		
14:15:50	-0:02:45	Initialize tracker		
14:16:00	-0:02:35	Set filter to 4		
14:16:08	-0:02:27	Load MASS AND INTENSITY run block	Activate WLN_5562	
14:16:39	-0:01:56	Turn off agc, set track & plasma gains to 0	Compute 118	
14:16:44	-0:01:51	Set extrapolate to 5 s.	Compute 198	
14:16:45	-0:01:50	Set frame ratio to 1:15 (Plume Tracker)	Compute 18	
14:16:51	-0:01:44	Open door to 51.24° (8db)	Compute 28	
14:17:11	-0:01:24	Turn on AGC		
14:17:12	-0:01:23	Turn on tape recorder, tape unit a		
14:17:13	-0:01:22	Swing gimbal to left (Az = -5.5°, El = 4.3°)		
14:17:18	-0:01:17	Swing gimbal to right (az = +5.6°, El = +1.4°)		
14:17:23	-0:01:12	Turn off tape recorder		
14:17:24	-0:01:11	Point to star (gamma velorum) using INFUNC 118		
14:17:25	-0:01:10	Set lost track function 198		
14:17:45	-0:00:50	KHEL AOS 5°		Open door 1 step, if req.
				Upload FIX STAR 198
				Point FIX STAR 198 (pred)
				Upload SCAN STAR 118
14:18:20	-0:00:15	<<<< GO/NO-GO Decision >>>>		Point SCAN STAR 118
			UMT-GMT	Upload ANTARES 28
		<scan star>	determine y. #	Upload ROCKET 18
				Upload FIX STAR 198 (calc)
				Point FIX STAR 198 (calc)
				Acquire FIX STAR 198
				Pl:Tk ratio 8:2
				Zoom On
				Filter Sequence J,2,1
			UMT - GMT	
14:18:35	0:00:00	<<<<<<<<< STRYPI LAUNCH >>>>>>>>		
			Compute ind 18	
14:19:15	0:00:40	STRYPI Castor B0		

Table C1 - Timeline of Events for the Strypi Observation (Cont'd)

Time (GMT)	Time-1 aunch	Delayed Execution Commands	Ground Operations	Real-Time Commands
14:19:57	0:01:22	Update Antares ignition time (24 s)	Compute inf 28	
14:20:26	0:01:51	Set filter to 4		
14:20:34	0:01:59	Turn off zoom		
14:20:35	0:02:00	Set frame ratio to 2:8 (p:t)		
14:20:36	0:02:01	Point to 0,0		
14:20:37	0:02:02	Open door fully for STRYPI viewing		
14:20:38	0:02:03	Initialize tracker		
14:20:47	0:02:12	Load MASS AND INTENSITY run block	Compute 18 (1 deg)	Upload ANTARES inf 28
14:20:57	0:02:22	Point to STRYPI using INFUNC 28		
14:20:58	0:02:23	Set lost track FUNC 28		
14:21:02	0:02:27	Turn on tape recorder, tape unit A		
14:21:03			Time Filter	Acquire ANTARES w/ inf28
14:21:07	0:02:32	STRYPI Antares ignition	0 - 4 4	Zoom On
			6 - 16 3	P:T 8:2
			18 - 23 2	Filter sequence
14:21:42	0:03:07	STRYPI Antares BO	23 - end 1	
14:21:47	0:03:12	Turn off zoom		
14:21:48	0:03:13	Set frame ratio to 2:8 (P:T)	Compute BOWSHK 28	Upload ROCKET inf 18
14:21:52	0:03:17	Turn off tape recorder		
14:22:24	0:03:49	Turn on tape recorder, tape unit A		
14:22:28	0:03:53	Point to STRYPI using INFUNC 18		
14:22:29	0:03:54	Set lost track FUNC 18		Acquire ROCKET w/inf 18
14:22:30	0:03:55		Time Filter	
14:22:34	0:03:59	STRYPI Star 27 ignition	0 - 15 1	Zoom On
			17 - 27 2	P:T ratio 8:2
			29 - end 3	Filter Sequence
14:23:10	0:04:35	Set extrapolate to 10 s	0 - 3 3	
14:23:10	0:04:35	Set tracker max gate to 11	5 - 8 4	
14:23:15	0:04:40	STRYPI Star 27 BO	10 - 13 3	Upload BOW SHOCK 28
14:23:15	0:04:40	STRYPI Bow shock start	15 - 18 2	Point BOW SHOCK
14:24:13	0:05:38	STRYPI LOS (40km)	20 - end 3	Activate joystick
14:24:23	0:05:48	Turn off AGC		
14:24:24	0:05:49	Set track and plume MCP gains to 0		
14:24:24	0:05:49	Perk gimbal mirror		
14:24:24	0:05:49	Turn off tape recorder		
14:24:25	0:05:50	Close door		
14:24:55	0:06:00	Start Dark Field Data Test		
14:24:57	0:06:22	Turn on tape recorder, tape unit A		
14:25:18	0:06:43	Turn off tape recorder		

Table C1 - Timeline of Events for the Strypi Observation (Cont'd)

Time (GMT)	Time-Launch	Delayed Execution Commands	Ground Operations	Real-Time Commands
14:26:56	0:08:21			command UVPI shutdown
14:27:26	0:08:51	Command UVPI shutdown		
14:27:26	0:08:51	KHEI LOS 5°		

### C.2.1.1 Pre-Encounter Activity

Three minutes prior to acquisition of signal (AOS) by the ground station, the UVPI is turned on. Two minutes later the UVPI door is opened and two star patterns are observed and recorded on the UVPI tape recorder. These star observations provide an independent set of data to confirm the attitude of UVPI during post-pass analysis. UVPI then points to the main target star, gamma Velorum, with a slow scan pattern in the yaw direction to determine the yaw attitude of the spacecraft.

At Kihei, the UVPI health and status is checked by the LACE engineer. If the UVPI status is in any way deemed unacceptable, the encounter manager will declare a Strypi NO-LAUNCH condition. Because of time limitations, initial pointing must be done by using predicted attitudes. The fixed star function based on the most recent predicted attitude will be transmitted and used to locate the main target star, gamma Velorum. If the target star cannot be located, which means the predicted attitude cannot be verified, a NO-LAUNCH condition is declared.

On the other hand, if the experiment status is acceptable and the predicted attitude is reasonable, the encounter manager will announce UVPI as GO FOR LAUNCH. The predicted scanning function is then transmitted and the star yaw scan starts. While UVPI is scanning, pointing functions for the Antares and Star 27 stages based on nominal conditions and the predicted attitude are transmitted.

UVPI is commanded to point to gamma Velorum by using the fixed star function based on the predicted attitude. A new fixed star function is generated by the ground software based on the yaw computed from the slow scan, and UVPI is pointed at the reference star using this function. The encounter manager will then select the better yaw value, computed or predicted, for computing the rocket pointing functions.

Gamma Velorum is acquired to collect star calibration data and to test the keypad commands for zoom rate transmission of images, plume-to-tracker ratio, and filter wheel changes. An equal amount of data is collected at each of the four plume-camera filter wheel positions.

### C.2.1.2 Antares Plume Observation

After the star calibration data activities are completed, the delayed-execution commands reset UVPI in preparation for viewing the Antares rocket plume.

After Strypi is launched, the actual launch time is incorporated into the real-time computations of the Antares and Star 27 rocket pointing functions. About 80 s after launch, the modified Antares ignition time and trajectory type, i.e. nominal or left, right, high or low dispersed, is incorporated into the real-time computation of the Antares pointing function, which is then transmitted.

The UVPI door will open fully for viewing Strypi; about 10 s before Antares ignition is expected, UVPI starts pointing at the expected Strypi trajectory by using a 0.65° radius circular scan with a 16-s period. The scan radius was selected to ensure that Strypi would appear in the tracker camera FOV at least during some portion of the circular scan, even with 3-sigma dispersion of the trajectory and expected spacecraft attitude errors.

Approximately 5 s before ignition, the command to acquire is sent. This ensures the minimum possible delay between ignition and lock-on by UVPI. If the Antares burn is not seen within about 10 s after expected ignition, a new pointing function with a  $1.0^\circ$  circular scan radius is transmitted and implemented.

After the Antares burn is seen and the tracker is in the process of locking onto it, the command to start the data-gathering sequence is sent. This single command starts the sequence of delayed-execution commands configuring UVPI for collecting data.

The planned filter sequence is commanded in real-time during the Antares plume observation. The filter change sequence, according to the Strypi Experiment Requirements Document (ERD) [10], is shown in Table C2. The Antares stage is expected to burn for approximately 35 s.

Table C2 - Planned Plume-Camera Filter Sequence for Antares Plume Observation

Data Interval	Time After Antares Ignition (s)	Filter Wheel Position
1	0 - 4	PC-4
2	6 - 16	PC-3
3	18 - 23	PC-2
4	25 - end of burn	PC-1

#### C.2.1.3 Star 27 Plume Observation

After Antares burnout, the delayed-execution commands reset UVPI to normal image transmission rate and a plume-to-tracker image ratio of 2:8. The newly computed pointing function for viewing the Star 27 burn is transmitted between Antares burnout and Star 27 ignition. At least 6 s prior to Star 27 ignition, UVPI is commanded, either by real-time or delayed-execution command, to point at Strypi using a  $0.5^\circ$  radius circular scan with a period of 16 s. At about 5 s before Star 27 ignition, the command to acquire is sent. If the Star 27 burn is not seen within about 10 s after expected ignition, a new pointing function with a  $1.0^\circ$  circular scan radius is transmitted and executed.

After acquisition of the Star 27 plume, the commands to configure UVPI for viewing the plume are sent. During the Star 27 plume observation, the planned filter sequence is commanded in real-time. The filter change sequence, according to the ERD [10], is shown in Table C3.

Table C3 - Planned Plume Camera Filter Sequence for Star 27 Plume Observation

Data Interval	Time After Star 27 Ignition (s)	Filter Wheel Position
5	0 - 15	PC-1
6	17 - 27	PC-2
7	29 - end of burn	PC-3

During the Star 27 burn, the UVPI pointing function to observe the bow shock portion of the trajectory is computed. The new bow shock pointing function is transmitted during the burn, immediately after the last filter change command. The Star 27 stage is expected to burn for approximately 41 s.

#### C.2.1.4 Bow Shock Observation

The Strypi bow shock region is expected to start at the end of the Star 27 burn. If UVPI keeps lock on Strypi during this portion of the trajectory, then the sequence of filters shown in Table C4 would be commanded as specified in the ERD [10].

Table C4 - Planned Plume Camera Filter Sequence for Bow Shock Observation

Data Interval	Time After Star 27 Burnout (s)	Filter Wheel Position
8	0-3	PC-3
9	5-8	PC-4
10	10-13	PC-3
11	15-18	PC-2
12	20-end of burn	PC-3

If the tracker would have lost lock on Strypi, then the following actions would be taken: UVPI would be commanded to point with the nonscanning bow shock function; normal image transmission rate would be selected; the plume-to-tracker image ratio would be changed to 2:8; the filter changed to PC-4; and the joystick would be activated. The joystick operator would then attempt to bring Strypi into the plume-camera's field of view. Radar data would be used to aid the joystick operator. The filter changes would be commanded from the joystick when the image is observed in the plume camera.

The predicted Strypi bow shock period is expected to last approximately 100 s and end at about 40-km altitude.

After the bow shock observation period, delayed-execution commands reset UVPI, close the door, and perform a dark field data test. The UVPI is turned off either by real-time command or by delayed-execution command.

### C.2.2 LOTB Testing

Testing on the LOTB of the commands and pointing functions used during this encounter was successfully completed on 17 February 1991. The delayed-execution commands and pointing functions were transmitted to the spacecraft from the Vandenberg TGS during LACE pass 5577 at about 06:01 GMT on 18 February 1991.

### C.2.3 Rehearsals with Ground Beacons

Five live rehearsals were held (13 - 17 February 1991). The last two were unscheduled and occurred because the launch attempts on those days were canceled. The rehearsals were scheduled for passes that had similar geometry and occurred at about the same time of day as the launch pass. Each rehearsal was designed to follow as closely as possible the timeline of the actual encounter pass. This provided the UVPI encounter team with practice in completing their activities in the time required to successfully observe Strypi during the actual encounter. The rehearsals also provided opportunities to test the radar support to the joystick operator and the range radar data link with the Sandia National Laboratories team at Kauai.

Ground beacons were used to simulate a plume target for the rehearsals. For the first two and the last rehearsals, a ground beacon located at the TGS site on Maui was used as a target to verify the attitude determination and pointing functions used. On the third and fourth rehearsals, the beacon was located near the launch site on Kauai. The ground beacon at each site consisted of two 6000-W metal halide bulbs. The beacons were switched on and off to coincide with the ignition and burnout of the Antares, Star 27, and bow shock stages of the Strypi trajectory relative to the simulated launch time.

Software, hardware, and operational problems were encountered in the rehearsals and were resolved in time to ensure a successful observation of Strypi on 18 February 1991.





## Appendix D TRACKER PERFORMANCE

### D.1.0 SERVO PERFORMANCE

The tracker commands to the gimbal servo electronics, to compensate for tracking error, are calculated as a function of: the target position ( $x$  and  $y$  tracker errors) on the tracker camera focal plane, and an error gain correction. This function transforms the gimbal position to the appropriate gimbal commands necessary to position the gimbal mirror such that the tracking errors are driven to zero. In the following expression, the gain coefficients  $C$  and  $F$  are nominally set to zero. The equation is:

$$\begin{bmatrix} \Phi \\ \Theta \end{bmatrix} = \begin{bmatrix} AB \\ DE \end{bmatrix} \begin{bmatrix} X \text{ TRKERR} \\ Y \text{ TRKERR} \end{bmatrix} + \begin{bmatrix} C \\ F \end{bmatrix}$$

where

$\Phi$ , is azimuth,  
 $\Theta$ , is elevation,

and

$$\begin{bmatrix} AB \\ DE \end{bmatrix} = \begin{bmatrix} \frac{-1}{2 \cos(\Theta)} & \frac{-\tan(\Theta) \tan(\Phi)}{2} \\ 0 & \frac{1}{2 \cos^2(\Phi)} \end{bmatrix}$$

Figure D1 shows the plot of the error gain corrections for converting the focal plane tracking errors into gimbal angles. A comparison of the values of the coefficients  $A$ ,  $B$ ,  $D$ , and  $E$ , with their calculated values based on the gimbal angles and tracker errors, confirms that these equations correctly describe the servo mechanism.

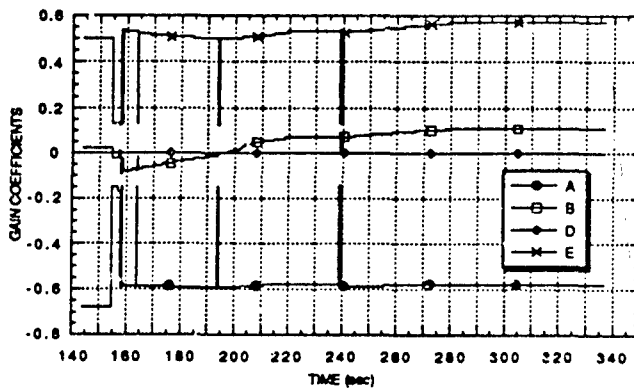


Fig. D1 - Gain coefficients vs time

#### D.1.1 Antares Acquisition

The tracking errors for the acquisition of the Antares rocket are plotted as a function of time in Fig. D2. The tracker servo response is determined from this plot as:

	X TRKERR	Y TRKERR
Rise time	< 0.2 s	< 0.43 s
% Overshoot	~ 171%	~ 24%
Settling time	< 1.2 s	< 1.2 s

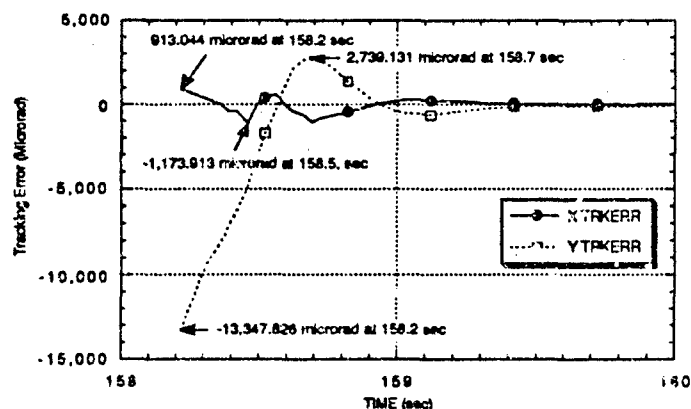


Fig. D2 - Antares acquisition tracking error vs time

These results compare favorably with the prior laboratory tests and tracker simulation results. The large overshoot is attributed to the "type 3" servo implementation, which provides zero steady state tracking error when tracking an accelerating target.

#### D.1.2 Star 27 Acquisition

The tracking errors for the acquisition of the Star 27 rocket are plotted as a function of time in Fig. D3. The tracker servo response is determined from this plot as:

	X TRKERR	Y TRKERR
Rise time	< 0.17 s	< 0.54 s
% Overshoot	~ 65%	~ 13%
Settling time	< 1.2 s	< 1.2 s

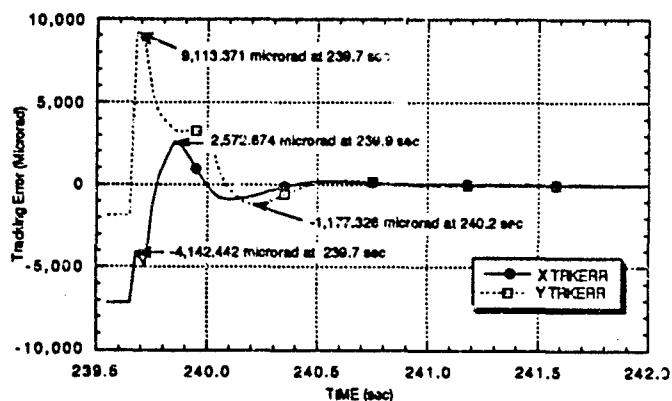


Fig. D3 - Star 27 acquisition tracking error vs time

These results compare favorably with the prior laboratory tests and tracker simulation results. The large overshoot is attributed to the "type 3" servo implementation, which provides zero steady state tracking error when tracking an accelerating target.

### D.1.3 Comparison With Previous Encounters

The comparison of servo responses from previous encounters, Nihka and Starbird, is given in Table D1. This table shows that the servo response has remained consistent throughout all the encounters.

Table D1 - Comparison of Servo Responses

	Overshoot (%)	Rise Time (s)	Settling Time (s)
<b>X Tracking Error</b>			
Nihka	40	0.2	1.0
Starbird 3rd Stage	100	0.11	1.2
Starbird 4th Stage	25	0.31	1.2
Antares	171	0.2	1.2
Star 27	65	0.17	1.2
<b>Y Tracking Error</b>			
Nihka	28	0.2	1.0
Starbird 3rd Stage	38	0.25	1.2
Starbird 4th Stage	28	0.31	1.2
Antares	24	0.43	1.2
Star 27	13	0.54	1.2

## D.2.0 TRACKING ERRORS

### D.2.1 Tracking Errors During Antares Burn

The four intervals chosen for analyzing the tracker performance during the Antares burn are approximately centered at 167, 170, 180, and 188 s after Strypi launch. Figures D4 and D5 present the tracking error and video signal for the complete Antares burn. Comparing Figs. D4 and D5 indicates that when a strong video signal is present, that is, when the peak video is almost full scale and the average signal is approximately 10% of full scale, tracking errors are near zero.

The four intervals are identified in Table D2 and their tracking errors are plotted in Figs. D6 through D13. The conversion from x-pixels to microradians is 60 microradians per pixel and the conversion from y-TV lines to microradians is 143 microradians per TV line. Note that the bias in the y-direction (Y TRKERR) is approximately -0.5 pixel and the error in the x-direction (X TRKERR) is  $\pm 1$  pixel in the tracker-camera focal plane. The target size is nominally 600  $\mu$ rad in both the x-direction (10 pixels) and the y-direction (4 pixels) on the tracker-camera focal plane. Occasionally, the target size jumps to double the nominal size. This is attributed to transients and does not affect the tracker performance.

Table D2 - Antares Data Intervals and Figure Numbers

Interval	Frames	Figure	Parameter
1	10,535 to 10,549	D5	X,Y Tracking Error
		D7	X,Y Target Size
2	10,656 to 10,913	D8	X,Y Tracking Error
		D9	X,Y Target Size
3	10,963 to 11,150	D10	X,Y Tracking Error
		D11	X,Y Target Size
4	11,266 to 11,413	D12	X,Y Tracking Error
		D13	X,Y Target Size

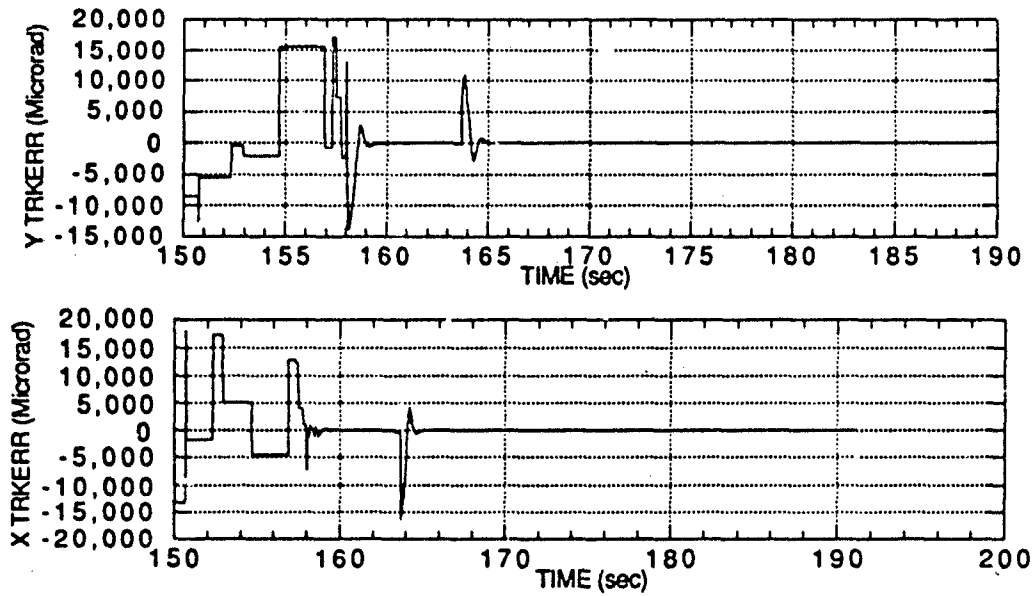


Fig. D4 - X and Y tracking error during Antares burn

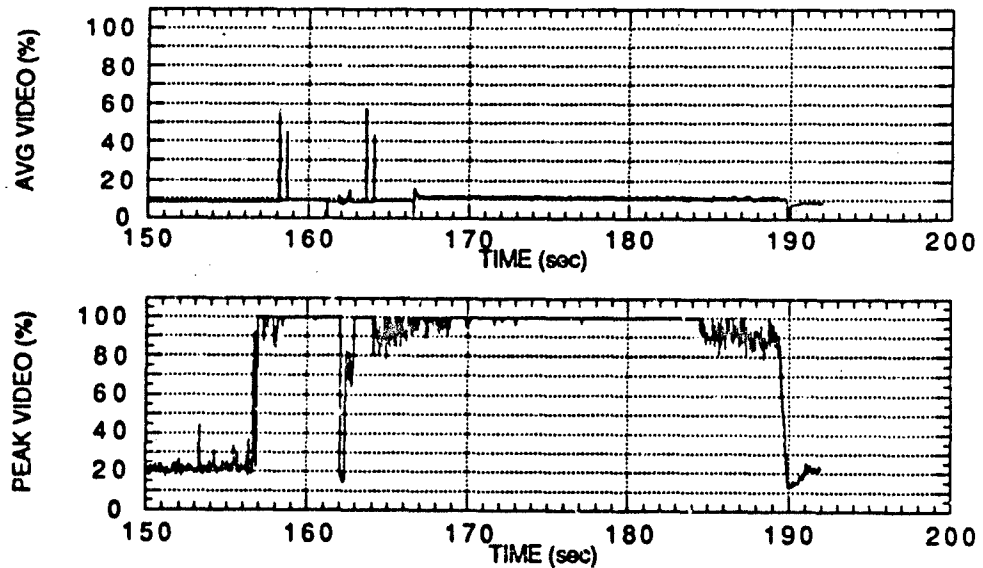


Fig. D5 - Average and peak video during Antares burn

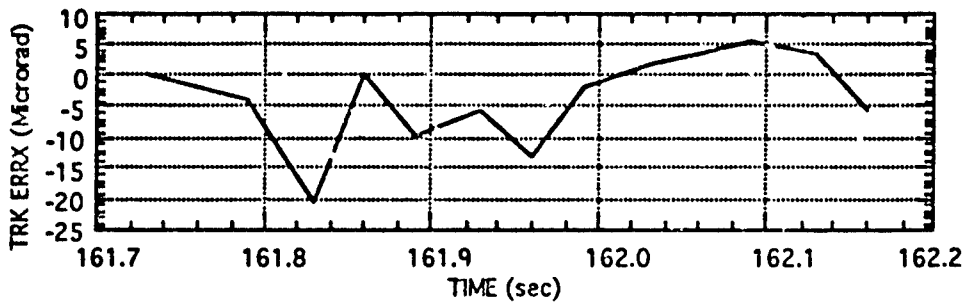
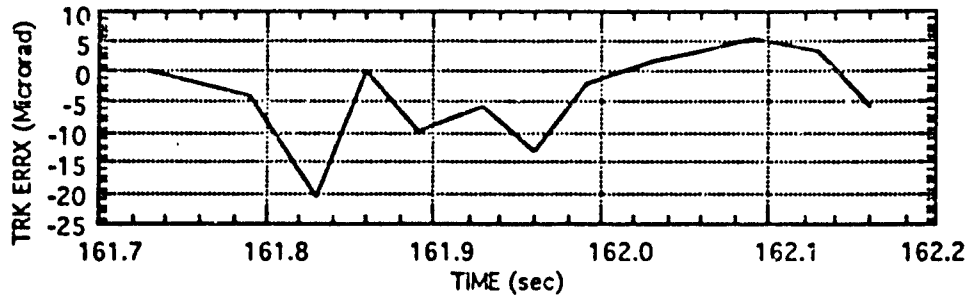


Fig. D6 - X and Y tracking errors, interval 1

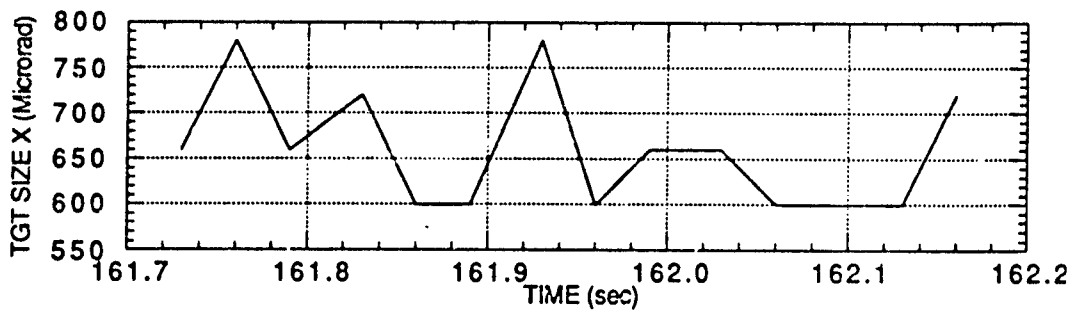
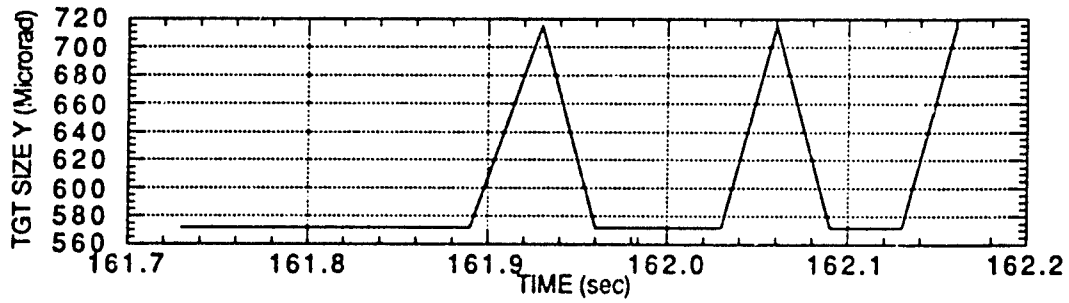


Fig. D7 - X and Y target size, interval 1

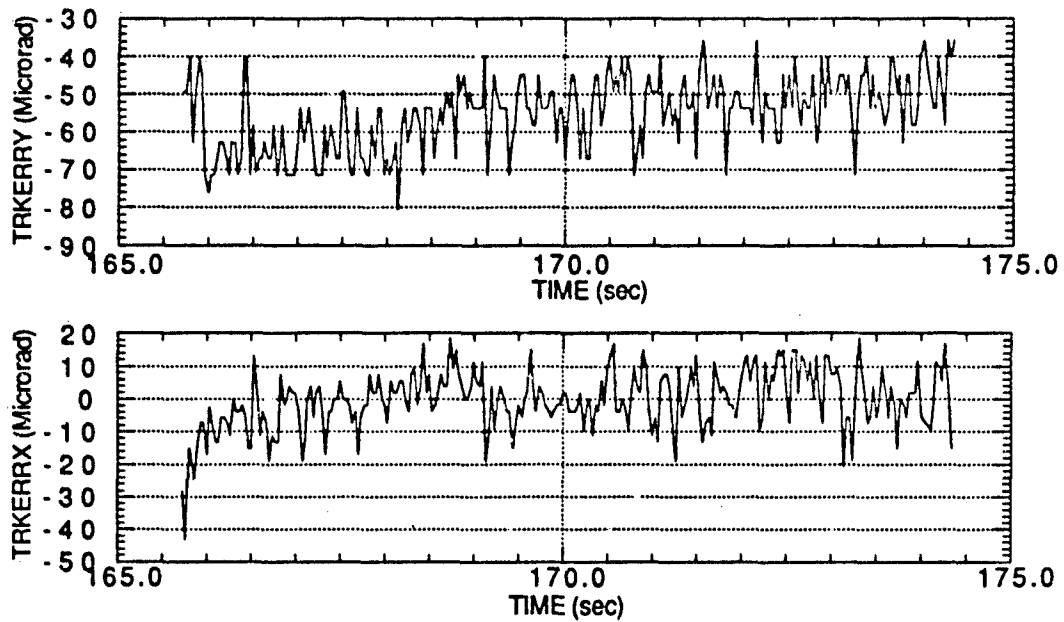


Fig. D8 - X and Y tracking errors, interval 2

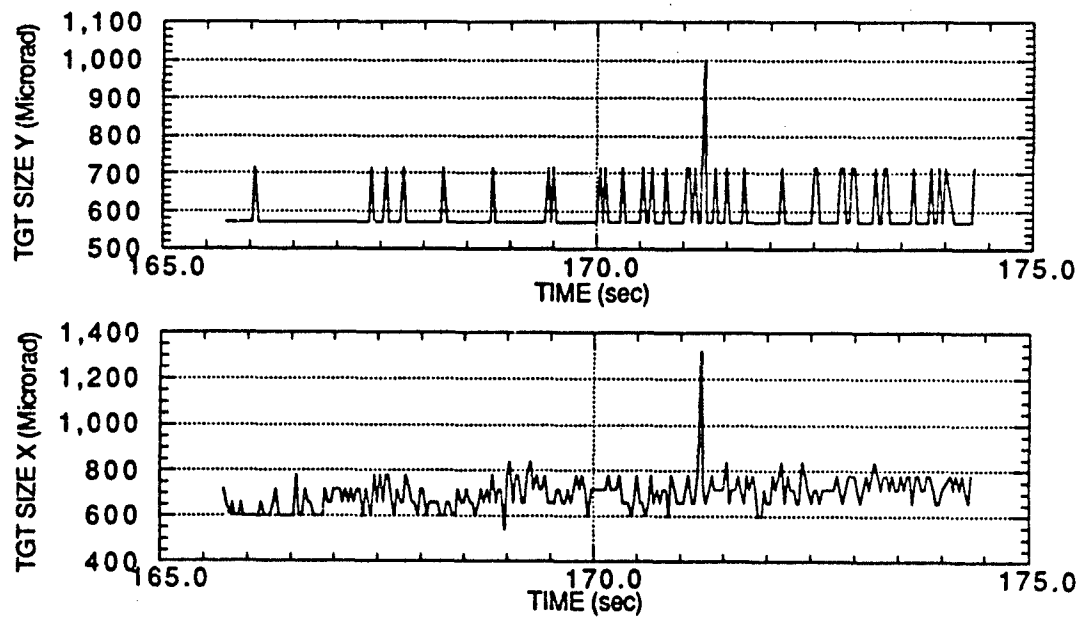


Fig. D9 - X and Y target size, interval 2

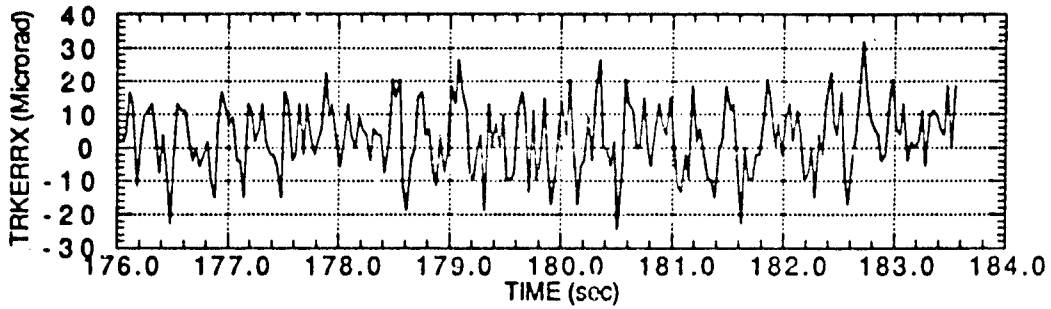
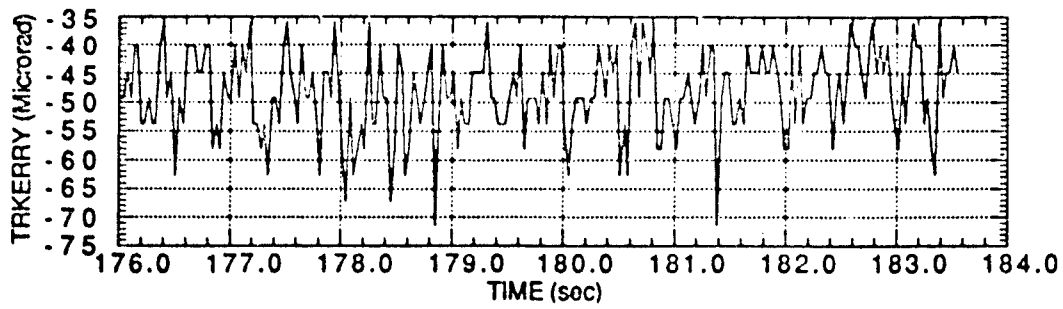


Fig. D10 - X and Y tracking errors, interval 3

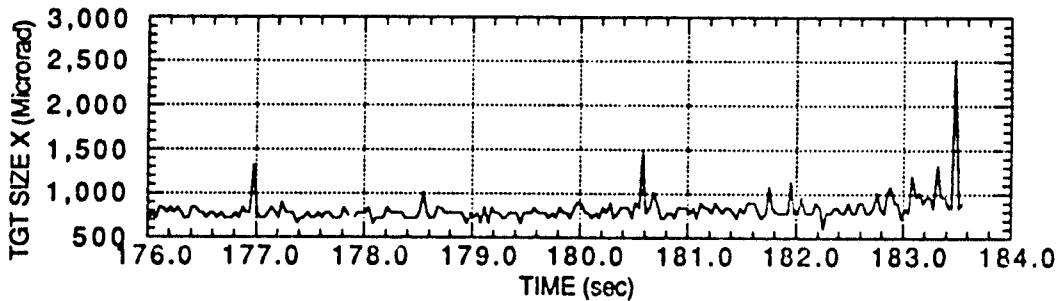
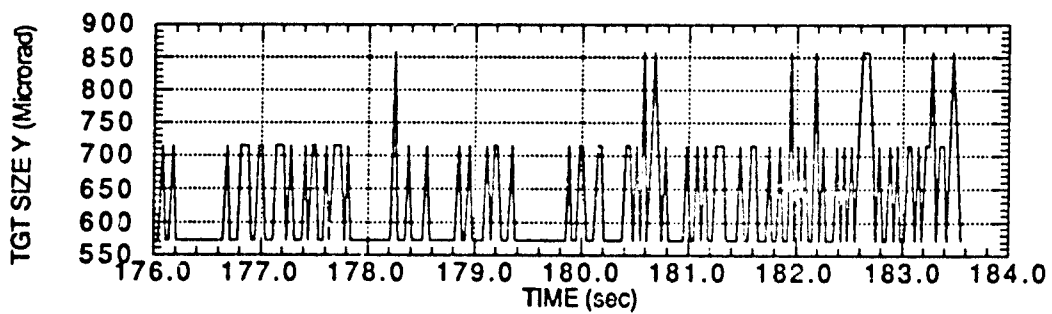


Fig. D11 - X and Y target size, interval 3



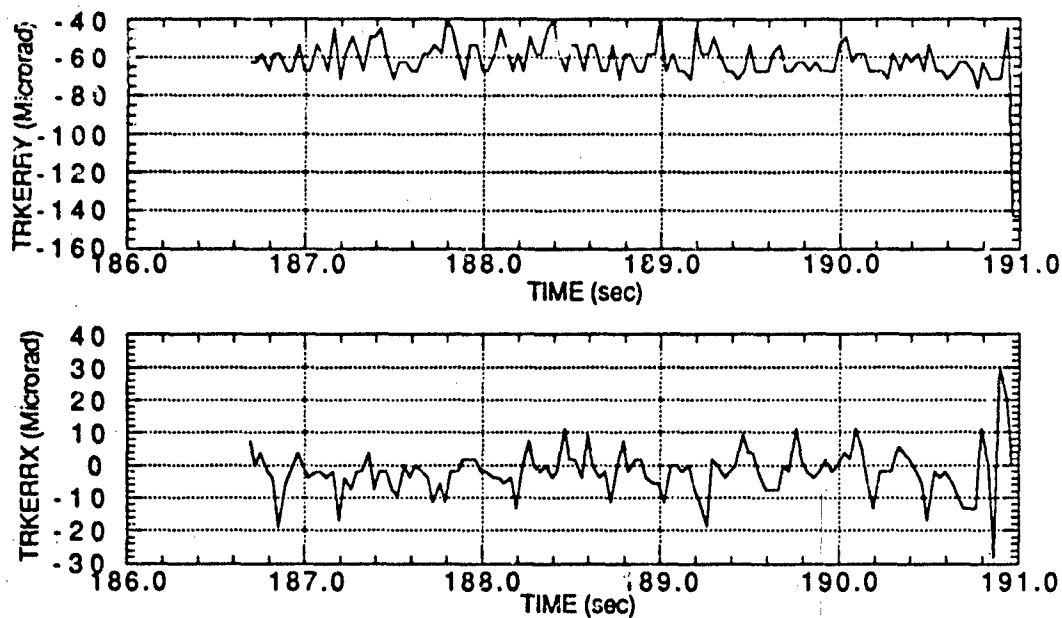


Fig. D12 - X and Y tracking errors, interval 4

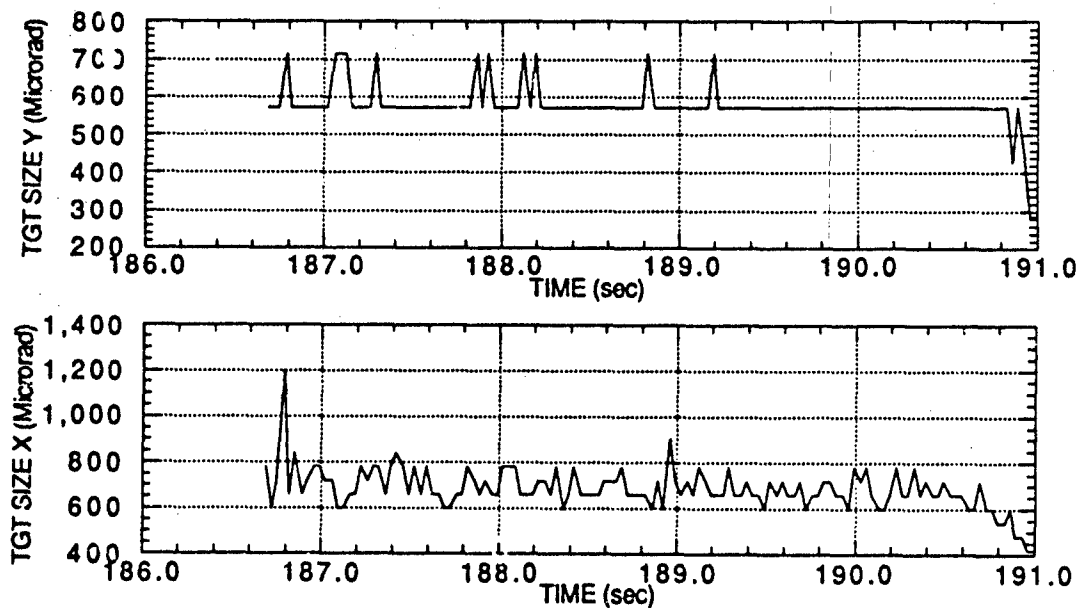


Fig. D13 - X and Y target size, interval 4

### D.2.2 Tracking Errors During Star 27 Burn

The three intervals chosen for analyzing the tracker performance during the Star 27 burn are approximately centered at 250, 262, and 270 s after Strypi launch. During this burn, the peak video

(Fig. D14) signal varied between 60 and 100% of full range. The low peak video level is attributed to the weak Star 27 signature and the fact that the tracker camera gain was not allowed to exceed level 10.

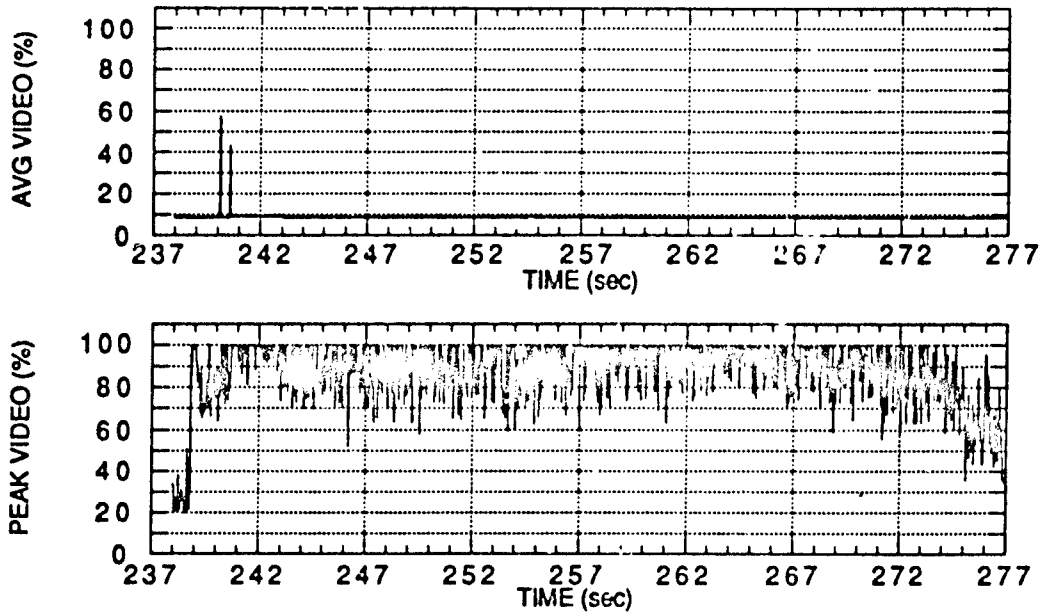


Fig. D14 - Average and peak video during Star 27 burn

The three intervals are identified in Table D3 and their tracking errors are plotted in Figs. D15 through D20. The bias in the y-direction ( $Y$  TRKERR) is approximately  $-0.5$  pixel, and the error in the x-direction ( $X$  TRKERR) ranges from  $\pm 1$  to  $\pm 20$  pixels in the tracker camera focal plane. This large tracking error is more evident as the Star 27 nears burnout. The target size is nominally  $25,000$   $\mu$ rad in both the x-direction (400 pixels) and the y-direction (175 pixels) on the tracker-camera focal plane. The large target size on the tracker-camera focal plane may be attributed to the fact that the Star 27 was coning during its thrusting period and thereby spreading the plume over a larger area.

Table D3 - Star 27 Data Intervals and Figure Numbers

Interval	Frames	Figure	Parameter
5	13,142 to 13,239	D15	X,Y Tracking Error
		D16	X,Y Target Size
6	13,489 to 13,599	D17	X,Y Tracking Error
		D18	X,Y Target Size
7	13,677 to 13,928	D19	X,Y Tracking Error
		D20	X,Y Target Size

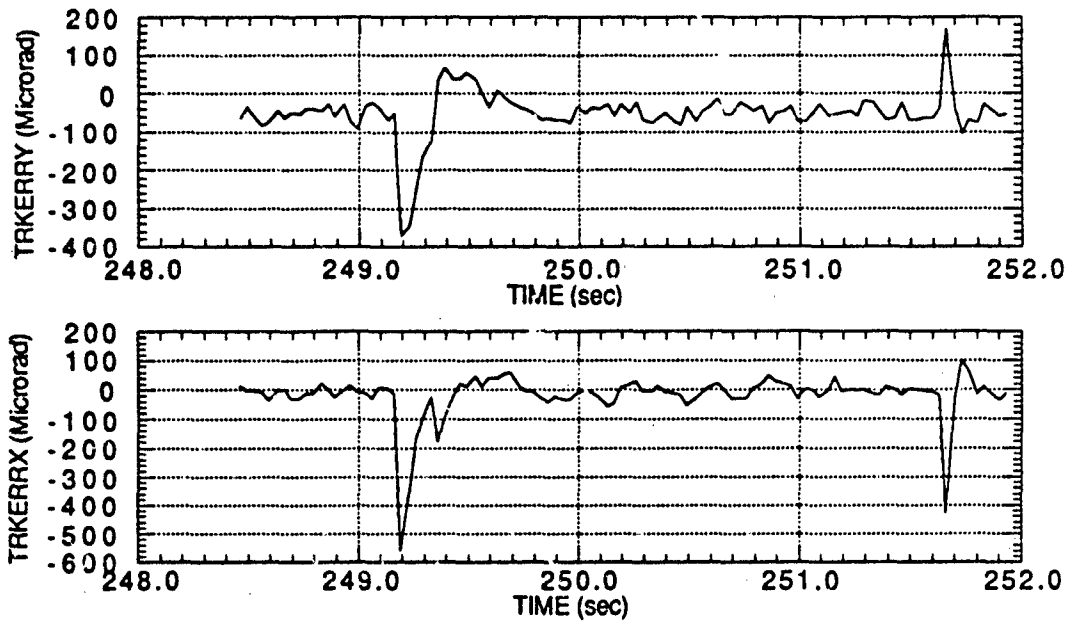


Fig. D15 - X and Y tracking errors, interval 5

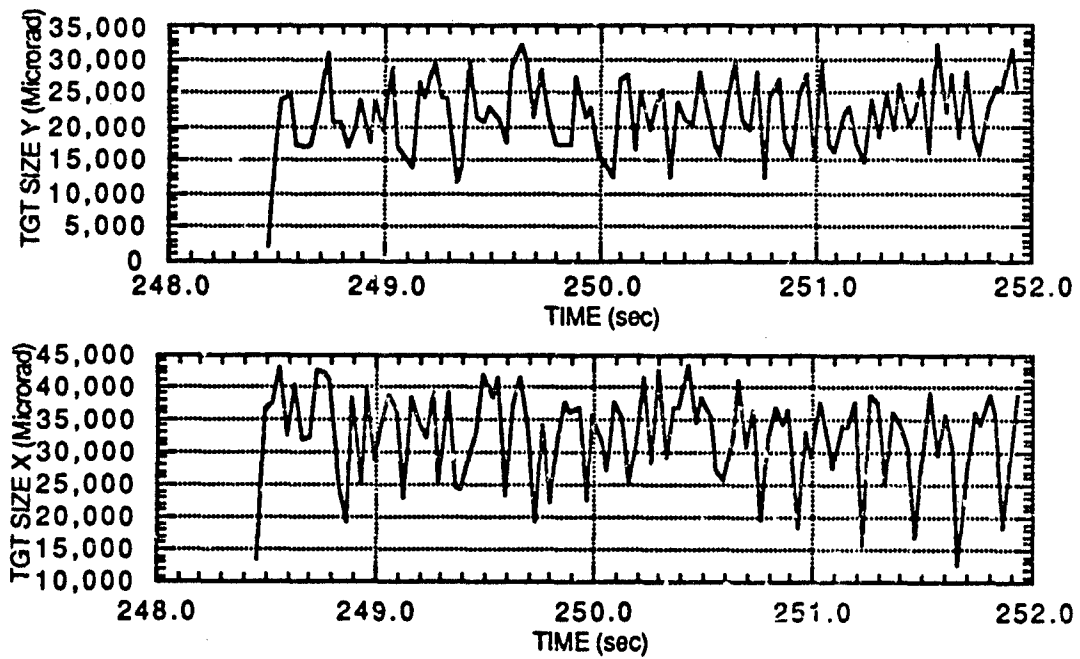


Fig. D16 - X and Y target size, interval 5

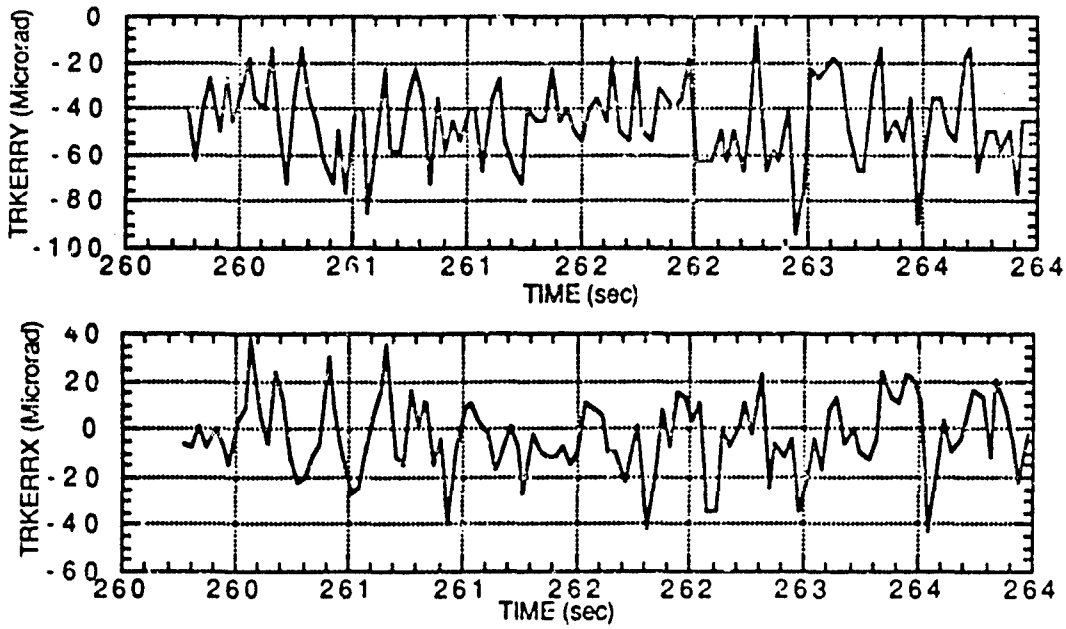


Fig. D17 - X and Y tracking errors, interval 6

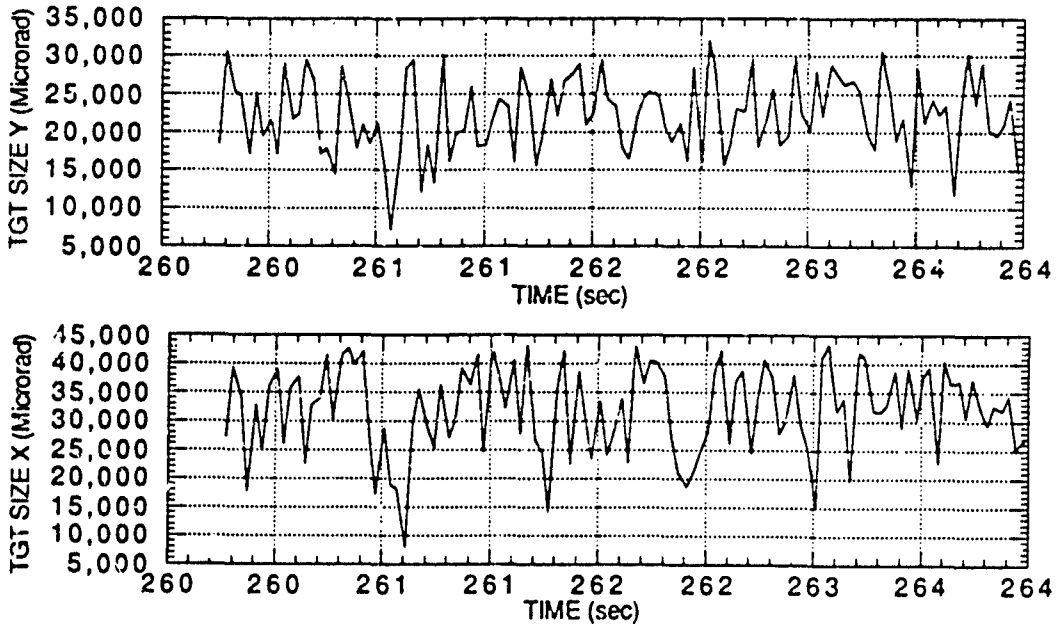


Fig. D18 - X and Y target size, interval 6

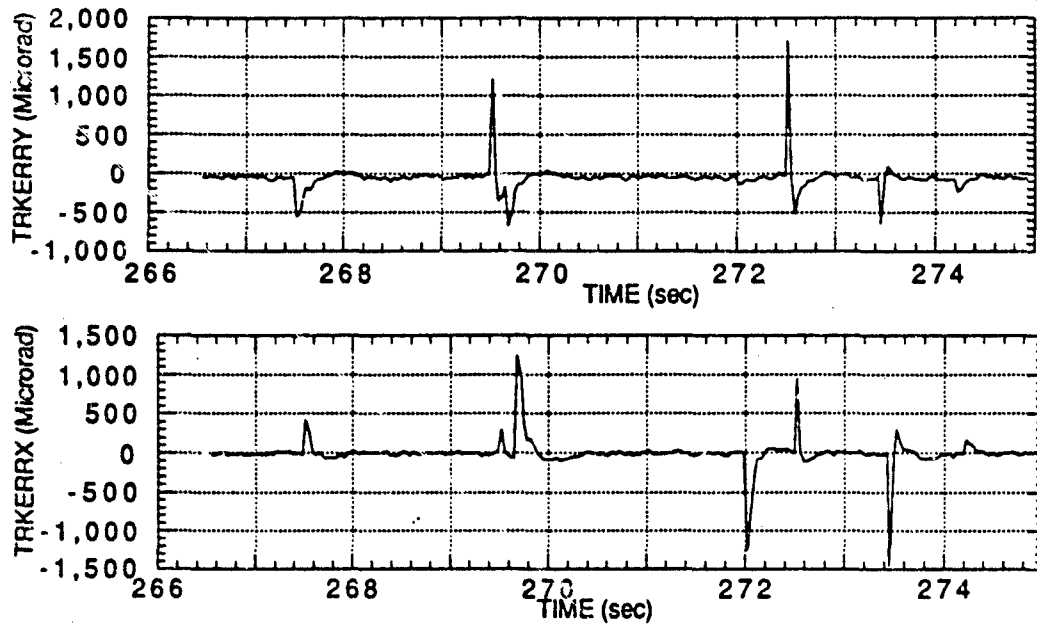


Fig. D19 - X and Y tracking errors, interval 7

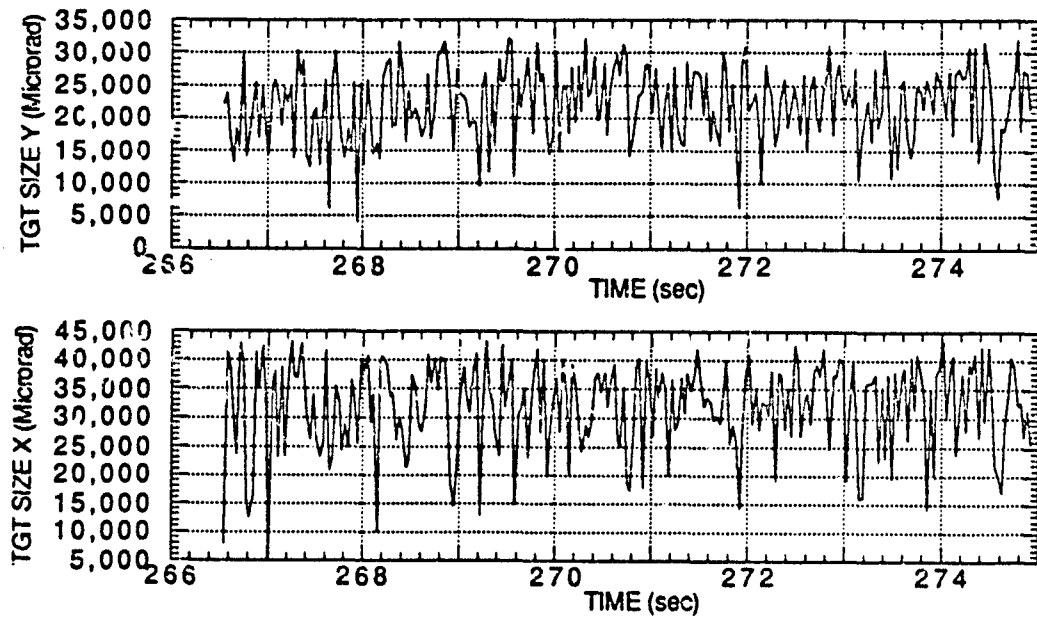


Fig. D20 - X and Y target size, interval 7

## Appendix E UVPI PARAMETERS

This appendix collects parameters and information that are useful for analyzing the data by using different assumptions for the source spectrum. The average number of photoevents per second for each of the intervals analyzed in this report is recorded in Table E1. Table E2 lists the net quantum efficiency in 5-nm steps for the tracker camera, and Table E3 lists plume-camera net quantum efficiency for each of the four filters.

Table E1 - Average Number of Photoevents/Second

Interval	Stage	Filter	Plume Camera		Tracker Camera	
			Bandpass (nm)	Photoevents/s	Bandpass (nm)	Photoevents/s*
1	Antares	PC-4	235-350	$1.46 \times 10^4$	255-450	$2.76 \times 10^5$
2	Antares	PC-3	195-295	$9.75 \times 10^2$	255-450	$5.13 \times 10^5$
3	Antares	PC-2	300-320	$1.91 \times 10^3$	255-450	$5.78 \times 10^5$
4	Antares	PC-1	220-320	$3.52 \times 10^3$	255-450	$4.22 \times 10^5$
5	Star 27	PC-1	220-320	$4.58 \times 10^2$	255-450	$5.32 \times 10^4$
6	Star 27	PC-2	300-320	$2.17 \times 10^2$	255-450	$5.37 \times 10^4$
7	Star 27	PC-3	195-295	$2.76 \times 10^2$	255-450	$4.57 \times 10^4$

\* For central 19 x 19 pixels

Table E2 - Net Quantum Efficiency for Tracker Camera

Wavelength (nm)	Tracker NQE	Wavelength (nm)	Tracker NQE
255	.00001	355	.022008
260	.000588	360	.018705
265	.00181	365	.018683
270	.003993	370	.018225
275	.005878	375	.01797
280	.0073	380	.018615
285	.00858	385	.019058
290	.00895	390	.018285
295	.010898	395	.01881
300	.01209	400	.018833
305	.014025	405	.017865
310	.014978	410	.018083
315	.012263	415	.016418
320	.01428	420	.016418
325	.017858	425	.016148
330	.017355	430	.016148
335	.015248	435	.013883
340	.011235	440	.010998
345	.014745	445	.00179
350	.017145	450	.00008

Table E3 - Net Quantum Efficiency for Plume Camera

Wavelength (nm)	PC-1	PC-2	PC-3	PC-4
195	0	0	0.000052	0
200	0	0	0.000129	0
205	0	0	0.000217	0
210	0	0	0.000228	0
215	0	0	0.000464	0
220	0.000015	0	0.00071	0
225	0.000038	0	0.001079	0
230	0.000075	0	0.001547	0
235	0.000092	0	0.002091	0.000119
240	0.0002	0	0.00247	0.000676
245	0.000385	0	0.002735	0.00198
250	0.00088	0	0.002542	0.003519
255	0.001873	0	0.002696	0.004922
260	0.003798	0	0.002413	0.006923
265	0.00546	0	0.00168	0.007535
270	0.006063	0	0.001124	0.009322
275	0.005503	0	0.000638	0.012336
280	0.003608	0	0.000345	0.013118
285	0.00211	0	0.000183	0.013089
290	0.001028	0	0.000123	0.01192
295	0.00048	0	0.000051	0.010684
300	0.000208	0.000053	0	0.009051
305	0.000095	0.001816	0	0.007641
310	0.000052	0.001497	0	0.006131
315	0.000015	0.000906	0	0.004956
320	0.000005	0.000021	0	0.003767
325	0	0	0	0.002863
330	0	0	0	0.001745
335	0	0	0	0.000985
340	0	0	0	0.000412
345	0	0	0	0.000119
350	0	0	0	0.000003

The digital number per photoevent is displayed in Figs. B8 and B9 for the tracker and plume cameras, respectively. Tables E4 and E5 list the values that make up those figures.

Table E4 - Gain Conversion Factor  $G_g$  for Tracker Camera

Gain Step $g$	Gain Conversion Factor $G_g$ (digital number per photoevent)
0	.001904
1	.00366
2	.007906
3	.016691
4	.034848
5	.079651
6	.149346
7	.279667
8	.512008
9	1.194808
10	2.298668
11	4.875681
12	10.15084
13	25.43053
14	45.58302
15	120.795

Table E5 - Gain Conversion Factor  $G_g$  for Plume Camera

Gain Step $g$	Gain Conversion Factor $G_g$ (digital number per photoevent)
0	.020287
1	.057107
2	.087467
3	.104575
4	.163667
5	.377368
6	.551453
7	2.85832
8	5.129954
9	10.80777
10	23.19167
11	39.75714
12	77.57491
13	143.6387
14	221.3121
15	292.9474

A scaled version of the beacon's point spread function (PSF) for the plume camera is presented in Table E6 in the form of a 16 by 16 pixel array. The intensity values were scaled such that the brightest pixel will map to 1. A row of intensity values representative of the full-width-half-maximum is highlighted in bold type. For the ground-based beacon, the equivalent full-width-half-maximum of the PSF along the major axis is about 40 m at a range of 450 km. A similar array for the tracker camera's PSF is presented in Table E7.

Table E6 - Scaled Version of Plume-Camera PSF Based on Ground Beacon

0.139	0.153	0.125	0.116	0.111	0.125	0.130	0.134	0.144	0.167	0.134	0.111	0.102	0.093	0.074	0.074
0.093	0.111	0.102	0.106	0.111	0.125	0.139	0.148	0.200	0.237	0.209	0.158	0.116	0.097	0.097	0.069
0.105	0.102	0.102	0.102	0.116	0.144	0.186	0.213	0.246	0.251	0.241	0.195	0.138	0.125	0.097	0.079
0.106	0.097	0.093	0.111	0.120	0.167	0.241	0.316	0.404	0.395	0.336	0.293	0.200	0.116	0.102	0.069
0.120	0.102	0.097	0.120	0.144	0.204	0.267	0.325	0.534	0.581	0.673	0.469	0.237	0.134	0.116	0.097
0.074	0.083	0.097	0.111	0.134	0.241	0.511	0.762	0.730	0.804	0.800	0.613	0.376	0.181	0.111	0.083
0.083	0.088	0.102	0.120	0.144	0.260	0.677	0.804	0.869	0.958	0.855	0.623	0.506	0.265	0.148	0.111
0.069	0.093	0.097	0.120	0.121	0.344	0.734	0.925	1.100	0.995	0.920	0.720	0.511	0.283	0.153	0.097
0.065	0.079	0.102	0.130	0.209	0.400	0.609	0.823	0.888	0.874	0.877	0.660	0.367	0.209	0.120	0.097
0.079	0.079	0.093	0.120	0.172	0.316	0.516	0.697	0.744	0.679	0.613	0.437	0.209	0.148	0.111	0.106
0.065	0.069	0.097	0.120	0.134	0.246	0.479	0.651	0.479	0.415	0.362	0.274	0.162	0.139	0.093	0.083
0.060	0.065	0.079	0.088	0.116	0.186	0.404	0.441	0.238	0.260	0.223	0.185	0.139	0.125	0.097	0.079
0.079	0.074	0.083	0.079	0.106	0.148	0.237	0.218	0.218	0.181	0.167	0.148	0.116	0.097	0.088	0.069
0.074	0.074	0.079	0.088	0.079	0.111	0.167	0.144	0.167	0.153	0.139	0.130	0.083	0.083	0.069	0.065
0.060	0.060	0.074	0.074	0.088	0.097	0.134	0.114	0.116	0.106	0.097	0.098	0.083	0.069	0.065	0.065
0.046	0.065	0.065	0.069	0.083	0.079	0.283	0.093	0.097	0.093	0.079	0.079	0.079	0.079	0.065	0.069



Table E7 - Scaled Version of Tracker-Camera PSF Based on Ground Beacon

0.046	0.041	0.046	0.021	0.037	0.049	0.074	0.046	0.030	0.034	0.046	0.001	0.046	0.008	0.047	0.021
0.012	0.035	0.017	0.026	0.037	0.044	0.049	0.019	0.032	0.008	0.031	0.003	0.042	0.000	0.029	0.025
0.047	0.016	0.018	0.037	0.043	0.036	0.053	0.022	0.015	0.058	0.034	0.024	0.035	0.027	0.032	
0.044	0.034	0.028	0.052	0.035	0.052	0.034	0.034	0.034	0.016	0.037	0.032	0.028	0.061	0.037	0.041
0.045	0.035	0.034	0.038	0.029	0.047	0.015	0.064	0.049	0.036	0.082	0.028	0.042	0.028	0.068	0.015
0.045	0.001	0.061	0.078	0.063	0.059	0.054	0.057	0.083	0.056	0.061	0.017	0.042	0.029	0.036	0.026
0.046	0.058	0.043	0.060	0.047	0.040	0.074	0.136	0.108	0.042	0.027	0.036	0.043	0.026	0.046	0.013
0.037	0.028	0.036	0.041	0.055	0.049	0.212	0.986	0.511	0.081	0.069	0.051	0.073	0.026	0.027	0.015
0.050	0.052	0.037	0.032	0.037	0.087	0.227	1.000	0.338	0.092	0.076	0.034	0.016	0.044	0.010	0.030
0.033	0.017	0.034	0.027	0.021	0.051	0.045	0.141	0.105	0.055	0.067	0.040	0.026	0.032	0.021	0.097
0.010	0.032	0.032	0.039	0.025	0.049	0.070	0.075	0.039	0.040	0.035	0.032	0.036	0.036	0.021	0.032
0.030	0.030	0.036	0.016	0.027	0.050	0.034	0.042	0.019	0.022	0.046	0.031	0.017	0.017	0.029	0.015
0.028	0.025	0.034	0.020	0.033	0.030	0.059	0.029	0.039	0.042	0.053	0.052	0.036	0.043	0.045	0.026
0.046	0.034	0.042	0.042	0.042	0.025	0.045	0.051	0.036	0.018	0.036	0.018	0.013	0.029	0.037	0.041
0.043	0.027	0.026	0.023	0.044	0.041	0.036	0.028	0.006	0.027	0.033	0.033	0.033	0.035	0.053	0.040
0.042	0.031	0.027	0.036	0.041	0.024	0.055	0.027	0.040	0.015	0.040	0.027	0.028	0.028	0.037	0.017

Finally, Table E8 lists all frames recorded for this encounter. The time and frame number are recorded in the first two columns. Note that the frame number carries a trailing P if it is a plume camera frame and a trailing T if it is a tracker camera frame. The third column lists the filter wheel position if it is a plume-camera frame. A filter wheel position of 0 denotes a tracker camera frame. The next two columns indicate the exposure time for the frame. For the plume camera, this is fixed at  $1/30$ th of a second, but it is variable for the tracker-camera, with a maximum allowed value of  $1/30$ th s. The next two columns list the tracker camera and plume camera gain steps.

For the zoom image transmission rate, 30 Hz, each telemetry frame carries one image. For the normal image transmission rate, 5 Hz, six telemetry frames carry one image.

UVPI mission time (UMT) is related to GMT for the Strypi observation pass by:

$$\text{UMT} = \text{GMT} + (0.29 + \text{Frame} \cdot 1.06 \times 10^{-5}) \text{ seconds.}$$

Table E8 - Telemetry Frames and Camera Parameters

UMT	Telemetry Frame	Filter	Tracker Exp. Time (ms)	Plume Exp. Time (ms)	Tracker Gain Step	Plume Gain Step	Comments
14 21 15.69	10505T	0	9.6633	33.3	8	11	Frame 10438: initial cloud puff in tracker camera FOV Frame 10457: Antares enters plume camera FOV
14 21 15.89	10511P	4	9.6633	33.3	8	11	
14 21 16.09	10517P	4	9.6633	33.3	8	11	
14 21 16.29	10523T	0	15.4018	33.3	7	10	
14 21 16.49	10529T	0	15.4018	33.3	7	10	
14 21 16.53	10530T	0	15.4018	33.3	7	10	
14 21 16.56	10531T	0	15.4018	33.3	7	10	

Table E8 - Telemetry Frames and Camera Parameters (Cont'd)

GMT	Telemetry Frame	Filter	Tracker Exp Time (ms)	Prime Exp Time (ms)	Tracker Gain Step	Prime Gain Step	Comments
14 21 16.59	10532T	0	15.4018	33.3	7	10	
14 21 16.63	10533T	0	15.4018	33.3	7	10	
14 21 16.66	10534T	0	15.4018	33.3	7	10	
14 21 16.69	10535T	0	15.4018	33.3	7	10	
14 21 16.73	10536P	4	15.4018	33.3	7	10	Begin data interval 1, PC-4
14 21 16.76	10537P	4	15.4018	33.3	7	10	
14 21 16.79	10538P	4	15.4018	33.3	7	10	
14 21 16.83	10539P	4	15.4018	33.3	7	10	
14 21 16.86	10540P	4	15.4018	33.3	7	10	
14 21 16.89	10541P	4	15.4018	33.3	7	10	
14 21 16.93	10542P	4	15.4018	33.3	7	10	
14 21 16.96	10543P	4	15.4018	33.3	7	10	
14 21 16.99	10544T	0	15.4018	33.3	7	10	
14 21 17.03	10545T	0	15.4018	33.3	7	10	Initial Cloud leaves tracker PO ✓
14 21 17.06	10546P	4	15.4018	33.3	7	10	
14 21 17.09	10547P	4	15.4018	33.3	7	10	
14 21 17.13	10548P	4	15.4018	33.3	7	10	
14 21 17.16	10549P	4	15.4018	33.3	7	10	End data interval 1, PC-4
14 21 18.73	10596P	4	15.4018	33.3	7	10	
14 21 18.76	10597P	4	15.4018	33.3	7	10	
14 21 18.80	10598P	4	15.4018	33.3	7	10	
14 21 18.83	10599P	4	15.4018	33.3	7	10	
14 21 18.86	10600P	4	15.4018	33.3	7	10	
14 21 18.90	10601P	4	15.4018	33.3	7	11	
14 21 18.93	10602P	4	15.4018	33.3	7	12	
14 21 18.96	10603P	4	15.4018	33.3	7	13	
14 21 19.00	10604T	0	15.4018	33.3	7	13	
14 21 19.03	10605T	0	15.4018	33.3	7	13	
14 21 19.06	10606P	4	15.4018	33.3	7	13	
14 21 19.10	10607P	4	15.4018	33.3	7	13	
14 21 19.13	10608P	4	15.4018	33.3	7	13	
14 21 19.16	10609P	4	15.4018	33.3	7	13	
14 21 19.20	10610P	4	15.4018	33.3	7	13	
14 21 19.23	10611P	4	15.4018	33.3	7	13	
14 21 19.26	10612P	4	15.4018	33.3	7	13	
14 21 19.30	10613P	4	15.4018	33.3	7	13	
14 21 19.33	10614T	0	15.4018	33.3	7	13	
14 21 19.36	10615T	0	15.4018	33.3	7	13	
14 21 19.40	10616P	4	15.4018	33.3	7	13	
14 21 19.43	10617P	4	15.4018	33.3	7	13	
14 21 19.46	10618P	4	15.4018	33.3	7	13	
14 21 19.50	10619P	4	15.4018	33.3	7	13	

Table E8 - Telemetry Frames and Camera Parameters (Cont'd)

GMT	Telemetry Frame	Fiber	Tracker Exp. Time (ms)	Plume Exp. Time (ms)	Tracker Gain Step	Plume Gain Step	Comments
14 21 19.53	10620P	4	15.4018	33.3	7	13	
14 21 19.56	10621P	4	15.4018	33.3	7	13	
14 21 19.60	10622P	4	15.4018	33.3	7	13	
14 21 19.63	10623P	4	15.4018	33.3	7	13	
14 21 19.66	10624T	0	15.4018	33.3	7	13	
14 21 19.70	10625T	0	15.4018	33.3	7	12	
14 21 19.73	10626P	4	15.4018	33.3	7	12	
14 21 19.76	10627P	4	15.4018	33.3	7	12	
14 21 19.80	10628P	4	15.4018	33.3	7	12	
14 21 19.83	10629P	4	15.4018	33.3	7	12	
14 21 19.86	10630P	4	15.4018	33.3	7	12	
14 21 19.90	10631P	4	15.4018	33.3	7	12	
14 21 19.93	10632P	4	15.4018	33.3	7	12	
14 21 19.96	10633P	4	15.4018	33.3	7	12	
14 21 20.00	10634T	0	15.4018	33.3	7	12	
14 21 20.03	10635T	0	12.1997	33.3	7	12	
14 21 20.06	10636P	4	12.1997	33.3	7	12	
14 21 20.10	10637P	4	12.1997	33.3	7	12	
14 21 20.13	10638P	4	12.1997	33.3	7	12	
14 21 20.16	10639P	4	12.1997	33.3	7	12	
14 21 20.20	10640P	4	12.1997	33.3	7	12	
14 21 20.23	10641P	4	12.1997	33.3	7	12	
14 21 20.26	10642P	4	12.1997	33.3	7	12	
14 21 20.29	10643P	3	12.1997	33.3	7	12	
14 21 20.33	10644T	0	9.6633	33.3	7	12	
14 21 20.36	10645T	0	9.6633	33.3	7	12	
14 21 20.40	10646P	3	9.6633	33.3	7	12	
14 21 20.43	10647P	3	9.6633	33.3	7	12	
14 21 20.46	10648P	3	9.6633	33.3	7	12	
14 21 20.50	10649P	3	9.6633	33.3	7	12	
14 21 20.53	10650P	3	9.6633	33.3	7	12	
14 21 20.56	10651P	3	9.6633	33.3	7	12	
14 21 20.60	10652P	3	9.6633	33.3	7	12	
14 21 20.63	10653P	3	9.6633	33.3	7	12	
14 21 20.66	10654T	0	9.6633	33.3	7	12	
14 21 20.70	10655T	0	9.6633	33.3	7	12	
14 21 20.73	10656P	3	9.6633	33.3	7	12	Begin data interval 2, PC-3
14 21 20.76	10657P	3	9.6633	33.3	7	12	
14 21 20.80	10658P	3	9.6633	33.3	7	12	
14 21 20.83	10659P	3	9.6633	33.3	7	12	
14 21 20.86	10660P	3	9.6633	33.3	7	12	
14 21 20.90	10661P	3	9.6633	33.3	7	12	
14 21 20.93	10662P	3	9.6633	33.3	7	12	

Table E8 - Telemetry Frames and Camera Parameters (Cont'd)

GMT	Telemetry Frame	Filter	Tracker Exp. Time (ms)	Plume Exp. Time (ms)	Tracker Gain Step	Plume Gain Step	Comments
14 21 20.96	10663P	3	9.6633	33.3	7	12	
14 21 21.00	10664T	0	9.6633	33.3	7	12	
14 21 21.03	10665T	0	9.6633	33.3	7	12	
14 21 21.06	10666P	3	9.6633	33.3	7	12	
14 21 21.10	10667P	3	9.6633	33.3	7	12	
14 21 21.13	10668P	3	9.6633	33.3	7	12	
14 21 21.16	10669P	3	9.6633	33.3	7	12	
14 21 21.20	10670P	3	9.6633	33.3	7	12	
14 21 21.23	10671P	3	9.6633	33.3	7	12	
14 21 21.26	10672P	3	9.6633	33.3	7	12	
14 21 21.30	10673P	3	9.6633	33.3	7	12	
14 21 21.33	10674T	0	9.6633	33.3	7	12	
14 21 21.37	10675T	0	9.6633	33.3	7	12	
14 21 21.40	10676P	3	9.6633	33.3	7	12	
14 21 21.43	10677P	3	9.6633	33.3	7	12	
14 21 21.47	10678P	3	9.6633	35.3	7	12	
14 21 21.50	10679P	3	9.6633	33.3	7	12	
14 21 21.53	10680P	3	9.6633	33.3	7	12	
14 21 21.57	10681P	3	9.6633	33.3	7	12	
14 21 21.60	10682P	3	9.6633	33.3	7	12	
14 21 21.63	10683P	3	9.6633	33.3	7	12	
14 21 21.67	10684T	0	9.6633	33.3	7	12	
14 21 21.70	10685T	0	9.6633	33.3	7	12	
14 21 21.73	10686P	3	9.6633	33.3	7	12	
14 21 21.77	10687P	3	9.6633	33.3	7	12	
14 21 21.80	10688P	3	9.6633	33.3	7	12	
14 21 21.83	10689P	3	9.6633	33.3	7	12	
14 21 21.87	10690P	3	9.6633	33.3	7	12	
14 21 21.90	10691P	3	9.6633	33.3	7	12	
14 21 21.93	10692P	3	9.6633	33.3	7	12	
14 21 21.97	10693P	3	9.6633	33.3	7	12	
14 21 22.00	10694T	0	9.6633	33.3	7	12	
14 21 22.03	10695T	0	9.6633	33.3	7	12	
14 21 22.07	10696P	3	9.6633	33.3	7	12	
14 21 22.10	10697P	3	9.6633	33.3	7	12	
14 21 22.13	10698P	3	9.6633	33.3	7	12	
14 21 22.17	10699P	3	9.6633	33.3	7	12	
14 21 22.20	10700P	3	9.6633	33.3	7	12	
14 21 22.23	10701P	3	9.6633	33.3	7	12	
14 21 22.27	10702P	3	9.6633	33.3	7	12	
14 21 22.30	10703P	3	9.6633	33.3	7	12	
14 21 22.33	10704T	0	9.6633	33.3	7	12	
14 21 22.37	10705T	0	9.6633	33.3	7	12	

Table E8 - Telemetry Frames and Camera Parameters (Cont'd)

GMT	Telemetry Frame	Filter	Tracker Exp. Time (ms)	Plume Exp. Time (ms)	Tracker Gain Step	Plume Gain Step	Comments
14 21 22.40	10706P	3	9.6633	33.3	7	12	
14 21 22.43	10707P	3	9.6633	33.3	7	12	
14 21 22.47	10708P	3	9.6633	33.3	7	12	
14 21 22.50	10709P	3	9.6633	33.3	7	12	
14 21 22.53	10710P	3	9.6633	33.3	7	12	
14 21 22.57	10711P	3	9.6633	33.3	7	12	
14 21 22.60	10712P	3	9.6633	33.3	7	12	
14 21 22.63	10713P	3	9.6633	33.3	7	12	
14 21 22.67	10714T	0	9.6633	33.3	7	12	
14 21 22.70	10715T	0	9.6633	33.3	7	12	
14 21 22.73	10716P	3	9.6633	33.3	7	12	
14 21 22.77	10717P	3	9.6633	33.3	7	12	
14 21 22.80	10718P	3	9.6633	33.3	7	12	
14 21 22.83	10719P	3	9.6633	33.3	7	12	
14 21 22.87	10720P	3	9.6633	33.3	7	12	
14 21 22.90	10721P	3	9.6633	33.3	7	12	
14 21 22.93	10722P	3	9.6633	33.3	7	12	
14 21 22.97	10723P	3	9.6633	33.3	7	12	
14 21 23.00	10724T	0	9.6633	33.3	7	12	
14 21 23.03	10725T	0	9.6633	33.3	7	12	
14 21 23.07	10726P	3	9.6633	33.3	7	12	
14 21 23.10	10727P	3	9.6633	33.3	7	12	
14 21 23.13	10728P	3	9.6633	33.3	7	12	
14 21 23.17	10729P	3	9.6633	33.3	7	12	
14 21 23.20	10730P	3	9.6633	33.3	7	12	
14 21 23.23	10731P	3	9.6633	33.3	7	12	
14 21 23.27	10732P	3	9.6633	33.3	7	12	
14 21 23.30	10733P	3	9.6633	33.3	7	12	
14 21 23.33	10734T	0	9.6633	33.3	7	12	
14 21 23.37	10735T	0	9.6633	33.3	7	12	
14 21 23.40	10736P	3	9.6633	33.3	7	12	
14 21 23.43	10737P	3	9.6633	33.3	7	12	
14 21 23.47	10738P	3	9.6633	33.3	7	12	
14 21 23.50	10739P	3	9.6633	33.3	7	12	
14 21 23.53	10740P	3	9.6633	33.3	7	12	
14 21 23.57	10741P	3	9.6633	33.3	7	12	
14 21 23.60	10742P	3	9.6633	33.3	7	12	
14 21 23.63	10743P	3	9.6633	33.3	7	12	
14 21 23.67	10744T	0	9.6633	33.3	7	12	
14 21 23.70	10745T	0	9.6633	33.3	7	12	
14 21 23.73	10746P	3	9.6633	33.3	7	12	
14 21 23.77	10747P	3	9.6633	33.3	7	12	
14 21 23.80	10748P	3	9.6633	33.3	7	12	

Table E8 - Telemetry Frames and Camera Parameters (Cont'd)

UMT	Telemetry Frame	Filter	Tracker Exp. Time (ms)	Frame Exp. Time (ms)	Tracker Gain Step	Frame Gain Step	Comments
14 21 23.83	10745P	3	9.6633	33.3	7	12	
14 21 23.87	10750P	3	9.6633	33.3	7	12	
14 21 23.90	10751P	3	9.6633	33.3	7	12	
14 21 23.93	10752P	3	9.6633	33.3	7	12	
14 21 23.97	10753P	3	9.6633	33.3	7	12	
14 21 24.00	10754T	0	9.6633	33.3	7	12	
14 21 24.03	10755T	0	9.6633	33.3	7	12	
14 21 24.07	10756P	3	9.6633	33.3	7	12	
14 21 24.10	10757P	3	9.6633	33.3	7	12	
14 21 24.13	10758P	3	9.6633	33.3	7	12	
14 21 24.17	10759P	3	9.6633	33.3	7	12	
14 21 24.20	10760P	3	9.6633	33.3	7	12	
14 21 24.23	10761P	3	9.6633	33.3	7	12	
14 21 24.27	10762P	3	9.6633	33.3	7	12	
14 21 24.30	10763P	3	9.6633	33.3	7	12	
14 21 24.34	10764T	0	9.6633	33.3	7	12	
14 21 24.37	10765T	0	9.6633	33.3	7	12	
14 21 24.40	10766P	3	9.6633	33.3	7	12	
14 21 24.44	10767P	3	9.6633	33.3	7	12	
14 21 24.47	10768P	3	9.6633	33.3	7	12	
14 21 24.50	10769P	3	9.6633	33.3	7	12	
14 21 24.54	10770P	3	9.6633	33.3	7	12	
14 21 24.57	10771P	3	9.6633	33.3	7	12	
14 21 24.60	10772P	3	9.6633	33.3	7	12	
14 21 24.64	10773P	3	9.6633	33.3	7	12	
14 21 24.67	10774T	0	9.6633	33.3	7	12	
14 21 24.70	10775T	0	9.6633	33.3	7	12	
14 21 24.74	10776P	3	9.6633	33.3	7	12	
14 21 24.77	10777P	3	9.6633	33.3	7	12	
14 21 24.80	10778P	3	9.6633	33.3	7	12	
14 21 24.84	10779P	3	9.6633	33.3	7	12	
14 21 24.87	10780P	3	9.6633	33.3	7	12	
14 21 24.90	10781P	3	9.6633	33.3	7	12	
14 21 24.94	10782P	3	9.6633	33.3	7	12	
14 21 24.97	10783P	3	9.6633	33.3	7	12	
14 21 25.00	10784T	0	9.6633	33.3	7	12	
14 21 25.04	10785T	0	9.6633	33.3	7	12	
14 21 25.07	10786P	3	9.6633	33.3	7	12	
14 21 25.10	10787P	3	9.6633	33.3	7	12	
14 21 25.14	10788P	3	9.6633	33.3	7	12	
14 21 25.17	10789P	3	9.6633	33.3	7	12	
14 21 25.20	10790P	3	9.6633	33.3	7	12	
14 21 25.24	10791P	3	9.6633	33.3	7	12	

Table E8 - Telemetry Frames and Camera Parameters (Cont'd)

UMI	Telemetry Frame	Filter	Tracker Exp. Time (ms)	Plume Exp. Time (ms)	Tracker Gain Step	Plume Gain Step	Comments
14 21 25.27	10792P	3	9.6633	33.3	7	12	
14 21 25.30	10793P	3	9.6633	33.3	7	12	
14 21 25.34	10794T	0	9.6633	33.3	7	12	
14 21 25.37	10795T	0	9.6633	33.3	7	12	
14 21 25.40	10796P	3	9.6633	33.3	7	12	
14 21 25.44	10797P	3	9.6633	33.3	7	12	
14 21 25.47	10798P	3	9.6633	33.3	7	12	
14 21 25.50	10799P	3	9.6633	33.3	7	12	
14 21 25.54	10800P	3	9.6633	33.3	7	12	
14 21 25.57	10801P	3	9.6633	33.3	7	12	
14 21 25.60	10802P	3	9.6633	33.3	7	12	
14 21 25.64	10803P	3	9.6633	33.3	7	12	
14 21 25.67	10804T	0	9.6633	33.3	7	12	
14 21 25.70	10805T	0	9.6633	33.3	7	12	
14 21 25.74	10806P	3	9.6633	33.3	7	12	
14 21 25.77	10807P	3	9.6633	33.3	7	12	
14 21 25.80	10808P	3	9.6633	33.3	7	12	
14 21 25.84	10809P	3	9.6633	33.3	7	12	
14 21 25.87	10810P	3	9.6633	33.3	7	12	
14 21 25.90	10811P	3	9.6633	33.3	7	12	
14 21 25.94	10812P	3	9.6633	33.3	7	12	
14 21 25.97	10813P	3	9.6633	33.3	7	12	
14 21 26.00	10814T	0	9.6633	33.3	7	12	
14 21 26.04	10815T	0	9.6633	33.3	7	12	
14 21 26.07	10816P	3	9.6633	33.3	7	12	
14 21 26.10	10817P	3	9.6633	33.3	7	12	
14 21 26.14	10818P	3	9.6633	33.3	7	12	
14 21 26.17	10819P	3	9.6633	33.3	7	12	
14 21 26.20	10820P	3	9.6633	33.3	7	12	
14 21 26.24	10821P	3	9.6633	33.3	7	12	
14 21 26.27	10822P	3	9.6633	33.3	7	12	
14 21 26.30	10823P	3	9.6633	33.3	7	12	
14 21 26.34	10824T	0	9.6633	33.3	7	12	
14 21 26.37	10825T	0	9.6633	33.3	7	12	
14 21 26.40	10826P	3	9.6633	33.3	7	12	
14 21 26.44	10827P	3	9.6633	33.3	7	12	
14 21 26.47	10828P	3	9.6633	33.3	7	12	
14 21 26.50	10829P	3	9.6633	33.3	7	12	
14 21 26.54	10830P	3	9.6633	33.3	7	12	
14 21 26.57	10831P	3	9.6633	33.3	7	12	
14 21 26.60	10832P	3	9.6633	33.3	7	12	
14 21 26.64	10833P	3	9.6633	33.3	7	12	
14 21 26.67	10834T	0	9.6633	33.3	7	12	

Table E8 - Telemetry Frames and Camera Parameters (Cont'd)

GMT	Telemetry Frame	Roller	Tracker Exp. Time (ms)	Plume Exp. Time (ms)	Tracker Gain Step	Plume Gain Step	Comments
14 21 26.70	10835T	0	9.6633	33.3	7	12	
14 21 26.74	10836P	3	9.6633	33.3	7	12	
14 21 26.77	10837P	3	9.6633	33.3	7	12	
14 21 26.80	10838P	3	9.6633	33.3	7	12	
14 21 26.84	10839P	3	9.6633	33.3	7	12	
14 21 26.87	10840P	3	9.6633	33.3	7	12	
14 21 26.90	10841P	3	9.6633	33.3	7	12	
14 21 26.94	10842P	3	9.6633	33.3	7	12	
14 21 26.97	10843P	3	9.6633	33.3	7	12	
14 21 27.00	10844T	0	9.6633	33.3	7	12	
14 21 27.04	10845T	0	9.6633	33.3	7	12	
14 21 27.07	10846P	3	9.6633	33.3	7	12	
14 21 27.10	10847P	3	9.6633	33.3	7	12	
14 21 27.14	10848P	3	9.6633	33.3	7	12	
14 21 27.17	10849P	3	9.6633	33.3	7	12	
14 21 27.21	10850P	3	9.6633	33.3	7	12	
14 21 27.24	10851P	3	9.6633	33.3	7	12	
14 21 27.27	10852P	3	9.6633	33.3	7	12	
14 21 27.31	10853P	3	9.6633	33.3	7	12	
14 21 27.34	10854T	0	9.6633	33.3	7	12	
14 21 27.37	10855T	0	9.6633	33.3	7	12	
14 21 27.41	10856P	3	9.6633	33.3	7	12	
14 21 27.44	10857P	3	9.6633	33.3	7	12	
14 21 27.47	10858P	3	9.6633	33.3	7	12	
14 21 27.51	10859P	3	9.6633	33.3	7	12	
14 21 27.54	10860P	3	9.6633	33.3	7	12	
14 21 27.57	10861P	3	9.6633	33.3	7	12	
14 21 27.61	10862P	3	9.6633	33.3	7	12	
14 21 27.64	10863P	3	9.6633	33.3	7	12	
14 21 27.67	10864T	0	9.6633	33.3	7	12	
14 21 27.71	10865T	0	9.6633	33.3	7	12	
14 21 27.74	10866P	3	9.6633	33.3	7	12	
14 21 27.77	10867P	3	9.6633	33.3	7	12	
14 21 27.81	10868P	3	9.6633	33.3	7	12	
14 21 27.84	10869P	3	9.6633	33.3	7	12	
14 21 27.87	10870P	3	9.6633	33.3	7	12	
14 21 27.91	10871P	3	9.6633	33.3	7	12	
14 21 27.94	10872P	3	9.6633	33.3	7	12	
14 21 27.97	10873P	3	9.6633	33.3	7	12	
14 21 28.01	10874T	0	9.6633	33.3	7	12	
14 21 28.04	10875T	0	9.6633	33.3	7	12	
14 21 28.07	10876P	3	9.6633	33.3	7	12	
14 21 28.11	10877P	3	9.6633	33.3	7	12	



Table E8 - Telemetry Frames and Camera Parameters (Cont'd)

UMT	Telemetry Frame	Filter	Tracker Exp. Time (ms)	Plume Exp. Time (ms)	Tracker Gain Step	Plume Gain Step	Comments
14 21 28.14	10878P	3	9.6633	33.3	7	12	
14 21 28.17	10879P	3	9.6633	33.3	7	12	
14 21 28.21	10880P	3	9.6633	33.3	7	12	
14 21 28.24	10881P	3	9.6633	33.3	7	12	
14 21 28.27	10882P	3	9.6633	33.3	7	12	
14 21 28.31	10883P	3	9.6633	33.3	7	12	
14 21 28.34	10884T	0	9.6633	33.3	7	12	
14 21 28.37	10885T	0	9.6633	33.3	7	12	
14 21 28.41	10886P	3	9.6633	33.3	7	12	
14 21 28.44	10887P	3	9.6633	33.3	7	12	
14 21 28.47	10888P	3	9.6633	33.3	7	12	
14 21 28.51	10889P	3	9.6633	33.3	7	12	
14 21 28.54	10890P	3	9.6633	33.3	7	12	
14 21 28.57	10891P	3	9.6633	33.3	7	12	
14 21 28.61	10892P	3	9.6633	33.3	7	12	
14 21 28.64	10893P	3	9.6633	33.3	7	12	
14 21 28.67	10894T	0	9.6633	33.3	7	12	
14 21 28.71	10895T	0	9.6633	33.3	7	12	
14 21 28.74	10896P	3	9.6633	33.3	7	12	
14 21 28.77	10897P	3	9.6633	33.3	7	12	
14 21 28.81	10898P	3	9.6633	33.3	7	12	
14 21 28.84	10899P	3	9.6633	33.3	7	12	
14 21 28.87	10900P	3	9.6633	33.3	7	12	
14 21 28.91	10901P	3	9.6633	33.3	7	12	
14 21 28.94	10902P	3	9.6633	33.3	7	12	
14 21 28.97	10903P	3	9.6633	33.3	7	12	
14 21 29.01	10904T	0	9.6633	33.3	7	12	
14 21 29.11	10907P	3	9.6633	33.3	7	12	
14 21 29.14	10908P	3	9.6633	33.3	7	12	
14 21 29.17	10909P	3	9.6633	33.3	7	12	
14 21 29.21	10910P	3	9.6633	33.3	7	12	
14 21 29.24	10911P	3	9.6633	33.3	7	12	
14 21 29.27	10912P	3	9.6633	33.3	7	12	
14 21 29.31	10913P	3	9.6633	33.3	7	12	
14 21 29.34	10914T	0	9.6633	33.3	7	12	
14 21 30.98	10963P	2	9.6633	33.3	7	12	End data interval 2, PC-3
14 21 31.01	10964T	0	9.6633	33.3	7	12	Begin data interval 3, PC-2
14 21 31.04	10965T	0	9.6633	33.3	7	12	
14 21 31.08	10966P	2	9.6633	33.3	7	12	
14 21 31.11	10967P	2	9.6633	33.3	7	12	
14 21 31.14	10968P	2	9.6633	33.3	7	12	
14 21 31.18	10969P	2	9.6633	33.3	7	12	

Table E8 - Tele.etry Frames and Camera Parameters (Cont'd)

GMT	Telemetry Frame	Fiber	Tracker Exp. Time (ms)	Frame Exp. Time (ms)	Tracker Gain Step	Frame Gain Step	Comments
14 21 31.21	10970P	2	9.6633	33.3	7	12	
14 21 31.24	10971P	2	9.6633	33.3	7	12	
14 21 31.28	10972P	2	9.6633	33.3	7	12	
14 21 31.31	10973P	2	9.6633	33.3	7	12	
14 21 31.34	10974T	0	9.6633	33.3	7	12	
14 21 31.38	10975T	0	9.6633	33.3	7	12	
14 21 31.41	10976P	2	9.6633	33.3	7	12	
14 21 31.44	10977P	2	9.6633	33.3	7	12	
14 21 31.48	10978P	2	9.6633	33.3	7	12	
14 21 31.51	10979P	2	9.6633	33.3	7	12	
14 21 31.54	10980P	2	9.6633	33.3	7	12	
14 21 31.58	10981P	2	9.6633	33.3	7	12	
14 21 31.61	10982P	2	9.6633	33.3	7	12	
14 21 31.64	10983P	2	9.6633	33.3	7	12	
14 21 31.68	10984T	0	9.6633	33.3	7	12	
14 21 31.71	10985T	0	9.6633	33.3	7	12	
14 21 31.74	10986P	2	9.6633	33.3	7	12	
14 21 31.78	10987P	2	9.6633	33.3	7	12	
14 21 31.81	10988P	2	9.6633	33.3	7	12	
14 21 31.84	10989P	2	9.6633	33.3	7	12	
14 21 31.88	10990P	2	9.6633	33.3	7	12	
14 21 31.91	10991P	2	9.6633	33.3	7	12	
14 21 31.94	10992P	2	9.6633	33.3	7	12	
14 21 31.98	10993P	2	9.6633	33.3	7	12	
14 21 32.01	10994T	0	9.6633	33.3	7	12	
14 21 32.04	10995T	0	9.6633	33.3	7	12	
14 21 32.08	10996P	2	9.6633	33.3	7	12	
14 21 32.11	10997P	2	9.6633	33.3	7	12	
14 21 32.14	10998P	2	9.6633	33.3	7	12	
14 21 32.18	10999P	2	9.6633	33.3	7	12	
14 21 32.21	11000P	2	9.6633	33.3	7	12	
14 21 32.24	11001P	2	9.6633	33.3	7	12	
14 21 32.28	11002P	2	9.6633	33.3	7	12	
14 21 32.31	11003P	2	9.6633	33.3	7	12	
14 21 32.34	11004T	0	9.6633	33.3	7	12	
14 21 32.38	11005T	0	9.6633	33.3	7	12	
14 21 32.41	11006P	2	9.6633	33.3	7	12	
14 21 32.44	11007P	2	9.6633	33.3	7	12	
14 21 32.48	11008P	2	9.6633	33.3	7	12	
14 21 32.51	11009P	2	9.6633	33.3	7	12	
14 21 32.54	11010P	2	9.6633	33.3	7	12	
14 21 32.58	11011P	2	9.6633	33.3	7	12	
14 21 32.61	11012P	2	9.6633	33.3	7	12	

Table E8 - Telemetry Frames and Camera Parameters (Cont'd)

GMT	Telemetry Frame	Filter	Tracker Exp. Time (ms)	Plume Exp. Time (ms)	Tracker Gain Step	Plume Gain Step	Comments
14 21 32.64	11013P	2	9.6633	33.3	7	12	
14 21 32.68	11014T	0	9.6633	33.3	7	12	
14 21 32.71	11015T	0	9.6633	33.3	7	12	
14 21 32.74	11016P	2	9.6633	33.3	7	12	
14 21 32.78	11017P	2	9.6633	33.3	7	12	
14 21 32.81	11018P	2	9.6633	33.3	7	12	
14 21 32.84	11019P	2	9.6633	33.3	7	12	
14 21 32.88	11020P	2	9.6633	33.3	7	12	
14 21 32.91	11021P	2	9.6633	33.3	7	12	
14 21 32.94	11022P	2	9.6633	33.3	7	12	
14 21 32.98	11023P	2	9.6633	33.3	7	12	
14 21 33.01	11024T	0	9.6633	33.3	7	12	
14 21 33.04	11025T	0	9.6633	33.3	7	12	
14 21 33.08	11026P	2	9.6633	33.3	7	12	
14 21 33.11	11027P	2	9.6633	33.3	7	12	
14 21 33.15	11028P	2	9.6633	33.3	7	12	
14 21 33.18	11029P	2	9.6633	33.3	7	12	
14 21 33.21	11030P	2	9.6633	33.3	7	12	
14 21 33.25	11031P	2	9.6633	33.3	7	12	
14 21 33.28	11032P	2	9.6633	33.3	7	12	
14 21 33.31	11033P	2	9.6633	33.3	7	12	
14 21 33.35	11034T	0	9.6633	33.3	7	12	
14 21 33.38	11035T	0	9.6633	33.3	7	12	
14 21 33.41	11036P	2	9.6633	33.3	7	12	
14 21 33.45	11037P	2	9.6633	33.3	7	12	
14 21 33.48	11038P	2	9.6633	33.3	7	12	
14 21 33.51	11039P	2	9.6633	33.3	7	12	
14 21 33.55	11040P	2	9.6633	33.3	7	12	
14 21 33.58	11041P	2	9.6633	33.3	7	12	
14 21 33.61	11042P	2	9.6633	33.3	7	12	
14 21 33.65	11043P	2	9.6633	33.3	7	12	
14 21 33.68	11044T	0	9.6633	33.3	7	12	
14 21 33.71	11045T	0	9.6633	33.3	7	12	
14 21 33.75	11046P	2	9.6633	33.3	7	12	
14 21 33.78	11047P	2	9.6633	33.3	7	12	
14 21 33.81	11048P	2	9.6633	33.3	7	12	
14 21 33.85	11049P	2	9.6633	33.3	7	12	
14 21 33.88	11050P	2	9.6633	33.3	7	12	
14 21 33.91	11051P	2	9.6633	33.3	7	12	
14 21 33.95	11052P	2	9.6633	33.3	7	12	
14 21 33.98	11053P	2	9.6633	33.3	7	12	
14 21 34.01	11054T	0	9.6633	33.3	7	12	
14 21 34.05	11055T	0	9.6633	33.3	7	12	

Table E8 - Telemetry Frames and Camera Parameters (Cont'd)

UMI	Telemetry Frame	Filter	Tracker Exp. Time (ms)	Frame Exp. Time (ms)	TRACKER Gain Step	Frame Gain Step	Comments
14 21 34.08	11053P	2	9.6633	33.3	7	12	
14 21 34.11	11057P	2	9.6633	33.3	7	12	
14 21 34.15	11058P	2	9.6633	33.3	7	12	
14 21 34.18	11059P	2	9.6633	33.3	7	12	
14 21 34.21	11060P	2	9.6633	33.3	7	12	
14 21 34.25	11061P	2	9.6633	33.3	7	12	
14 21 34.28	11062P	2	9.6633	33.3	7	12	
14 21 34.31	11063P	2	9.6633	33.3	7	12	
14 21 34.35	11064T	0	9.6633	33.3	7	12	
14 21 34.38	11065T	0	9.6633	33.3	7	12	
14 21 34.41	11066P	2	9.6633	33.3	7	12	
14 21 34.51	11069P	2	9.6633	33.3	7	11	
14 21 34.55	11070P	2	9.6633	33.3	7	11	
14 21 34.58	11071P	2	9.6633	33.3	7	11	
14 21 34.61	11072P	2	9.6633	33.3	7	11	
14 21 34.65	11073P	2	9.6633	33.3	7	11	
14 21 34.68	11074T	0	9.6633	33.3	7	11	
14 21 34.71	11075T	0	9.6633	33.3	7	11	
14 21 34.75	11076P	2	9.6633	33.3	7	11	
14 21 34.78	11077P	2	9.6633	33.3	7	11	
14 21 34.81	11078P	2	9.6633	33.3	7	11	
14 21 34.85	11079P	2	9.6633	33.3	7	11	
14 21 34.88	11080P	2	9.6633	33.3	7	11	
14 21 34.91	11081P	2	9.6633	33.3	7	11	
14 21 34.95	11082P	2	9.6633	33.3	7	11	
14 21 34.98	11083P	2	9.6633	33.3	7	11	
14 21 35.01	11084T	0	9.6633	33.3	7	11	
14 21 35.05	11085T	0	9.6633	33.3	7	11	
14 21 35.08	11086P	2	9.6633	33.3	7	11	
14 21 35.11	11087P	2	9.6633	33.3	7	11	
14 21 35.15	11088P	2	9.6633	33.3	7	11	
14 21 35.18	11089P	2	9.6633	33.3	7	11	
14 21 35.21	11090P	2	9.6633	33.3	7	11	
14 21 35.25	11091P	2	9.6633	33.3	7	11	
14 21 35.28	11092P	2	9.6633	33.3	7	11	
14 21 35.31	11093P	2	9.6633	33.3	7	11	
14 21 35.35	11094T	0	9.6633	33.3	7	11	
14 21 35.38	11095T	0	9.6633	33.3	7	11	
14 21 35.41	11096P	2	9.6633	33.3	7	11	
14 21 35.45	11097P	2	9.6633	33.3	7	11	
14 21 35.48	11098P	2	9.6633	33.3	7	11	
14 21 35.51	11099P	2	9.6633	33.3	7	11	
14 21 35.55	11100P	2	9.6633	33.3	7	11	

Table E8 - Telemetry Frames and Camera Parameters (Cont'd)

UMT	Telemetry Frame	Filter	Tracker Exp. Time (ms)	Prime Exp. Time (ms)	Tracker Gain Step	Prime Gain Step	Comments
14 21 35.58	11101P	2	9.6633	33.3	7	11	
14 21 35.61	11102P	2	9.6633	33.3	7	11	
14 21 35.65	11103P	2	9.6633	33.3	7	11	
14 21 35.68	11104T	0	9.6633	33.3	7	11	
14 21 35.71	11105T	0	9.6633	33.3	7	11	
14 21 35.75	11106P	2	9.6633	33.3	7	11	
14 21 35.78	11107P	2	9.6633	33.3	7	11	
14 21 35.81	11108P	2	9.6633	33.3	7	11	
14 21 35.85	11109P	2	9.6633	33.3	7	11	
14 21 35.88	11110P	2	9.6633	33.3	7	11	
14 21 35.91	11111P	2	9.6633	33.3	7	11	
14 21 35.95	11112P	2	9.6633	33.3	7	11	
14 21 35.98	11113P	2	9.6633	33.3	7	11	
14 21 36.02	11114T	0	9.6633	33.3	7	11	
14 21 36.05	11115T	0	9.6633	33.3	7	11	
14 21 36.08	11116P	2	9.6633	33.3	7	11	
14 21 36.12	11117P	2	9.6633	33.3	7	11	
14 21 36.15	11118P	2	9.6633	33.3	7	11	
14 21 36.18	11119P	2	9.6633	33.3	7	11	
14 21 36.22	11120P	2	9.6633	33.3	7	11	
14 21 36.25	11121P	2	9.6633	33.3	7	11	
14 21 36.28	11122P	2	9.6633	33.3	7	11	
14 21 36.32	11123P	2	9.6633	33.3	7	11	
14 21 36.35	11124T	0	9.6633	33.3	7	11	
14 21 36.38	11125T	0	9.6633	33.3	7	11	
14 21 36.42	11126P	2	9.6633	33.3	7	11	
14 21 36.45	11127P	2	9.6633	33.3	7	11	
14 21 36.48	11128P	2	9.6633	33.3	7	11	
14 21 36.52	11129P	2	9.6633	33.3	7	11	
14 21 36.55	11130P	2	9.6633	33.3	7	11	
14 21 36.58	11131P	2	9.6633	33.3	7	11	
14 21 36.62	11132P	2	9.6633	33.3	7	11	
14 21 36.65	11133P	2	9.6633	33.3	7	11	
14 21 36.68	11134T	0	9.6633	33.3	7	11	
14 21 36.72	11135T	0	9.6633	33.3	7	11	
14 21 36.75	11136P	2	9.6633	33.3	7	11	
14 21 36.78	11137P	2	9.6633	33.3	7	11	
14 21 36.82	11138P	2	9.6633	33.3	7	11	
14 21 36.85	11139P	2	9.6633	33.3	7	11	
14 21 36.88	11140P	2	9.6633	33.3	7	11	
14 21 36.92	11141P	2	9.6633	33.3	7	11	
14 21 36.95	11142P	2	9.6633	33.3	7	11	
14 21 36.98	11143P	2	9.6633	33.3	7	11	

Table E8 - Telemetry Frames and Camera Parameters (cont'd)

UMT	Telemetry Frame	Filter	Tracker Exp. Time (ms)	Plane Exp. Time (ms)	Tracker Gain Step	Plane Gain Step	Comments
14 21 37.02	11144I	0	9.6633	33.3	7	11	
14 21 37.05	11145I	0	9.6633	33.3	7	11	
14 21 37.08	11146P	2	9.6633	33.3	7	11	
14 21 37.12	11147P	2	9.6633	33.3	7	11	
14 21 37.15	11148P	2	9.6633	33.3	7	11	
14 21 37.18	11149P	2	9.6633	33.3	7	11	
14 21 37.22	11150P	2	9.6633	33.3	7	11	
14 21 37.25	11151P	2	9.6633	33.3	7	11	
14 21 37.28	11152P	2	9.6633	33.3	7	11	
14 21 37.32	11153P	2	9.6633	33.3	7	11	
14 21 37.35	11154I	0	9.6633	33.3	7	11	
14 21 37.38	11155I	0	9.6633	33.3	7	11	
14 21 37.42	11156P	2	9.6633	33.3	7	11	
14 21 37.45	11157P	2	9.6633	33.3	7	11	
14 21 37.48	11158P	2	9.6633	33.3	7	11	
14 21 37.52	11159P	2	9.6633	33.3	7	11	
14 21 37.55	11160P	2	9.6633	33.3	7	11	
14 21 37.58	11161P	2	9.6633	33.3	7	11	
14 21 37.62	11162P	2	9.6633	33.3	7	11	
14 21 37.65	11163P	2	9.6633	33.3	7	11	
14 21 37.68	11164I	0	9.6633	33.3	7	11	
14 21 37.72	11165I	0	9.6633	33.3	7	11	
14 21 37.75	11166P	2	9.6633	33.3	7	11	
14 21 37.78	11167P	2	9.6633	33.3	7	11	
14 21 37.82	11168P	2	9.6633	33.3	7	11	
14 21 37.85	11169P	2	9.6633	33.3	7	11	
14 21 37.88	11170P	2	9.6633	33.3	7	11	
14 21 37.92	11171P	2	9.6633	33.3	7	11	
14 21 37.95	11172P	2	9.6633	33.3	7	11	
14 21 37.98	11173P	2	9.6633	33.3	7	11	
14 21 38.02	11174I	0	9.6633	33.3	7	11	
14 21 38.05	11175I	0	9.6633	33.3	7	11	
14 21 38.08	11176P	2	9.6633	33.3	7	11	
14 21 38.12	11177P	2	9.6633	33.3	7	11	
14 21 38.15	11178P	2	9.6633	33.3	7	11	
14 21 38.18	11179P	2	9.6633	33.3	7	11	
14 21 38.22	11180P	2	9.6633	33.3	7	11	
14 21 38.25	11181P	2	9.6633	33.3	7	11	
14 21 38.28	11182P	2	9.6633	33.3	7	11	
14 21 38.32	11183P	2	9.6633	33.3	7	11	
14 21 38.35	11184I	0	9.6633	33.3	7	11	
14 21 38.39	11185I	0	9.6633	33.3	7	11	
14 21 38.42	11186P	2	9.6633	33.3	7	11	

Table E8 - Telemetry Frames and Camera Parameters (Cont'd)

UMT	Telemetry Frame	Filter	Tracker Exp. Time (ms)	Plume Exp. Time (ms)	Tracker Gain Step	Plume Gain Step	Comments
14 21 38.45	11187P	2	9.6633	33.3	7	11	
14 21 38.48	11188P	2	9.6633	33.3	7	11	
14 21 38.52	11189P	2	9.6633	33.3	7	11	
14 21 38.55	11190P	2	9.6633	33.3	7	11	End data interval 3, PC-2
14 21 40.12	11237P	2	9.6633	33.3	7	11	
14 21 40.15	11238P	2	9.6633	33.3	7	11	
14 21 40.25	11241P	2	9.6633	33.3	7	11	
14 21 40.29	11242P	2	9.6633	33.3	7	11	
14 21 40.32	11243P	2	9.6633	33.3	7	11	
14 21 40.35	11244T	0	9.6633	33.3	7	11	
14 21 40.39	11245T	0	9.6633	33.3	7	11	
14 21 40.41	11246P	2	9.6633	33.3	7	11	
14 21 40.45	11247P	2	9.6633	33.3	7	11	
14 21 40.49	11248P	2	9.6633	33.3	7	11	
14 21 40.52	11249P	2	9.6633	33.3	7	11	
14 21 40.55	11250P	2	9.6633	33.3	7	11	
14 21 40.59	11251P	2	9.6633	33.3	7	11	
14 21 40.62	11252P	2	9.6633	33.3	7	11	
14 21 40.65	11253P	2	9.6633	33.3	7	11	
14 21 40.69	11254T	0	15.4018	33.3	6	11	
14 21 40.72	11255T	0	15.4018	33.3	6	11	
14 21 40.75	11256P	2	15.4018	33.3	6	11	
14 21 40.79	11257P	2	15.4018	33.3	6	11	
14 21 40.82	11258P	2	15.4018	33.3	6	11	
14 21 40.85	11259P	2	15.4018	33.3	6	11	
14 21 40.89	11260P	2	15.4018	33.3	6	11	
14 21 40.92	11261P	2	15.4018	33.3	6	11	
14 21 40.95	11262P	2	15.4018	33.3	6	11	
14 21 40.99	11263P	2	15.4018	33.3	6	11	
14 21 41.02	11264T	0	15.4018	33.3	6	11	
14 21 41.05	11265T	0	15.4018	33.3	6	11	
14 21 41.09	11266P	2	15.4018	33.3	6	11	
14 21 41.12	11267P	2	15.4018	33.3	6	11	
14 21 41.15	11268P	2	15.4018	33.3	6	11	
14 21 41.19	11269P	2	15.4018	33.3	6	11	
14 21 41.22	11270P	2	15.4018	33.3	6	11	
14 21 41.25	11271P	2	15.4018	33.3	6	11	
14 21 41.29	11272P	2	15.4018	33.3	6	11	
14 21 41.32	11273P	1	15.4018	33.3	6	11	
14 21 41.35	11274T	0	15.4018	33.3	6	11	
14 21 41.39	11275T	0	15.4018	33.3	6	11	
14 21 41.42	11276P	1	15.4018	33.3	6	11	
14 21 41.45	11277P	1	15.4018	33.3	6	11	

Table E8 - Telemetry Frames and Camera Parameters (Cont'd)

GMT	Telemetry Frame	Filter	Tracker Exp. Time (ms)	Plume Exp. Time (ms)	Tracker Gain Step	Plume Gain Step	Comments
14 21 41.49	11275P	1	15.4018	33.3	6	11	
14 21 41.52	11275P	1	15.4018	33.3	6	11	
14 21 41.55	11280P	1	15.4018	33.3	6	11	
14 21 41.59	11281P	1	15.4018	33.3	6	11	
14 21 41.62	11282P	1	15.4018	33.3	6	11	
14 21 41.65	11283P	1	15.4018	33.3	6	11	
14 21 41.69	11284T	0	15.4018	33.3	6	11	Begin data interval 4, PC-1
14 21 41.72	11285T	0	15.4018	33.3	6	11	
14 21 41.75	11286P	1	15.4018	33.3	6	11	
14 21 41.79	11287P	1	15.4018	33.3	6	11	
14 21 41.82	11288P	1	15.4018	33.3	6	11	
14 21 41.85	11289P	1	15.4018	33.3	6	11	
14 21 41.89	11290P	1	15.4018	33.3	6	11	
14 21 41.92	11291P	1	15.4018	33.3	6	11	
14 21 41.96	11292P	1	15.4018	33.3	6	11	
14 21 41.99	11293P	1	15.4018	33.3	6	11	
14 21 42.02	11294T	0	15.4018	33.3	6	11	
14 21 42.05	11295T	0	15.4018	33.3	6	11	
14 21 42.09	11296P	1	15.4018	33.3	6	11	
14 21 42.12	11297P	1	15.4018	33.3	6	11	
14 21 42.16	11298P	1	15.4018	33.3	6	11	
14 21 42.19	11299P	1	15.4018	33.3	6	11	
14 21 42.22	11300P	1	15.4018	33.3	6	11	
14 21 42.26	11301P	1	15.4018	33.3	6	11	
14 21 42.29	11302P	1	15.4018	33.3	6	11	
14 21 42.32	11303P	1	15.4018	33.3	6	11	
14 21 42.36	11304T	0	15.4018	33.3	6	11	
14 21 42.39	11305T	0	15.4018	33.3	6	11	
14 21 42.42	11306P	1	15.4018	33.3	6	11	
14 21 42.46	11307P	1	15.4018	33.3	6	11	
14 21 42.49	11308P	1	15.4018	33.3	6	11	
14 21 42.52	11309P	1	15.4018	33.3	6	11	
14 21 42.56	11310P	1	15.4018	33.3	6	11	
14 21 42.59	11311P	1	15.4018	33.3	6	11	
14 21 42.62	11312P	1	15.4018	33.3	6	11	
14 21 42.66	11313P	1	15.4018	33.3	6	11	
14 21 42.69	11314T	0	15.4018	33.3	6	11	
14 21 42.72	11315T	0	15.4018	33.3	6	11	
14 21 42.76	11316P	1	15.4018	33.3	6	11	
14 21 42.79	11317P	1	15.4018	33.3	6	11	
14 21 42.82	11318P	1	15.4018	33.3	6	11	
14 21 42.86	11319P	1	15.4018	33.3	6	11	
14 21 42.89	11320P	1	15.4018	33.3	6	11	



Table E8 - Telemetry Frames and Camera Parameters (Cont'd)

GMT	Telemetry Frame	Filter	Tracker Exp. Time (ms)	Plume Exp. Time (ms)	Tracker Gain Step	Plume Gain Step	Comments
14 21 42.92	11321P	1	15.4018	33.3	6	11	
14 21 42.96	11322P	1	15.4018	33.3	6	11	
14 21 42.99	11323P	1	15.4018	33.3	6	11	
14 21 43.02	11324T	0	15.4018	33.3	6	11	
14 21 43.06	11325T	0	15.4018	33.3	6	11	
14 21 43.09	11326P	1	15.4018	33.3	6	11	
14 21 43.12	11327P	1	15.4018	33.3	6	11	
14 21 43.16	11328P	1	15.4018	33.3	6	11	
14 21 43.19	11329P	1	15.4018	33.3	6	11	
14 21 43.22	11330P	1	15.4018	33.3	6	11	
14 21 43.26	11331P	1	15.4018	33.3	6	11	
14 21 43.29	11332P	1	15.4018	33.3	6	11	
14 21 43.32	11333P	1	15.4018	33.3	6	11	
14 21 43.36	11334T	0	15.4018	33.3	6	11	
14 21 43.39	11335T	0	15.4018	33.3	6	11	
14 21 43.42	11336P	1	15.4018	33.3	6	11	
14 21 43.46	11337P	1	15.4018	33.3	6	11	
14 21 43.49	11338P	1	15.4018	33.3	6	11	
14 21 43.52	11339P	1	15.4018	33.3	6	11	
14 21 43.56	11340P	1	15.4018	33.3	6	11	
14 21 43.59	11341P	1	15.4018	33.3	6	11	
14 21 43.62	11342P	1	15.4018	33.3	6	11	
14 21 43.66	11343P	1	15.4018	33.3	6	11	
14 21 43.69	11344T	0	15.4018	33.3	6	11	
14 21 43.72	11345T	0	15.4018	33.3	6	11	
14 21 43.76	11346P	1	15.4018	33.3	6	11	
14 21 43.79	11347P	1	15.4018	33.3	6	11	
14 21 43.82	11348P	1	15.4018	33.3	6	11	
14 21 43.86	11349P	1	15.4018	33.3	6	11	
14 21 43.89	11350P	1	15.4018	33.3	6	11	
14 21 43.92	11351P	1	15.4018	33.3	6	11	
14 21 43.96	11352P	1	15.4018	33.3	6	11	
14 21 43.99	11353P	1	15.4018	33.3	6	11	
14 21 44.02	11354T	0	15.4018	33.3	6	11	
14 21 44.06	11355T	0	15.4018	33.3	6	11	
14 21 44.09	11356P	1	15.4018	33.3	6	11	
14 21 44.12	11357P	1	15.4018	33.3	6	11	
14 21 44.16	11358P	1	15.4018	33.3	6	11	
14 21 44.19	11359P	1	15.4018	33.3	6	11	
14 21 44.22	11360P	1	15.4018	33.3	6	11	
14 21 44.26	11361P	1	15.4018	33.3	6	11	
14 21 44.29	11362P	1	15.4018	33.3	6	11	
14 21 44.32	11363P	1	15.4018	33.3	6	11	

Table E8 - Telemetry Frames and Camera Parameters (Cont'd)

UMT	Telemetry Frame	Filter	Tracker Exp. Time (ms)	Plume Exp. Time (ms)	Tracker Gain Step	Plume Gain Step	Comments
14 21 44.36	11364T	0	15.4018	33.3	6	11	
14 21 44.39	11365T	0	15.4018	33.3	6	11	
14 21 44.42	11366P	1	15.4018	33.3	6	11	
14 21 44.46	11367P	1	15.4018	33.3	6	11	
14 21 44.49	11368P	1	15.4018	33.3	6	11	
14 21 44.52	11369P	1	15.4018	33.3	6	11	
14 21 44.56	11370P	1	15.4018	33.3	6	11	
14 21 44.59	11371P	1	15.4018	33.3	6	11	
14 21 44.62	11372P	1	15.4018	33.3	6	11	
14 21 44.66	11373P	1	15.4018	33.3	6	11	
14 21 44.69	11374T	0	15.4018	33.3	6	11	
14 21 44.72	11375T	0	15.4018	33.3	6	11	
14 21 44.76	11376P	1	15.4018	33.3	6	11	
14 21 44.79	11377P	1	15.4018	33.3	6	11	
14 21 44.82	11378P	1	15.4018	33.3	6	11	
14 21 44.86	11379P	1	15.4018	33.3	6	11	
14 21 44.89	11380P	1	15.4018	33.3	6	11	
14 21 44.93	11381P	1	15.4018	33.3	6	11	
14 21 44.96	11382P	1	15.4018	33.3	6	11	
14 21 44.99	11383P	1	15.4018	33.3	6	11	
14 21 45.03	11384T	0	15.4018	33.3	6	11	
14 21 45.06	11385T	0	15.4018	33.3	6	11	
14 21 45.09	11386P	1	15.4018	33.3	6	11	
14 21 45.13	11387P	1	15.4018	33.3	6	11	
14 21 45.16	11388P	1	15.4018	33.3	6	11	
14 21 45.19	11389P	1	15.4018	33.3	6	11	
14 21 45.23	11390P	1	15.4018	33.3	6	11	
14 21 45.26	11391P	1	15.4018	33.3	6	11	
14 21 45.29	11392P	1	15.4018	33.3	6	11	
14 21 45.33	11393P	1	15.4018	33.3	6	11	
14 21 45.36	11394T	0	15.4018	33.3	6	11	
14 21 45.39	11395T	0	15.4018	33.3	6	11	
14 21 45.43	11396P	1	15.4018	33.3	6	11	
14 21 45.46	11397P	1	15.4018	33.3	6	11	
14 21 45.49	11398P	1	15.4018	33.3	6	11	
14 21 45.53	11399P	1	15.4018	33.3	6	11	
14 21 45.56	11400P	1	15.4018	33.3	6	11	
14 21 45.59	11401P	1	15.4018	33.3	6	11	
14 21 45.63	11402P	1	15.4018	33.3	6	11	
14 21 45.66	11403P	1	15.4018	33.3	6	11	
14 21 45.69	11404T	0	15.4018	33.3	6	11	
14 21 45.73	11405T	0	15.4018	33.3	6	11	
14 21 45.76	11406P	1	15.4018	33.3	6	11	

Table E8 - Telemetry Frames and Camera Parameters (Cont'd)

UMT	Telemetry Frame	Filter	Tracker Exp. Time (ms)	Plume Exp. Time (ms)	Tracker Gain Step	Plume Gain Step	Comments
14 21 45.79	11407P	1	15.4018	33.3	6	11	
14 21 45.83	11408P	1	15.4018	33.3	6	11	
14 21 45.85	11409P	1	15.4018	33.3	6	11	
14 21 45.89	11410P	1	15.4018	33.3	6	11	
14 21 45.93	11411P	1	15.4018	33.3	6	11	
14 21 45.96	11412P	1	15.4018	33.3	6	11	
14 21 45.99	11413P	1	15.4018	33.3	6	11	
14 21 46.03	11414T	0	15.4018	33.3	6	11	End data interval 4, PC-1
14 21 46.06	11415T	0	19.4444	33.3	6	11	
14 21 46.09	11416P	1	19.4444	33.3	6	11	
14 21 46.13	11417P	1	19.4444	33.3	6	11	Antarcs burnout
14 21 46.16	11418P	1	19.4444	33.3	6	11	
14 21 46.19	11419P	1	19.4444	33.3	6	12	
14 21 46.23	11420P	1	19.4444	33.3	6	13	
14 21 46.26	11421P	1	19.4444	33.3	6	13	
14 21 46.29	11422P	1	19.4444	33.3	6	13	
14 21 46.33	11423P	1	19.4444	33.3	6	13	
14 21 46.36	11424T	0	24.5481	33.3	6	13	
14 21 46.39	11425T	0	30.9914	33.3	6	13	
14 21 46.43	11426P	1	30.9914	33.3	6	13	
14 21 46.46	11427P	1	30.9914	33.3	6	13	
14 21 46.49	11428P	1	30.9914	33.3	6	13	
14 21 46.53	11429P	1	30.9914	33.3	6	13	
14 21 46.56	11430P	1	30.9914	33.3	6	13	
14 21 46.60	11431P	1	30.9914	33.3	6	13	
14 21 46.63	11432P	1	30.9914	33.3	6	13	
14 21 46.66	11433P	1	30.9914	33.3	6	13	
14 21 46.69	11434T	0	16.3259	33.3	7	13	
14 21 46.73	11435T	0	21.8478	33.3	7	13	
14 21 46.76	11436P	1	21.8478	33.3	7	13	
14 21 46.79	11437P	1	21.8478	33.3	7	13	
14 21 46.83	11438P	1	21.8478	33.3	7	13	
14 21 46.86	11439P	1	21.8478	33.3	7	13	
14 21 46.89	11440P	1	21.8478	33.3	7	13	
14 21 46.93	11441P	1	21.8478	33.3	7	13	
14 21 46.96	11442P	1	21.8478	33.3	7	13	
14 21 46.99	11443P	1	21.8478	33.3	7	13	
14 21 47.03	11444T	0	27.5823	33.3	7	13	
14 21 47.06	11445T	0	16.3259	33.3	8	13	
14 21 47.26	11451P	1	16.3259	33.3	8	13	
14 21 47.46	11457P	1	16.3259	33.3	8	13	
14 21 47.66	11463P	1	16.3259	33.3	8	13	
14 21 47.86	11469P	1	16.3259	33.3	8	13	

Table E8 - Telemetry Frames and Camera Parameters (Cont'd)

UMT	Telemetry Frame	Filter	Tracker Exp. Time (ms)	Plume Exp. Time (ms)	Tracker Gain Step	Plume Gain Step	Comments
14 21 48.06	11475P	1	16.3259	33.3	8	13	
14 21 48.26	11481P	1	16.3259	33.3	8	13	
14 21 48.46	11487P	1	16.3259	33.3	8	13	
14 21 48.66	11493P	1	27.5823	33.3	9	13	Cloud trail appears in tracker camera FOV
14 21 48.86	11499T	0	27.5823	33.3	10	13	
14 21 49.06	11505T	0	27.5823	33.3	10	13	
14 21 49.26	11511T	0	27.5823	33.3	10	13	
14 21 49.46	11517T	0	27.5823	33.3	10	13	
14 21 49.66	11523T	0	27.5823	33.3	10	13	
14 21 49.86	11529T	0	27.5823	33.3	10	13	
14 21 50.06	11535T	0	27.5823	33.3	10	13	
14 21 50.26	11541T	0	27.5823	33.3	10	13	
14 21 50.46	11547P	1	27.5823	33.3	10	13	
14 21 50.66	11553P	1	27.5823	33.3	10	13	
14 21 50.87	11559T	0	27.5823	33.3	10	13	
14 21 51.07	11565T	0	27.5823	33.3	10	13	
14 21 51.27	11571T	0	27.5823	33.3	10	13	
14 21 51.47	11577T	0	27.5823	33.3	10	13	
14 21 51.67	11583T	0	27.5823	33.3	10	13	
14 21 51.87	11589T	0	27.5823	33.3	10	13	
14 21 52.07	11595T	0	27.5823	33.3	10	13	
14 21 52.27	11601T	0	27.5823	33.3	10	13	
14 21 52.47	11607P	1	27.5823	33.3	10	13	
14 21 52.67	11613P	1	27.5823	33.3	10	13	
14 21 52.87	11619T	0	27.5823	33.3	10	13	
14 21 53.07	11625T	0	27.5823	33.3	10	13	
14 21 53.27	11631T	0	27.5823	33.3	10	13	
14 21 53.47	11637T	0	27.5823	33.3	10	13	
14 21 53.67	11643T	0	27.5823	33.3	10	13	
14 21 53.87	11649T	0	27.5823	33.3	10	13	
14 21 54.07	11655T	0	27.5823	33.3	10	13	
14 21 54.27	11661T	0	27.5823	33.3	10	13	
14 21 54.47	11667P	1	27.5823	33.3	10	13	
14 21 54.67	11673P	1	27.5823	33.3	10	13	
14 21 54.87	11679T	0	27.5823	33.3	10	13	
14 21 55.07	11685T	0	27.5823	33.3	10	13	
14 21 55.27	11691T	0	27.5823	33.3	10	13	
14 21 55.47	11697T	0	27.5823	33.3	10	13	
14 21 55.67	11703T	0	27.5823	33.3	10	13	
14 21 55.87	11709T	0	27.5823	33.3	10	13	
14 21 56.07	11715T	0	27.5823	33.3	10	13	
14 21 56.27	11721T	0	27.5823	33.3	10	13	
14 21 56.47	11727P	1	27.5823	33.3	10	13	

Table E8 - Telemetry Frames and Camera Parameters (Cont'd)

UMT	Telemetry Frame	Filter	Tracker Exp. Time (ms)	Flame Exp. Time (ms)	Tracker Gain Step	Flame Gain Step	Comments
14 21 56.67	11733P	1	27.5823	33.3	10	13	
14 21 56.87	11739T	0	27.5823	33.3	10	13	
14 21 57.07	11745T	0	27.5823	33.3	10	13	
14 21 57.27	11751T	0	27.5823	33.3	10	13	
14 21 57.47	11757T	0	27.5823	33.3	10	13	
14 21 57.67	11763T	0	27.5823	33.3	10	13	
14 21 57.87	11769T	0	27.5823	33.3	10	13	
14 21 58.07	11775T	0	27.5823	33.3	10	13	
14 21 58.27	11781T	0	27.5823	33.3	10	13	
14 21 58.47	11787P	1	27.5823	33.3	10	13	
14 21 58.67	11793P	1	27.5823	33.3	10	13	
14 21 58.87	11799T	0	27.5823	33.3	10	13	
14 21 59.07	11805T	0	27.5823	33.3	10	13	
14 21 59.27	11811T	0	27.5823	33.3	10	13	
14 21 59.48	11817T	0	27.5823	33.3	10	13	
14 21 59.68	11823T	0	27.5823	33.3	10	13	
14 21 59.88	11829T	0	27.5823	33.3	10	13	
14 22 0.08	11835T	0	27.5823	33.3	10	13	
14 22 0.28	11841T	0	27.5823	33.3	10	13	
14 22 0.48	11847P	1	27.5823	33.3	10	13	
14 22 0.68	11853P	1	27.5823	33.3	10	12	
14 22 0.88	11859T	0	27.5823	33.3	10	12	
14 22 1.08	11865T	0	27.5823	33.3	10	12	
14 22 1.28	11871T	0	27.5823	33.3	10	12	
14 22 1.68	11883T	0	27.5823	33.3	10	12	
14 22 1.88	11889T	0	27.5823	33.3	10	12	
14 22 2.08	11895T	0	27.5823	33.3	10	12	
14 22 2.28	11901T	0	27.5823	33.3	10	12	
14 22 2.48	11907P	1	27.5823	33.3	10	13	
14 22 2.68	11913P	1	27.5823	33.3	10	13	
14 22 2.88	11919T	0	27.5823	33.3	10	13	
14 22 3.08	11925T	0	27.5823	33.3	10	13	
14 22 3.28	11931T	0	27.5823	33.3	10	13	
14 22 3.48	11937T	0	27.5823	33.3	10	13	
14 22 3.68	11943T	0	27.5823	33.3	10	13	
14 22 3.88	11949T	0	27.5823	33.3	10	13	
14 22 4.08	11955T	0	27.5823	33.3	10	13	
14 22 4.28	11961T	0	27.5823	33.3	10	13	
14 22 4.48	11967P	1	27.5823	33.3	10	13	
14 22 4.88	11979T	0	27.5823	33.3	10	13	
14 22 5.08	11985T	0	27.5823	33.3	10	13	
14 22 5.28	11991T	0	27.5823	33.3	10	13	
14 22 5.48	11997T	0	27.5823	33.3	10	13	

Table E8 - Telemetry Frames and Camera Parameters (Cont'd)

UMT	Telemetry Frame	Filter	Tracker Exp. Time (ms)	Plume Exp. Time (ms)	Tracker Gain Step	Plume Gain Step	Comments
14 22 5.68	12003T	0	27.5823	33.3	10	13	
14 22 5.88	12009T	0	27.5823	33.3	10	13	
14 22 6.38	12015T	0	27.5823	33.3	10	13	
14 22 6.28	12021T	0	27.5823	33.3	10	13	
14 22 6.48	12027P	1	27.5823	33.3	10	13	
14 22 6.68	12033P	1	27.5823	33.3	10	13	
14 22 6.88	12039T	0	27.5823	33.3	10	13	
14 22 7.08	12045T	0	27.5823	33.3	10	13	
14 22 7.28	12051T	0	27.5823	33.3	10	13	
14 22 7.48	12057T	0	27.5823	33.3	10	13	
14 22 7.68	12063T	0	27.5823	33.3	10	13	
14 22 7.88	12069T	0	27.5823	33.3	10	13	
14 22 8.29	12081T	0	27.5823	33.3	10	13	
14 22 8.49	12087P	1	27.5823	33.3	10	13	
14 22 8.69	12093P	1	27.5823	33.3	10	13	
14 22 8.89	12099T	0	27.5823	33.3	10	13	
14 22 9.09	12105T	0	27.5823	33.3	10	13	
14 22 9.29	12111T	0	27.5823	33.3	10	13	
14 22 9.49	12117T	0	27.5823	33.3	10	13	
14 22 9.69	12123T	0	27.5823	33.3	10	13	
14 22 9.89	12129T	0	27.5823	33.3	10	13	
14 22 10.09	12135T	0	27.5823	33.3	10	13	
14 22 10.29	12141T	0	27.5823	33.3	10	13	
14 22 10.49	12147P	1	27.5823	33.3	10	13	
14 22 10.69	12153P	1	27.5823	33.3	10	13	
14 22 10.89	12159T	0	27.5823	33.3	10	13	
14 22 11.09	12165T	0	27.5823	33.3	10	13	
14 22 11.29	12171T	0	27.5823	33.3	10	13	
14 22 11.49	12177T	0	27.5823	33.3	10	13	
14 22 11.69	12183T	0	27.5823	33.3	10	13	
14 22 11.89	12189T	0	27.5823	33.3	10	13	
14 22 12.09	12195T	0	27.5823	33.3	10	13	
14 22 12.29	12201T	0	27.5823	33.3	10	13	
14 22 12.49	12207P	1	27.5823	33.3	10	13	
14 22 13.09	12225T	0	27.5823	33.3	10	13	
14 22 13.29	12231T	0	27.5823	33.3	10	13	
14 22 13.49	12237T	0	27.5823	33.3	10	13	
14 22 13.69	12233T	0	27.5823	33.3	10	13	
14 22 13.89	12249T	0	27.5823	33.3	10	13	
14 22 14.09	12255T	0	27.5823	33.3	10	13	
14 22 14.29	12261T	0	27.5823	33.3	10	13	
14 22 14.69	12273P	1	27.5823	33.3	10	13	
14 22 14.89	12279T	0	27.5823	33.3	10	13	

Table E8 - Telemetry Frames and Camera Parameters (Cont'd)

GMT	Telemetry Frame	Filter	Tracker Exp. Time (ms)	Plume Exp. Time (ms)	Tracker Gain Step	Plume Gain Step	Comments
14 22 15.09	12285T	0	27.5823	33.3	10	13	
14 22 15.29	12291T	0	27.5823	33.3	10	13	
14 22 15.49	12297T	0	27.5823	33.3	10	13	
14 22 15.69	12303T	0	27.5823	33.3	10	13	
14 22 15.89	12309T	0	27.5823	33.3	10	13	
14 22 16.09	12315T	0	27.5823	33.3	10	13	
14 22 16.29	12321T	0	27.5823	33.3	10	13	
14 22 16.49	12327P	1	27.5823	33.3	10	13	
14 22 16.69	12333P	1	27.5823	33.3	10	13	
14 22 16.89	12339T	0	27.5823	33.3	10	13	
14 22 17.10	12345T	0	27.5823	33.3	10	13	Cloud trail disappears from tracker camera FOV
14 22 17.30	12351T	0	27.5823	33.3	10	13	
14 22 17.50	12357T	0	27.5823	33.3	10	13	
14 22 17.70	12363T	0	27.5823	33.3	10	13	
14 22 17.90	12369T	0	27.5823	33.3	10	13	
14 22 18.10	12375T	0	27.5823	33.3	10	13	
14 22 18.30	12381T	0	27.5823	33.3	10	13	
14 22 18.50	12387P	1	27.5823	33.3	10	13	
14 22 18.70	12393P	1	27.5823	33.3	10	13	
14 22 18.90	12399T	0	27.5823	33.3	10	13	
14 22 19.10	12405T	0	27.5823	33.3	10	13	
14 22 19.30	12429T	0	27.5823	33.3	10	13	
14 22 20.10	12435T	0	27.5823	33.3	10	13	
14 22 20.30	12441T	0	27.5823	33.3	10	13	
14 22 20.50	12447P	1	27.5823	33.3	10	13	
14 22 20.70	12453P	1	27.5823	33.3	10	13	
14 22 20.90	12459T	0	27.5823	33.3	10	13	
14 22 21.10	12465T	0	27.5823	33.3	10	13	
14 22 21.30	12471T	0	27.5823	33.3	10	13	
14 22 21.50	12477T	0	27.5823	33.3	10	13	
14 22 21.70	12483T	0	27.5823	33.3	10	13	
14 22 21.90	12489T	0	27.5823	33.3	10	13	
14 22 22.10	12495T	0	27.5823	33.3	10	13	
14 22 22.30	12501T	0	27.5823	33.3	10	13	
14 22 22.50	12507P	1	27.5823	33.3	10	13	
14 22 22.70	12513P	1	27.5823	33.3	10	13	
14 22 22.90	12519T	0	27.5823	33.3	10	13	
14 22 23.10	12525T	0	27.5823	33.3	10	13	
14 22 23.30	12531T	0	27.5823	33.3	10	13	
14 22 23.50	12537T	0	27.5823	33.3	10	13	
14 22 23.70	12543T	0	27.5823	33.3	10	13	
14 22 23.90	12549T	0	27.5823	33.3	10	13	

Table E8 - Telemetry Frames and Camera Parameters (Cont'd)

OMT	Telemetry Frame	Filter	Tracker Exp. Time (ms)	Plume Exp. Time (ms)	Tracker Gain Step	Plume Gain Step	Comments
14 22 24.10	12555T	0	27.5823	33.3	10	13	
14 22 24.30	12561T	0	27.5823	33.3	10	13	
14 22 24.50	12567P	1	27.5823	33.3	10	13	
14 22 24.70	12573P	1	27.5823	33.3	10	13	
14 22 24.90	12579T	0	27.5823	33.3	10	13	
14 22 25.10	12585T	0	27.5823	33.3	10	13	
14 22 25.30	12591T	0	27.5823	33.3	10	13	
14 22 25.50	12597T	0	27.5823	33.3	10	13	
14 22 25.70	12603T	0	27.5823	33.3	10	13	
14 22 25.90	12609T	0	27.5823	33.3	10	13	
14 22 26.11	12615T	0	27.5823	33.3	10	13	
14 22 26.31	12621T	0	27.5823	33.3	10	13	
14 22 26.51	12627P	1	27.5823	33.3	10	13	
14 22 26.71	12633P	1	27.5823	33.3	10	13	
14 22 26.91	12639T	0	27.5823	33.3	10	13	
14 22 27.11	12645T	0	27.5823	33.3	10	13	
14 22 27.31	12651T	0	27.5823	33.3	10	13	
14 22 27.51	12657T	0	27.5823	33.3	10	13	
14 22 27.71	12663T	0	27.5823	33.3	10	13	
14 22 27.91	12669T	0	27.5823	33.3	10	13	
14 22 28.11	12675T	0	27.5823	33.3	10	13	
14 22 28.31	12681T	0	27.5823	33.3	10	13	
14 22 28.51	12687P	1	27.5823	33.3	10	13	
14 22 28.71	12693P	1	27.5823	33.3	10	13	
14 22 29.11	12705T	0	27.5823	33.3	10	13	
14 22 29.31	12711T	0	27.5823	33.3	10	13	
14 22 29.51	12717T	0	27.5823	33.3	10	13	
14 22 29.71	12723T	0	27.5823	33.3	10	13	
14 22 29.91	12729T	0	27.5823	33.3	10	13	
14 22 30.11	12735T	0	27.5823	33.3	10	13	
14 22 30.51	12747P	1	27.5823	33.3	10	13	
14 22 30.71	12753P	1	27.5823	33.3	10	13	
14 22 30.91	12759T	0	27.5823	33.3	10	13	
14 22 31.11	12765T	0	27.5823	33.3	10	13	
14 22 31.31	12771T	0	27.5823	33.3	10	13	
14 22 31.51	12777T	0	27.5823	33.3	10	13	
14 22 31.71	12783T	0	27.5823	33.3	10	13	
14 22 31.91	12789T	0	27.5823	33.3	10	13	
14 22 32.11	12795T	0	27.5823	33.3	10	13	
14 22 32.31	12801T	0	27.5823	33.3	10	13	
14 22 32.51	12807P	1	27.5823	33.3	10	13	
14 22 32.71	12813P	1	27.5823	33.3	10	13	
14 22 32.91	12819T	0	27.5823	33.3	10	13	



Table E8 - Telemetry Frames and Camera Parameters (Cont'd)

UMT	Telemetry Frame	Filter	Tracker Exp. Time (ms)	Plume Exp. Time (ms)	Tracker Gain Step	Plume Gain Step	Comments
14 22 33.11	12825T	0	27.5823	33.3	10	13	
14 22 33.31	12831T	0	27.5823	33.3	10	13	
14 22 33.51	12837T	0	27.5823	33.3	10	13	
14 22 33.71	12843T	0	27.5823	33.3	10	13	
14 22 33.92	12849T	0	27.5823	33.3	10	13	
14 22 34.11	12855T	0	27.5823	33.3	10	13	
14 22 34.31	12861T	0	27.5823	33.3	10	13	
14 22 34.51	12867P	1	27.5823	33.3	10	13	
14 22 34.72	12873P	1	27.5823	33.3	10	13	
14 22 34.92	12879T	0	10.8577	33.3	10	13	
14 22 35.12	12885T	0	10.8577	33.3	10	13	
14 22 35.32	12891T	0	10.8577	33.3	10	13	
14 22 35.52	12903T	0	10.8577	33.3	10	13	
14 22 35.92	12909T	0	10.8577	33.3	10	13	
14 22 36.12	12915T	0	10.8577	33.3	10	13	
14 22 36.32	12921T	0	10.8577	33.3	10	13	
14 22 36.52	12927P	1	10.8577	33.3	10	13	
14 22 36.72	12933P	1	10.8577	33.3	10	13	
14 22 36.92	12939T	0	10.8577	33.3	10	13	
14 22 37.12	12945T	0	10.8577	33.3	10	13	
14 22 37.32	12957T	0	10.8577	33.3	10	13	
14 22 37.72	12963T	0	10.8577	33.3	10	13	
14 22 37.92	12969T	0	10.8577	33.3	10	13	
14 22 38.12	12975T	0	10.8577	33.3	10	13	
14 22 38.32	12981T	0	10.8577	33.3	10	13	
14 22 38.52	12987P	1	10.8577	33.3	10	13	Star 27 plume enters plume camera FOV
14 22 38.92	12999T	0	10.8577	33.3	10	13	
14 22 39.12	13005T	0	8.6003	33.3	10	13	
14 22 39.32	13017T	0	8.6003	33.3	10	13	
14 22 39.95	13030T	0	8.6003	33.3	10	13	
14 22 39.99	13031T	0	8.6003	33.3	10	13	
14 22 40.02	13032P	1	8.6003	33.3	10	13	
14 22 40.05	13033P	1	8.6003	33.3	10	13	
14 22 40.09	13034T	0	8.6003	33.3	10	13	
14 22 40.12	13035T	0	8.6003	33.3	10	13	
14 22 40.15	13036T	0	8.6003	33.3	10	13	
14 22 40.19	13037T	0	8.6003	33.3	10	13	
14 22 40.22	13038T	0	8.6003	33.3	10	13	
14 22 40.25	13039T	0	8.6003	33.3	10	13	
14 22 40.29	13040T	0	8.6003	33.3	10	13	
14 22 40.32	13041T	0	8.6003	33.3	10	13	
14 22 40.35	13042P	1	8.6003	33.3	10	13	
14 22 40.39	13043P	1	8.6003	33.3	10	13	

Table E8 - Telemetry Frames and Camera Parameters (Cont'd)

UMI	Telemetry Frame	Filter	Tracker Exp. Time (ms)	Plume Exp. Time (ms)	Tracker Gain Step	Plume Gain Step	Comments
14 22 40.42	130441	0	8.6003	33.3	10	13	
14 22 40.43	130451	0	8.6003	33.3	10	13	
14 22 40.49	130461	0	8.6003	33.3	10	13	
14 22 40.52	130471	0	8.6003	33.3	10	13	
14 22 40.55	130481	0	8.6003	33.3	10	13	
14 22 40.59	130491	0	8.6003	33.3	10	13	
14 22 40.62	130501	0	8.6003	33.3	10	13	
14 22 40.65	130511	0	8.6003	33.3	10	13	
14 22 40.69	13052P	1	8.6003	33.3	10	13	
14 22 40.72	13053P	1	8.6003	33.3	10	13	
14 22 40.76	130541	0	8.6003	33.3	10	13	
14 22 40.79	130551	0	8.6003	33.3	10	13	
14 22 40.82	130561	0	8.6003	33.3	10	13	
14 22 40.86	130571	0	8.6003	33.3	10	13	
14 22 40.89	130581	0	8.6003	33.3	10	13	
14 22 40.92	130591	0	8.6003	33.3	10	13	
14 22 40.96	130601	0	8.6003	33.3	10	13	
14 22 40.99	130611	0	8.6003	33.3	10	13	
14 22 41.02	13062P	1	8.6003	33.3	10	13	
14 22 41.06	13063P	1	8.6003	33.3	10	13	
14 22 41.16	130661	0	8.6003	33.3	10	13	
14 22 41.19	130671	0	8.6003	33.3	10	13	
14 22 41.22	130681	0	8.6003	33.3	10	13	
14 22 41.26	130691	0	8.6003	33.3	10	13	
14 22 41.29	130701	0	8.6003	33.3	10	13	
14 22 41.32	130711	0	8.6003	33.3	10	13	
14 22 41.36	13072P	1	8.6003	33.3	10	13	
14 22 41.39	13073P	1	8.6003	33.3	10	13	
14 22 41.42	130741	0	8.6003	33.3	10	13	
14 22 41.46	130751	0	8.6003	33.3	10	13	
14 22 41.49	130761	0	8.6003	33.3	10	13	
14 22 41.52	130771	0	8.6003	33.3	10	13	
14 22 41.56	130781	0	8.6003	33.3	10	13	
14 22 41.59	130791	0	8.6003	33.3	10	13	
14 22 41.62	130801	0	8.6003	33.3	10	13	
14 22 41.66	130811	0	8.6003	33.3	10	13	
14 22 41.69	13082P	1	8.6003	33.3	10	13	
14 22 41.72	13083P	1	8.6003	33.3	10	13	
14 22 41.76	130841	0	8.6003	33.3	10	13	
14 22 41.79	130851	0	8.6003	33.3	10	13	
14 22 42.39	13103P	1	8.6003	33.3	10	13	
14 22 42.49	131061	0	8.6003	33.3	10	12	
14 22 42.52	131071	0	8.6003	33.3	10	12	

Table E8 - Telemetry Frames and Camera Parameters (Cont'd)

UMI	Telemetry Frame	Filter	Tracker Exp. Time (ms)	Plume Exp. Time (ms)	Tracker Gain Step	Plume Gain Step	Comments
14 22 42.56	13108T	0	8.6003	33.3	10	12	
14 22 42.59	13109T	0	8.6003	33.3	10	12	
14 22 42.62	13110T	0	8.6003	33.3	10	12	
14 22 42.66	13111T	0	8.6003	33.3	10	12	
14 22 42.69	13112P	1	8.6003	33.3	10	12	
14 22 42.72	13113P	1	8.6003	33.3	10	12	
14 22 42.79	13115T	0	8.6003	33.3	10	12	
14 22 42.82	13116T	0	8.6003	33.3	10	12	
14 22 42.86	13117T	0	8.6003	33.3	10	12	
14 22 42.89	13118T	0	8.5003	33.3	10	12	
14 22 42.92	13119T	0	8.6003	33.3	10	12	
14 22 42.96	13120T	0	8.6003	33.3	10	12	
14 22 42.99	13121T	0	8.6003	33.3	10	12	
14 22 43.02	13122P	1	8.6003	33.3	10	12	
14 22 43.06	13123P	1	8.6003	33.3	10	12	
14 22 43.09	13124T	0	8.6003	33.3	10	12	
14 22 43.12	13125T	0	8.6003	33.3	10	12	
14 22 43.16	13126T	0	8.6003	33.3	10	12	
14 22 43.19	13127T	0	8.6003	33.3	10	12	
14 22 43.22	13128T	0	8.6003	33.3	10	12	
14 22 43.26	13129T	0	8.6003	33.3	10	12	
14 22 43.29	13130T	0	8.6003	33.3	10	12	
14 22 43.32	13131T	0	8.6003	33.3	10	12	
14 22 43.36	13132P	1	8.6003	33.3	10	12	
14 22 43.39	13133P	1	8.6003	33.3	10	12	
14 22 43.42	13134T	0	8.6003	33.3	10	12	
14 22 43.46	13135T	0	8.6003	33.3	10	12	
14 22 43.49	13136T	0	8.6003	33.3	10	12	
14 22 43.52	13137T	0	8.6003	33.3	10	12	
14 22 43.56	13138T	0	8.6003	33.3	10	12	
14 22 43.59	13139T	0	8.6003	33.3	10	12	
14 22 43.63	13140T	0	8.6003	33.3	10	12	
14 22 43.69	13142P	1	8.6003	33.3	10	12	Begin data interval 5, PC-1
14 22 44.16	13156T	0	8.6003	33.3	10	12	
14 22 44.19	13157T	0	8.6003	33.3	10	12	
14 22 44.23	13158T	0	8.6003	33.3	10	12	
14 22 44.26	13159T	0	8.6003	33.3	10	12	
14 22 44.29	13160T	0	8.6003	33.3	10	12	
14 22 44.33	13161T	0	8.6003	33.3	10	12	
14 22 44.36	13162P	1	8.6003	33.3	10	12	
14 22 44.39	13163P	1	8.6003	33.3	10	12	
14 22 44.43	13164P	1	8.6003	33.3	10	12	
14 22 44.46	13165P	1	8.6003	33.3	10	12	

Table E8 - Telemetry Frames and Camera Parameters (Cont'd)

UMT	Telemetry Frame	Filter	Tracker Exp. Time (ms)	Frame Exp. Time (ms)	Tracker Gain Step	Frame Gain Step	Comments
14 22 44.49	13166P	1	8.6003	33.3	10	12	
14 22 44.53	13167P	1	8.6003	33.3	10	12	
14 22 44.93	13179P	1	8.6003	33.3	10	12	
14 22 44.96	13180T	0	8.6003	33.3	10	12	
14 22 44.99	13181T	0	8.6003	33.3	10	12	
14 22 45.03	13182P	1	8.6003	33.3	10	12	
14 22 45.06	13183P	1	8.6003	33.3	10	12	
14 22 45.09	13184P	1	8.6003	33.3	10	12	
14 22 45.13	13185P	1	8.6003	33.3	10	13	
14 22 45.16	13186P	1	8.6003	33.3	10	13	
14 22 45.19	13187P	1	8.6003	33.3	10	13	
14 22 45.23	13188P	1	8.6003	33.3	10	13	
14 22 45.26	13189P	1	8.6003	33.3	10	13	
14 22 45.29	13190T	0	8.6003	33.3	10	13	
14 22 45.33	13191T	0	8.6003	33.3	10	13	
14 22 45.36	13192P	1	8.6003	33.3	10	13	
14 22 45.39	13193P	1	8.6003	33.3	10	13	
14 22 45.43	13194P	1	8.6003	33.3	10	13	
14 22 45.46	13195P	1	8.6003	33.3	10	13	
14 22 45.49	13196P	1	8.6003	33.3	10	13	
14 22 45.53	13197P	1	8.6003	33.3	10	13	
14 22 45.56	13198P	1	8.6003	33.3	10	13	
14 22 45.59	13199P	1	8.6003	33.3	10	13	
14 22 45.63	13200T	0	8.6003	33.3	10	13	
14 22 45.66	13201T	0	8.6003	33.3	10	13	
14 22 45.69	13202P	1	8.6003	33.3	10	13	
14 22 45.73	13203P	1	8.6003	33.3	10	13	
14 22 45.76	13204P	1	8.6003	33.3	10	13	
14 22 45.79	13205P	1	8.6003	33.3	10	13	
14 22 45.83	13206P	1	8.6003	33.3	10	13	
14 22 45.86	13207P	1	8.6003	33.3	10	13	
14 22 45.89	13208P	1	8.6003	33.3	10	13	
14 22 45.93	13209P	1	8.6003	33.3	10	13	
14 22 45.96	13210T	0	8.6003	33.3	10	13	
14 22 45.99	13211T	0	8.6003	33.3	10	13	
14 22 46.03	13212P	1	8.6003	33.3	10	13	
14 22 46.06	13213P	1	8.6003	33.3	10	13	
14 22 46.09	13214P	1	8.6003	33.3	10	13	
14 22 46.13	13215P	1	8.6003	33.3	10	13	
14 22 46.16	13216P	1	8.6003	33.3	10	13	
14 22 46.19	13217P	1	8.6003	33.3	10	13	
14 22 46.23	13218P	1	8.6003	33.3	10	13	
14 22 46.26	13219P	1	8.6003	33.3	10	13	

Table E8 - Telemetry Frames and Camera Parameters (Cont'd)

UMT	Telemetry Frame	Filter	Tracker Exp. Time (ms)	Flame Exp. Time (ms)	Tracker Gain Step	Flame Gain Step	Comments
14 22 46.29	13220T	0	8.6003	33.3	10	13	
14 22 46.33	13221T	0	8.6003	33.3	10	13	
14 22 46.36	13222P	1	8.6003	33.3	10	13	
14 22 46.39	13223P	1	8.6003	33.3	10	13	
14 22 46.43	13224P	1	8.6003	33.3	10	13	
14 22 46.46	13225P	1	8.6003	33.3	10	13	
14 22 46.49	13226P	1	8.6003	33.3	10	13	
14 22 46.53	13227P	1	8.6003	33.3	10	13	
14 22 46.56	13228P	1	8.6003	33.3	10	13	
14 22 46.60	13229P	1	8.6003	33.3	10	13	
14 22 46.63	13230T	0	8.6003	33.3	10	13	
14 22 46.66	13231T	0	8.6003	33.3	10	13	
14 22 46.70	13232P	1	8.6003	33.3	10	13	
14 22 46.73	13233P	1	8.6003	33.3	10	13	
14 22 46.76	13234P	1	8.6003	33.3	10	13	
14 22 46.80	13235P	1	8.6003	33.3	10	13	
14 22 46.83	13236P	1	8.6003	33.3	10	13	
14 22 46.86	13237P	1	8.6003	33.3	10	13	
14 22 46.90	13238P	1	8.6003	33.3	10	13	
14 22 46.93	13239P	1	8.6003	33.3	10	13	End data interval 5, PC-1
14 22 46.96	13240T	0	8.6003	33.3	10	13	
14 22 47.00	13241T	0	8.6003	33.3	10	13	
14 22 47.03	13242P	1	8.6003	33.3	10	13	
14 22 47.06	13243P	1	8.6003	33.3	10	12	
14 22 47.10	13244P	1	8.6003	33.3	10	11	
14 22 47.13	13245P	1	8.6003	33.3	10	11	
14 22 47.16	13246P	1	8.6003	33.3	10	11	
14 22 47.20	13247P	1	8.6003	33.3	10	11	
14 22 47.23	13248P	1	8.6003	33.3	10	11	
14 22 47.26	13249P	1	8.6003	33.3	10	1	
14 22 47.30	13250T	0	8.6003	33.3	10	11	
14 22 47.33	13251T	0	8.6003	33.3	10	12	
14 22 47.36	13252P	1	8.6003	33.3	10	12	
14 22 47.40	13253P	1	8.6003	33.3	10	12	
14 22 47.43	13254P	1	8.6003	33.3	10	12	
14 22 47.46	13255P	1	8.6003	33.3	10	12	
14 22 47.50	13256P	1	8.6003	33.3	10	12	
14 22 47.53	13257P	1	8.6003	33.3	10	12	
14 22 47.56	13258P	1	8.6003	33.3	10	12	
14 22 47.60	13259P	1	8.6003	33.3	10	12	
14 22 47.66	13261T	0	8.6003	33.3	10	12	
14 22 47.70	13262P	1	8.6003	33.3	10	12	
14 22 47.73	13263P	1	8.6003	33.3	10	12	

Table E8 - Telemetry Frames and Camera Parameter. (Cont'd)

GMT	Telemetry Frame	Filter	Tracker Exp. Time (ms)	Flume Exp. Time (ms)	Tracker Gain Step	Flume Gain Step	Comments
14 22 47.76	13254P	1	8.6003	33.3	10	12	
14 22 47.86	13255P	1	8.6003	33.3	10	12	
14 22 47.83	13256P	1	8.6003	33.3	10	12	
14 22 47.90	13258P	1	8.6003	33.3	10	12	
14 22 48.00	13271T	0	8.6003	33.3	10	13	
14 22 48.13	13275P	1	8.6003	33.3	10	13	
14 22 48.20	13277P	1	8.6003	33.3	10	13	
14 22 48.23	13278P	1	8.6003	33.3	10	13	
14 22 48.26	13279P	1	8.6003	33.3	10	12	
14 22 48.30	13280T	0	8.6003	33.3	10	12	
14 22 48.33	13281T	0	8.6003	33.3	10	12	
14 22 48.36	13282P	1	8.6003	33.3	10	12	
14 22 48.40	13283P	1	8.6003	33.3	10	12	
14 22 48.43	13284P	1	8.6003	33.3	10	12	
14 22 48.46	13285P	1	8.6003	33.3	10	12	
14 22 48.50	13286P	1	8.6003	33.3	10	12	
14 22 48.53	13287P	1	8.6003	33.3	10	12	
14 22 48.56	13288P	1	8.6003	33.3	10	12	
14 22 48.60	13289P	1	8.6003	33.3	10	12	
14 22 48.63	13290T	0	8.6003	33.3	10	12	
14 22 48.66	13291T	0	8.6003	33.3	10	12	
14 22 48.70	13292P	1	8.6003	33.3	10	12	
14 22 48.73	13293P	1	8.6003	33.3	10	12	
14 22 48.76	13294P	1	8.6003	33.3	10	12	
14 22 48.80	13295P	1	8.6003	33.3	10	12	
14 22 48.83	13295P	1	8.6003	33.3	10	13	
14 22 48.86	13297P	1	8.6003	33.3	10	13	
14 22 48.96	13300T	0	8.6003	33.3	10	13	
14 22 49.00	13301T	0	8.6003	33.3	10	13	
14 22 49.10	13304P	1	8.6003	33.3	10	12	
14 22 49.13	13305P	1	8.6003	33.3	10	12	
14 22 49.16	13306P	1	8.6003	33.3	10	12	
14 22 49.20	13307P	1	8.6003	33.3	10	12	
14 22 49.23	13308P	1	8.6003	33.3	10	12	
14 22 49.26	13309P	1	8.6003	33.3	10	12	
14 22 49.30	13310T	0	8.6003	33.3	10	12	
14 22 49.33	13311T	0	8.6003	33.3	10	12	
14 22 49.36	13312P	1	8.6003	33.3	10	12	
14 22 49.40	13313P	1	8.6003	33.3	10	12	
14 22 49.43	13314P	1	8.6003	33.3	10	12	
14 22 49.46	13315P	1	8.6003	33.3	10	13	
14 22 49.50	13316P	1	8.6003	33.3	10	13	
14 22 49.53	13317P	1	8.6003	33.3	10	13	

Table E8 - Telemetry Frames and Camera Parameters (Cont'd)

DMT	Telemetry Frame	Filter	Tracker Exp. Time (ms)	Plume Exp. Time (ms)	Tracker Gain Step	Plume Gain Step	Comments
14 22 49.57	13318P	1	8.6003	33.3	10	13	
14 22 49.60	13319P	1	8.6003	33.3	10	13	
14 22 49.63	13320T	0	8.6003	33.3	10	13	
14 22 49.67	13321T	0	8.6003	33.3	10	13	
14 22 49.70	13322P	1	8.6003	33.3	10	13	
14 22 49.73	13323P	1	8.6003	33.3	10	13	
14 22 49.77	13324P	1	8.6003	33.3	10	13	
14 22 49.80	13325P	1	8.6003	33.3	10	13	
14 22 49.83	13326P	1	8.6003	33.3	10	13	
14 22 49.87	13327P	1	8.6003	33.3	10	13	
14 22 49.90	13328P	1	8.6003	33.3	10	13	
14 22 49.93	13329P	1	8.6003	33.3	10	13	
14 22 49.97	13330T	0	8.6003	33.3	10	13	
14 22 50.00	13331T	0	8.6003	33.3	10	13	
14 22 50.03	13332P	1	8.6003	33.3	10	13	
14 22 50.07	13333P	1	8.5003	33.3	10	13	
14 22 50.10	13334P	1	8.6003	33.3	10	13	
14 22 50.13	13335P	1	8.6003	33.3	10	13	
14 22 50.17	13336P	1	8.6003	33.3	10	13	
14 22 50.20	13337P	1	8.6003	33.3	10	13	
14 22 50.23	13338P	1	8.6003	33.3	10	13	
14 22 50.27	13339P	1	8.6003	33.3	10	13	
14 22 50.30	13340T	0	8.6003	33.3	10	13	
14 22 50.33	13341T	0	8.6003	33.3	10	13	
14 22 50.37	13342P	1	8.6003	33.3	10	13	
14 22 50.40	13343P	1	8.6003	33.3	10	13	
14 22 50.43	13344P	1	8.6003	33.3	10	13	
14 22 50.47	13345P	1	8.6003	33.3	10	13	
14 22 50.50	13346P	1	8.6003	33.3	10	13	
14 22 50.53	13347P	1	8.6003	33.3	10	13	
14 22 50.57	13348P	1	8.6003	33.3	10	13	
14 22 50.60	13349P	1	8.6003	33.3	10	13	
14 22 50.63	13350T	0	8.6003	33.3	10	13	
14 22 50.67	13351T	0	8.6003	33.3	10	13	
14 22 50.70	13352P	1	8.6003	33.3	10	13	
14 22 50.73	13353P	1	8.6003	33.3	10	13	
14 22 50.77	13354P	1	8.6003	33.3	10	12	
14 22 50.80	13355P	1	8.6003	33.3	10	12	
14 22 50.83	13356P	1	8.6003	33.3	10	12	
14 22 50.87	13357P	1	8.6003	33.3	10	12	
14 22 50.90	1335P	1	8.6003	33.3	10	12	
14 22 50.93	13359P	1	8.6003	33.3	10	12	
14 22 50.97	13360T	0	8.6003	33.3	10	12	

Table E8 - Telemetry Frames and Camera Parameters (Cont'd)

UMT	Telemetry Frame	Filter	Tracker Exp. Time (ms)	Plume Exp. Time (ms)	Tracker Gain Step	Plume Gain Step	Comments
14 22 51.00	13361T	0	8.6003	33.3	10	12	
14 22 51.03	13362P	1	8.6003	33.3	10	12	
14 22 51.07	13363P	1	8.6003	33.3	10	12	
14 22 51.10	13364P	1	8.6003	33.3	10	12	
14 22 51.13	13365P	1	8.6003	33.3	10	12	
14 22 51.17	13366P	1	8.6003	33.3	10	12	
14 22 51.20	13367P	1	8.6003	33.3	10	13	
14 22 51.23	13368P	1	8.6003	33.3	10	13	
14 22 51.27	13369P	1	8.6003	33.3	10	13	
14 22 51.30	13370T	0	8.6003	33.3	10	13	
14 22 51.33	13371T	0	8.6003	33.3	10	13	
14 22 51.37	13372P	1	8.6003	33.3	10	13	
14 22 52.94	13419P	1	8.6003	33.3	10	13	
14 22 52.97	13420T	0	8.6003	33.3	10	13	
14 22 53.00	13421T	0	8.6003	33.3	10	13	
14 22 53.04	13422P	1	8.6003	33.3	10	13	
14 22 53.07	13423P	1	8.6003	33.3	10	13	
14 22 53.10	13424P	1	8.6003	33.3	10	13	
14 22 53.14	13425P	1	8.6003	33.3	10	13	
14 22 53.17	13426P	1	8.6003	33.3	10	13	
14 22 53.20	13427P	1	8.6003	33.3	10	13	
14 22 53.24	13428P	1	8.6003	33.3	10	13	
14 22 53.27	13429P	1	8.6003	33.3	10	13	
14 22 53.30	13430T	0	8.6003	33.3	10	13	
14 22 53.34	13431T	0	8.6003	33.3	10	13	
14 22 53.37	13432P	1	8.6003	33.3	10	13	
14 22 53.40	13433P	1	8.6003	33.3	10	13	
14 22 53.44	13434P	1	8.6003	33.3	10	13	
14 22 53.47	13435P	1	8.6003	33.3	10	13	
14 22 53.50	13436P	1	8.6003	33.3	10	13	
14 22 53.54	13437P	1	8.6003	33.3	10	13	
14 22 53.57	13438P	1	8.6003	33.3	10	13	
14 22 53.60	13439P	1	8.6003	33.3	10	13	
14 22 53.64	13440T	0	8.6003	33.3	10	13	
14 22 53.67	13441T	0	8.6003	33.3	10	13	
14 22 53.70	13442P	1	8.6003	33.3	10	13	
14 22 53.74	13443P	1	8.6003	33.3	10	13	
14 22 53.77	13444P	1	8.6003	33.3	10	13	
14 22 53.80	13445P	1	8.6003	33.3	10	13	
14 22 53.84	13446P	1	8.6003	33.3	10	13	
14 22 53.87	13447P	1	8.6003	33.3	10	13	
14 22 53.90	13448P	1	8.6003	33.3	10	13	
14 22 53.94	13449P	1	8.6003	33.3	10	12	



Table E8 - Telemetry Frames and Camera Parameters (Cont'd)

UMT	Telemetry Frame	Filter	Tracker Exp. Time (ms)	Plume Exp. Time (ms)	Tracker Gain Step	Plume Gain Step	Comments
14 22 53.97	13450T	0	8.6003	33.3	10	12	
14 22 54.00	13451T	0	8.6003	33.3	10	12	
14 22 54.04	13452P	1	8.6003	33.3	10	12	
14 22 54.07	13453P	1	8.6003	33.3	10	12	
14 22 54.16	13454P	1	8.6003	33.3	10	12	
14 22 54.14	13455P	1	8.6003	33.3	10	12	
14 22 54.17	13456P	1	8.6003	33.3	10	12	
14 22 54.20	13457P	1	8.6003	35.5	10	12	
14 22 54.24	13458P	1	8.6003	33.3	10	12	
14 22 54.27	13459P	1	8.6003	33.3	10	13	
14 22 54.30	13460T	0	8.6003	33.3	10	13	
14 22 54.34	13461T	0	8.6003	33.3	10	13	
14 22 54.37	13462P	2	8.6003	33.3	10	13	
14 22 54.40	13463P	2	8.6003	33.3	10	13	
14 22 54.44	13464P	2	8.6003	33.3	10	13	
14 22 54.47	13465P	2	8.6003	33.3	10	13	
14 22 54.50	13466P	2	8.6003	33.3	10	13	
14 22 54.54	13467P	2	8.6003	33.3	10	13	
14 22 54.57	13468P	2	8.6003	33.3	10	13	
14 22 54.60	13469P	2	8.6003	33.3	10	13	
14 22 54.64	13470T	0	8.6003	33.3	10	13	
14 22 54.67	13471T	0	8.6003	33.3	10	13	
14 22 54.70	13472P	2	8.6003	33.3	10	13	
14 22 54.74	13473P	2	8.6003	33.3	10	13	
14 22 54.77	13474P	2	8.6003	33.3	10	13	
14 22 54.80	13475P	2	8.6003	33.3	10	13	
14 22 54.84	13476P	2	8.6003	33.3	10	13	
14 22 54.87	13477P	2	8.6003	33.3	10	13	
14 22 54.90	13478P	2	8.6003	33.3	10	13	
14 22 54.94	13479P	2	8.6003	33.3	10	13	
14 22 54.97	13480T	0	8.6003	33.3	10	13	
14 22 55.00	13481T	0	8.6003	33.3	10	13	
14 22 55.04	13482P	2	8.6003	33.3	10	13	
14 22 55.07	13483P	2	8.6003	33.3	10	13	
14 22 55.10	13484P	2	8.6003	33.3	10	13	
14 22 55.14	13485P	2	8.6003	33.3	10	13	
14 22 55.17	13486P	2	8.6003	33.3	10	13	
14 22 55.20	13487P	2	8.6003	33.3	10	13	
14 22 55.24	13488P	2	8.6003	33.3	10	13	
14 22 55.27	13489P	2	8.6003	35.3	10	13	begin data interval 6, PC-2
14 22 55.30	13490T	0	8.6003	33.3	10	13	
14 22 55.34	13491T	0	8.6003	33.3	10	13	
14 22 55.37	13492P	2	8.6003	33.3	10	13	

Table E8 - Telemetry Frames and Camera Parameters (Cont'd)

UMI	Telemetry Frame	Filter	Tracker Exp. Time (ms)	Plume Exp. Time (ms)	Tracker Gain Step	Plume Gain Step	Comments
14 22 55.41	13493P	2	8.6003	33.3	10	13	
14 22 55.44	13494P	2	8.6003	33.3	10	13	
14 22 55.47	13495P	2	8.6003	33.3	10	13	
14 22 55.51	13496P	2	8.6003	33.3	10	13	
14 22 55.54	13497P	2	8.6003	33.3	10	13	
14 22 55.57	13498P	2	8.6003	33.3	10	13	
14 22 55.61	13499P	2	8.6003	33.3	10	13	
14 22 55.64	13500T	0	8.6003	33.3	10	13	
14 22 55.67	13501T	0	8.6003	33.3	10	13	
14 22 55.71	13502P	2	8.6003	33.3	10	13	
14 22 55.74	13503P	2	8.6003	33.3	10	13	
14 22 55.77	13504P	2	8.6003	33.3	10	13	
14 22 55.81	13505P	2	8.6003	33.3	10	13	
14 22 55.84	13506P	2	8.6003	33.3	10	13	
14 22 55.87	13507P	2	8.6003	33.3	10	13	
14 22 55.91	13508P	2	8.6003	33.3	10	13	
14 22 55.94	13509P	2	8.6003	33.3	10	13	
14 22 55.97	13510T	0	8.6003	33.3	10	13	
14 22 56.01	13511T	0	8.6003	33.3	10	13	
14 22 56.04	13512P	2	8.6003	33.3	10	13	
14 22 56.07	13513P	2	8.6003	33.3	10	13	
14 22 56.11	13514P	2	8.6003	33.3	10	13	
14 22 56.14	13515P	2	8.6003	33.3	10	13	
14 22 56.17	13516P	2	8.6003	33.3	10	13	
14 22 56.21	13517P	2	8.6003	33.3	10	13	
14 22 56.24	13518P	2	8.6003	33.3	10	13	
14 22 56.27	13519P	2	8.6003	33.3	10	13	
14 22 56.31	13520T	0	8.6003	33.3	10	13	
14 22 56.34	13521T	0	8.6003	33.3	10	13	
14 22 56.37	13522P	2	8.6003	33.3	10	13	
14 22 56.41	13523P	2	8.6003	33.3	10	13	
14 22 56.44	13524P	2	8.6003	33.3	10	13	
14 22 56.47	13525P	2	8.6003	33.3	10	13	
14 22 56.51	13526P	2	8.6003	33.3	10	13	
14 22 56.54	13527P	2	8.6003	33.3	10	13	
14 22 56.57	13528P	2	8.6003	33.3	10	13	
14 22 56.61	13529P	2	8.6003	33.3	10	13	
14 22 56.64	13530T	0	8.6003	33.3	10	13	
14 22 56.67	13531T	0	8.6003	33.3	10	13	
14 22 56.71	13532P	2	8.6003	33.3	10	13	
14 22 56.74	13533P	2	8.6003	33.3	10	13	
14 22 56.77	13534P	2	8.6003	33.3	10	13	
14 22 56.81	13535P	2	8.6003	33.3	10	13	

Table E8 - Telemetry Frames and Camera Parameters (Cont'd)

DMT	Telemetry Frame	Filter	Tracker Exp. Time (ms)	Plume Exp. Time (ms)	Tracker Gain Step	Plume Gain Step	Comments
14 22 56.84	13536P	2	8.6003	33.3	10	13	
14 22 56.87	13537P	2	8.6003	33.3	10	13	
14 22 56.91	13538P	2	8.6003	33.3	10	13	
14 22 56.94	13539P	2	8.6003	33.3	10	13	
14 22 56.97	13540T	0	8.6003	33.3	10	13	
14 22 57.01	13541T	0	8.6003	33.3	10	13	
14 22 57.04	13542P	2	8.6003	33.3	10	13	
14 22 57.07	13543P	2	8.6003	33.3	10	13	
14 22 57.11	13544P	2	8.6003	33.3	10	13	
14 22 57.14	13545P	2	8.6003	33.3	10	13	
14 22 57.17	13546P	2	8.6003	33.3	10	13	
14 22 57.21	13547P	2	8.6003	33.3	10	13	
14 22 57.24	13548P	2	8.6003	33.3	10	13	
14 22 57.27	13549P	2	8.6003	33.3	10	13	
14 22 57.31	13550T	0	8.6003	33.3	10	13	
14 22 57.34	13551T	0	8.6003	33.3	10	13	
14 22 57.37	13552P	2	8.6003	33.3	10	13	
14 22 57.41	13553P	2	8.6003	33.3	10	13	
14 22 57.44	13554P	2	8.6003	33.3	10	13	
14 22 57.47	13555P	2	8.6003	33.3	10	13	
14 22 57.51	13556P	2	8.6003	33.3	10	13	
14 22 57.54	13557P	2	8.6003	33.3	10	13	
14 22 57.57	13558P	2	8.6003	33.3	10	13	
14 22 57.61	13559P	2	8.6003	33.3	10	13	
14 22 57.64	13560T	0	8.6003	33.3	10	13	
14 22 57.67	13561T	0	8.6003	33.3	10	13	
14 22 57.71	13562P	2	8.6003	33.3	10	13	
14 22 57.74	13563P	2	8.6003	33.3	10	13	
14 22 57.77	13564P	2	8.6003	33.3	10	13	
14 22 57.81	13565P	2	8.6003	33.3	10	13	
14 22 57.84	13566P	2	8.6003	33.3	10	13	
14 22 57.87	13567P	2	8.6003	33.3	10	13	
14 22 57.91	13568P	2	8.6003	33.3	10	13	
14 22 57.94	13569P	2	8.6003	33.3	10	13	
14 22 57.97	13570T	0	8.6003	33.3	10	13	
14 22 58.01	13571T	0	8.6003	33.3	10	13	
14 22 58.04	13572P	2	8.6003	33.3	10	13	
14 22 58.07	13573P	2	8.6003	33.3	10	13	
14 22 58.11	13574P	2	8.6003	33.3	10	13	
14 22 58.14	13575P	2	8.6003	33.3	10	13	
14 22 58.17	13576P	2	8.6003	33.3	10	13	
14 22 58.21	13577P	2	8.6003	33.3	10	13	
14 22 58.24	13578P	2	8.6003	33.3	10	13	

Table E8 - Telemetry Frames and Camera Parameters (Cont'd)

UMI	Telemetry Frame	Filter	Tracker Exp. Time (ms)	Flume Exp. Time (ms)	Tracker Gain Step	Flume Gain Step	Comments
14 22 58.28	13579P	2	8.6003	33.3	10	13	
14 22 58.31	13580P	0	8.6003	33.3	10	13	
14 22 58.34	13581P	0	8.6003	33.3	10	13	
14 22 58.38	13582P	2	8.6003	33.3	10	13	
14 22 58.41	13583P	2	8.6003	33.3	10	13	
14 22 58.44	13584P	2	8.6003	33.3	10	13	
14 22 58.48	13585P	2	8.6003	33.3	10	13	
14 22 58.51	13586P	2	8.6003	33.3	10	13	
14 22 58.54	13587P	2	8.6003	33.3	10	13	
14 22 58.58	13588P	2	8.6003	33.3	10	13	
14 22 58.61	13589P	2	8.6003	33.3	10	13	
14 22 58.64	13590P	0	8.6003	33.3	10	13	
14 22 58.68	13591P	0	8.6003	33.3	10	13	
14 22 58.71	13592P	2	8.6003	33.3	10	13	
14 22 58.74	13593P	2	8.6003	33.3	10	13	
14 22 58.78	13594P	2	8.6003	33.3	10	13	
14 22 58.81	13595P	2	8.6003	33.3	10	13	
14 22 58.84	13596P	2	8.6003	33.3	10	13	
14 22 58.88	13597P	2	8.6003	33.3	10	13	
14 22 58.91	13598P	2	8.6003	33.3	10	13	
14 22 58.94	13599P	2	8.6003	33.3	10	13	End data interval 0, PC-2
14 22 58.98	13600P	0	8.6003	33.3	10	13	
14 23 0.58	13648P	3	8.6003	33.3	10	13	
14 23 0.61	13649P	3	8.6003	33.3	10	13	
14 23 0.64	13650P	0	8.6003	33.3	10	13	
14 23 0.68	13651P	0	8.6003	33.3	10	13	
14 23 0.71	13652P	3	8.6003	33.3	10	13	
14 23 0.74	13653P	3	8.6003	33.3	10	13	
14 23 0.78	13654P	3	8.6003	33.3	10	13	
14 23 0.81	13655P	3	8.6003	33.3	10	13	
14 23 0.84	13656P	3	8.6003	33.3	10	13	
14 23 0.88	13657P	3	8.6003	33.3	10	13	
14 23 0.91	13658P	3	8.6003	33.3	10	13	
14 23 0.94	13659P	3	8.6003	33.3	10	13	
14 23 0.98	13660P	0	8.6003	33.3	10	13	
14 23 1.01	13661P	0	8.6003	33.3	10	13	
14 23 1.04	13662P	3	8.6003	33.3	10	13	
14 23 1.08	13663P	3	8.6003	33.3	10	13	
14 23 1.11	13664P	3	8.6003	33.3	10	13	
14 23 1.14	13665P	3	8.6003	33.3	10	13	
14 23 1.18	13666P	3	8.6003	33.3	10	13	
14 23 1.21	13667P	3	8.6003	33.3	10	13	
14 23 1.24	13668P	3	8.6003	33.3	10	13	

Table E8 - Telemetry Frames and Camera Parameters (Cont'd)

UMT	Telemetry Frame	Filter	Tracker Exp. Time (ms)	Plume Exp. Time (ms)	Tracker Gain Step	Plume Gain Step	Comments
14 23 1.28	13669P	3	8.6003	33.3	10	13	
14 23 1.31	13670T	0	8.6003	33.3	10	13	
14 23 1.35	13671T	0	8.6003	33.3	10	13	
14 23 1.38	13672P	3	8.6003	33.3	10	13	
14 23 1.41	13673P	3	8.6003	33.3	10	13	
14 23 1.45	13674P	3	8.6003	33.3	10	13	
14 23 1.48	13675P	3	8.6003	33.3	10	13	
14 23 1.51	13676P	3	8.6003	33.3	10	13	
14 23 1.55	13677P	3	8.6003	33.3	10	13	
14 23 1.58	13678P	3	8.6003	33.3	10	13	Begin data interval 7, PC-3
14 23 1.61	13679P	3	8.6003	33.3	10	13	
14 23 1.65	13680T	0	8.6003	33.3	10	13	
14 23 1.68	13681T	0	8.6003	33.3	10	13	
14 23 1.71	13682P	3	8.6003	33.3	10	13	
14 23 1.75	13683P	3	8.6003	33.3	10	13	
14 23 1.78	13684P	3	8.6003	33.3	10	13	
14 23 1.81	13685P	3	8.6003	33.3	10	13	
14 23 1.85	13686P	3	8.6003	33.3	10	13	
14 23 1.88	13687P	3	8.6003	33.3	10	13	
14 23 1.91	13688P	3	8.6003	33.3	10	13	
14 23 1.95	13689P	3	8.6003	33.3	10	13	
14 23 1.98	13690T	0	8.6003	33.3	10	13	
14 23 2.01	13691T	0	8.6003	33.3	10	13	
14 23 2.05	13692P	3	8.6003	33.3	10	13	
14 23 2.08	13693P	3	8.6003	33.3	10	13	
14 23 2.11	13694P	3	8.6003	33.3	10	13	
14 23 2.15	13695P	3	8.6003	33.3	10	13	
14 23 2.18	13696P	3	8.6003	33.3	10	13	
14 23 2.21	13697P	3	8.6003	33.3	10	13	
14 23 2.25	13698P	3	8.6003	33.3	10	13	
14 23 2.28	13699P	3	8.6003	33.3	10	13	
14 23 2.31	13700T	0	8.6003	33.3	10	13	
14 23 2.35	13701T	0	8.6003	33.3	10	13	
14 23 2.38	13702P	3	8.6003	33.3	10	13	
14 23 2.41	13703P	3	8.6003	33.3	10	13	
14 23 2.45	13704P	3	8.6003	33.3	10	13	
14 23 2.48	13705P	3	8.6003	33.3	10	13	
14 23 2.51	13706P	3	8.6003	33.3	10	13	
14 23 2.55	13707P	3	8.6003	33.3	10	13	
14 23 2.58	13708P	3	8.6003	33.3	10	13	
14 23 2.61	13709P	3	8.6003	33.3	10	13	
14 23 2.65	13710T	0	8.6003	33.3	10	13	
14 23 2.68	13711T	0	8.6003	33.3	10	13	

Table E8 - Telemetry Frames and Camera Parameters (Cont'd)

UMT	Telemetry Frame	Filter	Tracker Exp. Time (ms)	Plur. Exp. Time (ms)	Tracker Gain Step	Plume Gain Step	Comments
14 23 2.71	13712P	3	8.6003	33.3	10	13	
14 23 2.75	13713P	3	8.6003	33.3	10	13	
14 23 2.78	13714P	3	8.6003	33.3	10	13	
14 23 2.81	13715P	3	8.6003	33.3	10	13	
14 23 2.85	13716P	3	8.6003	33.3	10	13	
14 23 2.88	13717P	3	8.6003	33.3	10	13	
14 23 2.91	13718P	3	8.6003	33.3	10	13	
14 23 2.95	13719P	3	8.6003	33.3	10	13	
14 23 2.98	13720T	0	8.6003	33.3	10	13	
14 23 3.01	13721T	0	8.6003	33.3	10	13	
14 23 3.05	13722P	3	8.6003	33.3	10	13	
14 23 3.08	13723P	3	8.6003	33.3	10	13	
14 23 3.11	13724P	3	8.6003	33.3	10	13	
14 23 3.15	13725P	3	8.6003	33.3	10	13	
14 23 3.18	13726P	3	8.6003	33.3	10	13	
14 23 3.21	13727P	3	8.6003	33.3	10	13	
14 23 3.25	13728P	3	8.6003	33.3	10	13	
14 23 3.28	13729P	3	8.6003	33.3	10	13	
14 23 3.31	13730T	0	8.6003	33.3	10	13	
14 23 3.35	13731T	0	8.6003	33.3	10	13	
14 23 3.38	13732P	3	8.6003	33.3	10	13	
14 23 3.41	13733P	3	8.6003	33.3	10	13	
14 23 3.45	13734P	3	8.6003	33.3	10	13	
14 23 3.48	13735P	3	8.6003	33.3	10	13	
14 23 3.51	13736P	3	8.6003	33.3	10	12	
14 23 3.55	13737P	3	8.6003	33.3	10	13	
14 23 3.58	13738P	3	8.6003	33.3	10	13	
14 23 3.61	13739P	3	8.6003	33.3	10	13	
14 23 3.65	13740T	0	8.6003	33.3	10	13	
14 23 3.68	13741T	0	8.6003	33.3	10	13	
14 23 3.71	13742P	3	8.6003	33.3	10	13	
14 23 3.75	13743P	3	8.6003	33.3	10	13	
14 23 3.78	13744P	3	8.6003	33.3	10	13	
14 23 3.81	13745P	3	8.6003	33.3	10	13	
14 23 3.85	13746P	3	8.6003	33.3	10	13	
14 23 3.88	13747P	3	8.6003	33.3	10	13	
14 23 3.91	13748P	3	8.6003	33.3	10	13	
14 23 3.95	13749P	3	8.6003	33.3	10	13	
14 23 3.98	13750T	0	8.6003	33.3	10	13	
14 23 4.01	13751T	0	8.6003	33.3	10	13	
14 23 4.05	13752P	3	8.6003	33.3	10	13	
14 23 4.08	13753P	3	8.6003	33.3	10	13	
14 23 4.11	13754P	3	8.6003	33.3	10	13	

Table E8 - Telemetry Frames and Camera Parameters (Cont'd)

UNIT	Telemetry Frame	Filter	Tracker Exp. Time (ms)	Flame Exp. Time (ms)	Tracker Gain Step	Flame Gain Step	Comments
14 23 4.15	13755P	3	8.6003	33.3	10	13	
14 23 4.18	13756P	3	8.6003	33.3	10	13	
14 23 4.22	13757P	3	8.6003	33.3	10	13	
14 23 4.25	13758P	3	8.6003	33.3	10	13	
14 23 4.28	13759P	3	8.6003	33.3	10	12	
14 23 4.32	13760I	0	8.6003	33.3	10	12	
14 23 4.35	13761I	0	8.6003	33.3	10	12	
14 23 4.38	13762P	3	8.6003	33.3	10	12	
14 23 4.42	13763P	3	8.6003	33.3	10	12	
14 23 4.45	13764P	3	8.6003	33.3	10	12	
14 23 4.48	13765P	3	8.6003	33.3	10	12	
14 23 4.52	13766P	3	8.6003	33.3	10	13	
14 23 4.55	13767P	3	8.6003	33.3	10	13	
14 23 4.58	13768P	3	8.6003	33.3	10	13	
14 23 4.62	13769P	3	8.6003	33.3	10	13	
14 23 4.65	13770I	0	8.6003	33.3	10	13	
14 23 4.68	13771I	0	8.6003	33.3	10	13	
14 23 4.72	13772P	3	8.6003	33.3	10	13	
14 23 4.75	13773P	3	8.6003	33.3	10	13	
14 23 4.78	13774P	3	8.6003	33.3	10	13	
14 23 4.82	13775P	3	8.6003	33.3	10	13	
14 23 4.85	13776P	3	8.6003	33.3	10	13	
14 23 4.88	13777P	3	8.6003	33.3	10	13	
14 23 4.92	13778P	3	8.6003	33.3	10	13	
14 23 4.95	13779P	3	8.6003	33.3	10	13	
14 23 4.98	13780I	0	8.6003	33.3	10	13	
14 23 5.02	13781I	0	8.6003	33.3	10	13	
14 23 5.05	13782P	3	8.6003	33.3	10	13	
14 23 5.08	13783P	3	8.6003	33.3	10	13	
14 23 5.12	13784P	3	8.6003	33.3	10	13	
14 23 5.15	13785P	3	8.6003	33.3	10	13	
14 23 5.18	13786P	3	8.6003	33.3	10	13	
14 23 5.22	13787P	3	8.6003	33.3	10	13	
14 23 5.25	13788P	3	8.6003	33.3	10	13	
14 23 5.28	13789P	3	8.6003	33.3	10	13	
14 23 5.32	13790I	0	8.6003	33.3	10	13	
14 23 5.35	13791I	0	8.6003	33.3	10	13	
14 23 5.38	13792P	3	8.6003	33.3	10	13	
14 23 5.42	13793P	3	8.6003	33.3	10	13	
14 23 5.45	13794P	3	8.6003	33.3	10	13	
14 23 5.48	13795P	3	8.6003	33.3	10	13	
14 23 5.52	13796P	3	8.6003	33.3	10	13	
14 23 5.55	13797P	3	8.6003	33.3	10	13	

Table E8 - Telemetry Frames and Camera Parameters (Cont'd)

UMI	Telemetry Frame	Filter	Tracker Exp. Time (ms)	Plume Exp. Time (ms)	Tracker Gain Step	Plume Gain Step	Comments
14 23 5.38	13798P	3	8.6003	33.3	10	13	
14 23 5.62	13799P	3	8.6003	33.3	10	13	
14 23 5.65	13800T	0	8.6003	33.3	10	13	
14 23 5.68	13801T	0	8.6003	33.3	10	13	
14 23 5.72	13802P	3	8.6003	33.3	10	13	
14 23 5.75	13803P	3	8.6003	33.3	10	13	
14 23 5.78	13804P	3	8.6003	33.3	10	13	
14 23 5.82	13805P	3	8.6003	33.3	10	13	
14 23 5.85	13806P	3	8.6003	33.3	10	13	
14 23 5.88	13807P	3	8.6003	33.3	10	13	
14 23 5.92	13808P	3	8.6003	33.3	10	13	
14 23 5.95	13809P	3	8.6003	33.3	10	13	
14 23 5.98	13810T	0	8.6003	33.3	10	13	
14 23 6.02	13811T	0	8.6003	33.3	10	13	
14 23 6.05	13812P	3	8.6003	33.3	10	13	
14 23 6.08	13813P	3	8.6003	33.3	10	13	
14 23 6.12	13814P	3	8.6003	33.3	10	13	
14 23 6.15	13815P	3	8.6003	33.3	10	13	
14 23 6.18	13816P	3	8.6003	33.3	10	13	
14 23 6.22	13817P	3	8.6003	33.3	10	13	
14 23 6.25	13818P	3	8.6003	33.3	10	13	
14 23 6.28	13819P	3	8.6003	33.3	10	13	
14 23 6.32	13820T	0	8.6003	33.3	10	13	
14 23 6.35	13821T	0	8.6003	33.3	10	13	
14 23 6.38	13822P	3	8.6003	33.3	10	13	
14 23 6.42	13823P	3	8.6003	33.3	10	13	
14 23 6.45	13824P	3	8.6003	33.3	10	13	
14 23 6.48	13825P	3	8.6003	33.3	10	13	
14 23 6.52	13826P	3	8.6003	33.3	10	13	
14 23 6.55	13827P	3	8.6003	33.3	10	13	
14 23 6.58	13828P	3	8.6003	33.3	10	13	
14 23 6.62	13829P	3	8.6003	33.3	10	13	
14 23 6.65	13830T	0	8.6003	33.3	10	13	
14 23 6.68	13831T	0	8.6003	33.3	10	13	
14 23 6.72	13832P	3	8.6003	33.3	10	13	
14 23 6.75	13833P	3	8.6003	33.3	10	13	
14 23 6.78	13834P	3	8.6003	33.3	10	13	
14 23 6.82	13835P	3	8.6003	33.3	10	13	
14 23 6.85	13836P	3	8.6003	33.3	10	13	
14 23 6.88	13837P	3	8.6003	33.3	10	13	
14 23 6.92	13838P	3	8.6003	33.3	10	13	
14 23 6.95	13839P	3	8.6003	33.3	10	13	
14 23 6.98	13840T	0	8.6003	33.3	10	13	



Table E8 - Telemetry Frames and Camera Parameters (Cont'd)

OMT	Telemetry Frame	Filter	Tracker Exp. Time (ms)	Plane Exp. Time (ms)	Tracker Gain Step	Plane Gain Step	Comments
14 23 7.02	13841T	0	8.6003	33.3	10	13	
14 23 7.05	13842P	3	8.6003	33.3	10	13	
14 23 7.09	13843P	3	8.6003	33.3	10	13	
14 23 7.12	13844P	3	8.6003	33.3	10	13	
14 23 7.15	13845P	3	8.6003	33.3	10	13	
14 23 7.19	13846P	3	8.6003	33.3	10	13	
14 23 7.22	13847P	3	8.6003	33.3	10	13	
14 23 7.25	13848P	3	8.6003	33.3	10	13	
14 23 7.29	13849P	3	8.6003	33.3	10	13	
14 23 7.32	13850T	0	8.6003	33.3	10	13	
14 23 7.35	13851T	0	8.6003	33.3	10	13	
14 23 7.39	13852P	3	8.6003	33.3	10	13	
14 23 7.42	13853P	3	8.6003	33.3	10	13	
14 23 7.45	13854P	3	8.6003	33.3	10	13	
14 23 7.49	13855P	3	8.6003	33.3	10	13	
14 23 7.52	13856P	3	8.6003	33.3	10	13	
14 23 7.55	13857P	3	8.6003	33.3	10	13	
14 23 7.59	13858P	3	8.6003	33.3	10	13	
14 23 7.62	13859P	3	8.6003	33.3	10	13	
14 23 7.65	13860T	0	8.6003	33.3	10	13	
14 23 7.69	13861T	0	8.6003	33.3	10	13	
14 23 7.72	13862P	3	8.6003	33.3	10	13	
14 23 7.75	13863P	3	8.6003	33.3	10	13	
14 23 7.79	13864P	3	8.6003	33.3	10	13	
14 23 7.82	13865P	3	8.6003	33.3	10	13	
14 23 7.85	13866P	3	8.6003	33.3	10	13	
14 23 7.89	13867P	3	8.6003	33.3	10	13	
14 23 7.92	13868P	3	8.6003	33.3	10	13	
14 23 7.95	13869P	3	8.6003	33.3	10	13	
14 23 7.99	13870T	0	8.6003	33.3	10	13	
14 23 8.02	13871T	0	8.6003	33.3	10	13	
14 23 8.05	13872P	3	8.6003	33.3	10	13	
14 23 8.09	13873P	3	8.6003	33.3	10	13	
14 23 8.12	13874P	3	8.6003	33.3	10	13	
14 23 8.15	13875P	3	8.6003	33.3	10	13	
14 23 8.19	13876P	3	8.6003	33.3	10	13	
14 23 8.22	13877P	3	8.6003	33.3	10	13	
14 23 8.25	13878P	3	8.6003	33.3	10	13	
14 23 8.29	13879P	3	8.6003	33.3	10	13	
14 23 8.32	13880T	0	8.6003	33.3	10	13	
14 23 8.35	13881T	0	8.6003	33.3	10	13	
14 23 8.39	13882P	3	8.6003	33.3	10	13	
14 23 8.42	13883P	3	8.6003	33.3	10	13	

Table E8 - Telemetry Frames and Camera Parameters (Cont'd)

UMT	Telemetry Frame	Filter	Tracker Exp. Time (ms)	Frame Exp. Time (ms)	Tracker Gain Step	Frame Gain Step	Comments
14 23 8.45	13884P	3	8.6003	33.3	10	13	
14 23 8.49	13885P	3	8.6003	33.3	10	13	
14 23 8.52	13886P	3	8.6003	33.3	10	13	
14 23 8.55	13887P	3	8.6003	33.3	10	13	
14 23 8.59	13888P	3	8.6003	33.3	10	13	
14 23 8.62	13889P	3	8.6003	33.3	10	13	
14 23 8.65	13890T	0	8.6003	33.3	10	13	
14 23 8.69	13891T	0	8.6003	33.3	10	13	
14 23 8.72	13892P	3	8.6003	33.3	10	13	
14 23 8.75	13893P	3	8.6003	33.3	10	13	
14 23 8.79	13894P	3	8.6003	33.3	10	13	
14 23 8.82	13895P	3	8.6003	33.3	10	13	
14 23 8.85	13896P	3	8.6003	33.3	10	13	
14 23 8.89	13897P	3	8.6003	33.3	10	13	
14 23 8.92	13898P	3	8.6003	33.3	10	13	
14 23 8.95	13899P	3	8.6003	33.3	10	13	
14 23 8.99	13900T	0	8.6003	33.3	10	13	
14 23 9.02	13901T	0	8.6003	33.3	10	13	
14 23 9.05	13902P	3	8.6003	33.3	10	13	
14 23 9.09	13903P	3	8.6003	33.3	10	13	
14 23 9.12	13904P	3	8.6003	33.3	10	13	
14 23 9.15	13905P	3	8.6003	33.3	10	13	
14 23 9.19	13906P	3	8.6003	33.3	10	13	
14 23 9.22	13907P	3	8.6003	33.3	10	13	
14 23 9.25	13908P	3	8.6003	33.3	10	13	
14 23 9.29	13909P	3	8.6003	33.3	10	13	
14 23 9.32	13910T	0	8.6003	33.3	10	13	
14 23 9.35	13911T	0	8.6003	33.3	10	13	
14 23 9.39	13912P	3	8.6003	33.3	10	13	
14 23 9.42	13913P	3	8.6003	33.3	10	13	
14 23 9.45	13914P	3	8.6003	33.3	10	13	
14 23 9.49	13915P	3	8.6003	33.3	10	13	
14 23 9.52	13916P	3	8.6003	33.3	10	13	
14 23 9.55	13917P	3	8.6003	33.3	10	13	
14 23 9.59	13918P	3	8.6003	33.3	10	13	
14 23 9.62	13919P	3	8.6003	33.3	10	13	
14 23 9.65	13920T	0	8.6003	33.3	10	13	
14 23 9.69	13921T	0	8.6003	33.3	10	13	
14 23 9.72	13922P	3	8.6003	33.3	10	13	
14 23 9.75	13923P	3	8.6003	33.3	10	13	
14 23 9.79	13924P	3	8.6003	33.3	10	13	
14 23 9.82	13925P	3	8.6003	33.3	10	13	
14 23 9.85	13926P	3	8.6003	33.3	10	13	

Table E8 - Telemetry Frames and Camera Parameters (Cont'd)

UMI	Telemetry Frame	Filter	Tracker Exp. Time (ms)	Plane Exp. Time (ms)	Tracker Gain Step	Plane Gain Step	Comments
14 23 9.89	13927P	3	8.6003	33.3	10	13	
14 23 9.92	13928P	3	8.6003	33.3	10	13	End data interval 7, PC-3
14 23 9.95	13929P	3	8.6003	33.3	10	13	
14 23 9.99	13930T	0	8.6003	33.3	10	12	
14 23 10.02	13931T	0	8.6003	33.3	10	12	
14 23 10.05	13932P	3	8.6003	33.3	10	12	
14 23 10.09	13933P	3	8.6003	33.3	10	12	
14 23 10.12	13934P	3	8.6003	33.3	10	12	
14 23 10.16	13935P	3	8.6003	33.3	10	12	
14 23 10.19	13936P	3	8.6003	33.3	10	12	
14 23 10.22	13937P	3	8.6003	33.3	10	12	
14 23 10.26	13938P	3	8.6003	33.3	10	12	
14 23 10.29	13939P	3	8.6003	33.3	10	13	
14 23 10.32	13940T	0	8.6003	33.3	10	13	
14 23 10.36	13941T	0	8.6003	33.3	10	13	
14 23 10.39	13942P	3	8.6003	33.3	10	13	
14 23 10.42	13943P	3	8.6003	33.3	10	13	
14 23 10.46	13944P	3	8.6003	33.3	10	13	
14 23 10.49	13945P	3	8.6003	33.3	10	13	
14 23 10.52	13946P	3	8.6003	33.3	10	13	
14 23 10.56	13947P	3	8.6003	33.3	10	13	
14 23 10.59	13948P	3	8.6003	33.3	10	13	
14 23 10.62	13949P	3	8.6003	33.3	10	13	
14 23 10.65	13950T	0	8.6003	33.3	10	13	
14 23 10.69	13951T	0	8.6003	33.3	10	13	
14 23 10.72	13952P	3	8.6003	33.3	10	13	
14 23 10.75	13953P	3	8.6003	33.3	10	13	
14 23 10.79	13954P	3	8.6003	33.3	10	13	
14 23 10.82	13955P	3	8.6003	33.3	10	13	
14 23 10.86	13956P	3	8.6003	33.3	10	13	
14 23 10.89	13957P	3	8.6003	33.3	10	13	
14 23 10.92	13958P	3	8.6003	33.3	10	13	
14 23 10.96	13959P	3	8.6003	33.3	10	13	
14 23 10.99	13960T	0	8.6003	33.3	10	13	
14 23 11.02	13961T	0	10.8577	33.3	10	13	
14 23 11.06	13962P	3	10.8577	33.3	10	13	
14 23 11.09	13963P	3	10.8577	33.3	10	13	
14 23 11.12	13964P	3	10.8577	33.3	10	13	
14 23 11.16	13965P	3	10.8577	33.3	10	13	
14 23 11.19	13966P	3	10.8577	33.3	10	13	
14 23 11.22	13967P	3	10.8577	33.3	10	13	
14 23 11.26	13968P	3	10.8577	33.3	10	13	
14 23 11.29	13969P	3	10.8577	33.3	10	13	

Table E8 - Telemetry Frames and Camera Parameters (Cont'd)

UPT	Telemetry Frame	Filter	Tracker Exp. Time (ms)	Frame Exp. Time (ms)	Tracker Gain Step	Frame Gain Step	Comments
14 23 11.32	139701	0	13.7076	33.3	10	13	
14 23 11.35	139711	0	16.3259	33.3	10	13	
14 23 11.39	13972P	3	16.3259	33.3	10	13	
14 23 11.42	13973P	3	16.3259	33.3	10	13	
14 23 11.46	13974P	3	16.3259	33.3	10	13	
14 23 11.49	13975P	3	16.3259	33.3	10	13	
14 23 11.52	13976P	3	16.3259	33.3	10	13	
14 23 11.56	13977P	3	16.3259	33.3	10	13	
14 23 11.59	13978P	3	16.3259	33.3	10	13	
14 23 11.62	13979P	3	16.3259	33.3	10	13	
14 23 11.65	139801	0	21.8478	33.3	10	13	
14 23 11.69	139811	0	27.5823	33.3	10	13	
14 23 11.72	13982P	3	27.5823	33.3	10	13	
14 23 11.76	13983P	3	27.5823	33.3	10	13	
14 23 11.79	13984P	3	27.5823	33.3	10	13	
14 23 11.82	13985P	3	27.5823	33.3	10	13	
14 23 11.85	13986P	3	27.5823	33.3	10	13	
14 23 11.89	13987P	3	27.5823	33.3	10	13	
14 23 11.92	13988P	3	27.5823	33.3	10	13	
14 23 11.96	13989P	3	27.5823	33.3	10	13	
14 23 11.99	139901	0	27.5823	33.3	10	13	
14 23 12.02	139911	0	27.5823	33.3	10	13	
14 23 12.06	13992P	3	27.5823	33.3	10	13	
14 23 12.09	13993P	3	27.5823	33.3	10	13	
14 23 12.12	13994P	3	27.5823	33.3	10	13	Star 27 burnout
14 23 12.16	13995P	3	27.5823	33.3	10	13	
14 23 12.19	13996P	3	27.5823	33.3	10	13	
14 23 12.22	13997P	3	27.5823	33.3	10	13	
14 23 12.25	13998P	3	27.5823	33.3	10	13	
14 23 12.29	13999P	3	27.5823	33.3	10	13	
14 23 12.32	140001	0	27.5823	33.3	10	13	
14 23 12.32	140011	0	27.5823	33.3	11	13	



## Appendix F STRYPI TRAJECTORY PARAMETERS

The following tables present various Strypi trajectory-related parameters as a function of time. The first column in each table is TALO, time after liftoff, in seconds. Table F1 shows the rocket's position in Earth center-fixed (ECF) coordinates and the rocket's speed. Table F2 shows the aspect angle, the angle of attack, and the distance between the satellite and the rocket. The aspect angle is defined as the angle between the line-of-sight (LOS) vector from the satellite to the target point and the longitudinal axis of the rocket. The angle of attack is defined as the angle between the longitudinal axis of the rocket and its velocity vector. Table F3 shows the rocket's altitude, geodetic latitude, and longitude. These data were provided by Sandia Laboratories.

Table F1 - Rocket Position and Speed in ECF Coordinates

TALO (s)	XPOS (km)	YPOS (km)	ZPCS (km)	SPEED (km/s)
150	-5657.022	-2069.442	2387.759	0.315
151	-5657.276	-2069.424	2387.575	0.311
152	-5657.524	-2069.402	2387.388	0.307
153	-5657.763	-2069.378	2387.197	0.303
154	-5657.993	-2069.350	2387.002	0.300
155	-5658.216	-2069.320	2386.804	0.302
156	-5658.433	-2069.299	2386.595	0.320
157	-5658.649	-2069.308	2386.360	0.340
158	-5658.864	-2069.348	2386.099	0.365
159	-5659.079	-2069.420	2385.813	0.396
160	-5659.294	-2069.526	2385.498	0.430
161	-5659.509	-2069.668	2385.154	0.467
162	-5659.725	-2069.847	2384.781	0.509
163	-5659.942	-2070.066	2384.376	0.553
164	-5660.161	-2070.326	2383.940	0.600
55	-5660.382	-2070.628	2383.471	0.650
166	-5660.606	-2070.972	2382.967	0.703
167	-5660.831	-2071.363	2382.429	0.757
168	-5661.060	-2071.800	2381.854	0.815
169	-5661.293	-2072.287	2381.243	0.874
170	-5661.529	-2072.823	2380.594	0.937
171	-5661.769	-2073.411	2379.905	1.000
172	-5662.014	-2074.050	2379.177	1.067
173	-5662.263	-2074.746	2378.407	1.134
174	-5662.518	-2075.496	2377.596	1.204
175	-5662.778	-2076.304	2376.742	1.276
176	-5663.043	-2077.170	2375.844	1.348
177	-5663.314	-2078.096	2374.902	1.423
178	-5663.591	-2079.082	2373.914	1.499
179	-5663.874	-2080.130	2372.880	1.578
180	-5664.164	-2081.242	2371.800	1.657

Table F1 - Rocket Position and Speed in ECF Coordinates (Cont'd.)

TALO (s)	XPOS (km)	YPOS (km)	ZPOS (km)	SPEED (km/s)
181	-5664.461	-2082.419	2370.671	1.740
182	-5664.765	-2083.664	2369.494	1.826
183	-5665.078	-2084.979	2368.265	1.915
184	-5665.399	-2086.366	2366.984	2.005
185	-5665.731	-2087.825	2365.649	2.098
186	-5666.071	-2089.359	2364.259	2.195
187	-5666.421	-2090.972	2362.812	2.292
188	-5666.782	-2092.663	2361.309	2.390
189	-5667.153	-2094.434	2359.747	2.490
190	-5667.535	-2096.287	2358.127	2.575
191	-5667.924	-2098.208	2356.457	2.591
192	-5668.308	-2100.141	2354.774	2.593
193	-5668.635	-2102.073	2353.087	2.592
194	-5669.053	-2104.003	2351.396	2.591
195	-5669.414	-2105.929	2349.701	2.590
196	-5669.767	-2107.852	2348.003	2.589
197	-5670.111	-2109.773	2346.301	2.588
198	-5670.449	-2111.690	2344.596	2.587
199	-5670.777	-2113.605	2342.887	2.586
200	-5671.099	-2115.517	2341.175	2.586
201	-5671.412	-2117.425	2339.459	2.585
202	-5671.716	-2119.331	2337.739	2.584
203	-5672.014	-2121.233	2336.017	2.583
204	-5672.303	-2123.132	2334.290	2.583
205	-5672.584	-2125.029	2332.561	2.581
206	-5672.857	-2126.922	2330.827	2.580
207	-5673.123	-2128.812	2329.091	2.580
208	-5673.379	-2130.700	2327.351	2.579
209	-5673.629	-2132.584	2325.607	2.578
210	-5673.870	-2134.464	2323.860	2.578
211	-5674.104	-2136.342	2322.110	2.577
212	-5674.329	-2138.217	2320.356	2.577
213	-5674.546	-2140.089	2318.599	2.576
214	-5674.756	-2141.957	2316.838	2.575
215	-5674.958	-2143.822	2315.074	2.575
216	-5675.151	-2145.684	2313.306	2.574
217	-5675.336	-2147.544	2311.535	2.574
218	-5675.514	-2149.399	2309.761	2.573
219	-5675.684	-2151.252	2307.983	2.573
220	-5675.845	-2153.102	2306.202	2.572
221	-5675.999	-2154.949	2304.418	2.572
222	-5676.144	-2156.792	2302.630	2.572
223	-5676.282	-2158.633	2300.838	2.571
224	-5676.412	-2160.470	2299.044	2.571
225	-5676.533	-2162.304	2297.246	2.571
226	-5676.647	-2164.134	2295.445	2.571
227	-5676.753	-2165.962	2293.640	2.571

Table F1 - Rocket Position and Speed in ECF Coordinates (Cont'd.)

TALO (s)	XPOS (km)	YPOS (km)	ZPOS (km)	SPEED (km/s)
228	-5676.851	-2167.787	2291.832	2.570
229	-5676.941	-2169.608	2290.020	2.571
230	-5677.023	-2171.426	2288.205	2.570
231	-5677.097	-2173.241	2286.387	2.570
232	-5677.163	-2175.054	2284.566	2.570
233	-5677.221	-2176.863	2282.741	2.570
234	-5677.271	-2178.668	2280.912	2.571
235	-5677.313	-2180.471	2279.081	2.570
236	-5677.347	-2182.269	2277.246	2.570
237	-5677.373	-2184.065	2275.408	2.570
238	-5677.391	-2185.859	2273.566	2.571
239	-5677.401	-2187.649	2271.721	2.588
240	-5677.402	-2189.450	2269.862	2.632
241	-5677.399	-2191.282	2267.972	2.678
242	-5677.395	-2193.139	2266.043	2.726
243	-5677.378	-2195.022	2264.072	2.775
244	-5677.352	-2196.940	2262.066	2.824
245	-5677.324	-2198.889	2260.024	2.872
246	-5677.291	-2200.864	2257.939	2.921
247	-5677.245	-2202.870	2255.816	2.969
248	-5677.192	-2204.909	2253.658	3.017
249	-5677.139	-2206.976	2251.462	3.065
250	-5677.076	-2209.070	2249.224	3.114
251	-5677.002	-2211.196	2246.950	3.163
252	-5676.925	-2213.355	2244.639	3.216
253	-5676.844	-2215.544	2242.285	3.270
254	-5676.752	-2217.765	2239.887	3.326
255	-5676.653	-2220.024	2237.448	3.383
256	-5676.551	-2222.320	2234.965	3.443
257	-5676.443	-2224.651	2232.433	3.506
258	-5676.325	-2227.021	2229.852	3.570
259	-5676.200	-2229.434	2227.225	3.636
260	-5676.074	-2231.890	2224.545	3.706
261	-5675.940	-2234.386	2221.810	3.777
262	-5675.796	-2236.929	2219.021	3.850
263	-5675.648	-2239.522	2216.179	3.925
264	-5675.498	-2242.162	2213.278	4.003
265	-5675.340	-2244.848	2210.315	4.084
266	-5675.172	-2247.588	2207.291	4.167
267	-5675.001	-2250.385	2204.206	4.254
268	-5674.827	-2253.237	2201.054	4.343
269	-5674.647	-2256.143	2197.832	4.438
270	-5674.458	-2259.112	2194.539	4.534
271	-5674.262	-2262.146	2191.176	4.632
272	-5674.066	-2265.245	2187.738	4.734
273	-5673.866	-2268.408	2184.222	4.835
274	-5673.659	-2271.635	2180.627	4.935



Table F1 - Rocket Position and Speed in ECF Coordinates (Cont'd.)

TALO (s)	XPOS (km)	YPOS (km)	ZPOS (km)	SPEED (km/s)
275	-5673.443	-2274.929	2176.956	5.011
276	-5673.222	-2278.273	2173.232	5.036
277	-5672.994	-2281.631	2169.486	5.044
278	-5672.759	-2284.991	2165.731	5.048
279	-5672.516	-2288.350	2161.970	5.050
280	-5672.265	-2291.706	2158.205	5.052
281	-5672.007	-2295.060	2154.436	5.053
282	-5671.741	-2298.412	2150.664	5.053
283	-5671.467	-2301.759	2146.889	5.055
284	-5671.185	-2305.104	2143.110	5.055
285	-5670.896	-2308.445	2139.328	5.056
286	-5670.599	-2311.784	2135.542	5.057
287	-5670.294	-2315.119	2131.753	5.058
288	-5669.981	-2318.451	2127.961	5.058
289	-5669.660	-2321.780	2124.166	5.060
290	-5669.332	-2325.106	2120.367	5.060
291	-5668.996	-2328.428	2116.565	5.061
292	-5668.652	-2331.748	2112.760	5.061
293	-5668.301	-2335.063	2108.952	5.063
294	-5667.941	-2338.376	2105.140	5.064
295	-5667.574	-2341.686	2101.325	5.064
296	-5667.199	-2344.992	2097.508	5.065
297	-5666.816	-2348.294	2093.687	5.066
298	-5666.426	-2351.594	2089.863	5.067
299	-5666.028	-2354.890	2086.035	5.067
300	-5665.622	-2358.183	2082.205	5.068

Table F2 - Rocket Aspect Angle, Attack Angle, and Range from Satellite

TALO (s)	ASPECT ANGLE (deg)	ATTACK ANGLE (deg)	RANGE FROM SATELLITE (km)
150	109.34	65.65	534.450
151	108.74	65.84	530.768
152	108.02	65.91	527.159
153	107.37	65.99	523.623
154	106.65	66.20	520.164
155	105.97	63.61	516.782
156	105.15	57.19	513.483
157	104.40	51.21	510.275
158	103.85	46.40	507.157
159	103.05	41.63	504.129
160	102.31	37.60	501.193
161	101.41	33.95	498.348
162	100.75	30.72	495.594
163	99.98	27.98	492.932
164	99.34	25.67	490.361
165	98.51	23.75	487.880

Table F2 - Rocket Aspect Angle, Attack Angle, and Range from Satellite (Cont'd.)

TALO (s)	ASPECT ANGLE (deg)	ATTACK ANGLE (deg)	RANGE FROM SATELLITE (km)
166	97.80	21.80	485.488
167	97.02	20.32	483.186
168	96.34	18.88	480.972
169	95.45	17.68	478.845
170	94.78	16.46	476.804
171	94.08	15.72	474.848
172	93.39	14.78	472.975
173	92.68	13.94	471.184
174	92.09	13.31	469.473
175	91.25	12.68	467.840
176	90.83	12.00	466.283
177	90.02	11.63	464.802
178	89.35	11.42	463.392
179	88.34	10.97	462.052
180	87.88	10.60	460.780
181	87.12	10.20	459.573
182	86.27	9.93	458.429
183	85.53	9.12	457.344
184	84.94	9.15	456.315
185	84.39	8.81	455.341
186	83.64	8.51	454.416
187	83.13	8.34	453.540
188	82.58	8.22	452.708
189	82.14	8.24	451.917
190	81.64	8.11	451.165
191	80.60	8.70	450.451
192	79.96	8.63	449.785
193	79.63	8.59	449.168
194	79.09	8.68	448.602
195	78.49	8.76	448.086
196	77.90	8.76	447.621
197	77.22	8.84	447.206
198	78.21	7.42	446.843
199	80.11	5.54	446.530
200	81.53	4.39	446.269
201	83.36	4.99	446.059
202	84.83	6.48	445.900
203	86.69	8.87	445.793
204	88.11	11.09	445.736
205	89.91	13.70	445.732
206	90.68	15.21	445.779
207	91.04	16.06	445.877
208	90.91	16.52	446.027
209	90.65	16.62	446.228
210	90.16	16.69	446.480

Table F2 - Rocket Aspect Angle, Attack Angle, and Range from Satellite (Cont'd.)

TALO (s)	ASPECT ANGLE (deg)	ATTACK ANGLE (deg)	RANGE FROM SATELLITE (km)
211	89.66	16.53	446.783
212	89.09	16.48	447.138
213	88.50	16.20	447.543
214	87.95	16.12	447.999
215	87.26	15.72	448.506
216	86.69	15.62	449.063
217	86.14	15.42	449.670
218	85.72	15.33	450.328
219	84.87	14.85	451.035
220	84.44	14.86	451.791
221	83.88	14.63	452.597
222	83.19	14.36	453.452
223	82.88	14.53	454.356
224	82.69	14.53	455.308
225	81.68	13.81	456.308
226	80.97	13.65	457.357
227	80.85	13.87	458.452
228	80.11	12.49	459.595
229	63.22	9.42	460.784
230	59.11	12.21	462.020
231	76.24	13.53	463.302
232	73.82	10.75	464.630
233	55.94	10.67	466.002
234	63.17	13.15	467.420
235	76.95	12.05	468.882
236	64.98	10.23	470.388
237	52.86	12.27	471.938
238	68.46	11.77	473.530
239	73.51	10.56	475.166
240	56.07	11.23	476.836
241	54.59	12.19	478.524
242	69.95	9.64	480.226
243	65.60	8.59	481.949
244	51.31	11.02	483.688
245	59.04	10.00	485.435
246	68.36	6.89	487.191
247	57.27	9.10	488.963
248	51.00	10.37	490.742
249	62.55	6.95	492.524
250	63.36	5.99	494.315
251	51.32	9.63	496.113
252	53.84	8.57	497.911
253	62.76	4.02	499.706
254	57.25	6.79	501.503
255	49.20	9.36	503.296

Table F2 - Rocket Aspect Angle, Attack Angle, and Range from Satellite (Cont'd.)

TALO (s)	ASPECT ANGLE (deg)	ATTACK ANGLE (deg)	RANGE FROM SATELLITE (km)
256	55.92	6.19	505.079
257	60.21	2.53	506.852
258	53.13	7.13	508.617
259	49.35	8.19	510.367
260	55.87	4.07	512.096
261	57.16	2.64	513.807
262	50.75	7.14	515.499
263	49.27	7.32	517.165
264	54.63	3.06	518.800
265	55.03	2.60	520.408
266	50.09	6.49	521.986
267	48.54	6.81	523.527
268	52.36	3.50	525.026
269	53.56	1.81	526.484
270	50.46	5.32	527.900
271	47.72	6.65	529.267
272	49.33	5.06	530.581
273	51.71	2.34	531.840
274	51.45	3.08	533.046
275	48.75	5.52	534.200
276	47.06	6.47	535.313
277	47.59	5.80	536.420
278	49.61	3.70	537.529
279	49.95	3.43	538.646
280	48.26	5.48	539.770
281	46.12	6.99	540.902
282	46.38	6.48	542.043
283	48.34	4.51	543.192
284	49.30	3.56	544.350
285	47.73	5.66	545.516
286	45.33	7.52	546.690
287	45.07	7.32	547.872
288	46.89	5.50	549.062
289	48.36	3.92	550.261
290	47.15	5.76	551.468
291	44.79	7.77	552.682
292	43.87	8.11	553.905
293	45.59	6.36	555.136
294	47.25	4.57	556.374
295	46.60	5.83	557.620
296	44.20	8.05	558.874
297	42.88	8.76	560.136
298	44.32	7.24	561.405
299	46.14	5.30	562.682
300	46.04	5.87	563.967

Table F3 - Rocket Altitude, Geodetic Latitude and Longitude

TALO (s)	ALTITUDE (km)	LATITUDE (deg)	LONGITUDE (deg)
150	104.432	21.7532	200.0934
151	104.581	21.7509	200.0925
152	104.720	21.7487	200.0914
153	104.850	21.7464	200.0905
154	104.970	21.7441	200.0894
155	105.081	21.7418	200.0885
156	105.186	21.7394	200.0876
157	105.291	21.7368	200.0869
158	105.395	21.7339	200.0866
159	105.499	21.7308	200.0865
160	105.603	21.7274	200.0868
161	105.709	21.7238	200.0873
162	105.817	21.7198	200.0882
163	105.927	21.7156	200.0895
164	106.039	21.7110	200.0911
165	106.155	21.7061	200.0930
166	106.273	21.7009	200.0954
167	106.396	21.6953	200.0982
168	106.523	21.6894	200.1013
169	106.656	21.6830	200.1049
170	106.793	21.6764	200.1089
171	106.936	21.6693	200.1134
172	107.085	21.6618	200.1183
173	107.241	21.6539	200.1237
174	107.404	21.6455	200.1295
175	107.574	21.6368	200.1359
176	107.752	21.6276	200.1427
177	107.938	21.6179	200.1501
178	108.132	21.6078	200.1580
179	108.334	21.5972	200.1664
180	108.546	21.5862	200.1754
181	108.768	21.5746	200.1849
182	109.000	21.5626	200.1950
183	109.244	21.5500	200.2057
184	109.500	21.5369	200.2170
185	109.768	21.5232	200.2289
186	110.049	21.5089	200.2414
187	110.344	21.4941	200.2546
188	110.653	21.4787	200.2685
189	110.977	21.4626	200.2830
190	111.315	21.4460	200.2982
191	111.665	21.4289	200.3140
192	112.011	21.4116	200.3300
193	112.349	21.3944	200.3459
194	112.679	21.3771	200.3618

Table F3 - Rocket Altitude, Geodetic Latitude and Longitude (Cont'd.)

TALO (s)	ALTITUDE (km)	LATITUDE (deg)	LONGITUDE (deg)
195	113.001	21.3598	200.3777
196	113.314	21.3426	200.3936
197	113.620	21.3253	200.4096
198	113.918	21.3080	200.4255
199	114.207	21.2908	200.4414
200	114.488	21.2735	200.4573
201	114.761	21.2562	200.4731
202	115.025	21.2389	200.4890
203	115.282	21.2216	200.5049
204	115.530	21.2043	200.5208
205	115.771	21.1871	200.5367
206	116.003	21.1698	200.5525
207	116.226	21.1525	200.5684
208	116.441	21.1352	200.5842
209	116.649	21.1179	200.6001
210	116.848	21.1006	200.6159
211	117.039	21.0833	200.6317
212	117.222	21.0661	200.6476
213	117.396	21.0488	200.6634
214	117.563	21.0315	200.6792
215	117.721	21.0142	200.6950
216	117.871	20.9969	200.7108
217	118.013	20.9796	200.7266
218	118.146	20.9623	200.7424
219	118.271	20.9450	200.7582
220	118.389	20.9277	200.7740
221	118.498	20.9103	200.7898
222	118.598	20.8930	200.8055
223	118.691	20.8757	200.8213
224	118.775	20.8584	200.8371
225	118.852	20.8411	200.8528
226	118.920	20.8238	200.8686
227	118.980	20.8064	200.8843
228	119.031	20.7891	200.9001
229	119.075	20.7718	200.9158
230	119.110	20.7545	200.9315
231	119.138	20.7372	200.9473
232	119.157	20.7198	200.9630
233	119.168	20.7025	200.9787
234	119.170	20.6852	200.9944
235	119.165	20.6678	201.0102
236	119.150	20.6505	201.0259
237	119.129	20.6331	201.0416
238	119.099	20.6158	201.0573
239	119.060	20.5984	201.0730
240	119.013	20.5810	201.0888

Table F3 - Rocket Altitude, Geodetic Latitude and Longitude (Cont'd.)

TALO (s)	ALTITUDE (km)	LATITUDE (deg)	LONGITUDE (deg)
241	118.965	20.5632	201.1049
242	118.909	20.5452	201.1212
243	118.840	20.5267	201.1378
244	118.761	20.5080	201.1547
245	118.681	20.4389	201.1719
246	118.591	20.4695	201.1894
247	118.488	20.4498	201.2071
248	118.380	20.4297	201.2252
249	118.269	20.4093	201.2435
250	118.145	20.3885	201.2621
251	118.012	20.3674	201.2809
252	117.876	20.3460	201.3001
253	117.733	20.3242	201.3196
254	117.578	20.3021	201.3393
255	117.417	20.2795	201.3595
256	117.253	20.2566	201.3799
257	117.080	20.2332	201.4007
258	116.896	20.2094	201.4218
259	116.708	20.1852	201.4433
260	116.517	20.1605	201.4653
261	116.316	20.1353	201.4875
262	116.106	20.1097	201.5103
263	115.893	20.0835	201.5334
264	115.676	20.0568	201.5570
265	115.451	20.0296	201.5810
266	115.216	20.0018	201.6055
267	114.980	19.9734	201.6305
268	114.741	19.9444	201.6560
269	114.495	19.9148	201.6819
270	114.240	19.8846	201.7085
271	113.983	19.8536	201.7356
272	113.725	19.8220	201.7633
273	113.463	19.7897	201.7915
274	113.194	19.7567	201.8203
275	112.919	19.7229	201.8497
276	112.642	19.6887	201.8796
277	112.361	19.6543	201.9096
278	112.075	19.6198	201.9396
279	111.784	19.5853	201.9696
280	111.488	19.5507	201.9997
281	111.187	19.5162	202.0297
282	110.881	19.4816	202.0597
283	110.570	19.4471	202.0897
284	110.253	19.4125	202.1197
285	109.932	19.3779	202.1497
286	109.606	19.3433	202.1797

Table F3 - Rocket Altitude, Geodetic Latitude and Longitude (Cont'd.)

TALO (s)	ALTITUDE (km)	LATITUDE (deg)	LONGITUDE (deg)
287	109.275	19.3086	202.2097
288	108.938	19.2740	202.2396
289	108.596	19.2393	202.2696
290	108.250	19.2047	202.2995
291	107.898	19.1700	202.3294
292	107.541	19.1353	202.3594
293	107.179	19.1006	202.3893
294	106.813	19.0659	202.4192
295	106.441	19.0312	202.4491
296	106.064	18.9965	202.4789
297	105.681	18.9618	202.5088
298	105.294	18.9270	202.5387
299	104.902	18.8923	202.5685
300	104.504	18.8575	202.5984





## ADDENDUM

### Statistical Discrimination of Photoevents

When a single photoevent is generated in the microchannel plate (MCP) of the UVPI plume camera, it is registered as a spatial distribution of charge in the CCD focal plane array (FPA). In general, a photoevent gets registered within a 3 x 3 pixel region with the largest FPA response at the center pixel. Note that the blurring of a single photoevent over the 3 x 3 pixel region is a relatively small component of the overall system point spread function.

When UVPI is looking at a dim source, compared to the instrument sensitivity, the instrument gain is automatically set high, for example, gain 13. At these high gains the calibration procedure, i.e., the estimation of photoevents from the measured DN, is sensitive to any mismatch between the estimated dark field level used for calibration and the actual dark field level. Although a small bias error in the dark field estimate would have a small impact on the photoevent estimate for a single pixel, it could have a large impact on the results when summing the contribution of groups of pixels. Hence, for dim signal levels, such as the Nihka rocket plume, a statistical discrimination scheme was developed which fixes the probability of false alarm for every pixel. In the context of calibrating UVPI data, a false alarm occurs when the noise in a pixel that contains no target is large enough to be considered part of a photoevent.

Working with the already calibrated images, the discrimination scheme consists of estimating a statistical decision threshold for each image. The threshold is given in terms of the background mean, standard deviation, and the accepted probability of false alarm. Estimates for each image of the background mean and variance are made using 4 image blocks located at each corner of the image and with dimensions of 8 by 8 pixels. The estimated threshold will exactly correspond to a probability of false alarm of  $PF$  if the following assumptions hold [24]:

- the local mean and local variance background statistics are the same over the whole FPA, and
- the density function of the background follows a Gaussian distribution.

Mathematically the decision threshold is given by:

$$t' = \mu + \sigma \cdot t'$$

where

- $\mu$  is the estimated background mean,
- $\sigma$  is the estimated background standard deviation, and
- $t'$  is must satisfy the following integral equation

$$PF = \text{erfc}(t'),$$

where the standard complementary error function was used.[24]

All the plume camera images which were used in this report to estimate radiance or radiant intensities were subjected to the above discrimination scheme using a probability of false alarm of 0.0001. False alarms were, in fact, observed in approximately 1 out of every 10000 pixels, indicating that the two assumptions stated above are generally representative of these data. Recalling that a

photoevent may spread over a 3 x 3 pixel region, for all those pixels where a photoevent took place immediate neighbors were also included as possible signal contributors. A new estimate for the number of photoevents from the  $k$ th pixel was computed based on the following rule,

$$P_k = \max(0, P_k - \mu) \quad \text{if condition (A) holds or} \quad P_k = 0, \text{ otherwise.}$$

In the above, condition (A) states that if any pixel in the local neighborhood of the  $k$ th pixel exceeds  $t'$  then the value at the  $k$ th pixel is adjusted to be the maximum of zero or  $P_k - \mu$ . Thus, pixels containing no photoevent contribution are set to exactly zero, eliminating the possibility of an "erroneous" contribution due to uncertainties in the dark field estimate for that pixel. This adjustment can be significant when large numbers of pixels contain no photoevents, i.e., few photoevents per image.

## GLOSSARY

ACS	Attitude Control System
AMOS	Air Force Maui Optical Site
AOS	Acquisition of signal
ARI	Average radiant intensity
CCD	Charge-coupled device
CFC	Camera frame controller
CHARM	Composite High Altitude Radiation Model
CMOS	Complementary metal oxide semiconductor
CPU	Central processing unit
DN	Digital number
DN/PE	Digital number per photoevent
ECF	Earth center-fixed
EIA	Electronics interface assembly
ERD	Experiment requirements document
FOR	Field of regard
FOV	Field of view
FWHM	Full-width-half-maximum
GMT	Greenwich Mean Time
Hz	Hertz
ICC	Instrument control computer
ICCD	Intensified charge-coupled device
IDA	Institute for Defense Analyses
IR	Infrared
ITT	International Telephone and Telegraph
IUE	International Ultraviolet Explorer
K	Degrees Kelvin
KTF	Kauai Test Facility
LACE	Low-power Atmospheric Compensation Experiment
LOS	Loss of signal; line of sight
LOTB	LACE Operational Test Bed
Mbps	Megabits per second
MCP	Microchannel plate
MHz	Megahertz
NER	Noise-equivalent radiance
NQE	Net quantum efficiency
NRL	Naval Research Laboratory
QAO	Orbiting Astrophysical Observatory
OLES	One line element set
PC-N	Plume camera filter, N = 1, 2, 3, 4
PE	Photoevent
PMRF	Pacific Missile Range Facility
PSAG	Phenomenology Steering and Analysis Group
PSF	Point spread function
RMS	Root mean square
SDIO	Strategic Defense Initiative Organization
SIRRM	Standardized Infra-Red Radiation Model
SNR	Signal-to-noise ratio
sr	Steradian
TALO	Time after liftoff
TGS	Transportable ground station
ULTRASEEK	Ultraviolet seeker
UMT	UVPI mission time
UV	Ultraviolet
UVPI	Ultraviolet Plume Instrument
VAFB	Vandenberg Air Force Base
W	Watt

END  
FILMED

DATE:

11-93

DTIC